UTS UNIVERSITY OF TECHNOLOGY SYDNEY

Modelling Transition Zones and Optimal Design Adjoining Tunnels and Bridges

by Muhammad Babar Sajjad

Thesis submitted in fulfilment of the requirements for the degree of

Doctor of Philosophy

under the supervision of Dr. Trung Ngo and Distinguished Professor Buddhima Indraratna

University of Technology Sydney
Faculty of Engineering and Information Technology

August 2023

CERTIFICATE OF ORIGINAL AUTHORSHIP

I, Muhammad Babar Sajjad, declare that this thesis is submitted in fulfilment of the requirements for the award of Doctor of Philosophy, in the School of Civil and Environmental Engineering, Faculty of Engineering and Information Technology at the University of Technology Sydney.

This thesis is wholly my own work unless otherwise referenced or acknowledged. In addition, I certify that all information sources and literature used are indicated in the thesis.

This document has not been submitted for qualifications at any other academic institution.

This research is supported by the Australian Government Research Training Program.

Signature: Production Note:
Signature removed prior to publication.

Date: August 08, 2023

ABSTRACT

Track transitions, such as bridge approaches, road crossings, and shifts from slab track to ballasted track, are known to be locations where track degradation accelerates due to dynamic and high impact forces. As a result, there is a higher differential settlement, which can cause an abrupt change in the structural response of the track due to variations in stiffness and track damping. This can cause accelerated deterioration of track material and geometry leading to reduced efficiency and compromised track longevity, increased passenger discomfort, and elevated maintenance costs. In order to mitigate these issues, transition zones are provided at sudden discontinuities of track stiffness to minimize instability and reduce vibrations, and to ensure a smoother train passage over sections of significantly different track characteristics. By ensuring a smooth and gradual transition between flexible (less stiff) and rigid (stiff) track substructure, a well-designed transition zone can mitigate the impact of dynamic loads generated by moving trains.

This study proposes a novel approach to smoothen the abrupt stiffness variation along railway transitions and provides a step-by-step design of a multistep transition zone comprising adjoining segments with changing stiffness values, and design optimization guidelines. The influence of stiffness on the track dynamic response applied to transition zones is investigated analytically, considering a beam on elastic foundation. Vertical track displacements for varying stiffness values under different combinations of axle loads and speeds are calculated analytically and numerically, and they are found to be in good agreement. The results indicate that stiffer tracks undergo lesser settlements compared to those having smaller stiffness. Furthermore, the effect of abrupt stiffness variation at transition sections is analysed under four-carriage loading causing considerable differential settlement, which is further exacerbated by increased train speeds.

A mathematical process is introduced to determine the optimum stiffness of each segment to ensure a gradual change in stiffness while minimizing the corresponding differential settlement to allowable limits. The proposed methodology is further validated through Finite Element Modelling (2D & 3D) approach and worked-out examples, considering multiple loading conditions, epitomizing the effects of stiffness

variation along the number of transition steps. From a practical perspective, this study provides a significant extension for the design rejuvenation of transition zones by minimizing the differential settlement at any two consecutive transition segments. The proposed approach can be implemented to improve the durability and effectiveness of railway tracks during both their construction and upkeep, resulting in decreased passenger discomfort and reduced expenses for maintenance.

ACKNOWLEDGEMENTS

In the name of ALLAH, the Most Compassionate, the Most Merciful. All praise and gratitude are due to Him, the Lord of the worlds, and may His blessings and peace be upon His messenger MUHAMMAD, his family, and his companions.

I would like to express my heartfelt appreciation to my supervisors, Distinguished Professor Buddhima Indraratna and Dr. Trung Ngo, for their invaluable guidance, support, and encouragement throughout my PhD journey. Their dedication, expertise, and insightful feedback have been instrumental in shaping my research and helping me overcome challenges.

Australian Research Council, (ARC) is gratefully acknowledged for its financial support through the ITTC-RAIL scholarship. I wish also to thank the University of Wollongong (UOW) and the University of Technology Sydney (UTS) for awarding me the tuition scholarships that have covered my full tuition fee for the first half and the later part of my PhD tenure, respectively.

I would like to express my sincere gratitude to Dr. Richard Kelly, the representative of SMEC (our industry partner) for his invaluable support and contribution to my PhD research.

To my dear friends and colleagues, I am indebted to you for your support, encouragement, and laughter. Your constant support and camaraderie have made this journey more bearable, and I will cherish the memories we have created together.

I am also deeply grateful to my mother, Safia Begum, my wife, Tanzila, and my siblings for their unconditional love, unwavering support, and constant motivation. Their patience, sacrifices and encouragement have been the bedrock of my academic and personal success.

Last but not least, I'm thrilled to welcome my newborn boy, Muhammad Bakar, to the world. Your arrival has brought immense joy and inspiration to my life, and I look forward to sharing the milestones and the journey ahead with you.

Thank you all for your unwavering support, guidance, and love. I couldn't have done this without you.

LIST OF PUBLICATIONS

1. Journal Papers:

- Indraratna, B., Sajjad, M. B., Ngo, T., Correia, A. G., and Kelly, R. (2019), "Improved performance of Ballasted Tracks at Transition Zones: A Review of Experimental and Modelling Approaches", *Transportation Geotechnics*, 21, 100260.
- Sajjad, M. B., Indraratna, B., Ngo, T., Kelly, R., and Rujikiatkamjorn, C. (2022), "A Computational Approach to Smoothen the Abrupt Stiffness Variation along Railway Transitions", *J. Geotech. Geoenviron. Eng.,* 2023, 149(8): 04023063.
- Sajjad, M. B., Indraratna, B., Ngo, T, Kelly, R. (2023), " Enhancing Multi-Step Transitions through Comprehensive Analytical Solution and Advanced 3D Numerical Modeling Techniques ", *in preparation to be submitted*. (Under progress)

2. Peer-reviewed Conferences:

- Sajjad, M. B., Indraratna, B., Ngo, T. (2019), “Rail Track Transitions: Problems and Mitigation Measures”, at *9th Asian Young Geotechnical Engineers Conference (9AYGEC) & 15th International Conference on Geotechnical Engineering (15ICGE)*, in Lahore, Pakistan.
- Sajjad, M. B., Indraratna, B., Ngo, T. (2022), “Rail Track Transitions: Benefits of Multi-step Transition Zone”, at *16th International Conference on Geotechnical Engineering (16ICGE)*, in Lahore, Pakistan, (December 7-8, 2022)
- Sajjad, M. B., Indraratna, B., Ngo, T. and Rujikiatkamjorn, C. (2023), “Modelling of Tracks at Transition Zones: Analytical and Numerical Modelling Approach”, at Geo-Congress 2023, in Los Angeles, California.

LIST OF SYMBOLS

A	Rail cross sectional area
C	Damping matrix
c	Track damping
C_1-C_4	Constants
c_b, c_s	Track damping of ballasted track and slab track, respectfully
c_R	Damping ratio
D	Train wheel diameter
D_1, D_2, D_3	Distance between two consecutive wheels, bogies, and cars of the train, respectively
d_p	Distance of a certain load point from point x
E	Modulus of elasticity
E_1, E_2, E_3	Modulus of elasticity of ballast, sub-ballast and subgrade layers, respectively
E_s	Equivalent modulus of elasticity of layered foundation
F	Train dynamic load
h_1, h_2, h_3	Thickness of ballast, sub-ballast and subgrade layers, respectively
I	Rail second moment of area
i	Segment number in a multistep transition zone, stiff to soft
K	Stiffness matrix
k	Track equivalent stiffness,
k_b	Track equivalent stiffness of ballasted track
k_b, k_s	Track equivalent stiffness of ballasted track and slab track, respectfully
$k_{ballast}$	Stiffness of ballast layer

k_i	Track equivalent stiffness of the i^{th} segment at multistep transition zone
k_{max}	Track equivalent stiffness of stiffer side at track transition
k_{min}	Track equivalent stiffness of softer side at track transition
k_n	Track equivalent stiffness of the n^{th} segment at multistep transition zone
k_{n+1}	Track equivalent stiffness of the most-soft segment at multistep transition zone
k_o	Track equivalent stiffness of the most-stiff segment at multistep transition zone
$k_{railpad}$	Stiffness of rail pads
$k_{Sleeper}$	Stiffness of sleepers
$k_{sub\text{-}ballast}$	Stiffness of sub-ballast layer
$k_{subgrade}$	Stiffness of subgrade layer
l	Length of each segment in a multistep transition zone
L	Total length of a multistep transition zone
L_c	Characteristic length
M	Mass matrix
N	Total number of load points
n	Total number of transition segments in a multistep transition zone
P	Train wheel load
P_{axle}	Train axle load
P_d	Dynamic wheel load
S	Spring stiffness
U_1, U_2, U_3	Track deflection in X, Y and Z direction, respectively

UR_1, UR_2, UR_3	Track rotations in X, Y and Z direction, respectively
v	Train speed
v_R	Speed ratio
w	Track vertical displacement (i.e. settlement)
w_b, w_s	Vertical deflection of ballasted track and slab track, respectfully
w_i	Maximum settlement of the i^{th} segment at multistep transition zone
w_{max}	Maximum settlement
w_{n+1}	Maximum settlement of the most-soft segment at multistep transition zone
w_o	Maximum settlement of the most-stiff segment at multistep transition zone
w_{soft}	Maximum settlement for a track with lesser stiffness value
w_{stiff}	Maximum settlement for a track with higher stiffness value
x	Position of wheel load along the track
X_i	Distance of endpoint of segment i from track junction
Δk	Stiffness variation
Δw	Differential settlement
$\Delta w_{allowed}$	Maximum allowable differential settlement, ζ (zeta)
Δw_{max}	Maximum differential settlement
α, β	Damping coefficients
δ	Dirac-delta function
ζ	Maximum allowable differential settlement
ρ	Rail density

υ	Poisson`s ratio
φ	Friction angle
ϕ	Dynamic amplification factor
ψ	Dilation angle

ABBREVIATIONS

Acm	Accelerometers
AR	Auxiliary Rails
AS	Approach Slab
BCW	Backfill Confinement with Walls
BOEF	Beam on Elastic Foundation
BPA	Ballast Particles Acceleration),
BS	Ballast/subgrade Stresses
BsTAS	Ballast-less Track on Asphalt Slab
BsTCd	Ballast-less Track on Concrete deck
BsTR	Ballast-less Track on Rock
BsTS	Ballast-less Track on Soil
BTCc	Ballast Track on Concrete culvert
BTCd	Ballast Track on Concrete deck
BTCv	Ballast Track on Concrete viaduct
BTR	Ballast Track on Rock
BTS	Ballast Track on Soil
CF	Contact Forces
CMS	Changing Material of Sleepers
CW	Concrete Wedge/slab
DAF	Dynamic Amplification Factor
DEM	Discrete Element Method
Dyn.	Dynamic
EB	Euler-Bernoulli

EP	Elastoplastic
FEM	Finite Element Method
FT	Freight Track
Gp	Geophones
HL	Hughes-Liu
HMA	Hot Mix Asphalt Wedge/layer
HSb	Hydraulic Sub-base
IT	Inclinometer Tubes
iHPC	Interactive High-Performance Computing
LE	Linear Elastic
LS	Longer Sleeper
LU	LASER Units
LVDT	Linear Variable Differential Transducer
LVE	Linear Visco- elastic
MCE	Moisture Content Effect
MDD	Multidepth Deflectometers
MT	Mixed Traffic/Track
NLE	Non-linear Elastic
NLVE	Non-linear Visco-elastic
PSD	Position Sensitive Devices
PT	Passenger Track
QS	Quasi-static
RB	Rectangular Beam

RD	Rail Deflection
RP	Rail Pads
RpF	Rail pad Force
RS	Resilient Sleepers
SB	Simple Beam
SE	Survey Equipment
SG	Strain Gauges
SoTSt	Soft to Stiff
SRG	Soil Reinforcement with Geogrid
SRP	Soil Reinforcement with Piles
SS	Sleeper Spacing/Location
St.	Static
StTSo	Stiff to Soft
TA	Track Acceleration
TLV	Track Loading Vehicle
TM	Track Modulus/Stiffness
TS	Timoshenko
TV	Track Velocity
USP	Under Sleeper Pads
USPs	Under Sleeper Pads
UTS	University of Technology Sydney
VC	Video Cameras
VGS	Video Gauge System

VtD	Vertical Displacement/Deflection
WL	Wheel Load
WS	Wider Sleeper
WSB	Wedge-Shaped Backfill
2D	Two Dimensional
3D	Three Dimensional

TABLE OF CONTENTS

LIST OF FIGURES

LIST OF TABLES

CHAPTER ONE

1. INTRODUCTION

1.1 Research Background

Cities around the world are increasingly getting congested and expensive owing to limited space and increased population (Sterling & Nelson 2013; Gonzalez 2019). Therefore, the mass rapid transportation system is growing into a basic need of the time to connect the major cities and the countryside areas especially with high speed trains (Cui & Nelson 2019). Interestingly, most often it becomes comparatively quick and economical to connect the major cities and country side area by crossing below the mountains through tunnels (Zhao et al. 2019), but it requires numerous changeovers for the rail track from one type to the other (Aggestam & Nielsen 2019).

Railway transitions are locations along the track characterized by the presence of an abrupt variation of their stiffness, such as rail tracks change from a stiff structure (concrete bridge deck) to soft structure (ballasted track) or vice versa. They occur when a conventional ballasted track transitions to a stiffer track to traverse roadways, water bodies (such as river or canal), valleys or mountains. This transition could happen via level crossings, bridges, culverts or tunnels. Such transitions can be due to a sudden change in track substructural components, track superstructural components (as at special trackwork, level crossings, sleeper types, etc.) or both (Li et al. 2016). Figure 1.1 provides some examples of track transitions as a result of sudden change in substructural components. Figure 1.1a shows two rail track transitions indicating a ballasted track to concrete bridge deck on both sides of Berry Bridge crossing Tannery road in NSW, Australia. In contrast, Figure 1.1b illustrates a ballasted track to slab track transition having an alignment issue that is often a problem associated with such transitions. Figure 1.2 provides some examples of track transitions as a result of sudden change in the superstructural components. Figure 1.2a shows a single level crossing on a conventional track at Unanderra, NSW, Australia, whereas, Figure 1.2b illustrates several other types of such transitions that can generate extreme dynamic loadings attributed to associated gaps and discontinuities causing variations on the rail running surface (Li et al. 2016).

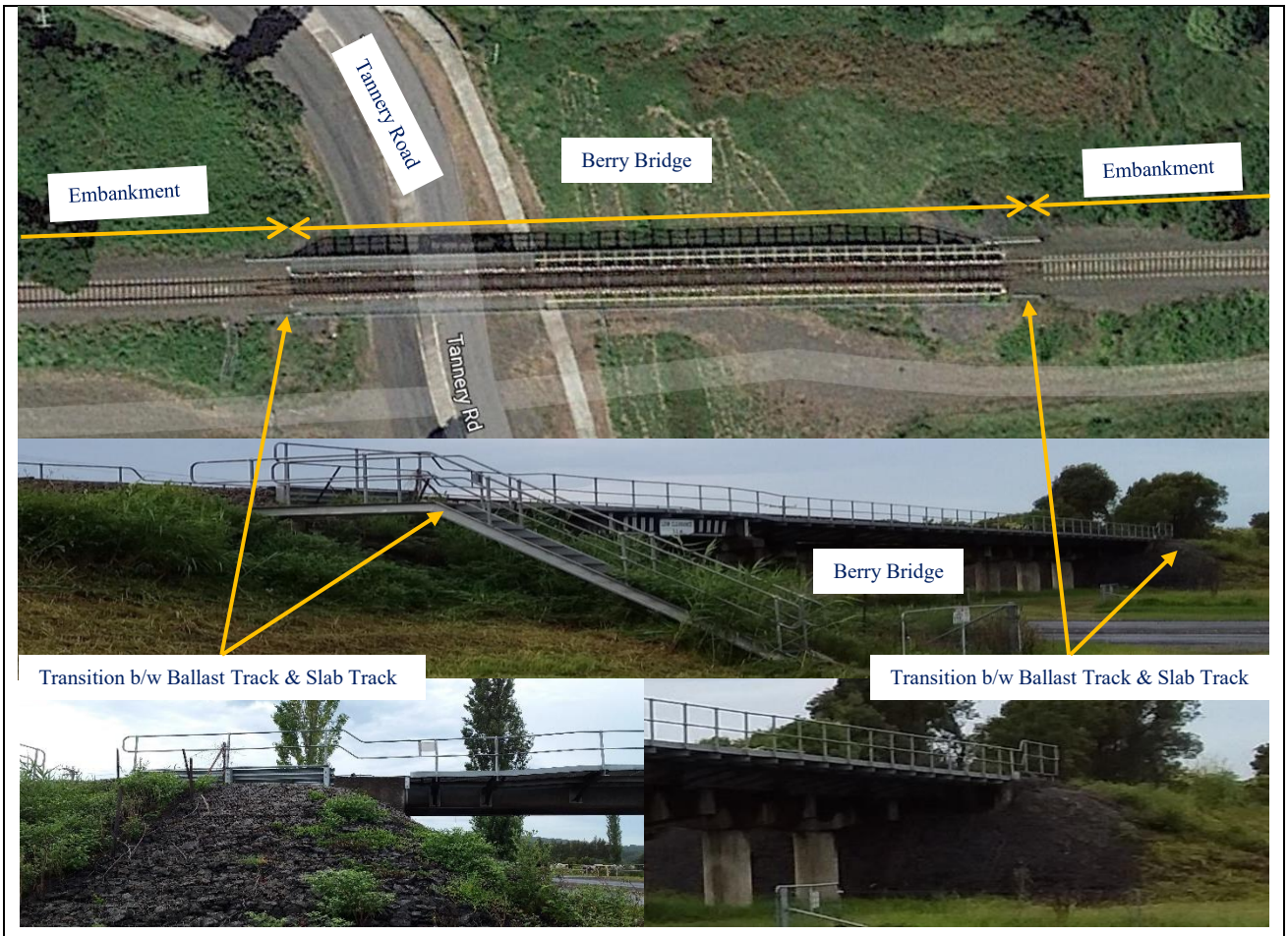

(a) Track transitions at Berry bridge crossing Tannery road, NSW, Australia

(b) Slab track to ballast track transitions indicating alignment error (Li et al. 2016)

Figure 1.1: Rail track transitions due to sudden change in substructural components, after (Indraratna et al. 2019)

(a) Level crossing on a conventional track at Unanderra, NSW, Australia

(b) Two crossing diamond, a level crossing, and a turnout (Li et al. 2016)

Figure 1.2: Rail track transitions due to the change of superstructural components, after Indraratna et al. (2019)

1.2 Problem Statement and Research Gaps

Transitions in rail tracks results in abrupt stiffness variations, sudden changes in track damping and corresponding subgrade reactions. Such changes in their structural properties results in increases dynamic loading and, differential settlements which further lead to track degradation. As a consequence, track components, materials, and geometry progressively deteriorate (Plotkin & Davis 2008; Dahlberg 2010; Choi 2013; Huang & Brennecke 2013; Zhou et al. 2020). Furthermore, the impact of moving train loads can exacerbate the adverse effects of transitions on rail deflections, dynamic loads, and track acceleration (Li & Davis 2005; Berggren 2009; Banimahd et al. 2012; Tutumluer et al. 2012).

This effect can be seen in Figure 1.3 that has been reproduced from the modelling data presented by Esmaeili et al. (2018) and Zakeri & Ghorbani (2011). Figure 1.3 illustrates how these values vary suddenly in a short length at the junction point of a ballasted and slab track, while loads move from the ballast track to the slab track. It

has been suggested that such abrupt variation in track acceleration causes oscillations or vibrations which further cause destructive effects (Zakeri & Ghorbani 2011). Failing to adopt any appropriate measures may results in escalated deterioration of track/vehicle components, leading to reduced ride quality for all rail traffic types, including accelerated ballast degradation(breakage). This will have significant repercussions on railway operations, including train speed restrictions, schedule delays, heightened passenger discomfort, and increased maintenance expenses (Zarembski & Palese 2003; Teixeira et al. 2006; Li et al. 2010; Heydari-Noghabi et al. 2017).

The expenses incurred in addressing issues related to track transitions to ensure the smooth functioning of railways are typically considerable (Sasaoka & Davis 2005; Hyslip et al. 2009; Sañudo et al. 2016), For example, in the United States and Europe, annual cost for the maintenance of track transitions are approximately 200 million dollars and 110 million dollars, respectively (Sasaoka & Davis 2005; Hyslip et al. 2009; Tutumluer et al. 2012). Repairing bridge-related transitions alone in the United States costs US$26 million per year, whereas in Spain the maintenance of tracks employs a significant amount of allocated budget for infrastructure materials (Nicks 2009; Sañudo et al. 2016). Previous research has shown that the cost of maintaining track transitions at discontinuities is considerably higher (up to 8 times) than that of conventional track maintenance (Kerr & Moroney 1993; Hölscher & Meijers 2007; Varandas et al. 2011; Sañudo et al. 2016).

Transition zones are provided at track junctions to alleviate the problems associated with structural discontinuities (Zuada Coelho 2011; J. Pires et al. 2014; Sañudo et al. 2016; Heydari-Noghabi et al. 2017) and to mitigate the dynamic effect of moving loads through smooth and gradual stiffness transitions (Aggestam & Nielsen 2019). With the increasing demand for long and heavy haul trains to travel at fast speeds, crossing bridge decks, concrete culverts or tunnels with stiff foundations towards softer soils or very soft estuarine plains, the precise and economic design of transition zones is a challenge for designers and practising engineers (Sañudo et al. 2016; Zhou et al. 2020).

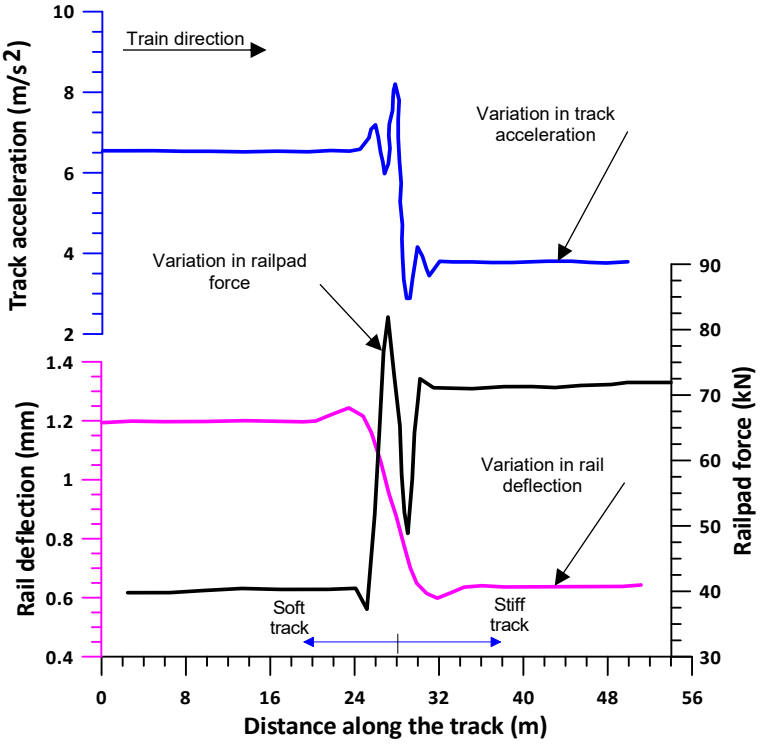

Figure 1.3: Variation in rail deflection, railpad force and track acceleration at track transition (Indraratna et al. 2019)

There have been several mitigation measures adopted, to minimise the track transition problems, and a few computational processes in relation to transition zones, as reported in following sections. After critically reviewing that, the Author has found the following research gaps in the literature, that have been the main reason for the motivation of this study.:

- There have not been any rigorous guidelines or comprehensive procedures for design of transition zones
- The literature in this field is lacking in respect to any specific fundamental approach that can be used in the design of track transitions incorporating the actual ground conditions, especially to cater for long and heavy haul freight in Australia.
- There have been limited studies focused particularly on the effects of abrupt stiffness variations and a fundamental optimization procedure to minimize the differential settlements.

- A precise and step-by-step design of transition zones remains a challenge for rail practicing engineers.

1.3 Research Objectives

The main objective of the current research is to model the transition zones using advanced modelling techniques and analytical approach to optimize their design considering moving train loads. The novelty of this current study lies in its aim to assist practitioners in designing transition zones while considering crucial factors such as the total length of the transition zone, the number of transition steps, and appropriate stiffness values, along with their variations along the track. The specific objectives of the study are as follows:

1. Analysing the behaviour of railway tracks, subjected to various loading condition relevant to transport corridors.
2. Developing mathematical models of track transitions for different ground conditions considering abrupt stiffness variation.
3. Analysing the track dynamic response at transitions using Finite Element Method (FEM) for various loading conditions.
4. Optimizing the multi-step transition zone in terms of its total length and the number of transition steps along with their lengths and stiffness values.
5. Recommending step-by-step design guidelines for the provision of multi-step transition zone for specific ground conditions.

1.4 Significance and Innovation

This study provides a major extension for design rejuvenation of transition zones by optimising the calculated differential settlement (both analytically and numerically) reflecting significant innovation compared to available literature on the computational design aspects of transition zones. It presents a novel analytical approach to design track transition zones considering the abrupt change of stiffness at any transition. The practical outcomes of this study including the salient flow charts can inspire better design solutions, as well as revised specifications and guidelines for track transition zones. Consequently, finding the appropriate length of transition zones to gradually

transform the track stiffness should reduce the differential settlement at these critical locations to minimise track degradation.

Furthermore, the significance and novelty of the current study can be more specifically described as below:

1. This study proposes a fundamental approach that can be used in the design of rail track transition zones. This approach provides a step-by-step design of a multi-step transition zone considering the abrupt change of stiffness at any transition. It determines the optimum stiffness of each segment at a transition zone to ensure a smooth and gradual change in stiffness values along the track.

2. The optimum stiffness of each segment at a transition zone is then utilised as input stiffness parameters for a layered track that is simulated in an FEM model to capture the response of different track elements (e.g. ballast, sub-ballast and subgrade). This modelling approach considers varied values of stiffness to simulate the moving wheel load on the layered track, where they are determined on the basis of the analytical approach.

3. Based on the analytical and numerical approaches, this study provides a significant extension for design rejuvenation of transition zones by minimising the differential settlement at any two consecutive transition segments.

1.5 Thesis Outline

This PhD thesis comprises of eight chapters, as briefly outlined as follows. This current chapter 1 describes the research background, research gaps, main objectives, and innovation of the current study along with its significance. The outline of the subsequent Chapters in this thesis is succinctly described below.

Chapter 2 reviews various aspects of railway transition zones by first defining a track transition and its importance with respect to the structural integrity of track catering for passenger and heavy haul trains. It also presents the various problems associated with track transition, and their causes and consequences on railway operations.

Chapter 3 presents the past research into rail tracks and transitions, and investigates the multiple measures adopted to minimise and mitigate these problems with reference to their limitations and effectiveness. The design and modelling of tracks at transition

zones, including large-scale laboratory testing and prototype experiments, mathematical and computational modelling and field measurements is also discussed in this chapter. At the end of this chapter detailed comparisons of computational modelling and field measurements are also provided in tabular forms.

Chapter 4 presents the dynamic response of railways investigating the effect of stiffness on track settlement through analytical and numerical modelling.

Chapter 5 elaborates further on the dynamic responses of tracks extending to the transition zones. This chapter highlights the severity of the problem in terms of enhanced differential settlement at track transitions due to abrupt stiffness variation.

Chapter 6 explains the design optimisation of transition zones through a novel approach, providing the step-by-step design guidelines and optimisation criterion. This chapter also highlights the research significance through its practical implications along with the worked-out design examples.

Chapter 7 provides three-dimensional modelling of the multistep transition zone. This investigation is aimed at studying the effect of train speed and load on the dynamic response of various segments in terms of track settlement and the corresponding differential settlement in order to optimize the proposed design.

Chapter 8 summarises and synthesises the main conclusions of this research along with its limitations and recommendations for future studies in the same discipline.

CHAPTER TWO

2. RAIL TRACKS AND TRANSITION ZONES

2.1 Introduction

A brief overview of various aspects of rail transitions and their importance with respect to the structural integrity is provided in this chapter. Following a basic introduction of the rail track structure and associated components, along with their specifications, the various types of tracks are categorised according to their usage and type of components/materials. The requirements of the provision of track transitions, the associated problems, and their causes and consequences on railway operations, are also discussed in this chapter. The PhD candidate has published part of this Chapter as a Review article in a Q1-Journal: Transportation Geotechnics.

2.2 Rail Track Structure

A railway track, generally, comprises of superstructure and substructure as shown in Figure 2.1 and Figure 2.2. The superstructure is composed of structural components including rails, and sleepers. The substructure is mainly consisted of ballast, sub-ballast and subgrade. The combined effect of all the components provides a durable surface to the train wheels for their smooth movements. Both the substructure and the superstructure are equally important in ensuring better ride quality and, the safety and comfort of passengers. Every component of overall track structure is equally responsible to dissipate the stresses induced by the dynamic wheel loads properly without compromising the integrity of rail track structure (Selig & Waters 1994; Esveld 2001). The properties and the functionality of each component are described in succeeding sections.

2.2.1 Rail

Rail is the only component of the railway track structure which has direct contact with the wheels of the train. It is made of steel and the length of single rail varies between

11m to 24m (depending upon country standards). The rails are then welded together and placed longitudinal on the sleepers in pairs at some standard spacing (called as gauge), typically 1435mm in Australia (Mills 2006), to form the railway track. Fasteners are used to fix the rails to sleepers restricting their movements caused by moving trains and thermal stresses. The main function of the rails is to guide the trains as well as transfer the train load to the supporting sleepers. Any defects or undulations in rail track can cause serious problems to track structure due to enhanced impact load of fast-moving loads (Li & Davis 2005; Dahlberg 2010).

2.2.2 Sleepers

The sleepers are provided to transfer the wheel load from rails to wider area on ballast and also to restrain the rail movement in lateral, vertical or longitudinal direction through proper anchoring (Selig & Waters 1994). In the past, the most common type of sleeper is the wooden sleeper, however, with the increase in train speeds and loads, concrete sleepers (ties) are becoming very common nowadays (Nicks 2009). The other types of sleepers made from steel, plastic and composite materials have also been used (Sasaoka & Davis 2005; Namura & Suzuki 2007). The range of total length and centre to centre spacing between two sleepers for a standard track in Australia, is 2.4m-2.6m and 0.6m-0.75m, respectively (Indraratna & Ngo 2018).

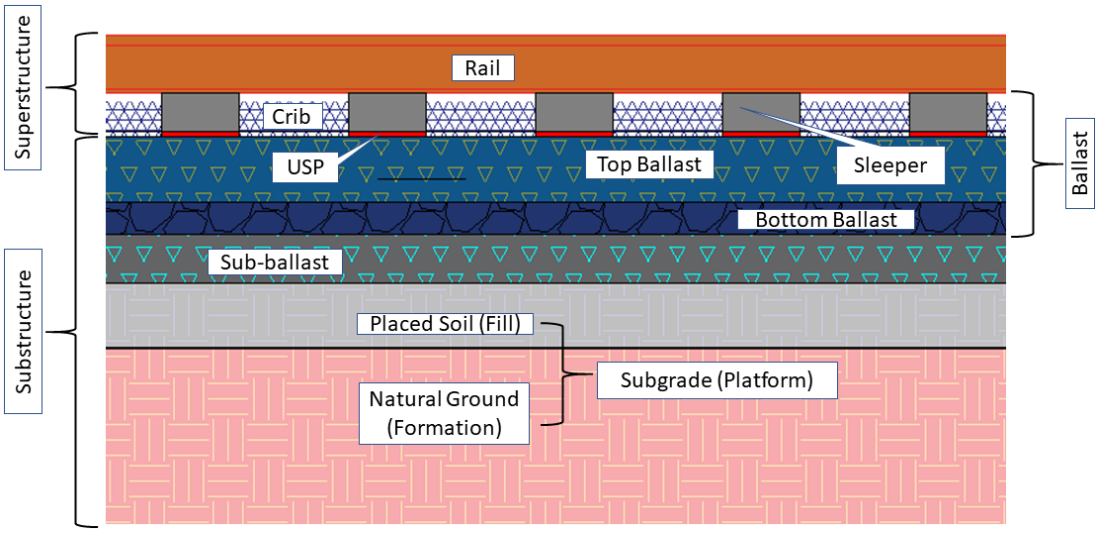

Figure 2.1: Rail track layout: side view (modified after Selig & Waters 1994)

2.2.3 Ballast

Ballast is a granular material (natural or crushed), which helps in transmitting the train load to the underlying layers at an acceptable level of stress (Indraratna et al. 1998) and also helps in restraining the movement of sleepers. The ballast placed between sleepers and the sub-ballast has typical thickness of 250mm to 450mm (Sun et al. 2015). According to Selig & Waters (1994) the ballast can be subdivided into three categories, e.g. crib, top ballast and bottom ballast, depending upon its position. Coarse-sized angular material is considered good ballast material consisting of uniformly graded crushed or natural stones or rocks without the presence of any dust or cementing material (Selig & Waters 1994; Lackenby et al. 2007; Tutumluer et al. 2007).

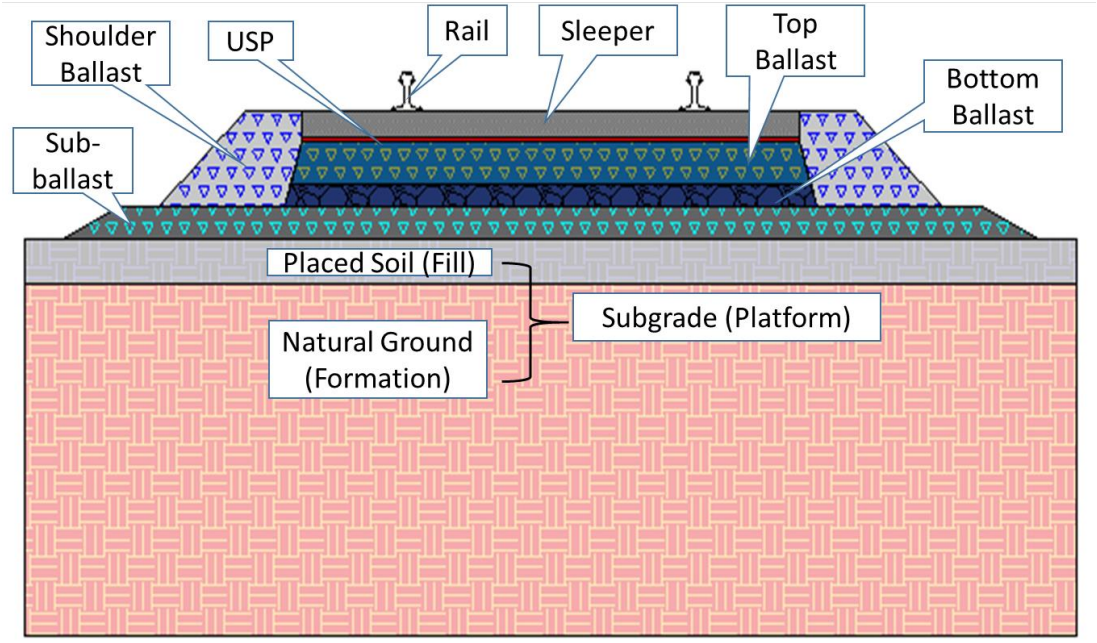

Figure 2.2: Rail track layout: cross-section (modified after Selig & Waters 1994)

2.2.4 Sub-Ballast

To avoid the penetration of ballast into the subgrade, a layer of granular material (sub-ballast) with particle size lesser than the ballast, is provided between the ballast and the subgrade. Sub-ballast also called as capping generally is a mixture of well graded

sand, gravel or crushed rock with a usual thickness of 150mm (Indraratna & Ngo 2018). Most often, the sub-ballast layer acts as a filter layer and drainage medium and helps in dissipating cyclic pore water pressure and preventing upward migration of fine particles from the subgrade. It also acts as a separating layer and helps in transmitting imposed loading from ballast to subgrade (Selig & Waters 1994; Wang et al. 2017).

2.2.5 Subgrade

The subgrade or formation layer is the ultimate foundation of the rail track structure, which provides a platform on which the track is constructed. Sometimes, a portion of subgrade (natural ground) is replaced with quality soil as a fill material (placed soil); however, it is not necessary for all cases (Nicks 2009). The subgrade should be stiff enough to support the traffic-induced stresses at the interface of sub-ballast and subgrade and these stresses reduce with depth making the top zone as main stress controller (Indraratna et al. 2011).

2.3 Types of Rail Tracks

Railway tracks can be divided into different categories depending upon their intended use, type of structure and type of supporting materials (Esveld 2001). A few of these categories can be further subdivided as follows:

1. Based on type of traffic: Passenger train tracks, freight tracks
2. Depending upon train speed: High-speed train tracks, normal speed tracks
3. Depending upon Gauge: Broad gauge, standard gauge and narrow-gauge tracks
4. Based on sleeper type: Wooden sleeper tracks, concrete sleeper tracks
5. Depending upon track component material:
    - Ballast track on soil
    - Concrete slab track on soil

- Slab track on concrete deck (bridges, aqueducts, etc.)
- Ballast-less tracks (level crossings, combined tracks, etc.)
- Ballast track on rock
- Slab tracks on rock (in tunnels)

2.4 Rail Track Transition

Rail track transitions involve a changeover of rail track structure from one type (i.e. ballast track) to the other (i.e. slab track) at their junction. These transitions are essential in railways to navigate natural or man-made obstacles. For instance, when a conventional ballasted track needs to traverse roadways, water bodies, or valleys, a transition to a stiffer track is provided. This may occur through level crossings, bridges, or culverts (Read & Li 2006). Similarly, transitions are necessary when the rail track passes through tunnels in mountains. At the tunnel entrance, the track changes from ballast to a slab track on rock, and upon exiting the tunnel, it transitions from slab track to ballast track again.

Figure 2.3 provides an example of two rail track transitions, the one which is at the lower left corner of the given picture, is showing a viaduct crossing where the ballasted track changes to slab track on the concrete deck. Whereas, on the other side of the viaduct, the transition is between slab track on the concrete deck and the ballast track on rock formation.

At these junctions of rail track, the structure of the track changes suddenly, causing abrupt change in track stiffness. Hence, an accelerated deterioration of material and geometry takes place at these transitions, especially when subjected to the movement of high-speed trains (Pita et al. 2004; Li & Davis 2005). There are numerous problems associated with track transitions which can lead to track degradation causing increased maintenance cost, if not addressed properly (Li & Davis 2005; Mishra et al. 2014; Sañudo et al. 2016). These problems, their major causes and different mitigation approaches are discussed in subsequent sections.

Figure 2.3: Local train crossing the Brusio spiral viaduct, Switzerland (Gubler 2012)

2.5 Problems of Track Transitions

Major problems associated with railway transitions include (i) differential settlement, (ii) enhanced dynamic load, and (iii) accelerated track deterioration; and they are discussed as follows.

2.5.1 Differential Settlement

Differential settlement, or geometric irregularity, occurs when there is uneven deformation on both sides of a track transition, causing ballasted tracks to experience higher settlement at certain sections than the stiffer side, which is typically designed for lesser settlements (Gallage et al. 2013; J. Pires et al. 2014; Sañudo et al. 2016). Li & Davis (2005) carried out measurements at four bridge sites and found that the highest settlement takes place at the bridge approaches (track transition) among the settlements on either side of the transition (Figure 2.4), causing differential settlements at these locations.

Field investigations generally report the maximum deformations at a given location resulting from repeated train loading. This maximum deformation encompasses both the elastic component, which recovers back upon unloading, and the irrecoverable plastic settlements that keep on accumulating with furhter load applications. A minimal value of differential settlement indicates an elastic track response, whereas significant differential settlements imply a plastic track response, particularly in the substructural components (Sañudo et al. 2016). It is also noted that some research based on computational modelling (Mishra et al. 2014; Real et al. 2016; Aggestam & Nielsen 2019) addresses the occurrence of transient deformations where the materials considered in the analysis are assumed fully elastic (i.e. small strain behaviour).

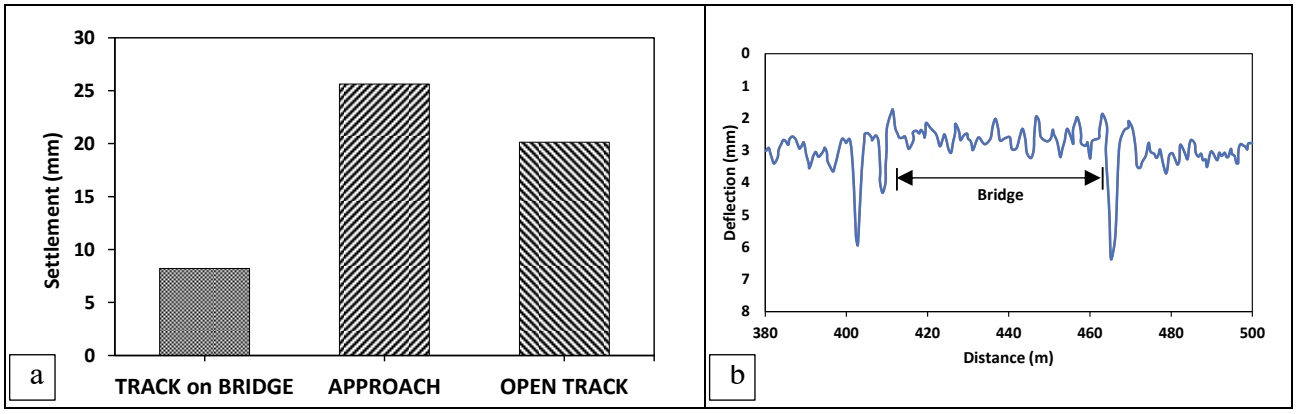

Figure 2.4: (a) Comparison of average settlement of track measured at track transition for four bridge sites, (b) Track deflection profile in loaded case (adopted from Li & Davis 2005)

A detailed comparison on the differential settlements of various rail transitions is given in Figure 2.5. Figure 2.5a shows a sudden increase in vertical displacement (Zhai & True 2000; Sañudo et al. 2016; Heydari-Noghabi et al. 2017; Heydari-Noghabi et al. 2018) at the location where a slab track changes to a ballast track, resulting in significant differential settlement. Figure 2.5b compares the field measurements of two studies for vertical displacements on each side of a bridge where the sudden variation in values is quite obvious. Figure 2.5c shows the increasing trend of rail displacement along the approach zones towards bridges at three different sites which could be due to hanging sleepers (Wang et al. 2018). Figure 2.5d compares the vertical displacement at concrete culverts (Read & Li 2006; Coelho et al. 2011) where approach slabs have been provided on each side. In this specific Figure 2.5, the part (a) indicates the elastic

settlements that have been obtained by load application for a shorter duration, whereas (b), (c) and (d) include the plastic deformations as well.

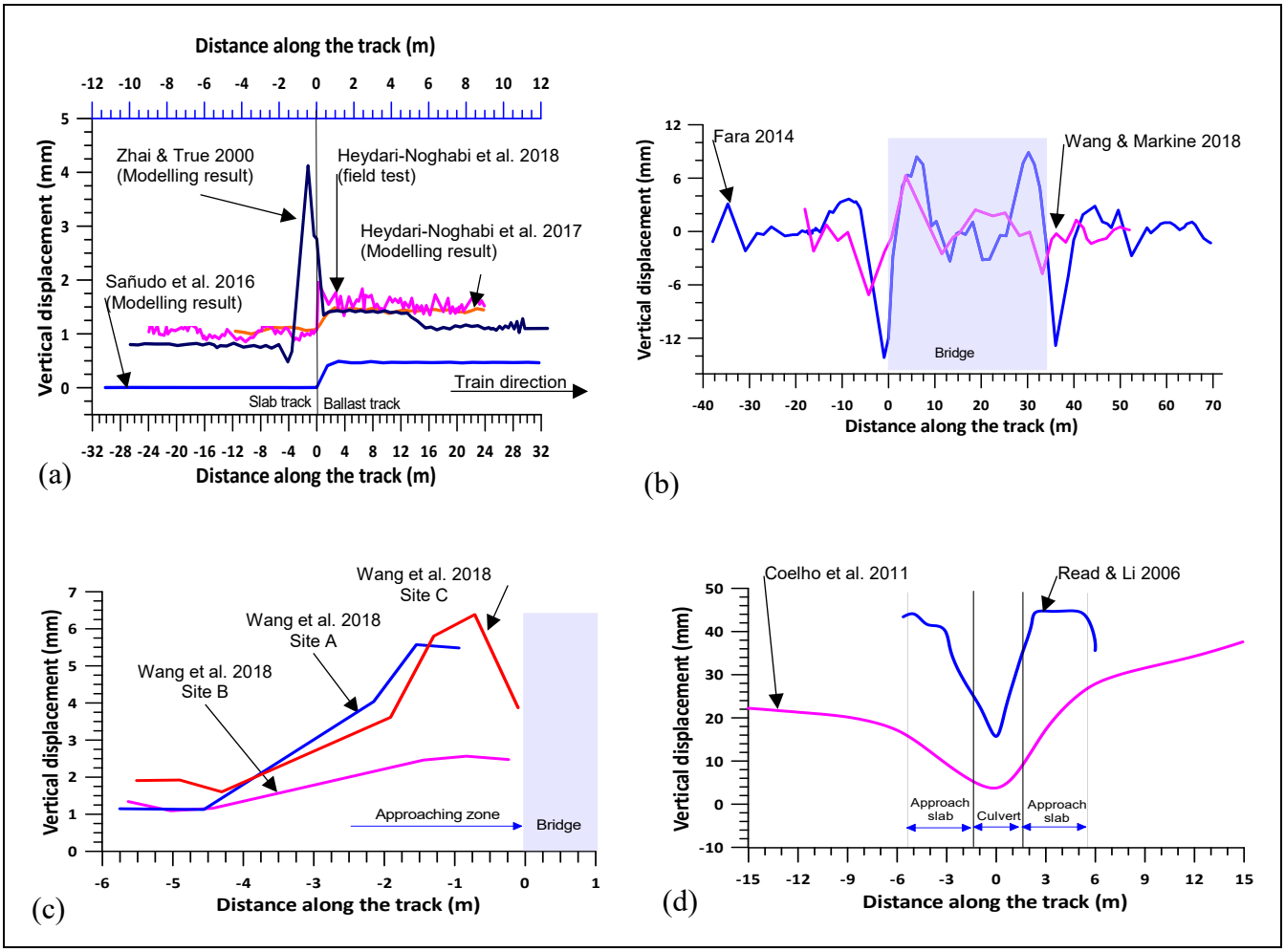

Figure 2.5: Comparison of differential settlements measured at various track transitions; (a) slab track to ballast track, (b) bridge crossing, (c) bridge approaches and (d) culvert crossing (adopted from Indraratna et al. 2019)

2.5.2 Enhanced Dynamic Loading

The amplification of dynamic loads at track transitions due to abrupt changes in the structural properties of tracks is another major problem associated with rail transitions. Sudden variations in stiffness and differential movement at track junctions often increase the dynamic force at track transition under vehicle loading (Zuada Coelho 2011; Paixao et al. 2015; Mishra et al. 2017; Coelho et al. 2018). Mishra et al. (2017) measured wheel loads using strain gauges at two bridge approaches considering the

elastic (transient) response and found an increase of up to 100% or more in the dynamic force on top of sleepers at bridge approaches compared to ballasted tracks. This could be due to poor sleeper support at the bridge approach sections, on both sides of the bridge, which affects the dynamic response of train suspension (Mishra et al. 2017).

Lei & Mao (2004) demonstrated that the transitions with differential settlement result in dynamic force amplification between the wheel and the rail, as compared to sudden changes in track stiffness, which is consistent with the findings of other studies (Lundqvist & Dahlberg 2005; Banimahd & Woodward 2007; Gallego Giner et al. 2012). Figure 2.6 offers a comprehensive analysis of the modeling outcomes that show the dynamic loads enhancement in relation to the wheel/rail interaction across various transitions (Zhai & True 2000; Nicks 2009; Lei & Zhang 2010; Wang et al. 2017). It can be noted that by using the actual load data in Figure 2.6, the figure maintains a closer resemblance to the original data sources from which the information was compiled. It allows readers to see the actual dynamic loads experienced by the tracks at different transitions and to relate the data to specific real-world conditions.

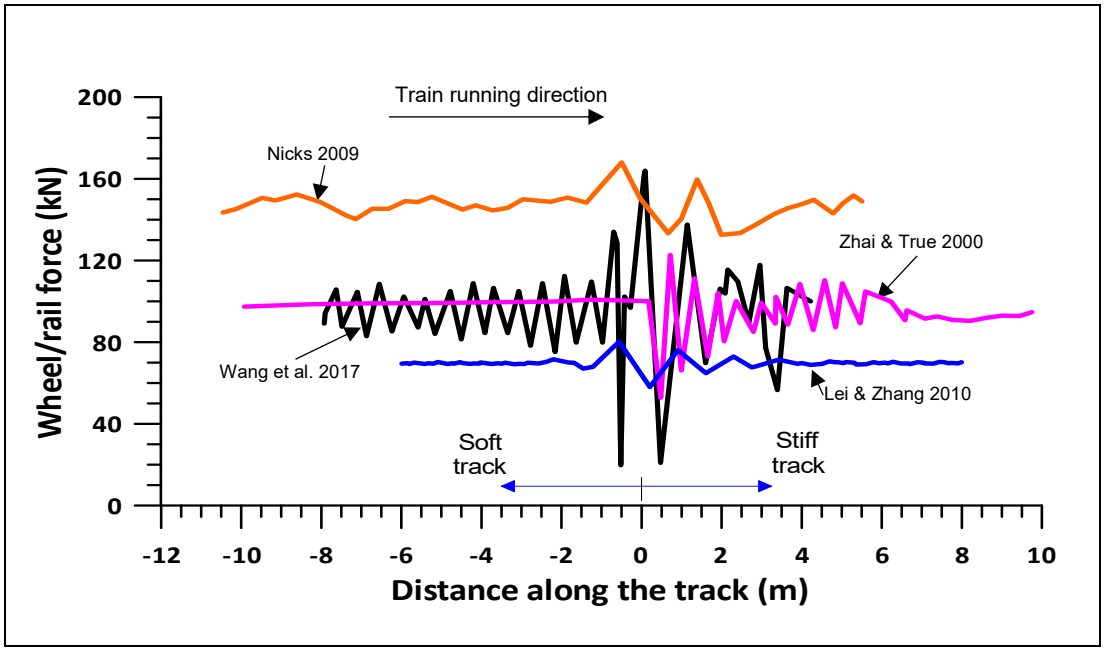

Figure 2.6: Variation in wheel-rail interaction forces at track transition (Indraratna et al. 2019)

2.5.3 Track Degradation

The relationship between dynamic load and differential settlement at transition zones is evident, where the differential settlement causes increase in dynamic load impact which results in more differential settlement. This effect becomes more pronounced under the impact of heavier trains moving at faster speeds (Frohling 1997; Lundqvist et al. 2006; Banimahd & Woodward 2007; Lei & Zhang 2010). Inter-dependency of the major problems, associated with track transitions, and their main causes are presented in Figure 2.7 (motivated by Paixão 2014). If these problems are not addressed properly, they can lead to enhanced track deterioration and increased maintenance costs (Li & Davis 2005; Mishra et al. 2014; Sañudo et al. 2016). Figure 2.7 also shows the various causes of these problems and the probable consequences of not intervening properly; further details of these causes and consequences are discussed in subsequent sections.

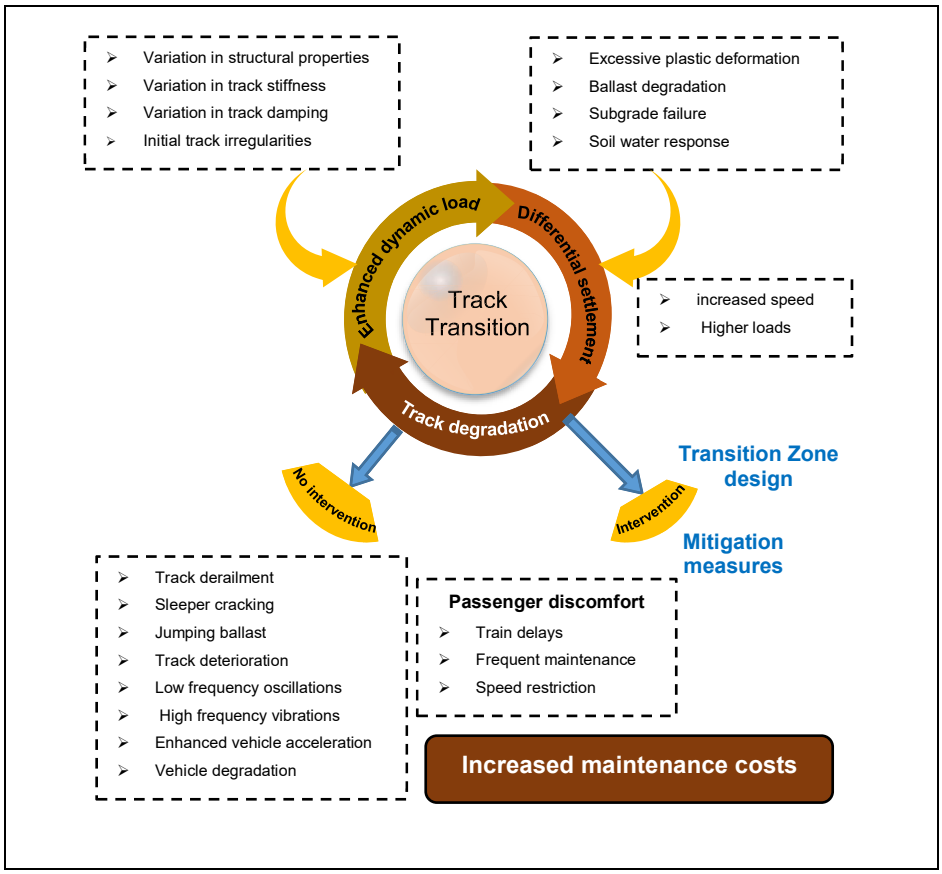

Figure 2.7: Summarised track transition problems: causes and effects (after Indraratna et al. 2019)

2.5.4 Development of Dips and Bumps

One issue that arises due to differential settlement is the formation of dips, bumps, and undulations near the track transition junction, which can cause passenger discomfort and lead to higher maintenance costs (Kerr & Moroney 1993; Frohling et al. 1996; Hunt & Winkler 1997; Nicks 2009; Fara 2014). Fara (2014) has coined the term "Jump and Bump" to describe the development of such dips and bumps at both sides of a bridge track transition, as illustrated in Figure 2.8. While dips and bumps in railway and highway bridge approaches have been seen by various researchers (Zaman et al. 1991; Briaud 1997; Long et al. 1998; Nicks 2009). It has been reported that more than 50% of bridge transitions in the USA are affected by this problem where the average height of bumps is 33mm and the average length is 5.2m (Nicks 2009).

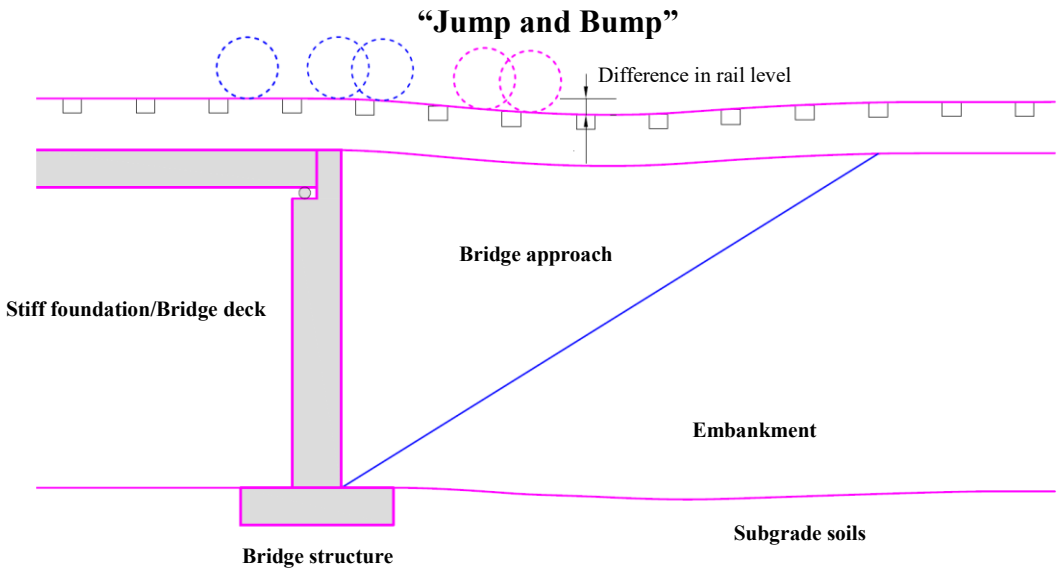

Figure 2.8: Schematic diagram of the development of bump/dip at bridge approaches after Indraratna et al. (2019)

2.5.5 Material and Track Geometry Deterioration

It is known that rail tracks deteriorate faster at transition zones than normal ballasted tracks (Dahlberg 2003; Li & Davis 2005) and this deterioration is triggered by the uneven settlement at rail transition zones which also increases the track degradation process. The deterioration of railway tracks encompasses various issues, such as rail

wear and corrugation, track irregularities, sleeper cracking, ballast and rail fastening loosening, and hanging sleepers (Zhai & True 2000; Momoya et al. 2005; Le Pen & Powrie 2011; Wang et al. 2015). In addition, ballast breakage and particle migration near sleepers can cause sleepers to hang or swing due to differential settlement and dynamic loads at track transitions (Coelho et al. 2011; Gallage et al. 2013; Alves Ribeiro et al. 2015; Stark & Wilk 2016; Mishra et al. 2017). According to Pita et al. (2004) the main factor accelerating track degradation at transitions, is the response of track components under increased dynamic loads of fast moving trains. As tracks deteriorate, it can also result in the degradation of vehicles due to increased oscillation, vibrations, and acceleration (Lundqvist & Dahlberg 2005; Zhai et al. 2009; Esveld 2010; Lei & Zhang 2011; Banimahd et al. 2012).

2.6 Major Causes of Track Transition Problems

The primary sources of track degradation at any transition zone are the uneven stiffness and damping between two different subgrade materials, the variation of moisture and geotechnical causes (Kerr & Moroney 1993; Li & Davis 2005; Nicks 2009; J. Pires et al. 2014). Gallage et al. (2013) identified two categories of causes for transition-related issues: primary causes and secondary causes. Primary causes include factors such as stiffness variations, damping variations, subgrade failure, permanent settlements, soil water response, progressive shear failure, among others. Secondary causes, on the other hand, include factors such as traffic conditions, train speed and loads, types of bridge abutments, and embankment heights. The direction of train movement (stiff to soft side and from soft to stiff side of the track transition) also causes different behaviour of transition problems (Namura & Suzuki 2007; Wang & Markine 2018). Some of the major causes are described below:

2.6.1 Track Stiffness Variation

Track stiffness, k is represented in units of kN/mm, which corresponds to the force causing a unit deflection under the load. It may either be dynamic, which varies based on the applied load and frequency of excitation, or static, which remains constant (Puzavac et al. 2012; Sañudo et al. 2016). Track modulus is sometimes used instead of

track stiffness because it can be defined as the load to produce a unit deflection per unit length of rail (Read & Li 2006). The value of track stiffness depends on the type of material and height of track embankments (Gallego et al. 2011). Figure 2.9 shows the track stiffness at various locations on a west coast line in Sweden; note that the track on a pile-deck bridge is almost twice as stiff as the normal track. The influence that subgrade (formation soils) has on track stiffness is also evident, hence the rapid change in stiffness for various types of track (Dahlberg 2003).

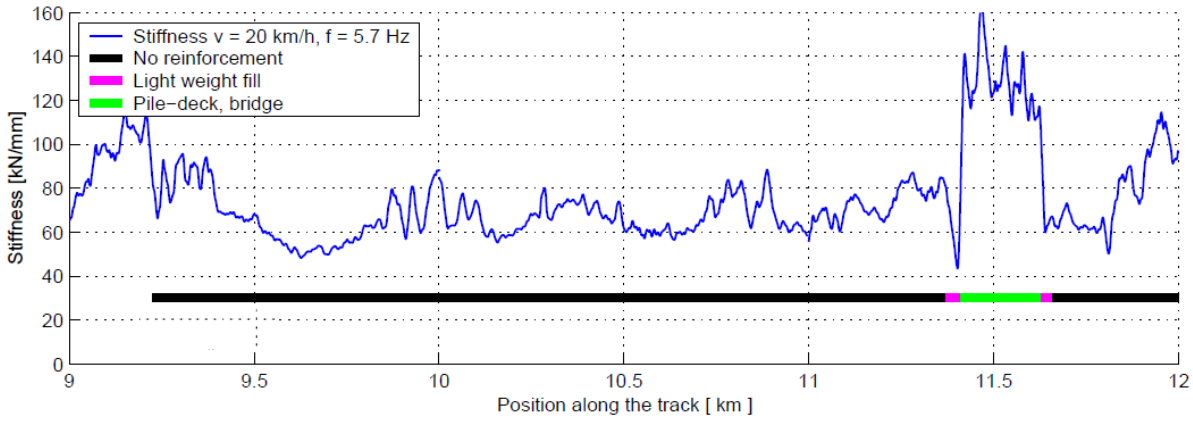

Figure 2.9: Variation in track stiffness for various track types along the railway track (Dahlberg 2003)

The abrupt variation in stiffness at track transition is the major reason for track problems (Kerr & Moroney 1993; Lundqvist et al. 2006; Li & Wu 2008; Lei & Zhang 2010; Chen & Mcdowell 2016). Figure 2.10 shows a typical example of variations in track stiffness where the total track stiffness k_b (ballast track) suddenly changes to k_s (slab track on a bridge deck); these sudden variations cause differential settlement and expedite track degradation (Berggren 2009; Dahlberg 2010). High values of track stiffness can also cause hanging sleepers as sleeper-ballast contact decreases and the gap between ballast and sleepers increases (Coelho et al. 2011).

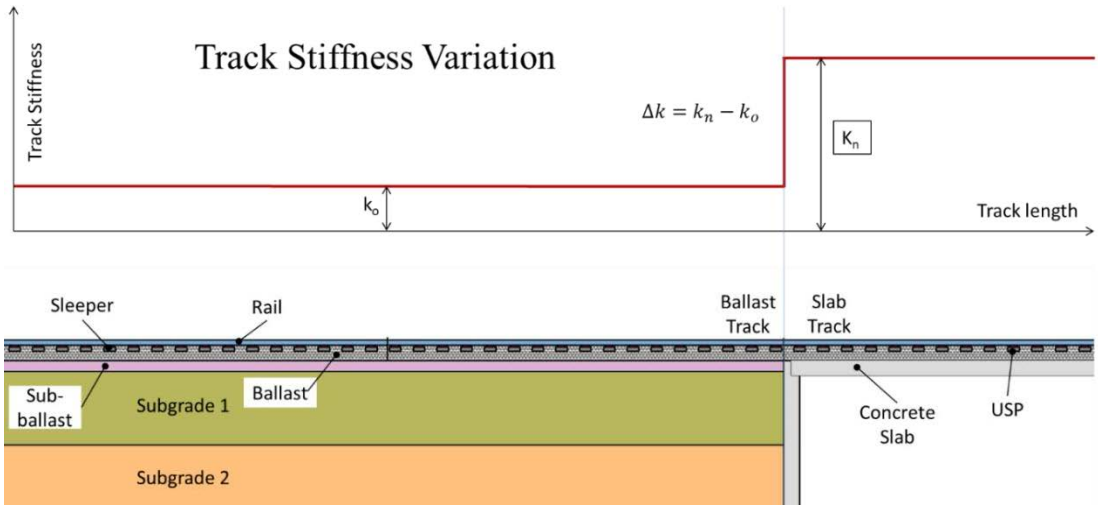

Figure 2.10: Stiffness variation at track transition between ballasted track and slab track

The knowledge of the effect of track stiffness variation is of great help in understanding the poor behavior of transition zones under dynamic loads and can be found in many past studies (Plotkin & Davis 2008; Dahlberg 2010; Choi 2013; Huang & Brennecke 2013). A detailed comparison of variations in track stiffness/modulus at various sites is given in Figure 2.11. Figure 2.11a shows the sudden variations in track modulus on both sides of the bridge (Read & Li 2006), whereas Figure 2.11b shows how the track modulus/stiffness increases when a track changes from being less stiff to stiffer (Nicks 2009; Varandas 2013; Germonpré et al. 2017). Note that stiff tracks such as bridges have higher modulus values than tracks that are not as stiff. While stiffer tracks can increase their lifespan by reducing track settlement, they can be susceptible to track degradation due to the greater contact forces at wheel-rail interaction and between sleepers and ballast that result from the increased stiffness, which could potentially amplify dynamic pressures acting on the track substructure (Li & Wu 2008; Berggren 2009; Choi 2013).

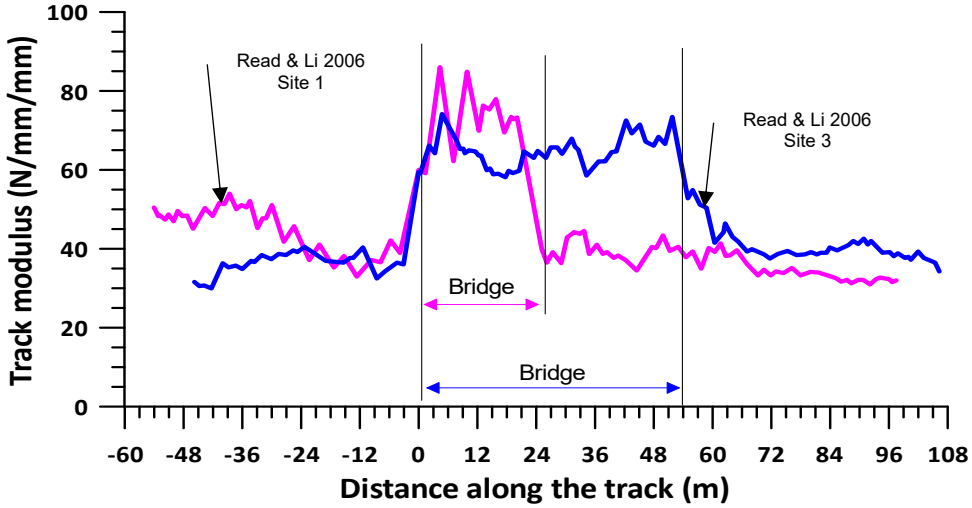

(a)

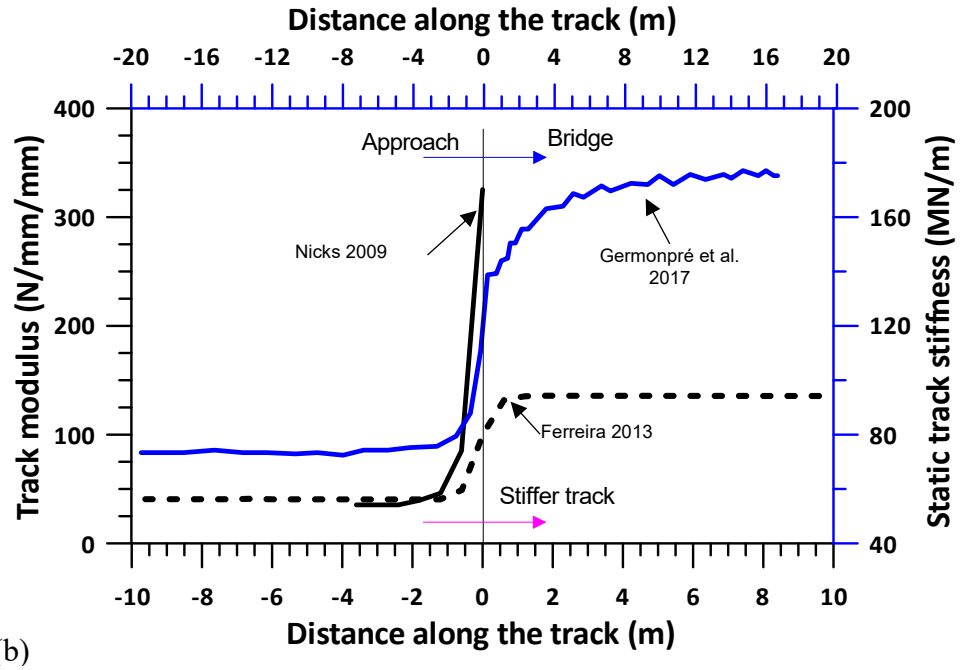

(b)

Figure 2.11: Abrupt variation in track modulus/stiffness at various track transitions; (a) at bridge crossings, (b) soft to stiff track transition (Indraratna et al. 2019)

2.6.2 Change in Damping Characteristics

The damping of track components at transition zones plays a crucial role in defining dynamic interaction at the wheel-track interface and helps to reduce track vibrations

(Esveld 2009; Choi 2013; Lei 2017; Shan et al. 2017)., and abrupt changes in its values at transition zones are critical factors in the development of differential settlements (Mishra et al. 2014). Additionally, the damping assists in energy dissipation, produced by moving loads. However, there is a risk of damage due to wheel impact while moving from a ballasted track on embankment (i.e. highly damped track) to a slab track on a bridge deck (i.e. low damped). The energy imparted onto embankment tracks can be dissipated through its structural components and the subgrade and surrounding ground, and while the ballast layer in a ballasted-deck bridge track will dissipate some of the energy and most of it will still reach the bridge structures (Sasaoka & Davis 2005).

2.6.3 Ballast Degradation

One of the primary reasons for progressive track deterioration is the degradation of ballast at track transitions (Li & Davis 2005; J. Pires et al. 2014; Indraratna et al. 2019). The degradation of ballast at track transitions happens as a result of frictional sliding, where ballast particles under sleepers moves laterally, and volumetric compaction, which involves particle breakage and ballast compaction (Selig & Waters 1994; Sato 1995; Iwnicki et al. 2000; Dahlberg 2001; Suiker & De Borst 2003; Indraratna et al. 2010; Varandas et al. 2010; Coelho et al. 2011; Wang & Markine 2018). It has been observed that the ballasted track side of the transitions undergoes more ballast degradation, which could be due to many factors including; (i) plastic deformation ballast fouling, moisture and temperature variations, and chemical actions (Indraratna et al. 2006; Zuada Coelho 2011; Chen 2013; Stark & Wilk 2016; Wang et al. 2017). However, no such degradation occurs on a slab track (Aggestam & Nielsen 2019).

As a consequence, the subsequent differential settlement does increase the dynamic loads and ballast stresses at transition zones (Mishra et al. 2014; Sañudo et al. 2016). As a result, ballast degradation keeps on increasing continuously mainly due to induced stresses. A comparison of the variation in the ballast stresses/pressure along the length of track for various transitions (Nicks 2009; Wang & Markine 2018; Wang & Markine 2018) is provided in Figure 2.12. The sudden change in ballast stresses can be observed on both sides of the bridge that indicates a significant variation in ballast

stresses due to higher stiffness variation in those areas.

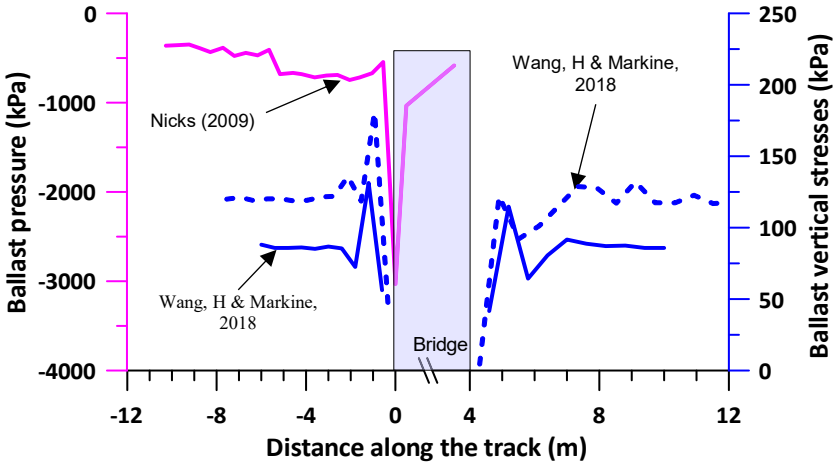

Figure 2.12: Variation in measured ballast stresses at various track transitions (Indraratna et al. 2019)

2.6.4 Structural Fill or Subgrade Settlement

The permanent settlement of the structural fill and subgrade layers causes issues such as hanging sleepers at transition zones due to differential settlement caused by the vertical movement of ballast particles, which results in increased dynamic loads (Mishra et al. 2012; Tutumluer et al. 2012; Mishra et al. 2014; Sañudo et al. 2016; Koch et al. 2018). Subgrade settlement can be accelerated by factors such as hindered track drainage, insufficient compaction of low-quality backfill materials, and restricted access adjacent to these structures t (Li & Davis 2005; Nicks 2009; Puppala et al. 2009; Sañudo et al. 2016). According to Plotkin & Davis (2008), subgrade settlement due to poor quality foundation has much more impact on the differential settlement than the track stiffness. A detailed analysis on how subgrade settlement is affected by the application of higher loads can be found in (Li 2000).

2.7 Chapter Summary

This chapter presents a detailed review of rail track transitions, various associated issues and their solutions. After defining the importance of rail transitions, their related problems are discussed, including their causes and effects on railway operations. It is noted that the provision of transitions in railways is necessary to avoid any natural or manmade obstacles, however, this results in faster track degradation due to arise of many problems. Differential settlement and enhanced dynamic loads are the main problems associated with track transition and are thus responsible for track degradation. The major cause of these problems is the abrupt change in stiffness, which can only be controlled by designing smooth and gradual transition zones.

CHAPTER THREE

3. RESEARCH INTO TRACK TRANSITION ZONES

3.1 Introduction

As the demand for high-speed passenger and heavy haul freight trains continues to rise, there is a growing necessity to design transition zones that provide smooth and gradual changes in track stiffness at track junctions. In this regard, rail tracks have undergone dynamic analysis to better understand the response of tracks at transition zones under moving loads, as well as the associated track problems and possible countermeasures. The dynamic analysis of railway track transition zones sets out to understand how traffic loads affect track components in terms of stresses, strains and deformation using established theories on the interaction between vehicle components and the track (Steffens 2005).

According to Esveld (2001), dynamic analysis is the interaction between an applied load and the structure where the structural components react according to their inherent frequencies (governed by mass elastic properties) to the applied load, and large amplifications occur when the frequencies of these structural components become equal to their natural frequencies. In the context of rail transition zones, it's important to note that various components, such as track damping, stiffness, rail modulus, and inertia, as well as train loads, exhibit spatial and temporal variations. The impact of train load on track components is influenced by factors like load type (static, dynamic, cyclic) and its velocity of application. These dynamics in rail systems are somewhat analogous to the considerations in road pavements, although with notable differences due to the unique characteristics of railways.

In track dynamic analysis, factors like mass (which resists geometric changes under loading), inertia (providing resistance against velocity changes), damping (for energy absorption), stiffness (counteracting deflection), and the mechanical and geometric attributes of track components all play critical roles (Steffens 2005). While there are similarities to road pavements in terms of load and response principles, the specific

conditions and behaviors of rail transition zones introduce their own intricacies that necessitate tailored analysis and design approaches (Steffens 2005).

This chapter provides an in-depth exploration of the ongoing research on the dynamic analysis of tracks at transition zones. The following sections present a critical review of this research, which includes laboratory experiments, mathematical and computational modelling, and field investigations. It is important to note that some of the content in this chapter has been previously published as a review article in Transportation Geotechnics (Indraratna et al. 2019). Through this chapter, the author aims to enhance understanding of the current state of research in this field and provide insights into future directions for investigation.

3.2 Laboratory Testing and Prototype Physical Modelling

Numerous laboratory experiments have been conducted globally to evaluate how different materials and components perform under various conditions in rail tracks. Several researchers have published a substantial number of findings in the field of railway engineering based on these experiments (Hussaini et al. 2016; Indraratna et al. 2016; Esmaeili et al. 2017; Estaire et al. 2017; Lima et al. 2017; Ngo et al. 2018).

However, there has been limited work carried out in laboratories to model transition zones due to limitations of size and composition. Momoya et al. (2016) performed some laboratory experiments on railway track transitions between ballasted embankments and concrete box culverts. This model was a $1/5^{th}$ scaled model of a transition onto which a moving load was applied onto rail sleepers by electric-hydraulic actuators to simulate an actual load from a 10-car train with four axles each. The four models tested were (a) without any buffering, (b) with an approach block, (c) with an approach slab, and (d) with a resilient mat. Results were reported in terms of track settlement, the hanging sleeper phenomenon, deformation of the ballast layer, and mobilized friction angle along ballast settlement. The conclusion of this extensive laboratory study was that the countermeasures are expected to reduce any large local settlement and an approach block will reduce settlement by almost one-half.

Likewise, Namura & Suzuki (2007) performed the cyclic loading tests on a $1/5^{th}$ scaled

model to evaluate the effectiveness of precast prestressed crossing (PPC). The model represents the transition between a ballasted track (consisting of sleeper, ballast and subgrade) and a slab track (consisting of concrete block and subgrade). Train loading was simulated by a movement loading device with 15 actuators (nine on ballasted track and six on PPC), considering the loading pattern of a single wheel load running cyclically at a speed of 1.2 m/s. Track dynamic analysis was carried out to investigate the effect of the rail fastening system on the reaction forces and vertical displacements at transition zones. With no rail fastening system, loose sleepers were observed on the ballasted track side soon after track maintenance by tamping (i.e. after 1000 passes of movement loading); however, no such loose sleepers have occurred even after 20000 passes of loading in case of rail fastening provision. It was concluded that the rail fastening system provides a better alignment to longitudinal irregularities, which minimises the disturbance of ballast components caused by tamping work.

3.3 Theoretical Background and Mathematical Modelling

There have been a number of researchers used the theory of beams on elastic foundations (BOEF) to model railway tracks and transitions (Kang et al. 2008; Senalp et al. 2010; Ding et al. 2012; Czyczula et al. 2017; Froio et al. 2018; Yu et al. 2018). This theory is based mainly on the Euler-Bernoulli beam (rail of infinite length) or Timoshenko beam resting on a Winkler foundation. The mathematical framework for the motion of a track built on a viscoelastic foundation using this theory can be found in Czyczula et al. (2017). Previous studies (Li & Davis 2005; Varandas et al. 2016; Heydari-Noghabi et al. 2017; Esmaeili et al. 2018; Paixão et al. 2018) applied the Euler-Bernoulli beam theory to model a transition zone, while some researchers used a Timoshenko beam to consider transverse shear deformation and beam vibration theory (Namura & Suzuki 2007; Aggestam & Nielsen 2019; Hu et al. 2019). However, after comparing these two conventional approaches for various cases, Czyczula et al. (2017) concluded that if either monotonic or moving loads are considered, the results through a Timoshenko beam are almost the same as an Euler- Bernoulli beam. A detailed comparison of the deflection of rail beams predicted by different theories subjected to varying train speeds can be found in Czyczula et al. (2017).

It is also noted that the use of BOEF theory to analyses the dynamic response of railway substructure has several limitations. Firstly, a foundation with distributed Winkler springs for soil reactions only gives approximate results if the speed of a moving load (train speed) is less than the critical velocity (Varandas 2013). Secondly, a Winkler springs foundation assumes there is no deformation of the adjacent soil elements, which does not always represent an actual rail track embankment (Walker & Indraratna 2018). Thirdly, granular materials (ballast, sub-ballast) under track substructure do not exhibit tension, whereas springs have some tension (Walker & Indraratna 2018). Lastly, this approach does not consider the interaction between train and track while representing the train loading by a constant moving load (Varandas 2013; Walker & Indraratna 2018). Moreover, the load-deformation response of track has frequently been assumed to be linear (Nicks 2009), whereas a highly non-linear response of ballasted tracks under dynamic loading often occurs, especially in stage-1 (rapid) settlement (Sato 1995; Indraratna & Ionescu 2000; Dahlberg 2001; Indraratna et al. 2006; Indraratna et al. 2010).

In spite of lacking of a comprehensive model to predict the actual response of rail track while considering the complex nature of track substructure (Steffens 2005), the BOEF model has been used extensively in practice, albeit using an analytical approach to solve the dynamic response of tracks at transition zones is limited because the problem of sudden changes in track stiffness is complex. Walker & Indraratna (2018) recently used a semi-analytical approach to solve the moving loads at transition zones; this model considers a Euler-Bernoulli beam (pinned) of finite length on viscoelastic foundations and the approach considers the spatial variation of rail characteristics (i.e. damping, mass, bending stiffness and cross-sectional area) as well as track stiffness and damping. The governing equation for a moving load used in this study is given as:

$$\frac{EI\partial^4 w}{\partial x^4} + \frac{\rho A\partial^2 w}{\partial t^2} + c\frac{\partial w}{\partial t} + kw = -P\delta(x - vt) \tag{3.1}$$

where, E = modulus of elasticity (N/m^2), I = second moment of area (m^4), ρ = rail density (kg/m^3), A = cross sectional area (m^2), k = track stiffness (kN/m/m), c = damping (Ns/m^2), w = track deflection (mm), P = dynamic load (kN), v = train speed (m/s) and δ = Dirac-delta function.

Equation (3.1) is solved for normalised track displacement (w), using the semi-analytical spectral Galerkin method that assumes 'n' terms truncated series. A general transition from soft (low stiffness value, k_1) to stiff track (higher stiffness value, k_2) over a given transition length (L_t) is investigated under single and multiple moving loads. The differential settlements are simulated by comparing the deflections on each side of the transition. The deflection amplification factor (DAF_{wrt1}), is calculated using Eq. (3.2), which considers various speed ratios (v_R=v/v_{cr}), damping ratios (c_R=c/c_{cr}), and stiffness ratios (k_1/k_2); these ratios can be determined as:

$$DAF_{wrt1} = \left(\frac{k_1}{k_2}\right)^{3/4} \times DAF_2 \tag{3.2}$$

$$\frac{v_{R2}}{v_{R1}} = \left(\frac{k_1}{k_2}\right)^{\mathbf{1/4}} \tag{3.3}$$

$$\frac{c_{R2}}{c_{R1}} = \left(\frac{k_1}{k_2}\right)^{\mathbf{1/2}} \tag{3.4}$$

where, v_{cr} = critical speed (m/s) = $\sqrt{2\frac{\sqrt{kEI}}{\rho A}}$,

and c_{cr} = critical damping (Ns/m2) = $2\sqrt{\rho A k}$

To find an optimum length for a transition zone, Walker & Indraratna (2018) examined the beam deflection of various transition length ratios with a characteristic length (L_c), as described in Eq. (3.5); they concluded that the minimum transition length should be 8-10 times of system's characteristic length (L_c) to avoid stiffness transition deflection spikes. One of the main outcomes of this study is how valid the conventional theory of BOEF is for long transitions with gradual changes in stiffness; the conclusion is that the dynamic response of transition zones can be described adequately with this theory. Furthermore, the model is validated by comparing the results of maximum displacement at the transition zone with field data, as shown in Figure 3.1; This figure shows that as the distance from the abutment increases, track stiffness decreases and peak displacement increases. This figure also indicates the

abrupt variation in track stiffness and displacement at the junction between the bridge approach and the abutment.

$$L_c = \sqrt[1/4]{\frac{4EI}{k}} \tag{3.5}$$

Mass spring-dashpot models have been used in previous studies to model a multilayer track system (Dimitrovová & Varandas 2009; Beskou & Theodorakopoulos 2011; Heydari-Noghabi et al. 2017; Shan et al. 2017). Sometimes these models are simplified by using over-all track stiffness and damping values by combining the values of all structural components and layers, as suggested by Berggren (2009).

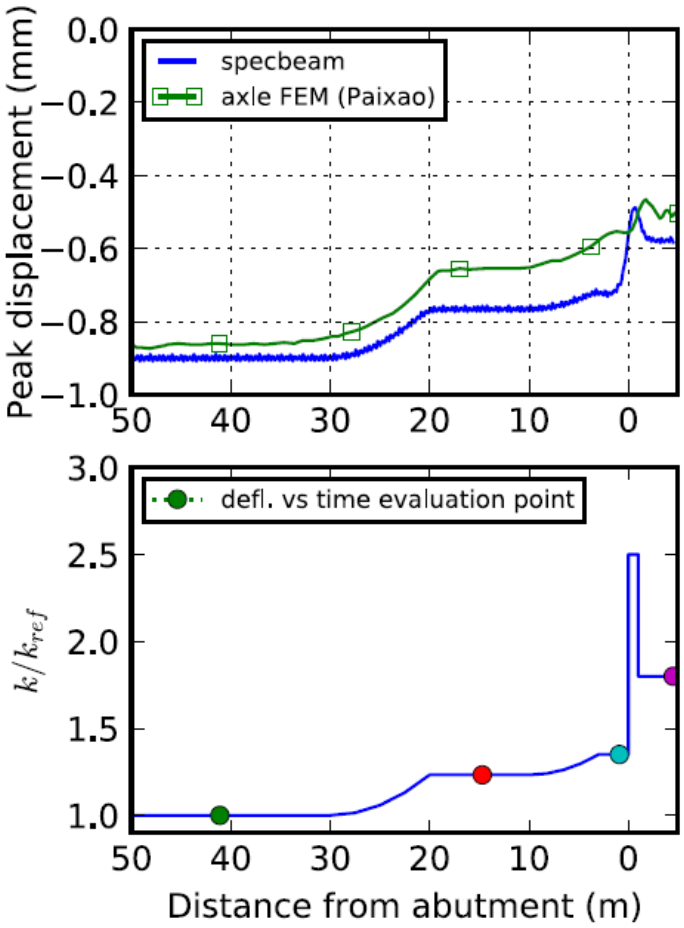

Figure 3.1: : Peak displacement and stiffness distribution at transition zone (Walker & Indraratna 2018)

To understand the nature of the transition between a ballast track and a slab track, a simplified mass spring-dashpot model can be developed, as shown in Figure 3.2. In this model the total stiffness of the track is represented by the "spring" with spring constants k_b and k_s for ballast track and slab track, respectively, while damping of the track substructure is represented as dashpots c_b and c_s for ballast track and slab track, respectively. However, to examine the effect of individual track layers, a full layered model can be used because they simulate all the supporting layers and also incorporate the additional elements for under sleeper pads (USPs), under ballast mats, geogrid, geotextile, and polystyrene, among others (Esveld 2001; Esveld et al. 2001; Sasaoka & Davis 2005; Lei 2017; Paixão et al. 2018).

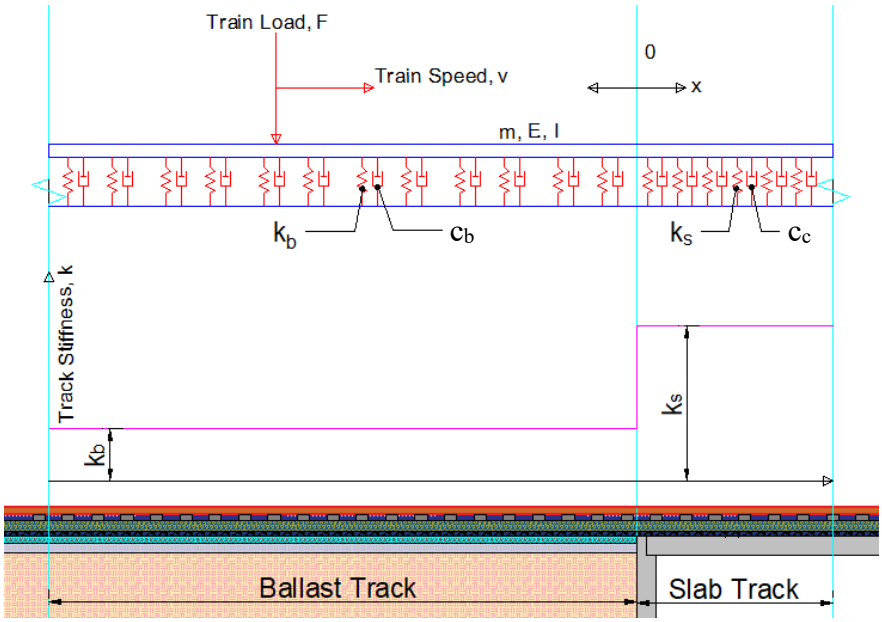

Figure 3.2: Mass and spring-dashpot models for ballast track to slab track transition

Varandas (2013) presented a linear mathematical model for the response analysis of inhomogeneous foundations using the two-layer mass spring-dashpot system shown in Figure 3.3. In this model two Euler-Bernoulli beams, one for the rail and another for the concrete slab are linked together by visco-elastic elements to represent rail pads and fill materials. The whole system is supported by soil represented by a visco-elastic foundation. The stiffness of the upper and lower visco-elastic elements is assumed to change abruptly at the x=0 section from k_{11} and k_{21} to k_{12} and k_{22} respectively. The vertical displacements are defined as $U_{ij}(x,t)$, as mentioned in Figure 3.3, and are

calculated using the dynamic equilibrium equations for the forced vibration of beams by considering the load (F) acting on the left side. The governing equations used to solve this linear mathematical model for the response analysis of an inhomogeneous foundation using a two-layer mass spring-dashpot model, are given as follows.

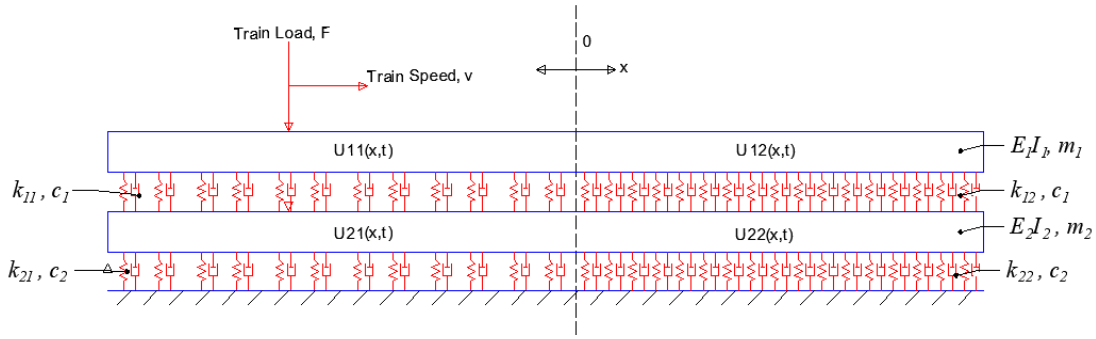

Figure 3.3: Two layers mass spring-dashpot model for track transition

The governing equation for $x < 0$ is as:

$$\begin{cases} \dfrac{E_1 I_1 \partial^4 u_{11}}{\partial x^4} + m_1 \dfrac{\partial^2 u_{11}}{\partial t^2} + c_1 \left(\dfrac{\partial u_{11}}{\partial t} - \dfrac{\partial u_{21}}{\partial t} \right) + k_{11}(u_{11} - u_{21}) = -F\delta(x - vt) \\ \dfrac{E_2 I_2 \partial^4 u_{21}}{\partial x^4} + m_2 \dfrac{\partial^2 u_{21}}{\partial t^2} + c_1 \left(\dfrac{\partial u_{21}}{\partial t} - \dfrac{\partial u_{11}}{\partial t} \right) + k_{11}(u_{21} - u_{11}) + k_{21} u_{21} + c_2 \dfrac{\partial u_{21}}{\partial t} \\ \qquad = 0 \end{cases}$$

and for $x > 0$ is as:

$$\begin{cases} \dfrac{E_1 I_1 \partial^4 u_{12}}{\partial x^4} + m_1 \dfrac{\partial^2 u_{12}}{\partial t^2} + c_1 \left(\dfrac{\partial u_{12}}{\partial t} - \dfrac{\partial u_{22}}{\partial t} \right) + k_{12}(u_{12} - u_{22}) = 0 \\ \dfrac{E_2 I_2 \partial^4 u_{22}}{\partial x^4} + m_2 \dfrac{\partial^2 u_{22}}{\partial t^2} + c_1 \left(\dfrac{\partial u_{22}}{\partial t} - \dfrac{\partial u_{12}}{\partial t} \right) + k_{12}(u_{22} - u_{12}) + k_{22} u_{22} + c_2 \dfrac{\partial u_{22}}{\partial t} \\ \qquad = 0 \end{cases}$$

These equations are solved for vertical displacements in each section by considering the boundary conditions at x=0. The solution for these equations of differential settlements is a complex process that involves many assumptions and the substitution of many variables, as described in (Van Dalen 2006; Varandas 2013). This mathematical model considers an inhomogeneous foundation so it can be applied to

rail transitions for a dynamic response analysis under train moving loads; it can also be utilised for the design of transition zones, but it would require extensive calculations that may not be solved analytically.

3.4 Finite Element Simulation

The numerical modelling approach is increasingly being used to simulate railway using fully calibrated models of track transitions under various loading and boundary conditions (Heydari-Noghabi et al. 2017; Wu et al. 2018). Various countermeasures have been modelled and analysed using FEM (finite element method) or DEM (discrete element method). In addition to the extensive use of FEM in rail track modelling (Table 3.1), the DEM has also been increasingly used to study the micromechanical behaviour of railway ballast because it can capture the discrete nature of ballast aggregates (Tutumluer et al. 2013; Qian et al. 2018; Bian et al. 2019). Furthermore, the DEM can examine the mechanical behaviour of a granular assembly of arbitrarily shaped discrete particles under quasi-static and dynamic conditions (Huang et al. 2009; Mcdowell & Li 2016; Ngo et al. 2016; Zhang et al. 2016). A comparison of several numerical and analytical models used to evaluate the dynamic response of railway tracks under moving train loads can be seen in Steffens (2005); Hyslip et al. (2009), among others. Numerical modelling through proper calibration and field validation is an appropriate tool to predict the dynamic response of any transition zone with various design options, remedial measures, train speeds and loads. A detailed comparison of several computational models of transition zones is given in Table 3.1.

One of the benefits of numerical modelling is that a single model can be utilised to work out multiple design options for a specific transition. For example, Sañudo et al. (2017) placed sleepers at six different locations using 2D FEM modelling and at every location the dynamic response was investigated for the overall design optimization. Likewise, in Wang & Markine (2018), a 3D FE model is used to analyse the dynamic response of track transitions by considering the differential settlement, stiffness variation, vehicle dynamics and hanging sleepers. Similarly, using a 3D FE model, various subgrade structural fills have been investigated to determine the most

economic structural fill materials for a high-speed railway transition zone (Hu et al. 2019).

Another use of numerical modelling is to investigate the effect that complex site situations can have on the dynamic response of track. These situations may include large-scale excavation close to a track transition, variations in the moisture of track substructure, and ballast fouling, among others (Ngo et al. 2016; Wang et al. 2017; Shan et al. 2018). Likewise, numerical modelling can assist in determining the track dynamic response at various levels and locations of track components at any time. Mishra et al. (2014) observed deformation at various levels using a 3D FE model to fully calibrate it with field values measured with multi-depth deflectometers.

The reliability and accuracy of dynamic response analysis in transition zones are affected by the type of model and modelling software used. Factors that impact the selection of appropriate parameters include the required analysis type (i.e. static or dynamic), material type (elastic or plastic), material behaviour (linear or nonlinear), the required time and computational powers available, calculation time, and the anticipated results. Previous studies (e.g. Duan & Yang 2013; Zhang et al. 2016; Wei et al. 2017) show the use of two types of finite element programs: (i) vehicle modelling packages, and (ii) track modelling packages. The vehicle modelling software packages concentrate more on vehicle dynamics while over-simplifying the modelling of ballast and subgrade materials, whereas track modelling packages mostly deal with a substructure model that over-simplifies the vehicle model (Nicks 2009). At transition zones, even though the main variation is in the structural properties of the track, utilising the model while considering the vehicle and track responses would enable a better understanding of the dynamic response of the track subjected to moving loads.

Likewise, selecting a vehicle model which considers various suspended, semi-suspended, and non-suspended loads can also help to enhance the track dynamic response accuracy. Hunt & Winkler (1997) used four vehicle models with (i) axle load only, (ii) axle and bogie, (iii) axle, bogie, and vehicle body, and (iv) two axles and bogies with the same static axle loads and found similar settlement results from every model; they then concluded that there was no effect on the increased settlement rate, even for closely spaced axles. Paixão et al. (2016) found a similar track response for a

train with different cars in terms of the wheel/rail interaction and vertical displacements; they concluded that a 2-car model could be just as practical as a full train model, and therefore it can be useful in reducing the calculation time. However, a simplified (one bogie) vehicle model is not always appropriate for considering responses such as the pitching motion of a vehicle (Aggestam & Nielsen 2019).

Selecting appropriate models relies on the level of complexity and precision required for the analysis. 2D models are usually insufficient for representing the distribution of train load in a longitudinal direction, so a 2D plane strain model with continuous support has been considered for a transversal track profile instead of real field conditions with the discrete support of rails by sleepers (Hunt & Winkler 1997; Lei & Mao 2004; Paixão et al. 2016). However, a 3D model can overcome these limitations (Shahraki et al. 2015), which is why Galvín et al. (2010) suggested using 3D models that include track non-linearity to obtain an accurate response of track transitions under moving loads.

In the study conducted by Paixão et al. (2016), a 2D numerical model was employed to investigate the impact of backfill settlement on train and track interaction, with a focus on measuring the wheel-rail contact force in the transition zone. The researchers explored four scenarios representing varying maximum backfill settlements: 1mm, 5mm, 10mm, and 15mm. Their findings revealed substantial interacting forces in each case, attributed to the negative effects of existing settlement associated with hanging sleepers. These results align with similar findings reported in other studies by Lundqvist & Dahlberg (2005); Zhang et al. (2008); and Zhu et al. (2011).

Numerical modelling can be utilised to investigate the response of track subjected to various train speeds and axle loads. Coelho et al. (2011) found that train speeds up to a certain limit (160 km/h for that specific case) had limited impact on the track, but as the speed became critical (180km/h), the response of track (i.e. settlements) became higher due to resonance. Likewise, in more recent research, Labrado Palomo et al. (2018) investigated the effect of train speeds on four different types of approaches at embankment-bridge transition using a 3D finite element model. The input parameters of ballast, sub-ballast and soil were optimised through model calibration and validation with field results. It is found that the peak and average particle velocities for vehicle

speeds of 100 km/h are higher than at 160 km/h and 220 km/h, possibly due to the train speed reached the critical speed of the entire system. However, Heydari-Noghabi et al. (2017) observed an increasing trend of track displacements for different track sections in response to a single loading cycle of one bogie (two axles) as the train speed and loads increased, as depicted in Figure 3.4. Note here that as the train speed (Figure 3.4a) and loads (Figure 3.4b) increase, track displacement also increases. Moreover, the ballasted track has a higher displacement than a slab track. Figure 3.4 also shows that the auxiliary rails help to smooth the differential settlement at the transition zone.

Numerical modeling is frequently employed to examine how the direction of train movement influences the dynamic response of the track, specifically regarding enhanced train-track interactions at transition zones. Many studies showed that trains passing through a transition zone from soft to stiff medium such as embankment to bridge are the worst-case scenarios (Namura & Suzuki 2007; Paixão et al. 2016; Wang & Markine 2018). This could be due to trains moving from a deformable structure to a non-deformable structure (i.e. concrete bridge) which enhances the impact load. However, Chen (2013) found more settlement when moving from a stiff to a soft transition zone because the boundary conditions for his model could be case specific. Despite this, other studies have reported that the effect of train direction on the dynamic behaviour of track is negligible, which is the case when the quality of tracks is high and there is no sharp variation in the track stiffness (Paixão et al. 2014; Alves Ribeiro et al. 2015; Aggestam & Nielsen 2019)

A 3D finite element model was simulated by Hu et al. (2019) to evaluate how effective different filling materials were for a wedge-shaped backfill at a tunnel-culvert transition zone. Three different materials were used; (i) graded gravel with 5% cement, (ii) graded gravel with no cement (c=160kPa, ϕ=39.5), and (iii) coarse-grained soil that is evenly distributed and contains less than 30% of fine-grained soil (c =200kPa, ϕ=41.8); their properties were calculated through laboratory (for new materials) and field testings (for in-situ material). In every case, maximum deflection occurred under maximum allowed values, however lower wheel loads were used in this study.

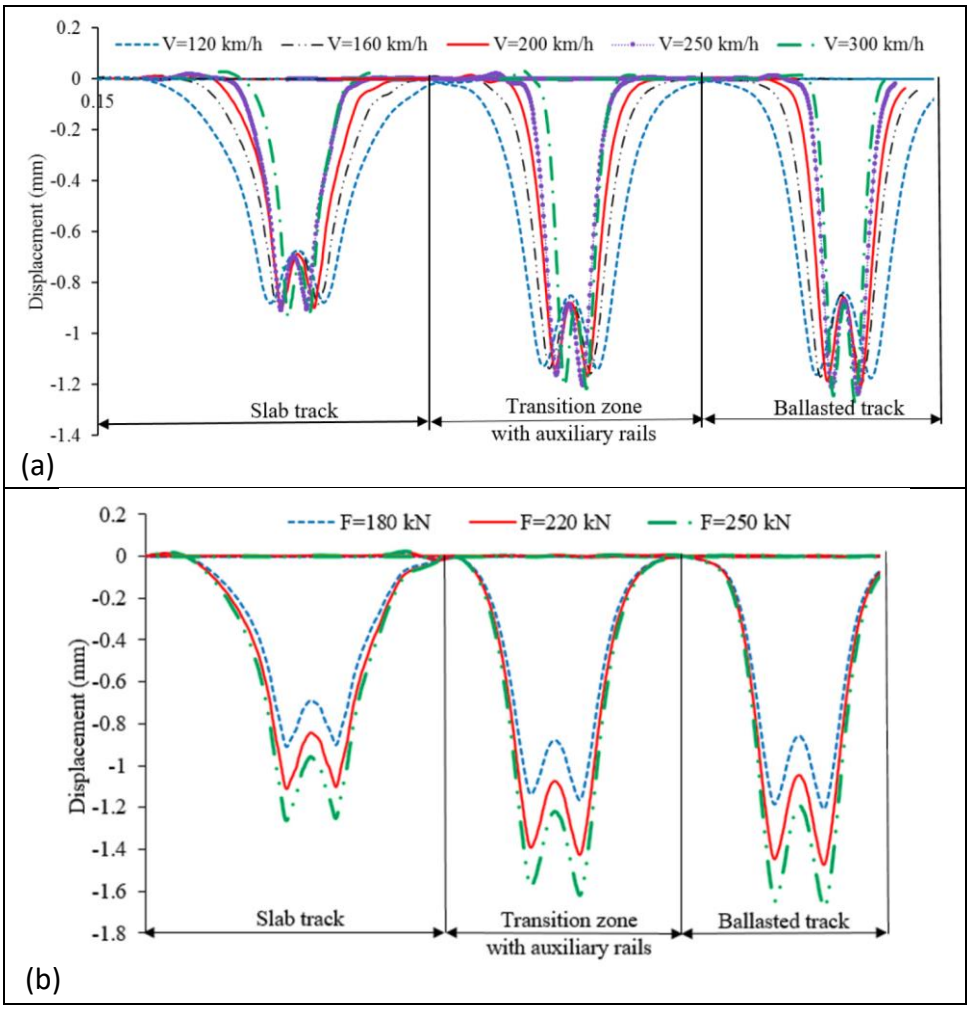

Figure 3.4: Rail deflection along the transition zone (a) for 180 kN vehicle load and various speeds, (b) for various loads moving at 200 km/h speed (Heydari-Noghabi et al. 2017).

The interaction between trains and tracks at transition zones has been investigated using a 3D finite element model (Banimahd & Woodward 2007; Banimahd 2008; Banimahd et al. 2012). This model incorporates variations in stiffness and considers the non-linear behaviour of ballast and subgrade. The conclusion is that simple variations in stiffness at track transitions is not the primary cause of transition problems, it is the soft subgrade, voids, and other faults at transition zones that increase the interaction forces as train speeds increase that cause passenger discomfort. It is therefore suggested that the difference in deflection at the junction of two different tracks over a 4-10 m long transition will lead to a smooth transition.

To study the dynamic response of bump at bridge approaches, a detailed investigation using a 3D FEM that incorporates train and track structure/substructure is given in

Nicks (2009). The response of this track is observed by varying the sizes of the bumps and dips, the thickness of the ballast, the sleeper material, train speed direction, and the type of abutment and length of the sleepers. It is found that the enhanced load impact and ballast/subgrade pressure due to variations in the track modulus cause dips and bumps to develop; as a result, the track dynamic response further increases at bridge transitions.

3.5 Field Monitoring

Different approaches for controlling differential settlement at transition zones have been evaluated through several field investigations conducted globally, including in the USA, Europe, Japan, and China. Various instruments were employed to monitor the track response in transition areas under real-time conditions. These instruments included multi-depth deflectometers (MDD), strain gauges, linear variable displacement transducers (LVDTs), settlement pegs, accelerometers, pressure cells, position-sensitive devices, geophones, inclinometers, and video gauge systems (Indraratna et al. 2014; Coelho et al. 2018; Paixão et al. 2018; Stanislav et al. 2018; Stark & Wynn 2018; Wang & Markine 2018; Boler et al. 2019). Furthermore, the structural health monitoring of rail tracks at transition zones was carried out with the help of conventional data measuring coaches and advanced techniques including digital image correlation (DIC) device and satellite synthetic aperture radar (InSAR) system which is developed by Wang et al. (2018).

Stone blowing is a process of adjusting the track geometry by adding crushed rock to ballast surface under the lifted sleeper. It is a relatively new method involving less damage to sleepers as compared to the tamping process where adjustment is achieved by ballast rearrangement to fill the voids under the lifted sleeper (Stanislav et al. 2018). The effectiveness of stone blowing instead of tamping was investigated by Boler et al. (2019) where comparison was made by analyzing the performance of track before and after stone blowing. Results show that stone blowing led to an almost 60% reduction in transient peak displacement, and moreover, the vertical acceleration and gaps at the sleeper-ballast interface also decreased.

In a study conducted by Paixão et al. (2018), the effectiveness of Under Sleeper Pads

(USPs) in transition zones was investigated. It was discovered that the use of USPs resulted in a decrease in the overall stiffness of the track. Fortunato et al. (2013) used a wedge-shaped approach at the transition zone and reported that a gradual transition of vertical stiffness can be achieved with this approach. They also discussed various types of wedge-shaped countermeasures that are commonly used at transition zones worldwide.

Stark & Wynn (2018) reported on the use of geosynthetic reinforcement systems in the railway transition zones to mitigate the differential settlement at these locations. They concluded that reinforced ballast with a geoweb underlay helps to mitigate transition problems by providing enhanced lateral confinement to ballast and improved load distribution. They also showed there is a large reduction in cost and installation time when geoweb underlay is used; in fact, this research shows that geosynthetic reinforcement will help to reduce differential settlement because it can increase the stiffness values (when used at approaches) and decrease the stiffness (when used under the bridge abutment).

Coelho et al. (2018) presented the results based on a fully-instrumented field measurement for a track crossing with a concrete culvert. The box culvert is almost 1.5 m deep from the track and is made within a sand embankment that carries the railway track. The culvert is supported by piles founded within dense sand below the embankment. Approach slabs, each measuring 4 meters in length and 300mm in thickness, are present within the sand embankment on both sides of the culvert. The study revealed that the primary cause of track displacement, leading to increased impact loading and accelerated track degradation, is attributed to hanging sleepers in the transition zone resulting from long-term track differential settlements.

A summary of the most recent field investigations of the transition zones in terms of the project description, transition types, countermeasures used and the outcome of the overall research, is given in Table 3.2.

Table 3.1: Comparison of computational modelling approaches and summarised key research findings on track transition zones

Reference	Model type	Numerical method	Software	Analysis type	Beam type	Foundation type	Model length (m)	Transition length (m)	Model calibration	Model validation	Transition type	Train speed (km/h)	Axle load (kn)	Parameters studied	Train direction	Mitigation measures	Innovations / Findings
(Aggestam & Nielsen 2019),Sweden	2D	FEM	-	Dyn.	TS	LE	60	23.4	-	Yes	BTS ~ BTCd	250-350	170	CF, BS	Both	SS, RP	Considering certain responses of vehicle, especially car body pitching motion, simplified (one bogie) vehicle model is not appropriate. Train direction has almost no effect on the dynamic response of track for an optimised transition design
(Hu et al. 2019), China	3D	FEM	ANSYS	Dyn.	TS	EP	52.2	46.2	No	Yes	BsTR ~ BTCc	350	140	VtD, TV, TA, BS	Both	WSB	Graded gravel with 5% cement is the best filling material, followed by simple graded gravel, and then well graded coarse-grained soil
(Esmaeili et al. 2018), Iran	2D	FEM	ANSYS	Dyn.	EB	LE	42.2	18	No	Yes	BTS ~ BTCc	120-340	160, 200	RD, TA, RpF	SoTSt	AR	Rail deflections and track acceleration decrease with stiffer rail pads & damping but increase with increased train speed, auxiliary rails transition is smoother and the dynamic performance improved
(Koch et al. 2018), Hungary	3D	FEM	PLAXIS	Dyn.	RB	LE	96	18	-	-	BTS ~ BTCd	80, 250	125	VtD, TV	SoTSt	BCW	Vertical displacement and Velocity amplitudes decrease with depth. Transition zone design is more important for higher train speed than lower speeds
(Labrado Palomo et al. 2018), Spain	3D	FEM	ANSYS	Dyn.	SB	LE	54	36	Yes	Yes	BTS ~ BTCd	50-300	24	TV, TA	SoTSt	CW, HMA, SRG, SRP	Geogrids are not the right approach to modify the vertical stiffness of track. Peak vibration increases with an increase in train speeds. concrete wedge is more effective technique, then HMA wedge and the Piles
(Paixão et al. 2018), Portugal	3D	FEM	Pegasus/ MATLAB	Dyn.	EB	NLVE	75	17.4	Yes	Yes	BTS ~ BTCv	220	250	VtD, CF, BS	SoTSt	WSB, USPs	USPs reduce the vibration transmitted to the ballast & sleeper-ballast contact forces so as the ballast degradation & diff. settlement in the long run
(Wang & Markine 2018), Netherlands	3D	FEM	LS-DYNA	Dyn.	HL	NLE	120	Varies	-	Yes	BTS ~ BTCd	200	142	VtD, WL, BS	SoTSt	WS, LS, WS+LS	The dips in transition zones increase, expand & propagate farther away from bridges with loading cycles. Number of iteration steps have strong effect on settlement prediction
(Wang & Markine 2018), Netherlands	3D	FEM	LS-DYNA	Dyn.	HL	LE	120	Varies	-	Yes	BTS ~ BTCd	72-288	178	VtD, WL, BS	Both	WS, LS, WS+LS	Diff. settlement & train speed, enhance the dynamic effect (wheel loads, ballast stress), longer sleepers are recommended for economy and longer & wider for performance, fasteners are effective but complex
(Heydari-Noghabi et al. 2017), Iran	3D	FEM	MATLAB	Dyn.	EB		52.2	18	Yes	Yes	BsTR ~ BTCc	120-300	180-250	RD, CF	StTSo	AR	Track deflection increases with an increase in train speed and vehicle load. Auxiliary rails reduce rail deflection, the optimum no. of additional rails is 2
(Sañudo et al. 2017), Spain	2D	FEM	ANSYS	Dyn.	-	LE	200	Varies	-	-	BTS ~ BTCd	300		VtD, BS, TA	Both	SS	The position & separation of sleepers influences the vertical acceleration and vibration, while slab to ballast track train movement is more critical

Table 3.1 (continued)

Reference	Model type	Numerical method	Software	Analysis type	Beam type	Foundation type	Model length (m)	Transition length (m)	Model calibration	Model validation	Transition type	Train speed (km/h)	Axle load (kn)	Parameters studied	Train direction	Mitigation measures	Innovations / findings
(Paixão et al. 2016), Portugal	2D	FEM	ANSYS	Dyn.	RB	NLE	172.5		Yes	Yes	BTS ~ BTCd	220	132	VtD, CF, TA	Both	WSB,	Soft to stiff train movements are more critical when considering track degradation and wheel/rail contact loss, wedge-shaped backfill is a good approach for train-track system
(Varandas et al. 2016), Portugal	3D	FEM	Pegasus MATLAB	Dyn.	EB	NLE	47.75	4.1	Yes	Yes	BTS ~ BTCc	130	174	VtD, BS	Both	AS	Ballast stresses are more than their strength and create a tendency towards sliding/rolling. The flow ability of ballast is due to high shear stresses. Ballast settlement depends mainly on the movement and inclination of the approach slab
(Real et al. 2016), Spain	3D	FEM	ANSYS	St. & Dyn.	SB	LE	60	20	Yes	Yes	BTS ~ BsTAS ~ BsTCd	35	90	TM, TA	Both	AR, RP	Stiffness variation between concrete and asphalt slab tracks can be smoothen by using rubber mats. No contribution from the addition of auxialiary rail in smoothening the transition. No significant effect on track dynamic response
(Shahraki et al. 2015), Germany	3D	FEM	ANSYS	Dyn.	RB	LE	80	7.5	-	-	BTS ~ BsTCd	300	180	VtD, TA, BS	SoTSt	LS,AR, WSB	More improvement in the dynamic performance of track with auxiliary rails, improved subgrade helps the entire system to perform better. Larger sleepers are the most effective way of reducing ballast stress
(Mishra et al. 2014), Illinois	2D, 3D	FEM, DEM	GEOTRACK BLOKS3D	Dyn.	EB	LE	2.22	-	Yes	Yes	-	177-241	270	BS, BPA	-	RP	Ballast is not a continuum medium therefore ballast particles accelerate at different speeds depending on its location with respect to load application
(Chen 2013), UK	3D	DEM	PFC^{3D}	Dyn.	-	LE	2.1	1.9	-	Yes	-	25-380	160-320	VtD, TA	Both	SRG	Stiff to soft train movement causes larger settlement than soft to stiff, multi-step stiffness is better at reducing the differential settlement, while geogrid in ballast over a soft subgrade is ineffective
(Banimahd 2008; Banimahd et al. 2012), UK	3D	FEM	GEOTRACK	Dyn.	-	LE, NLE	60	4~10	-	-	BTS ~ BTCd	180-250	170	VtD, CF, TA	SoTSt	-	Soft subgrade, Voids and other faults at transition zones produce increased interaction forces, while increased train speed causes passenger discomfort. Simple variations in stiffness is not the primary issue, a 4-10 m long transition based on deflection is enough
(Gallego et al. 2011; Gallego Giner et al. 2012), Spain	3D	FEM	ANSYS	St	SB	EP	7.2	4.8	-	Yes	BTS ~ BTCd	300	180	VtD, TM	Both	WSB	Effect of the type of material in natural ground and the embankment, and the height of an embankment on the vertical track stiffness. The vertical stiffness of track should be important when designing a transition zone

Table 3.1 (continued)

Reference	Model type	Numerical method	Software	Analysis type	Beam type	Foundation type	Model length (m)	Transition length (m)	Model calibration	Model validation	Transition type	Train speed (km/h)	Axle load (kn)	Parameters studied	Train direction	Mitigation measures	Innovations / Findings
(Coelho et al. 2011), Netherlands	3D	FEM	-	Dyn.	RB		20	5.0	-	Yes	BTS ~ BTCc	96 - 200	124 - 193	VtD, BS	Both	AS, MCE	Dynamic response found to be 20% higher than static, Higher response for soft to stiff train movement, development of hanging sleepers and their effect on the long-term performance of track
(Varandas et al. 2011), Portugal	1D	-	-	Dyn.	EB	NLE	60	5.0	-	Yes	BTS ~ BTCc	120 - 130	108 - 174	VtD, CF	Both	AS	Hanging sleepers were observed on both sides of the culvert, ballast settlement above the approach slab is caused by sleeper loading and ballast flow in a horizontal direction
(Galvín et al. 2010), Spain	3D	FEM	-	QS & Dyn	EB	NLE	90	15.4	-	Yes	BTS ~ BsTCd	298	152	TV,	SoTSt	RP, HSb	Rail pads used in ballast-less tracks play very important role in the vibration induced under moving train loads
(Nicks 2009), Texas	3D	FEM	LS-DYNA	Dyn.	EB	LE	16	1.6-8.4	No	Yes	BTS ~ BTCd, BTS ~ BsTCd	32 - 161	292	CF, TA, VtD, BS	Both	CMS, USPs, SB, RP	Going from soft to stiff structure causes higher impact loads, increased velocity has more impact for bumps than dips, track modulus is linearly proportional to soil modulus, ballast deck bridge is better than the ballast-less deck, steel bars of varying lengths will reduce track deflection and subgrade pressure
(Witt 2008), Sweden	3D	FEM	LS-DYNA	Dyn.	RB	LE	18	-	-	-	BTS ~ BTCd	324	215	CF	SoTSt	RP, USPs	Medium strength USPs (with vertical stiffness of 400kn/mm) are better at reducing the wheel/rail contact forces, Softer USPs help to reduce the ballast contact forces
(Namura & Suzuki 2007), Japan	3D	FEM	-	Dyn.	TB	LE	~5	-	-	Yes,	BTS ~ BsTCd	100-300	~160	WL,	SoTSt	LS, RS	Ballast settlement increased with the use of longer sleepers (more) and the resilient sleepers (less), length of approach track should be more than 22 m. Resilient sleepers are best at reducing ballast vibration
(Read & Li 2006), Colorado	2D	FEM	GEOTRACK	QS	SB	LE	115	0	-	-	-	80	54, 67, 100	VtD, BS, TM	-	CW, AR, HMA, WS+LS	Concrete slab is the best approach, followed by HMA, and then additional rails. Longer and wider sleepers at reduced spacing have an insignificant effect
(Li & Davis 2005), Colorado	3D	FEM	NUCARS	Dyn.	EB	LE	-	30	-	-	BTS ~ BTCd	160	178	WL, CF	-	-	Variations in stiffness lead increase the variations in dynamic load and wheel-rail interaction forces

Table 3.1 (continued)

Reference	Model type	Numerical method	Software	Analysis type	Beam type	Foundation type	Model length (m)	Transition length (m)	Model calibration	Model validation	Transition type	Train speed (km/h)	Axle load (kn)	Parameters studied	Train direction	Mitigation measures	Innovations / Findings
(Lei & Mao 2004), China	2D	FEM	-	Dyn.	SB	LE	231	20	Yes	-	BTS ~ BTCd	60-300	170	CF, TA	SoTSt	-	Variations in vertical stiffness have no direct effect on wheel/rail dynamic interaction forces. Permanent settlement is the main cause of transition related problems. Suggestions for irregularity angle and length of transition zone
(Hunt & Winkler 1997), UK	2D	DEM	-	Dyn.	SB	LE	10	2.0	-	-	BTS ~ BTCd	150	110	VtD, CF	SoTSt	USPs	Rate of track settlement mainly depends on the Initial settlement (voids under sleepers) owing to accelerated settlement under impulsive loads

Numerical Method (**FEM**: Finite Element Method, **DEM**: Discrete Element Method)
Analysis Type (**St**.: Static, **Dyn**.: Dynamic, **QS**: Quasi-static),
Beam Type (**TS**: Timoshenko, **EB**: Euler-Bernoulli, **HL**: Hughes-Liu, **SB**: Simple Beam, **RB**: Rectangular Beam),
Foundation Type (**LE**: Linear Elastic, **NLE**: Non-linear Elastic, **LVE**: Linear Visco- elastic, **NLVE**: Non-linear Visco-elastic, **EP**: Elastoplastic)
Transition Type (**BTR**: Ballast Track on Rock, **BTS**: Ballast Track on Soil, **BTCd**: Ballast Track on Concrete deck, **BsTR**: Ballast-less Track on Rock, **BsTS**: Ballast-less Track on Soil, **BsTCd**: Ballast-less Track on Concrete deck, **BTCc**: Ballast Track on Concrete Culvert, **BTCv**: Ballast Track on Concrete Viaduct, **BsTAS**: Ballast-less Track on Asphalt Slab),
Parameter Studied (**VtD**: Vertical displacement/deflection, **TV**: Track Velocity, **TA**: Track Acceleration, **BS**: Ballast/subgrade Stresses, **WL**: Wheel Load, **TM**: Track Modulus/Stiffness, **RD**: Rail Deflection, **RpF**: Railpad Force, **CF**: Contact Forces, **BPA**: Ballast Particles Acceleration),
Train Direction (**SoTSt**: Soft to Stiff, **StTSo**: Stiff to Soft),
Mitigation Measures (**WSB**: Wedge-Shaped Backfill, **AR**: Auxiliary Rails, **SRP**: Soil Reinforcement with Piles, **HMA**: Hot Mix Asphalt Wedge/layer, **USPs**: Under Sleeper Pads, **RP**: Rail Pads, **BCW**: Backfill Confinement with Walls, **CW**: Concrete Wedge/slab, **AS**: Approach Slab, **SRG**: Soil Reinforcement with Geogrid, **WS**: Wider Sleeper, **LS**: Longer Sleeper, **RS**: Resilient Sleepers, **CMS**: Changing Material of Sleepers, **SS**: Sleeper Spacing/Location, **MCE**: Moisture Content Effect, **SB**: Steel Bars, **HSb**: Hydraulic sub-base)

Table 3.2: Summary of outcomes of field monitoring on track transition zones

Author	Description	Transition type	Transition length (m)	Train speed (km/h)	Loading (kN)	Train direction	Track type	Parameters studied	Instrumentation	Outcomes
(Boler et al. 2019), USA	Stone blowing	BTS ~ BTCd		177	150		PT	VtD, WL, TA, BS	MDD, SG	60% reduction in transient displacements, Reduction in vertical acceleration and in gaps at sleeper-ballast interface, increased effectiveness and longevity
(Paixão et al. 2018), Portugal	WSB+USPs	BTS ~ BTCv	20	220	250		MT	RD, TA, SD	SG, LU, PSD, Acm, LVDT	Variations in the vertical stiffness of various sections along the transition, USPs with t=7mm reduced the stiffness by 30% of embankment but increases by 22% for UGM, USPs with t=10mm reduced the stiffness by 27% for CBM but remains same for CBM and concrete
(Wang & Markine 2018), Netherlands	methodology for comprehensive analysis of railway transition zones	BTS ~ BTCd	24	104	186	Both	PT	VtD	VGS	Maximum displacement close to bridge is higher than the far end, maximum displacement is larger for embankment ~ bridge case than the bridge ~ embankment case of train movement, Differential settlement at transition zones causes hanging sleepers
(Coelho et al. 2018), Netherlands	Approach slab	BTS ~ BTCc	4	65-106	76-142	Both	PT	VtD, WL, TS	Gp, Acm, VC, SG	Large differences in displacement and increased wheel loads show the presence of hanging sleepers. Non-symmetric response and non-uniform distribution of track displacements indicates inefficiency at the transition zone. Pivoting about the culvert generates enhanced impact loading
(Stark & Wynn 2018), USA	Reinforcement (Geoweb, HMA, Grout)	BTS ~ BTCd	15		30 MGT		FT	VtD, TA	VC, Acm	Geosynthetic reinforced transitions are less expensive, perform well for freight loads and reduce differential vertical displacements. Geoweb can be used as an alternative to HMA. With Geosynthetic reinforcement stiffness increases (in approaches) and decreases (while used under bridge abutments)
(Wilk et al. 2016), USA	Sleeper support effect, BCW, HMA	BTS ~ BsTCd	8.2	16, 40, 177	280	Both	PT, FT, MT	VtD, WL, TA, VF	Acm	For tracks with better sleeper support, peak acceleration remains below 5g for various types of trains, speeds, and loads, indicating smooth load transfer between track components, whereas poor sleeper support means that acceleration varies from 5g to 10g. Accelerometer data indicates a qualitative analysis of the track support and not quantitative
(Mishra et al. 2014), Illinois	Railpads,	BTS ~ BTCd		177-241	135	Both	MT	VtD, WL, TA	MDD, SG	Data obtained for track deformation and corresponding loading through field instrumentation is utilised to calibrate a 3D track dynamic model
(Fortunato et al. 2013), Portugal	Wedge-shaped approach	BTS ~ BTCd	20	220	66-125	SoTSt	MT	VtD	SG, LU, PSD, Acm, LVDT, IT	Passenger trains at higher speed cause more acceleration amplitude at sleepers than heavy freight at lower speeds. Using wedge-shaped approach leads to a gradual transition of vertical stiffness, and settlement seems to stabilise after one year of construction
(Namura & Suzuki 2007), Japan	Railpads,subgrade stabilization, Auxiliary rails, Ggluing resin	BTS ~ BTCd	20	100-300		Both	PT	WL, TA	SG, TLV	Variations in loads occur on ballast track at transition zone. Application of rail pads has no effect on track irregularities. Axle load variation at track transition found which increased with increasing speed. More variations in acceleration while travelling from a ballast track to a slab track
(Li & Davis 2005), Colorado	HMA, geocell, Thick ballast, cement stabilised	BTS ~ BTCd	30	160	178	Both	FT	RD, VtD, TS	SE, TLV	More track geometry degradation at bridge approaches, No improvement in track performance, a very high initial settlement rate of 100 to 180 mm in just six months (80 MGT), Rubber mats reduce track stiffness and increase track damping

Description (**WSB**: Wedge-Shaped Backfill, **AR**: Auxiliary Rails, **SRP**: Soil Reinforcement with Piles, **HMA**: Hot Mix Asphalt Wedge/layer, **USPs**: Under Sleeper Pads, **RP**: Rail Pads, **BCW**: Backfill Confinement with Walls, **CW**: Concrete Wedge/slab, **AS**: Approach Slab, **SRG**: Soil Reinforcement with Geogrid, **WS**: Wider Sleeper, **LS**: Longer Sleeper, **RS**: Resilient Sleepers, **CMS**: Changing Material of Sleepers, **SS**: Sleeper Spacing/Location, **MCE**: Moisture Contenet Effect, **SB**: Steel Bars, **HSb**: Hydraulic sub-base)
Transition Type (**BTR**: Ballast Track on Rock, **BTS**: Ballast Track on Soil, **BTCd**: Ballast Track on Concrete deck, **BsTR**: Ballast-less Track on Rock, **BsTS**: Ballast-less Track on Soil, **BsTCd**: Ballast-less Track on Concrete deck, **BTCc**: Ballast Track on Concrete Culvert, **BTCv**: Ballast Track on Concrete Viaduct), Train Direction (**SoTSt**: Soft to Stiff, **StTSo**: Stiff to Soft), Track Type (**PT**: Passenger Track, **FT**: Freight Track, **MT**: Mixed Traffic/Track),
Parameter Studied (**VtD**: Vertical displacement/deflection, **TV**: Track Velocity, **TA**: Track Acceleration, **BS**: Ballast/subgrade Stresses, **WL**: Wheel Load, **TM**: Track Modulus, **RD**: Rail Deflection, **RpF**: Railpad Force, **CF**: Contact Forces, **BPA**: Ballast Particles Acceleration),
Instrumentation (**MDD**: Multidepth Deflectometers, **SG**: Strain gauges, **LU**: LASER Units, **PSD**: Position Sensitive Devices, **Acm**: Accelerometers, **LVDT**: Linear Variable Differential Transducer, **VGS**: Video Gauge System,

VC: Video Cameras, **Gp**: Geophones, **IT**: Inclinometer Tubes, **SE**: Survey Equipment, **TLV**: Track Loading Vehicle

3.6 Mitigation Measures to Transition Problems

A proper transition zone must be able to minimise the impact of dynamic loads applied by moving trains. Different approaches for providing a smooth and gradual transition have been proposed and implemented through laboratory experiments, model testing, field investigations and mathematical and numerical modelling; they are reviewed and discussed in the following sections.

Transition wedges are widely used to smooth the tracks at transition areas; these wedge-shaped backfills are combinations of cement bond granular materials (CBM), unbound granular material (UGM), graded gravels with some percentage of cement, simple graded gravels, and well graded coarse grained soils (Li & Davis 2005; Coelho et al. 2011; Fortunato et al. 2013; J. Pires et al. 2014; Paixão et al. 2016; Paixão et al. 2018; Hu et al. 2019). The implementation of this system at bridge approaches results in an instant enhancement of the track system's dynamic response subjected to moving trains (Shahraki et al. 2015). The primary emphasis of this method is on the careful selection of materials based on their properties such as stiffness, cementation, and type, among others, for the transition wedge. Additionally, the geometry of the wedge, including its thickness, layer distribution, and slope is also carefully designed to ensure a gradual transition from softer to stiffer materials in the transition zones. Recommendations for such selections based on variations from soft to stiff, and even from sleeper to sleeper, can be found in (Gallego Giner et al. 2012). Currently, there is no standardized global approach to designing a transition wedge. As a result, various countries have developed their own specific parameters and criteria for designing this component. A comparison of various transition wedges, including their material configurations and geometric shapes that are used in different countries, is described in (Fortunato et al. 2013).

Varying the size and spacing of sleepers is another common approach for reducing abrupt change in track stiffness at transition zones; In this method, the dimensions of the sleepers, including their width, height, and length, increase gradually, while the spacing between them decreases progressively as the track structure transitions from a less stiff to a stiffer state (Namura et al. 2004; Read & Li 2006; Namura & Suzuki 2007). Larger sleepers have proven to be effective in reducing ballast settlement and

sleepers-ballast contact pressure (Namura & Suzuki 2007; Shahraki et al. 2015), but not as effective in minimising the load factor (Nicks 2009). Unlike maintaining the uniformity and compaction of ballast, this mitigation approach is not enhancing track stiffness directly, it can help reducing induced stresses and vertical displacement by wider load distribution (Sañudo et al. 2016).

Sleepers composed of materials such as composites, plastic, or rubber can be utilized in the transition zone (Sasaoka & Davis 2005; Read & Li 2006; Namura & Suzuki 2007). Especially, for high-speed railway lines, rubber sleepers that can adjust the sleeper/ballast stiffness are very effective in minimising the ballast vibration (Namura & Suzuki 2007). Frame sleepers, where every two sleepers are connected by additional supports to distribute the load over a wider area can also be used in the transition zone (Admetlla Pérez 2010). Considering dip and bump conditions near bridge approaches, Nicks (2009) conducted a study to investigate the impact of sleeper material on the dynamic response utilising concrete, plastic, and wooden sleepers. The study revealed that wooden sleepers are more effective than the other materials in mitigating bumps and dips.

Rail pads have recently been used to reduce the noise and vibration due to train moving loads, improving damping properties of track substructure (Dahlberg 2003; Read & Li 2006; Sol-Sánchez et al. 2015). Softer rail pads when utilised on stiffer track at transition improve the ride quality by making it smoother (Namura & Suzuki 2007). Further studies on such installation of softer rail pads at track transitions are documented in Varandas (2013) and Heydari-Noghabi et al. (2017). Research on the use of rubber pads that have the same stiffness as bridge approaches is discussed in Kerr & Bathurst (2001). It should be noted that thermoplastic elastomer rail pads (seat plates), which are commonly used in railway maintenance, are temperature-dependent and this aspect must be taken into account in design practices, as highlighted by Carrascal et al. (2005). The temperature-dependency of static stiffness of various types of rail pads is documented in Wei et al. (2017), which showed a nonlinear variation of static stiffness of rail pads across a temperature range of -40ºC to 70ºC.

The use of under sleeper pads (USPs) is becoming more prevalent in addressing the challenges associated with transition zones. USPs are effective in reducing ballast

degradation, allowing the stiffness on the stiffer side to be comparable to that of the softer side, and minimizing the impact of dynamic load (Dahlberg 2003; Namura et al. 2004; Nicks 2009; Insa et al. 2012; Varandas 2013; Sol-Sánchez et al. 2015; Navaratnarajah et al. 2018; Abadi et al. 2019). It has been noted that if the USPs are placed at bridge approaches, they can further soften the already soft side, hence reducing their effectiveness in minimising stiffness variations (Nicks 2009); however, they can result in a significant reduction in ballast stresses. This is because the improved contact between sleepers and the ballast, as a result, ballast degradation is minimised (Navaratnarajah et al. 2018). The use of resilient material mats (rubber mats) under slab tracks has proven to reduce track vibration (Galvín et al. 2010). A summary of the various effects of under sleeper pads can be found in (Lundqvist & Dahlberg 2005; Witt 2008), and a detailed investigation of their effectiveness through laboratory experiments and numerical simulations can be found in (Navaratnarajah et al. 2018; Jayasuriya et al. 2019).

Adding an extra rail (auxiliary rail) is another mitigation measure where additional support is provided on the softer side (ballasted track) of the transition to evenly distribute the dynamic load, and this can be achieved by adding extra rails along the main rails (Kerr & Moroney 1993; Read & Li 2006; Namura & Suzuki 2007; Heydari-Noghabi et al. 2017; Esmaeili et al. 2018); one example of this is where guard rails are extended from the bridge abutments to the bridge approaches (Read & Li 2006). This technique helps to improve the bending stiffness of the track and also reduce ballast stresses by distributing the load to the sleepers (Shahraki et al. 2015). According to Shahraki et al. (2015), auxiliary rails improve the dynamic response of the track by providing a smooth transition over sudden changes in stiffness. In some cases, auxiliary rails may not be as good at reducing the dynamic response compared to some other mitigation approaches, so proper consideration should be given to its benefit-cost ratio before making a final selection (Read & Li 2006; Shan et al. 2013). However, two extra rails along the transition zone are the optimum number of rails needed to decrease rail deflections(Heydari-Noghabi et al. 2017).

Constructing concrete confinement walls (also called as wing walls) alongside the bridge approaches is another way of mitigating transition issue. The utilisation of this

approach can help in reducing ballast loosening, deformations and ultimately the overall track settlement by providing the lateral confinement to ballast and subgrade layers (Read & Li 2006; Wilk et al. 2016). However, there may be a large increase in track modulus due to increased confinement and associated ballast breakage and this must be considered during design (Sañudo et al. 2016). Apart from wing walls, Nicks (2009) installed steel bars of varying lengths between sleepers into the subgrade to increase the confinement and strength of ballast; this approach is much better at reducing subgrade stress and the track deflection, and ultimately mitigating the development of dips.

While increasing the thickness of ballast and sub-ballast (capping) at transition zones will enhance track performance, it might also cause excessive track settlement (Li 2000; Li & Davis 2005; Lei 2017). However, if there are bumps in the track, increasing the thickness of ballast at the bridge approaches is the best approach because the extra depth helps to attenuate stress and reduce the deviatoric stresses applied on the substructural layers (Nicks 2009; Sayeed & Shahin 2017). Moreover, increasing the ballast thickness also increases the track modulus; Selig & Li (1994) report an increase in the track modulus from 24 MPa to 34 MPa after increasing the ballast from 0.3 m to 1.07 m thick.

The use of resin and polyurethane compound to glue ballast aggregates to reduce track settlement (Namura & Suzuki 2007; Woodward et al. 2009, 2010; Woodward et al. 2012, 2012; Kennedy et al. 2013; Gundavaram & Hussaini 2019) has been tested. Kennedy et al. (2013) reported that using polymer-treated tracks can result in an almost 99% decrease in permanent settlement. This is because the performance of a ballast track can be similar to that of a slab track when treated with polymers. Similarly, reinforcing ballast with 3D polyurethane and 3D polymer not only improves the efficiency and safety of a railway track, it also helps to reduce the cost of track maintenance (Woodward et al. 2009, 2010). However, Stanislav et al. (2018), while investigating the effectiveness of expanding polyurethane resin at bridge transition zone, found no improvement in track dynamic performance. Although the lifespan of polymeric material and its ability to withstand harsh track environments, including UV damage, are unknown, there is no conclusive evidence to suggest that it is ineffective.

However, the use of this method does raise concerns about the advantages of using highly angular ballast particles, which may provide intrinsic friction in the microscale. This friction could be reduced by bonding of particles when using polymeric materials.

Approach slabs (submerged approach structure) are often used on both sides of buried structures such as viaducts, culverts or bridges to reduce the high impact loads associated with sudden changes in track stiffness (Nassif et al. 2003; Cai et al. 2005; Sasaoka & Davis 2005; Varandas et al. 2011; Varandas et al. 2016; Coelho et al. 2018). In European railways, it is common to achieve a seamless transition between concrete culvert and ballasted track by providing horizontal and vertical concrete slab transitions as noted by Coelho et al. (2011). However, the recent research by Coelho et al. (2018) shows that the track vertical displacements on approach slab are four times higher than that of embankment and eight times higher than culvert. This could be due to high impact loading as a result of hanging sleepers and tracks rocking under moving trains.

Another effective mitigation approach to improve the performance of tracks at transitions, is the placement of hot mix asphalt (HMA) layer under the ballast (Li & Davis 2005; Read & Li 2006; Wilk et al. 2016; Labrado Palomo et al. 2018; Stark & Wynn 2018). When an HMA layer is placed under ballast and protected from the effects of climate, it can increase the life of the track substructure and enhance track performance by reducing stress at the ballast/capping interface and reducing the maintenance cycles (Rose et al. 2002). Moreover, since HMA is impervious, it prevents water from seeping into the underlying subgrade layer (Li & Davis 2005), so the drainage capacity of tracks increases. An HMA layer may also help to strengthen the substructure layer by improving its load-bearing capacity and further reducing the stresses acting on the subgrade (Seara & Correia 2008).

Improving the load-bearing capacity of track embankments with soil treatment such as grouting, dynamic compaction, soil cement, geosynthetics, geocells, cement gravels, etc., has been widely adopted (Li & Davis 2005; Puppala et al. 2009; Sañudo et al. 2016; Stanislav et al. 2018). According to Li (2000), the track performance can be improved by increasing the infill stiffness through the inclusion of geocells (honeycomb structure) in sub-ballast layer. A variety of soil improvement techniques

commonly used for embankments at track transitions, especially for bridge approaches, can be found in Puppala et al. (2009); Puppala et al. (2012); J. Pires et al. (2014); and Stanislav et al. (2018). These techniques can be categorized into three groups: (i) Mechanical techniques (excavation and replacement, preloading and surcharge, dynamic compaction), (ii) Hydraulic techniques (sand drains, prefabricated drains, surcharge loading), and (iii) Reinforcement techniques including: columns (stone and lime columns, concrete injected columns, deep soil mixing columns, geo-piers), piles (compacted piles, continuous flight auger cast piles, driven piles), deep foundations, geosynthetics, geotextiles/geogrids, geocells.

Improving the foundation of track embankments using piles made from reinforced concrete, steel, gravel, timber, sand column, and stone column, etc., can be very helpful in mitigating transition zone problems by increasing track stiffness and reducing settlement on the softer side of the transition (Wahls 1990; Woldringh & New 1999; Sew & Chin 2001; Sañudo et al. 2016; Lazorenko et al. 2019). However, this solution may not be cost-effective because it depends mainly on the length of the piles and the material used (Read & Li 2006). The effectiveness of piles at a transition zone can be enhanced by arranging them in a proper pattern, and by varying their lengths depending on whether the structures are soft or stiff, as shown in (Labrado Palomo et al. 2018); the length of any transition zone can be optimised by these arrangements.

Other mitigation measures may include lightweight fills (Sew & Chin 2001; Luna 2004; Puppala et al. 2009), precast prestressed crossings (PPC) (Namura & Suzuki 2007), increasing the length of the stiffness transition zone (Sañudo et al. 2016) and improving the treatment of subbase materials (Sasaoka & Davis 2005). The use of lightweight fills (expanded polystyrene, geofoam lightweight concrete or aggregate, among others) at transition zones (i.e. bridge approaches) reduces the dead weight (self-weight load) of embankments, which further increases their stability and reduces track settlement (Sew & Chin 2001; Luna 2004; Puppala et al. 2009). Although this approach has been widely used for the approaches to highway bridges, it can also be used for railways provided that the selected material is suitable (i.e. high stiffness, strength, compressibility, etc.) (Puppala et al. 2009). Similarly, precast prestressed crossings (PPC), which are approximately 1m long concrete blocks with larger

sleepers or rubber sleepers at each end towards the ballast track, have also been used for level crossings (Namura & Suzuki 2007).

For a smooth and gradual transition, more than one mitigation approach can be used to improve track performance (Sañudo et al. 2016). For example, the cost of maintenance has been reduced considerably using sleepers of varying lengths, and transition slabs (Read & Li 2006). Kang et al. (2008), implemented a combined approach by utilising auxiliary rails, stiffness pads, and geo-grids, and no abnormal response was observed. Similarly, longer rubber sleepers result in a larger base plane which, through the fastening system, also helps to avoid loose sleepers; this has proven to be the best countermeasure against differential settlement used by Namura & Suzuki (2007).

Some countermeasures are better at fulfilling the desired function, while others are either partly effective or completely unsuccessful; for example, according to Read and Li (2006), pads under rails and slab is the best way to reduce structural stiffness, whereas Seara & Correia (2008) and Read & Li (2006) indicate that longer sleepers with a reduced spacing in the transition zones do not increase structural stiffness. However, a Hot Mix Asphalt (HMA) layer definitely improves the load-bearing capacity and reduces the stress in subgrade (Seara & Correia 2008), but it does not improve the behaviour of ballast on rigid pavements (Kerr & Bathurst 2001; Read & Li 2006).

3.7 Recommendations for Improved Track Design

Despite the effort that has gone into studying the performance of tracks at transition zones using advanced modelling techniques, an optimal solution to transition-related problems is still not fully understood (J. Pires et al. 2014; Sañudo et al. 2016), hence the need to find an effective and low-cost solution (to eradicate/minimise the problems), with minimum disruption to traffic and longer life (Hyslip et al. 2009). The main aim of designing these transition zones is to maintain track quality while reducing maintenance cycles and costs (Sañudo et al. 2016). In order to use computational models properly for predicting the true dynamic track performance, the model parameters require realistic calibration either using large-scale laboratory simulations

or instrumented field trials.

Vertical track stiffness at transition zones is mainly influenced by the type of materials used in the embankment and its slope and height in the transition zone. The natural ground beneath an embankment also affects the stiffness of track depending on the material used in the embankment, so it should be replaced if it is highly compressible (Gallego Giner & López Pita 2009; Gallego et al. 2011; Gallego Giner et al. 2012). Therefore, to design a transition zone efficiently, a proper selection of materials along with the shape and height of the embankment should be considered, as should a proper consideration of natural ground characteristics.

To produce a decent design, the difference between the response of a track before and after a transition zone is set as low as possible. For a stable structure, it should have a uniform track stiffness for which the maximum vertical deflection should not be more than 6.4 mm (0.25 in.) under the applied vehicle load (Hay 1982; Sussman et al. 2001). Various factors found in the literature that affect the structural response of track transitions are summarised in Figure 3.5; these factors should receive enough attention to achieve the appropriate design of transition zones in terms of selecting different design techniques and approaches. To make a precise model, every individual component must be modelled separately by considering characteristics such as elastic/plastic, linear/non-linear, continuum/particulate (discrete), and their interaction with neighbouring components. These factors can be addressed by selecting proper modelling techniques such as 1D, 2D or 3D and commercially available advanced modelling software packages. Note that each model and modelling software has some limitations that should be considered before designing track transitions.

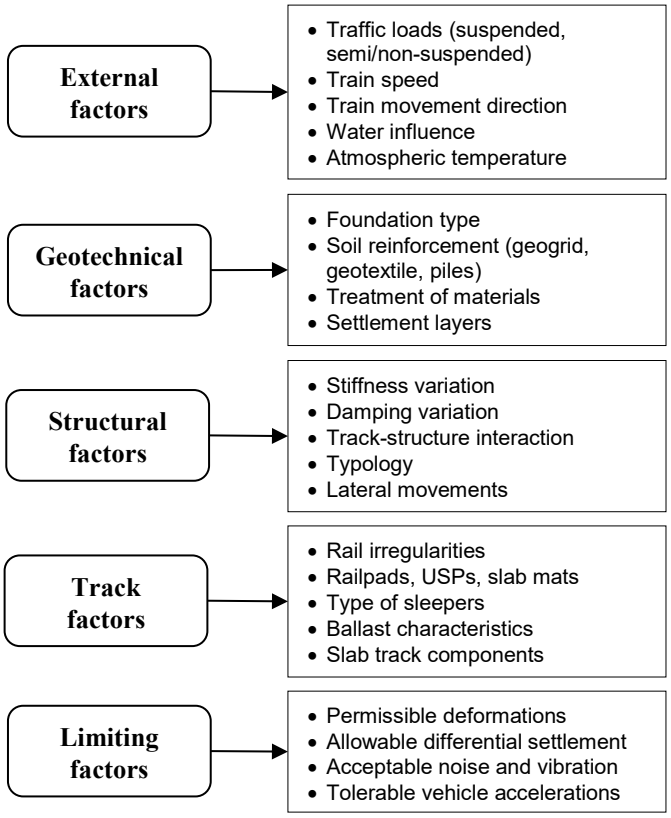

Figure 3.5: Summarised important factors for transition zone design considerations

3.8 Chapter Summary

This his chapter provides a comprehensive review of ongoing research on the design of transition zones to minimize the impact of sudden changes in the structural properties of the track. The review is based on laboratory testing and prototype physical modelling, Analytical and numerical approaches, and field monitoring. In addition, various mitigation measures aimed at improving the performance of ballasted tracks at transition zones are discussed in detail, and their effectiveness is evaluated. After examining several design approaches, recommendations for improving the performance of ballasted tracks at transitions are presented.

It is noted that one of many reasons for not having a precise and economical design of transition zones is that the problem is complex due to the interaction of several structures and structural components. Since conventional rail track structure consists of various structural components, it is a composite structure, but in transition zones, this complexity is enhanced due to the sudden variations in the structural properties of

the track. This makes the prediction of the dynamic performance of the overall structure a challenging task because every component behaves differently under various loading conditions. Furthermore, the interaction between these components (vehicle-track-structure) makes the model more complex.

Most current design practices are based mainly on empiricism established through trial and error basis. However, various mitigation measures have been utilised but without any theoretical reasoning, and therefore they are not overcoming the need for frequent maintenance. Therefore, transition zones should be designed to cope with the required variations in stiffness and possible initial settlement, which may vary depending on the case. If the variations in stiffness are known, a proper design of transition zone in terms of its total length and the type of materials can be established to provide a smooth and gradual variation in track stiffness at the junction.

CHAPTER FOUR

4. DYNAMIC RESPONSE OF RAILWAYS

4.1 Introduction

Research into track dynamics involves the study of induced vibrations of track and vehicle in all directions under the effect of moving loads (Van Dalen 2006; Zhai et al. 2013; Kouroussis et al. 2014; Real et al. 2016). It considers various components of a track structure that react to the applied loads according to their inherent frequencies and finds that a significant amplification of track vibrations (i.e. resonant effect) could occur when these frequencies reach their natural frequencies (Esveld 2001). Increased train speed can lead to amplified dynamic vibrations on track structure due to the propagation of surface waves and bending waves in track (Kouroussis et al. 2014). For conventional tracks, these vibrations become exacerbated, especially when the train speed reaches critical speed; causing strong vibrations to track structures and noise to surrounding buildings, apart from increased track settlements (Dimitrovová & Varandas 2009; Galvín et al. 2010; Zhai et al. 2013).

Considering the complexity of the track transitions, study presented in this chapter focuses on the investigation of the dynamic response of rail tracks by examining the impact of track stiffness on track settlements. In this regard, an analytical model is developed for a rail track employing the beam on elastic foundation theory (BOEF), and analysed for the maximum settlements under train wheel loads. The results obtained from analytical models are verified with those simulated by Finite Element Method (FEM) using ABAQUS, considering track substructure as elastic springs model. The model was further extended to 2D FEM layered tracks simulating a conventional ballasted track. These developed models are then utilised to investigate the effect of track stiffness on track settlement subjected to a single, multiple and moving wheel load, the details of which can be found in subsequent sections. It is noteworthy to mention that part of this chapter has been published as a technical article in the Journal ASCE- Journal of Geotechnical and Geoenvironmental Engineering.

4.2 Analytical Modelling of Rail Tracks

In this study, a fundamental approach using the BOEF theory has been used to compute the track displacement for a given wheel load. Initially, this model is developed for a general track without any transition, and then updated to incorporate one-step and multistep transitions. The following sections explain the calculation of vertical displacements analytically under various types of wheel loadings for a general track.

4.2.1 Beam on Elastic Foundation (BOEF) Model

The Euler-Bernoulli beam on elastic foundation theory has been extensively used to model railway tracks and transitions (Esveld 2001; Li & Davis 2005; Mishra et al. 2014; Paixão et al. 2018), and it is adopted in this study to investigate the stiffness effect on track dynamic responses under multiple loadings. Following this approach, a continuous beam resting on an elastic foundation can be considered as a rail track structure to develop the corresponding load-deformation equation. In this study, a rail track is modelled by considering a steel beam with the modulus of elasticity (E), the moment of inertia (I), and mass per unit length (m), resting on a foundation with stiffness (k), and damping (c), as shown in Figure 4.1(a). The term "foundation stiffness" or "track equivalent stiffness (k)" is adopted in this study in accordance with some previous studies, e.g. Lei (2017) and Priest & Powrie (2009). This foundation stiffness represents the original definition of stiffness magnitude, relating the line load amplitude to the corresponding vertical displacement, with the units of MN/m/m or MN/m^2. The differential equation for the track system can be described as introduced by several authors (Kenney 1954; Esveld 2001; Zhang et al. 2017):

$$EI\frac{\partial^4 w}{\partial x^4} + m\frac{\partial^2 w}{\partial t^2} + c\frac{\partial w}{\partial t} + kw = -P\delta(x - vt) \tag{4.1}$$

where, w represents the vertical displacement (i.e. settlement) of rail at point x, at any time t, under a wheel load P, moving at speed, v. δ is Dirac-delta function whose value is zero everywhere except at zero.

The approximate solution for the vertical displacement of the rail under static wheel load, ($v = 0$) for an undamped case for Equation (4.1) gets the following general form (Ugural & Fenster 2003; Lei 2017; Zhang et al. 2017):

$$w = e^{\beta x}(C_1 cos\beta x + C_2 sin\beta x) + e^{-\beta x}(C_3 cos\beta x + C_4 sin\beta x) \tag{4.2}$$

where,

$$\beta = \sqrt[4]{\frac{k}{4EI}} \tag{4.3}$$

and C_1 to C_4 are constants that can be found as introduced by Ugural & Fenster (2003) by taking a physical example of an infinite beam with concentrated midpoint loading as P resting on an elastic foundation, as shown in Figure 4.1(b). The decision to consider the beam with infinite length is made to facilitate a simplified analysis and better illustrate the underlying principle of the structural behaviour under certain conditions. The assumption of infinite length allows to focus on the general behaviour and avoids the complexities introduced by boundary effects, which often arise with finite-length beams.

In many engineering and mathematical models, the concept of an infinite beam is often used as a simplified assumption for its convenience in steady-state analyses in theoretical studies and mathematical modelling related to railway tracks (Esveld 2001; Ugural & Fenster 2003; Mallik et al. 2006; Nguyen & Duhamel 2008; Yu & Yuan 2013; Lei 2017; Zhang et al. 2017; Froio et al. 2018; Li et al. 2018; De Oliveira Barbosa & Van Dalen 2019). The infinite length assumption is a common simplification that allows to explore the fundamental response of the structure without getting entangled in the particulars of localized effects.

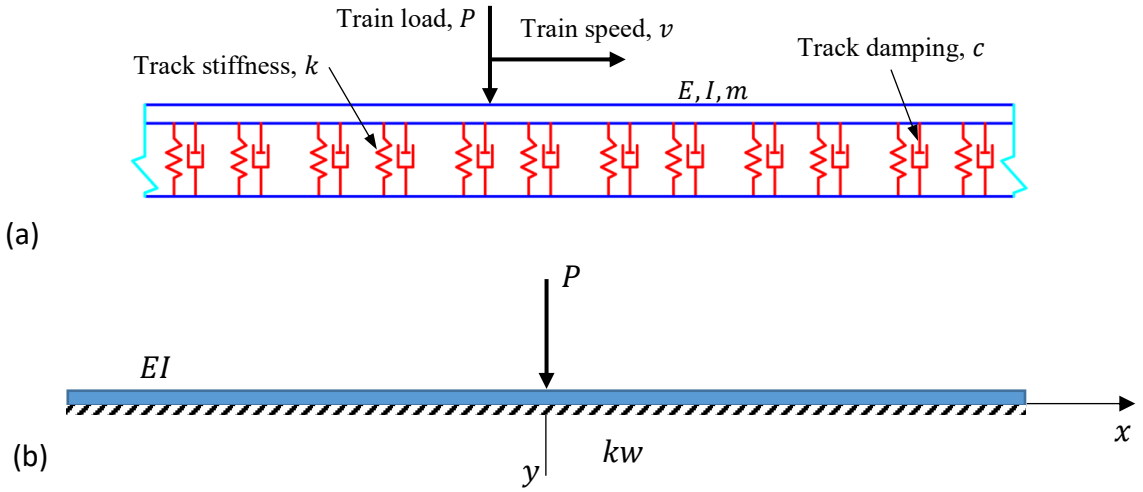

Figure 4.1: (a) BOEF model (mass-spring-dashpot) for analytical modelling, (b) Infinite beam on elastic foundation with a midpoint loading

To ensure a finite deflection for this beam, the following boundary conditions must be satisfied:

(i) at $x = \infty$: $C_1 = C_2 = 0$

$$w = e^{-\beta x}(C_3 cos\beta x + C_4 sin\beta x) \tag{4.4}$$

(ii): at $x = 0$, the slope of the deflection curve should be zero (i.e., for the symmetric shape of the deflected beam): $\frac{dw}{dx} = 0$

$$\frac{dw}{dx} = e^{-\beta x}(C_3 cos\beta x + C_4 sin\beta x) + e^{-\beta x}(\beta)(C_3 cos\beta x + C_4 sin\beta x) = 0 \tag{4.5}$$

which gives: $C_3 = C_4 = C$

The symmetric deflected shape indicates that the track stiffness remains constant along the track, whereas, while it varies spatially in case of track transition. Therefore, at the junction of two consecutive segments, symmetric boundary conditions were assumed for the analytical solution. In this approach, the analytical solution calculates the maximum settlement for each segment to provide an assessment of the differential

settlement at the track transition. Although the analysis assumes an infinite rail length (also conforms to plane strain), the symmetric assumption has a minimal impact on the evaluation of the spatial variability of stiffness, which is more a dependent on the subgrade conditions (Selig & Li 1994).

The solution for the rail deflection becomes:

$$w = Ce^{-\beta x}(cos\beta x + sin\beta x) \tag{4.6}$$

Considering the symmetry of the deflected shape, the loading condition should satisfy (Ugural & Fenster 2003):

$$P = 2\int_0^\infty kCe^{-\beta x}(cos\beta x + sin\beta x)dx \tag{4.7}$$

Integrating by parts gives: $C = \frac{P\beta}{2k}$

Substituting *C* to Equation (4.6) gives (Ugural & Fenster 2003):

$$w(x) = \frac{P\beta}{2k}e^{-\beta x}(cos\beta x + sin\beta x) \tag{4.8}$$

Hence, the vertical displacements of a rail can be predicted considering it as a steel beam with flexural stiffness, EI, and solving it through Equation (4.8). Considering a steel rail for a standard UIC60 profile with 60kg/m as the unit mass, (i.e. EI =6.23 MN.m^2), under a wheel load, P of 10 tonnes (representing 20 tonne axle load), the predicted vertical displacements for various foundation stiffness values (k = 5-80 MN/m/m) are shown in Figure 4.2.

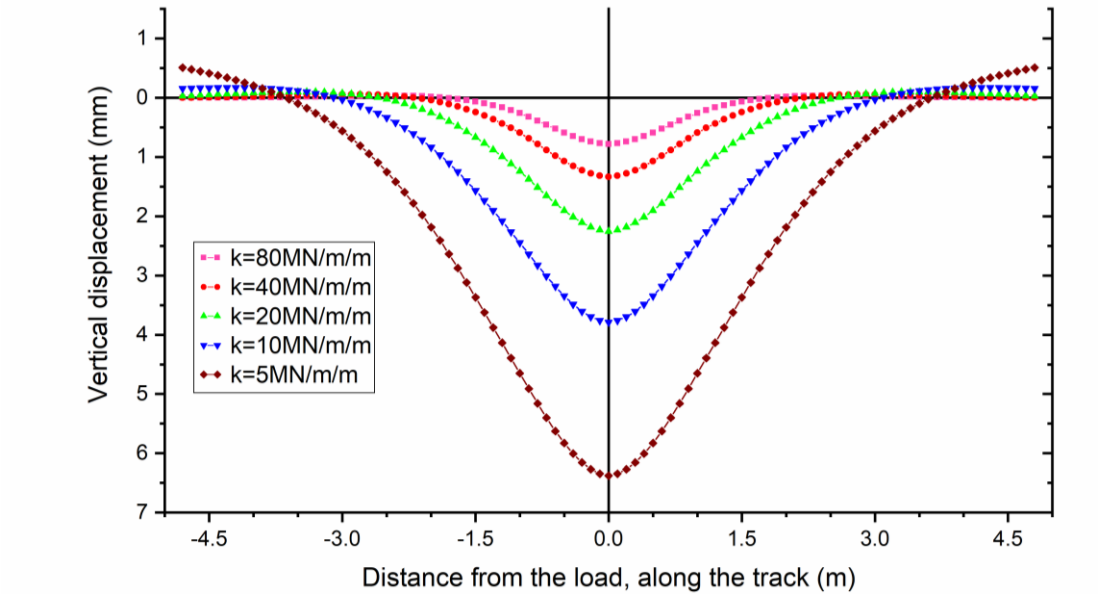

Figure 4.2: Predicted vertical displacements of rail tracks subjected to 10 tonnes wheel load for different track stiffness values

Equation of motion (4.8) is also solved through the Fourier transform technique for faster analysis using a developed MATLAB code (Appendix A). This approach has been adopted to gain confidence in applying analytical methods, thus streamlining the calculation process and enhancing efficiency, especially when dealing with more complex data sets The vertical displacements of a rail track obtained through this approach are presented in Figure 4.3, and are found to be exactly similar as obtained by simple hand calculations (as given in above).

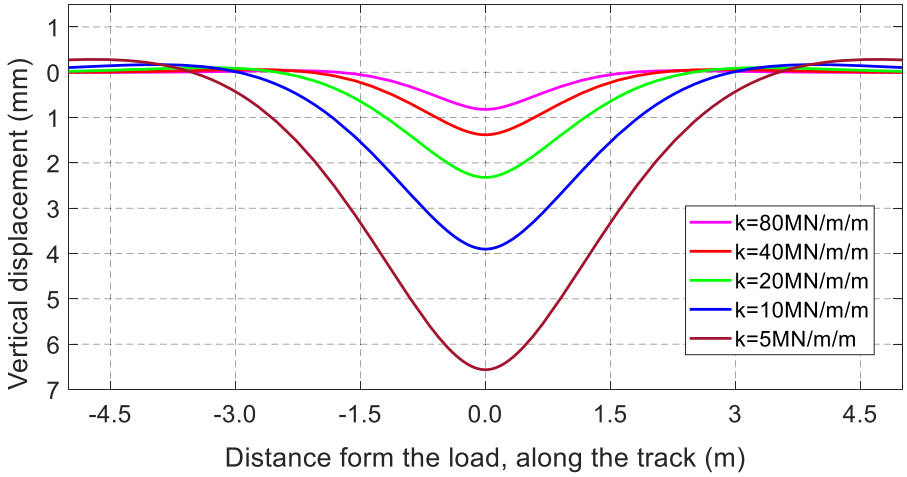

Figure 4.3: Predicted vertical displacements of rail tracks subjected to 10 tonnes wheel load for different track stiffness values, using the Fourier transform approach.

4.3 Numerical Modelling of Rail Tracks

In order to verify the accuracy of the analytical modelling and to investigate the complex behaviour of transition zones under dynamic loads, a comprehensive plan for the Numerical (finite element) modelling is developed. Initially, a 2D elastic spring model is developed and verified with the analytical modelling results. Later, this model is updated to a 2D layered model for the conventional ballast track, which is then further updated to incorporate one-step and multistep transition zones, and then finally to a 3D FE model (presented in Chapter 7). This chapter describes the numerical analysis of 2D elastic spring and layered models for a conventional ballast track subjected to single, multiple and moving wheel loads.

4.3.1 Elastic Spring Model

In this study, the development of a complex finite element model of the rail track transition zone was carried out in a systematic manner, starting from a simple model and then gradually increasing its sophistication to predict the settlement under train loading. Initially, a beam on springs model was developed under static general conditions, using Finite Element Modelling software ABAQUS, to verify the analytical modelling technique. In this model, a steel beam of flexural rigidity, *EI* is considered to be connected to the ground with equally spaced springs of specific stiffness *S*, as shown in Figure 4.4(a). The material properties and cross-sectional profile of the steel beam, as well as the spring stiffness and spacing, have been selected to align with the material parameters used for analytical modelling for varying stiffness values (Table 4.1). The total length of the model has been considered as 10m to avoid any boundary effect for single midpoint loading, *P* (Figure 4.4a). This straightforward and relatively simple numerical model can be used to examine how track stiffness affects track settlement under train loadings. The model is analysed for various stiffness values and loadings and the results are compared with those that are calculated through analytical modelling as provided in the next sections. This numerical model provided similar results as the analytical model considering the BOEF concept (beam on elastic foundation) as shown in Figure 4.1(a).

4.3.2 2D FEM Layered Model

The beam on springs model was further developed to a layered model consisting of rail, ballast, sub-ballast and subgrade layers, simulating a conventional ballasted track. To investigate the effect of train wheel load, a 2D plane strain model was developed using FEM software ABAQUS, with a total length of 9.86m and a height of 5.68m, as illustrated in Figure 4.4(b). The steel rail is modelled as a modified rectangular section, (width=50mm, height=194mm), for a standard UIC60 profile with 60kg/m as the unit mass (Shahraki et al. 2015). The model included 17 reinforced concrete sleepers, each measuring 0.26 meters in width and 0.23 meters in height, spaced 0.6 meters apart (Nimbalkar & Indraratna 2016). Ballast and sub-ballast layers have been simulated with thicknesses of 300 mm and 150 mm, respectively, and are situated on top of a homogenous subgrade that is 5 metres thick.

The total length and height of the 2D plane strain model were chosen to accommodate the 17 sleepers with a 0.6-meter centre-to-centre spacing, based on the beam on springs model. The total height of the model was determined through calibration, adjusting the heights and stiffness values of ballast, sub-ballast, and subgrade layers to achieve the track's equivalent stiffness and corresponding deflections. The calculated total height of the model was 5.86m, considering the thicknesses of all track components, except for the steel rail, which was represented as a line element resembling a steel beam with a rectangular cross-section.

Due to the anticipated non-yielding behaviour, the steel rail and concrete sleepers are modelled as linear-elastic materials. However, to accurately represent the damping and nonlinear behaviour of track substructure, the ballast, sub-ballast and subgrade are modelled as viscoelastic materials with the inclusion of damping behaviour (Nimbalkar et al. 2012; Lamprea-Pineda et al. 2021). In this regard, the Rayleigh viscous damping technique is utilised, where the global damping matrix (C) is related to the mass matrix (M), and stiffness matrix (K), through Rayleigh damping coefficients; α and β, as shown below (Chumyen et al. 2022).

$$C = \alpha M + \beta K \tag{4.9}$$

The geometry and model input parameters for the substructural elements used in the current FE analysis are obtained from Indraratna & Ngo (2018), which were derived from extensive laboratory testing and field measurements in Bulli and Singleton tracks (Indraratna et al. 2010; Indraratna et al. 2014) carried out in New South Wales, Australia (Indraratna et al. 2011). The summary of the mechanical parameters for each component of the track models used for this investigation can be found in Table 4.1.

Track geometry, boundary conditions, element size, and dynamic calculation time-step for this model have been selected properly to ensure an adequate level of accuracy and model convergence for the track dynamic analysis. A mesh sensitivity analysis was conducted to assess the influence of varying mesh sizes on the numerical outcomes of the model. The mesh sensitivity analysis involved systematically refining and coarsening the mesh to observe the effects on the track vertical displacements. Considering the size of the transition model, the goal was to determine an appropriate mesh size that strikes a balance between accuracy and computational efficiency. After carrying out the mesh sensitivity analysis, a typical mesh for the model is shown in Figure 4.4(b).

The model represents a vertical cross-section through the centreline of one of the rails along the track, for a conventional ballast track, as shown in Figure 4.4(b). Vertical displacement has been allowed on both the vertical boundaries of the model, whereas, the encastre boundary condition has been applied at the bottom of the model to constrain all displacements and rotations at a node to zero, meaning U1 = U2 = U3 = UR1 = UR2 = UR3 = 0. It is noted that the sides and base of the model do not transmit waves, however, the wave reflection during the current analysis is not an issue due to the applied static loadings.

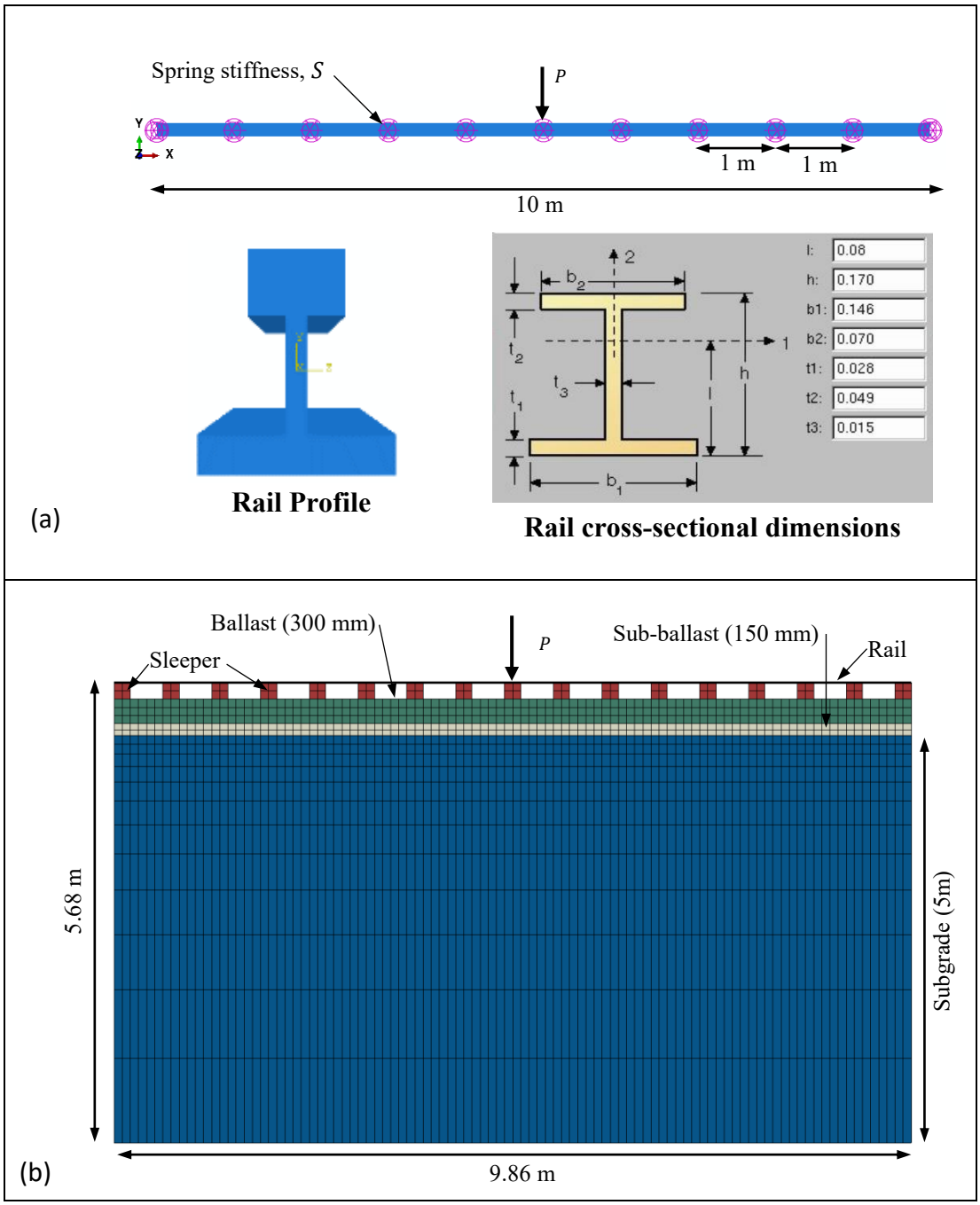

Figure 4.4: (a) Numerical model considering beam on springs, with rail profile and dimensions, after Onesteel (2017) (b) 2D FEM mesh model for conventional layered ballast track

The maximum element sizes for sub-ballast, ballast, and subgrade layers have been kept as 0.075m, 0.13m, and 0.1-1m, respectively. Hence, the discretised mesh grid has 2234 nodes and 1834 hourglass-controlled quadrilateral plain strain elements (element type: CPE4R), including 100 linear line elements for the steel rail. In order to improve

the analysis accuracy, the node continuity at the interface is well maintained between all the layers (Abaqus 2020). Additionally, surface-to-surface contact was established between various layers of the track model using a penalty method to ensure the accurate transmission of normal and shear stresses at the interface (Hibbitt et al. 2014).

4.3.3 Model Calibration and Validation

The input parameters for beam on elastic springs model are the same as used in analytical modelling, hence a good match of the obtained results with the analytical analysis would be sufficient to prove its credibility. However, the 2D FEM layered track model required various input parameters that were calibrated through the beam on elastic springs model by comparing the maximum settlement under wheel loads for various track stiffness (k) and wheel loading (P). The fully calibrated model is further validated with the analytical modelling results for single and multiple loadings.

Both the numerical models; the beam on spring and the 2D layered, are validated with the analytical model and field data reported by Read & Li (2006), by comparing the maximum settlement under wheel loads for various track stiffness. In this regard, the analytic response was obtained by solving Equation (4.8) for stiffness values, k = 9 MN/m/m and 64 MN/m/m, under wheel loads, P = 7 tonnes. The track stiffness values, and the wheel load are adopted in accordance with the data reported by Read & Li (2006) for model validation under similar loading conditions.

Beam on spring model is then solved numerically for the same loads considering a steel beam resting on equally spaced springs with stiffness, S values of 9 MN/m and 64 MN/m placed at the one-meter centre-to-centre distance. The wheel load is applied at the centre of the model to determine the maximum settlement under the applied loading. The deformation contour showing the maximum settlement and the deformed shape of this FE model with 9 MN/m/m stiffness springs, is given in Figure 4.5(a), which indicates a maximum settlement of 2.9 mm under 7 tonnes wheel loading which is in good agreement with the one obtained analytically.

Likewise, the 2D layered FEM model is solved numerically for the same loading conditions where an equivalent track stiffness (k) for this model is used to match its

values with the analytical model. The equivalent track stiffness is a combination of stiffness from various track components, that contribute in a series form, for example in the case of a layered ballast track, it can be calculated as given below (Powrie & Le Pen 2016):

$$\frac{1}{k_b} = \frac{1}{k_{railpad}} + \frac{1}{k_{sleeper}} + \frac{1}{k_{ballast}} + \frac{1}{k_{sub-ballast}} + \frac{1}{k_{subgrade}} \tag{4.10}$$

The stiffness of rail pads and sleepers is primarily determined by the resilience and stiffness of their elastomeric components. As a result, equivalent stiffness of rail fastening system is more uniform and easier to predict compared to the track substructural components (e.g. ballast, sub-ballast, subgrade). However, the stiffness of track substructure can be related to its fundamental properties; the Poisson ratio, Young's modulus, and the thickness of individual layers as introduced by Lei (2017), as below:

$$k = \frac{0.65E_s}{1 - v_s} \sqrt[12]{\frac{E_s B^4}{EI}} \tag{4.11}$$

where, k represents the track foundation stiffness in MN/m per meter length (MN/m/m); E_s and v_s represent foundation elastic modulus in MN/m^2 and Poisson's ratio, respectively. B is the sleeper length, and EI is the flexural modulus of the rail in MN m^2.

For a three layered model, the foundation elasticity modulus, E_s can be calculated as per Zhang et al. (1998), that can be reproduced as below:

$$E_s = \left\{ \frac{h_1 \sqrt[3]{E_1} + h_2 \sqrt[3]{E_2} + h_3 \sqrt[3]{E_3}}{h_1 + h_2 + h_3} \right\}^3 \tag{4.12}$$

where, E_1, E_2, E_3 and h_1, h_2, h_3 are the modulus of elasticity in MN/m^2 and thickness

of model layers from top to bottom.

This indicates that any change in the material properties of the track components will result in the corresponding change in its overall stiffness. In this model, the change in overall stiffness values has been achieved by changing the E values of ballast, sub-ballast and subgrade where the other material properties are kept the same (as given in Table 4.1) for all cases. Hence, to achieve the overall stiffness of 9 MN/m/m and 64 MN/m/m, the E values of ballast, sub-ballast and subgrade are calculated using Equations (4.10), (4.11), & (4.12) as given in Table 4.2.

The wheel load is applied at the centre of the model as a point load to determine the maximum settlement under the applied loading. The deformation contour showing the maximum settlement and the deformed shape of this FE model with overall stiffness of 9 MN/m/m, is given in Figure 4.5(b). It is seen that the maximum settlement of 2.9 mm is predicted under 7 tonnes wheel loading, which is almost the same as the analytical solution and beam on springs model.

The comparison of vertical displacements of tracks for these models is presented in Figure 4.5(c). To validate the FEM model, predicted settlements were compared with field data reported by Read & Li (2006). Although Read & Li (2006) presented results for various conditions, only those results that had similar or comparable conditions to the current 2D FE model were utilized for the verification process. As seen in Figure 4.5(c), both studies show a comparable maximum settlement and deformation pattern under similar loading conditions, albeit some discrepancy in the deformation pattern obtained from 2D FE modelling (layered) and from the authors' analytical model. This could be attributed to the differences in modelling assumptions, especially where the analytical model assumes the loads being supported by a series of vertical springs with zero deformation for nearby soil elements, while the FEM numerical model distributes the applied loads in both transverse and horizontal directions.

Additionally, the non-linearity of layered materials and the damping (that captures the dissipation of energy and the time-dependent material response) may result in a more spatial distribution of deformation as suggested by Walker & Indraratna (2018). However, it can be noted that the maximum displacement, under a given wheel load

P, for all the three models (analytical, beam on spring, 2D layered) is almost similar. For example, the maximum settlement under 7 tonnes wheel loading for all three models having a track stiffness value of 9 MN/m/m is about 2.9mm which is identical for all.

In case of track transition, the maximum settlement calculated for each sides segment provides an assessment of the differential settlement, which is the main design criterion. Hence, the 2D layered model can be used to study the dynamic response of ballasted tracks under various loading conditions. Figure 4.5(c) also shows an increase in vertical displacement with a decrease in track stiffness, a detailed discussion of this phenomenon is given in the next section.

Table 4.1: Material properties used in ballasted track model

Track Components	Value
Rail	
Density (kg/m^3)	7850
Young's modulus (MPa)	210000
Poisson's ratio, ν	0.3
Sleeper	
Density (kg/m^3)	2500
Young's modulus (MPa)	30000
Poisson's ratio, ν	0.25
Ballast	
Density (kg/m^3)	1530
Young's modulus (MPa)	200
Poisson's ratio, ν	0.3
Cohesion (kPa)	1
Friction angle, ϕ (degrees)	50
Dilation angle, ψ (degrees)	20
Rayleigh Damping Coefficient, α (1/s)	6.14
Rayleigh Damping Coefficient, β (s)	0.000195
Thickness (m)	0.3
Sub-ballast	
Density (kg/m^3)	1800
Young's modulus (MPa)	110
Poisson's ratio, ν	0.3
Cohesion (kPa)	1
Friction angle, ϕ (degrees)	35
Dilation angle, ψ (degrees)	5
Rayleigh Damping Coefficient, α (1/s)	4.8
Rayleigh Damping Coefficient, β (s)	0.000152
Thickness (m)	0.15
Subgrade	
Density (kg/m^3)	1730
Young's modulus (MPa)	50
Poisson's ratio	0.4
Cohesion (kPa)	30
Friction angle, ϕ (degrees)	24
Dilation angle, ψ (degrees)	4
Rayleigh Damping Coefficient, α (1/s)	4.8
Rayleigh Damping Coefficient, β (s)	0.000152

Table 4.2: Material properties for equivalent track stiffnesses

$\boldsymbol{k}$ (MN/m/m)	$\boldsymbol{E_b}$ (MPa)	$\boldsymbol{E_c}$ (MPa)	$\boldsymbol{E_s}$(MPa)
5	200	110	8.5
9.2	200	150	15.7
10	200	150	17.2
13.6	200	150	23.6
20	250	150	35
22.8	250	150	40.5
40	250	175	75
41.5	250	175	80
80	300	175	175

Where, k is track equivalent stiffness, and E_b, E_c, and E_s is modulus of elasticity of ballast, sub-ballast and subgrade, respectively.

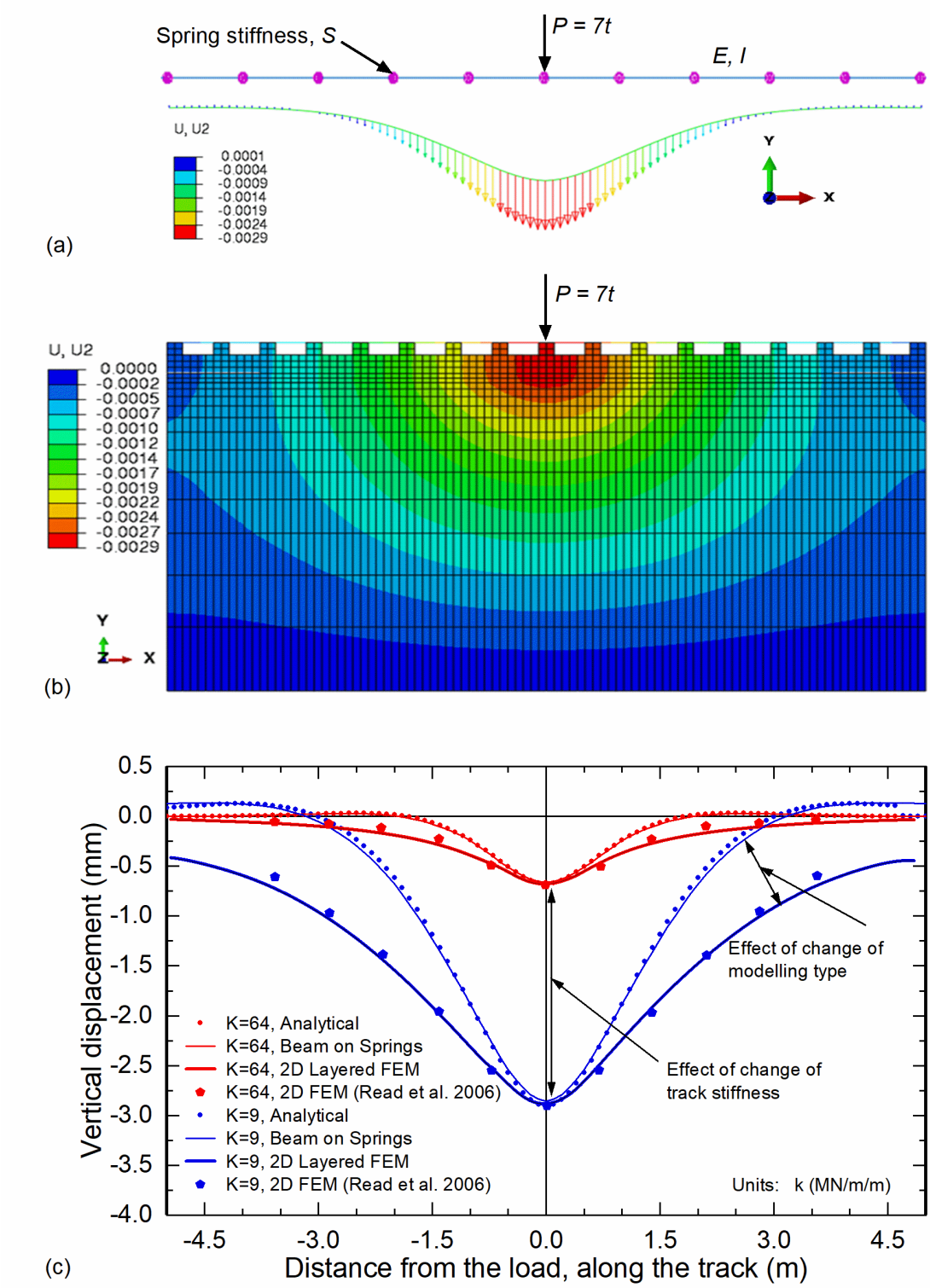

Figure 4.5: (a) Deformation contours for 10m long steel beam resting on equally spaced springs with spring stiffness of 9MN/m, (b) Deformation contours for 2D FEM layered model with track stiffness as 9MN/m/m, (c) Comparison of vertical displacements of rail tracks for analytical and Numerical (i.e. beam on spring and 2D FEM layered) models.

4.4 Effect of Stiffness on Track Settlement

Track stiffness, k is directly related to track settlement under the applied load; if the magnitude or position of load changes, there will be a corresponding change in track settlement and the resulting accelerations and forces in the vehicle (Powrie & Le Pen 2016). The following sections explain how the track stiffness affects the track settlement and its extent in the longitudinal direction for various types of wheel loads.

4.4.1 Effect of Stiffness on Settlement under single-wheel loading

In order to investigate the effect of track stiffness in terms of track settlement under train loading, Equation (4.8) is solved for various stiffnesses under a given wheel load of P = 7.5-17.5 tonnes (representing 15-35 tonne axle loads). The stiffness values (k = 5-80 MN/m/m) have been adopted in this study based on past studies (Dahlberg 2010; Powrie & Le Pen 2016; Sung et al. 2020). In this chapter, k represents the overall track stiffness, demonstrating the load required to produce a unit track deflection and can be determined from field measurements either by measuring rail/sleeper deflection under actual train passing or by falling weight techniques (Powrie & Le Pen 2016). The loading range has been selected to incorporate typical Australian heavy-haul railways that correspond to 35-tonne axle loading (i.e. P = 17.5 tonnes). Additionally, the track stiffness effect was also analysed numerically using the beam on spring model under the above loading for various spring stiffness values (i.e. k = 5-80 MN/m/m).

The results obtained from analytical and numerical modelling are presented in Figure 4.6, which demonstrates exactly similar observations for both modelling approaches. The results indicate a decrease in vertical displacement (w) with an increase in track stiffness (k) for a given applied load (P), as expected (Choudhury et al. 2008). For example, Figure 4.6a shows the decrease in maximum track settlement, w_{max} under 15-tonne axle load, from 4.9mm to just 0.6mm for an increase in track stiffness from k =5MN/m/m to 80MN/m/m. This affirms that the stiffer tracks undergo lesser settlements than the tracks having a smaller stiffness. It can also be noted that the settlement increases with the increase in applied load, indicating the higher differential

settlements at track transitions due to load amplification. A maximum track settlement (w_{max}) for the case of 15-tonne axle load and k =5MN/m/m (Figure 4.6a) is predicted as about w_{max} =4.9mm, compared to w_{max} =11.5mm for similar track stiffness subjected to 35-tonne axle load (Figure 4.6d). Hence, it can be concluded that higher differential settlements occurring at the track transitions can be amplified by sudden stiffness variation and train loading.

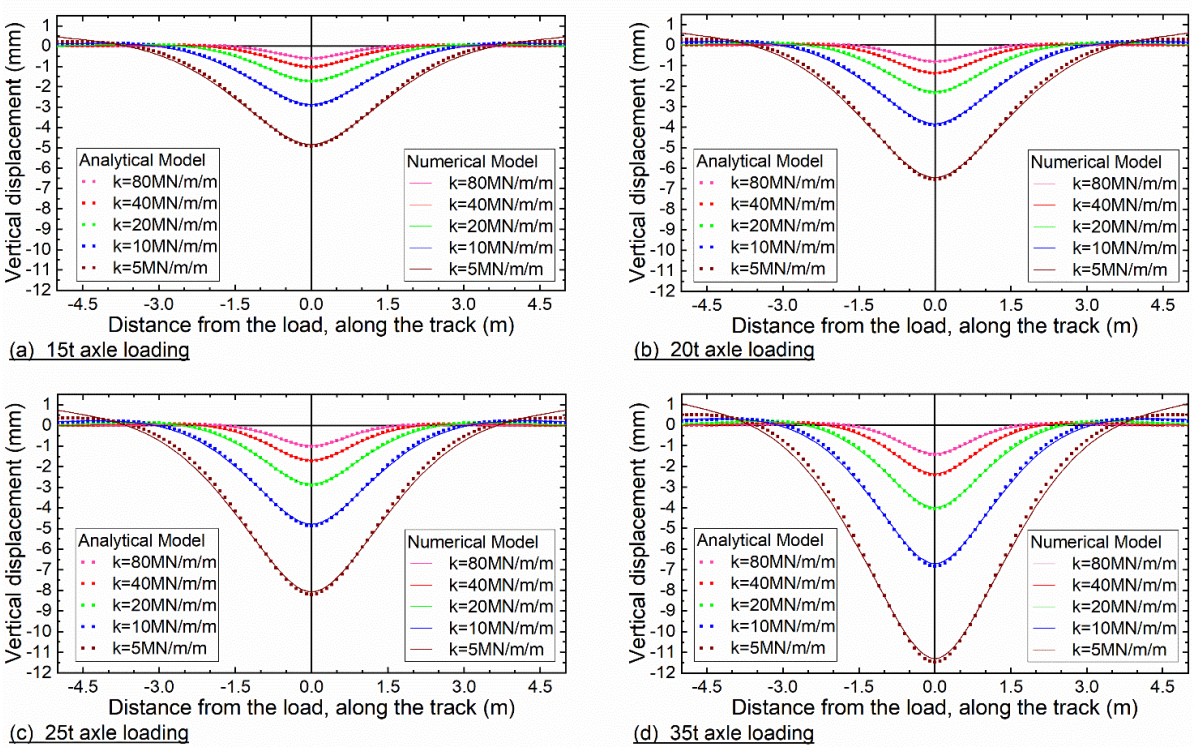

Figure 4.6: Predicted vertical displacements of rail tracks subjected to different axle loadings; (a) 15-tonne axle load, (b) 20-tonne axle load, (c) 25-tonne axle load, and (d) 35-tonne axle load

4.4.2 Effect of Stiffness on Settlement for Multiple and Moving Wheel Loads

The effect of multiple loading can be considered by modifying Equation (4.8) for multiple loadings, introduced by (Esveld 2001):

$$w(x) = \sum_{p=1}^{N} \frac{P\beta}{2k} e^{-\beta(x-d_p)}\left(\cos(\beta(x-d_p)) + \sin(\beta(x-d_p))\right) \qquad (4.13)$$

where, $w(x) =$ Maximum track settlement at any point x under the effect of multiple loadings, $N =$ Total number of load points for the whole train; $P =$ Wheel load; and $d_p =$ Distance of a certain load point from point x.

In order to investigate the effect of multiple loading, Equation (4.13) was solved analytically (to optimise accuracy and expedite the solving process) for a four-carriage loading (16 wheels), as shown in Figure 4.7(a). In this study, the values of D_1, D_2 and D_3 have been considered 2.5m, 12m and 4m, respectively (Hendry 2007). The equation was solved for three different track stiffnesses (5MN/m/m, 10MN/m/m, and 40MN/m/m) under P=10-tonne. A similar problem was also solved numerically by extending the length of 2D FEM layered model (as discussed above) to 120m, simulating a four-carriage train loading and using the material properties as given in Table 4.1 and Table 4.2.

The vertical displacements of the rail under the effect of multiple (16 wheels) loadings obtained through analytical and numerical modelling are presented in Figure 4.7(b). A reasonable agreement is found for maximum displacements under combined loading obtained from both analytical and numerical modelling approaches. Furthermore, comparing Figure 4.6(b) and Figure 4.7(b), it can be noted that the maximum track settlement (w_{max}) for k =5MN/m/m under 10-tonne single wheel loading (Figure 4.6b) increases from 6.5mm to 8mm when considering the effect of multiple train loadings (Figure 4.7b). A considerable increase in track settlement under each wheel load can be observed, demonstrating the pronounced effect of multiple-wheel loading.

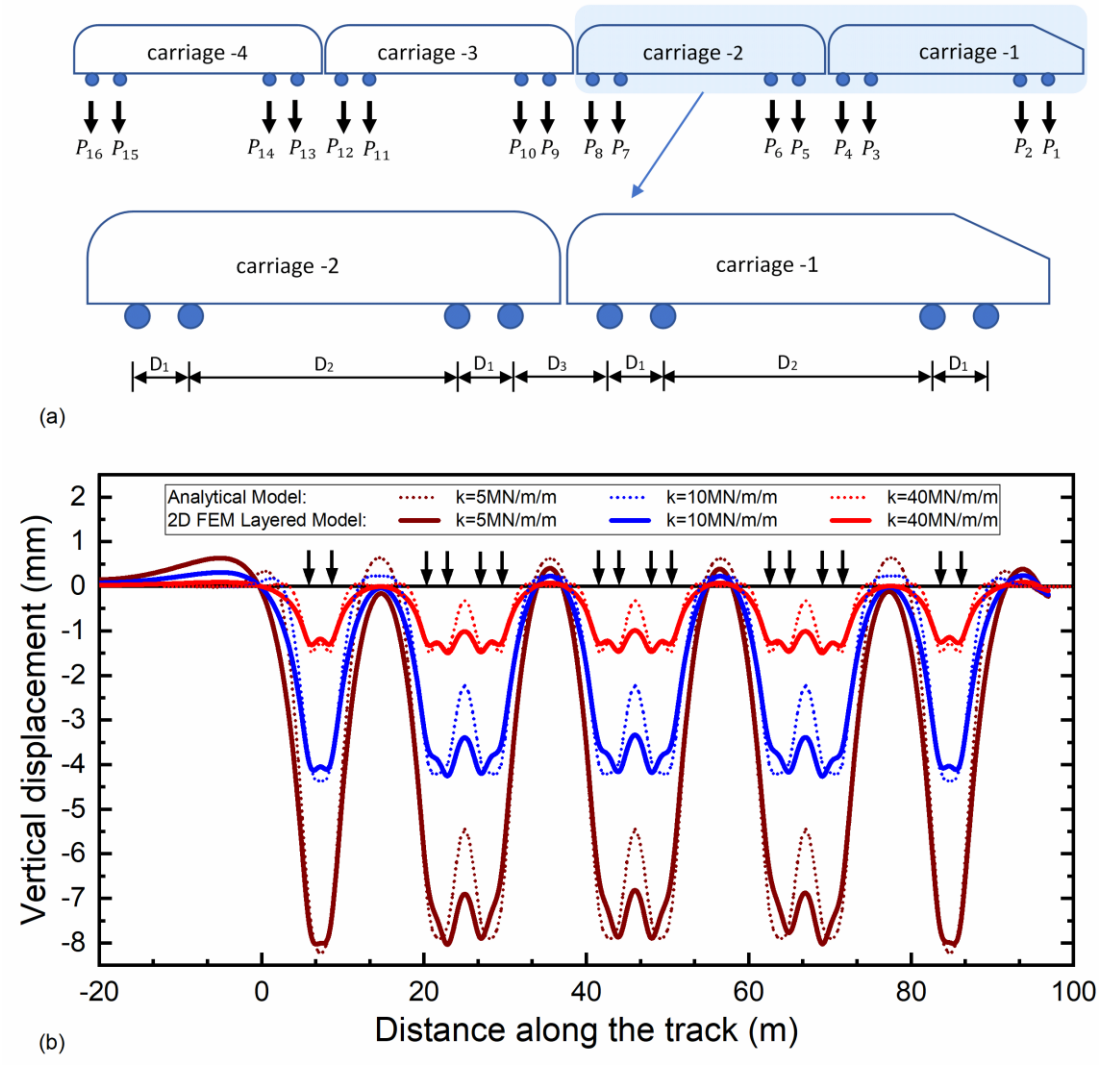

Figure 4.7: (a) Four-carriage loading (b) Vertical displacements of rail tracks under four-carriage loading considering the effect of multiple loadings

The effect of moving train with speed v, at any point x along the track with respect to time t, can be calculated using Equation (4.14) as introduced by Powrie & Le Pen (2016):

$$w(x,t) = \sum_{p=1}^{N} \frac{P_d \beta}{2k} e^{-\beta(vt-d_p)} \left(\cos(\beta(vt-d_p)) + \sin(\beta(vt-d_p))\right) \qquad (4.14)$$

where, $w(x,t)$ = Maximum track settlement at point x with respect to time t, under the effect of multiple loadings, N = Total number of load points; P_d = Dynamic wheel load; d_p = Distance of a certain load point from point x; and v is the speed of

the moving train.

The dynamic behaviour of tracks is captured in terms of increased deformations with increased speeds, as a function of the dynamic amplification factor (DAF). DAF determines the quasi-dynamic stress due to moving loads and incorporates the train speed, sleeper passing frequency, and dynamic train-track interaction (Esveld 2001; Punetha et al. 2021), and this approach has been widely adopted to accurately depict track dynamics, as demonstrated by the works of Li & Selig (1998); Kennedy et al. (2013); Nimbalkar & Indraratna (2016); Indraratna & Ngo (2018); Punetha et al. (2020), among others. To determine a dynamic wheel load, P_d for a moving train due to DAF, an empirical relationship as proposed by Li & Selig (1998) based on American Railway Engineering Association (AREA) is used, as given:

$$P_d = \emptyset P \tag{4.15}$$

where, $P_d =$ Dynamic wheel load; $P =$ Static wheel load; $\emptyset =$ Dynamic amplification factor and is determined by:

$$\emptyset = 1 + 5.21\frac{v}{D} \tag{4.16}$$

However, in this equation, $v =$ train speed (km/h); and $D =$ wheel diameter in mm (970mm considered in this study).

Equation (4.14) is employed for the cases of four-carriage train loading (P =10-tonne) moving at four different speeds (v = 60, 100, 150, and 200 km/h) with five different track stiffness values (k = 5, 10, 20, 40 and 80 MN/m/m), and the calculated vertical displacements of rail tracks are presented in Figure 4.8. Comparing Figure 4.7 and Figure 4.8, it can be noted that the maximum track settlement (w_{max}) for k =5MN/m/m under P =10 tonnes increases from 8mm to 10.1mm, 11.7mm, 13.8mm, and 15.8mm under the train speed of 60 km/h, 100km/h, 150km/h, and 200km/h, respectively. A similar increasing trend can also be observed for other stiffness values. Hence, a further increase in track settlement under each wheel load can be observed, demonstrating the enhanced dynamic loading effect of moving loads.

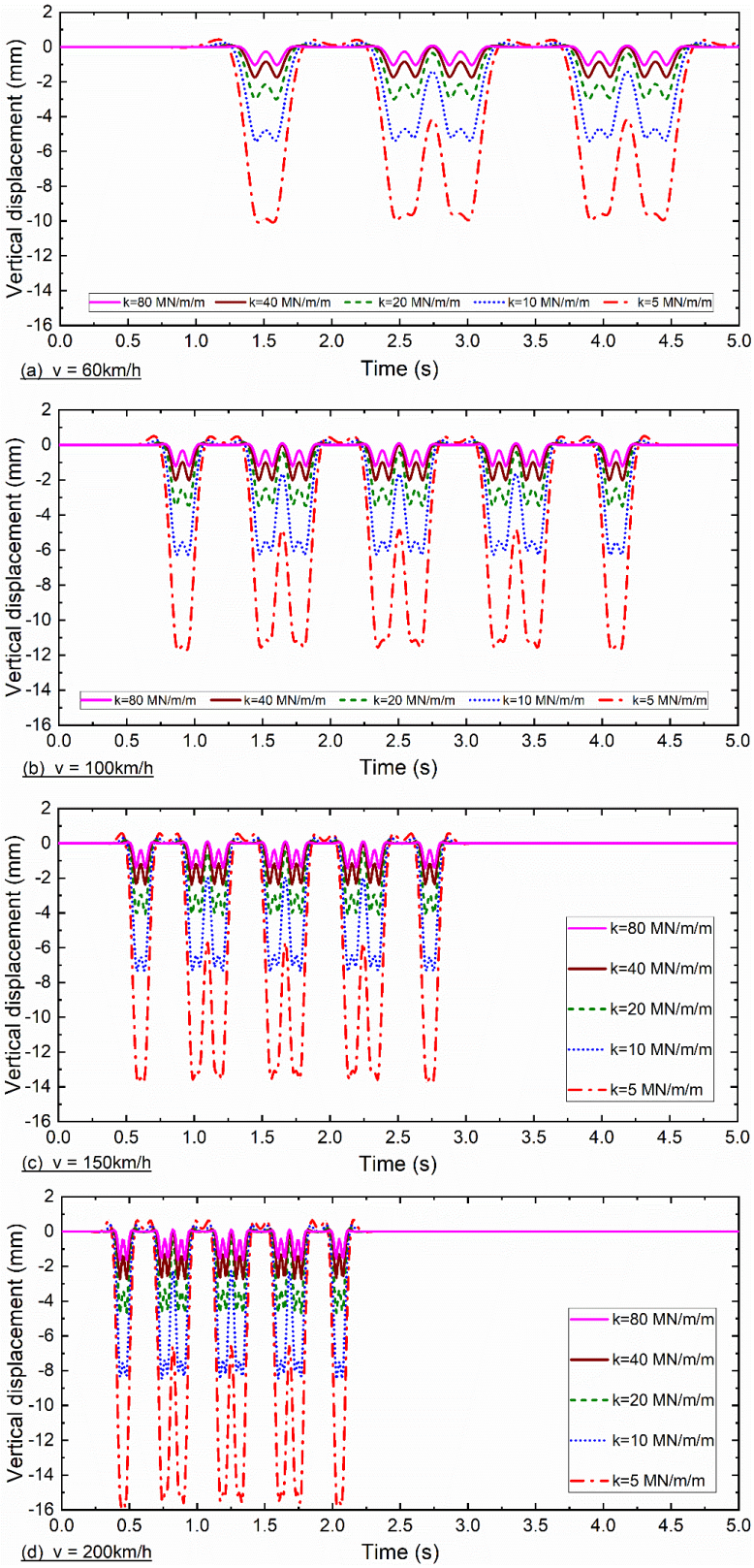

Figure 4.8: Vertical displacements of the track calculated at various times considering 4- carriage ($P = 10$ tonnes) moving at various speeds; (a) v=60 km/h, (b) v=100 km/h, (c) v=150 km/h, and (d) v=200 km/h

Figure 4.9 shows the calculated maximum vertical displacements of the tracks subjected to train (P =10 tonnes), moving at various speeds and track stiffnesses in comparison with similar data reported from case studies. It can be seen that the effect of moving train loading (e.g. settlement) increases with the increase in train speed, however, this effect becomes less noticeable for higher track stiffness. The comparison with some past studies (Karlsson & Hjelm 2016; Lamas-Lopez et al. 2017; Lei 2017; Coelho et al. 2018) shows that despite different sites and loading conditions, there are similar trends in the increase in vertical displacements with the increase in train speeds. It can also be observed from Figure 4.9 that the absolute differential settlement (Δw) between any two tracks with different stiffness values, increases with the increase in train speed. For example, for a stiffness variation of Δk = 75MN/m/m (from 5 to 80 MN/m/m) is Δw=10.5mm and Δw=17.8mm for the train moving at v=100km/h and v=300km/h, respectively. This indicates that the trains moving at higher speeds can lead to higher differential settlements.

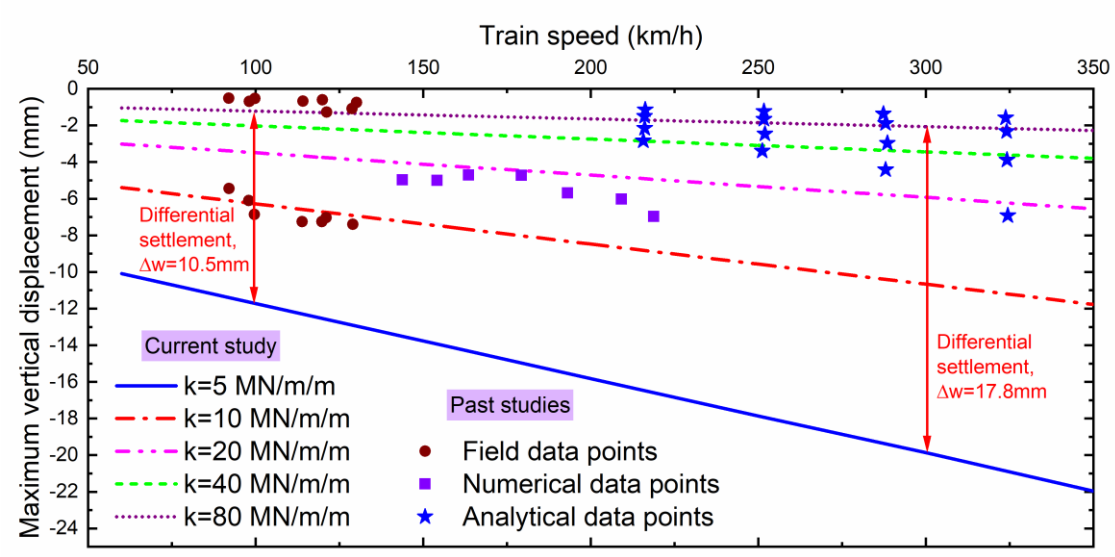

Figure 4.9: Maximum vertical displacement of the rail track subjected to train moving at various speeds

4.5 Chapter Summary

In this chapter the dynamic response of a conventional track is investigated in terms of maximum settlement under various wheel loads, through analytical solution (considering the BOEF theory) and numerical modelling (2D-FEM; elastic spring and layered track models). The results for the vertical track displacements obtained through analytical and numerical modelling for different combinations of wheel loads and speeds are found to be in good agreement. The models are then utilised to investigate the effect of track stiffness considering its five different values, i.e. (k = 5, 10, 20, 40, & 80 MN/m/m). It is noted that the tracks with higher stiffness undergo less settlements compared to those having lower stiffness, as expected. For example, the results showed a significant increase in track settlements, w_{max} (i.e., increased from w_{max}=0.6 mm to w_{max}=4.9 mm, for a change in track stiffness from k=80MN/m/m (stiff track) to k=5MN/m/m (soft track).

In order to investigate the effect of applied load, the models are analysed for various wheel loads as P = 7.5-17.5 tonnes (representing 15-35 tonne axle loads) and an increase in track settlement is observed with the increase in applied load. Similarly, the increase in dynamic load corresponding to the increased train speed, also resulted in higher settlements for any specific load and stiffness. For instance, increase in train speed from 60 km/h to 200km/h for a wheel load of P=10 tonnes and track stiffness k=5 MN/m/m, the track settlement increased from w_{max}=8 mm to w_{max}=15.8 mm, which demonstrates the enhanced dynamic loading due to moving loads. Hence, this modelling approach affirmed that the tracks with lower stiffness values undergo higher settlement, which further exacerbates with the increase in train speed.

CHAPTER FIVE

5. DYNAMIC RESPONSE AT TRANSITION ZONES

5.1 Introduction

The dynamic response of rail tracks at transition zones can be investigated by further extending the track models (Chapter 4) to incorporate the sudden change in track structural properties (i.e. stiffness). In this regard, the track models considered in the previous chapter is extended to incorporate the one-step transition from a stiff to the soft track, as shown in Figure 5.1. Such transitions are responsible for a sudden change in track stiffness and hence produce uneven settlements on both sides of the junction when subjected to the train passing. The dynamic analysis of one-step transition results in the differential settlement and highlights the importance of sudden stiffness variation at track transitions. Further details about the dynamic response of transitions, and the effect of track stiffness on differential settlement is provided in this chapter. Part of this chapter has been submitted as a technical article to the Journal ASCE-Journal of Geotechnical and Geoenvironmental Engineering (pending for approval after the second round of revisions).

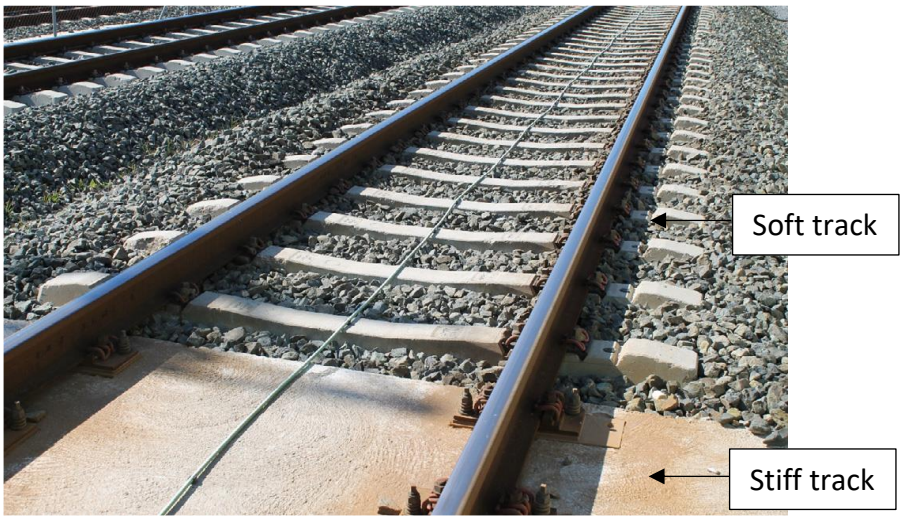

Figure 5.1: Track transition between ballasted track and slab track sections on the high-speed line Cordoba-Malaga, Spain, (Sañudo et al. 2016)

5.2 Design Concept

In order to identify the severity of the research problem, a typical track transition between a soft track (conventional ballast track) and a stiff track (concrete bridge deck), as shown Figure 5.2(a), is considered in this study. This is a common transition when a traditional ballast track changes to a concrete slab track section (e.g. when crossing a bridge). In this study, the soft track is considered as a layered structure that consists of rails, concrete sleepers, ballast, sub-ballast and subgrade, whereas the track on a concrete bridge deck has no sub-ballast or soft subgrade layers, and becomes considerably much stiffer than a ballasted track.

An abrupt change in track stiffness has been assumed to be the main effect of this track transition where overall (global) track stiffness, k_s of the stiff track suddenly decreases to k_b which is the total track stiffness of ballast track as shown in Figure 5.2(b). Primarily, both the stiffness values are known or they can be determined from field measurements. A total variation in track stiffness values ($\Delta k = k_s - k_b$) at a given transition can then be determined accordingly. This stiffness variation (Δk) serves as an input parameter for the design of the track transition zone.

5.3 Development of Analytical Model

To develop the analytical model for a rail track at railway transition zone, the typical track transition in Figure 5.2(a) is utilised considering sudden stiffness variation at the junction of two tracks. A mass spring-dashpot model as shown in Figure 5.3, is developed to understand the nature of problem for the given transition. In this model, the total track stiffness is represented by the "spring" with spring constants k_b and k_s for ballast track and slab track, respectively, whereas the damping (c) of the track structure is represented as dashpots.

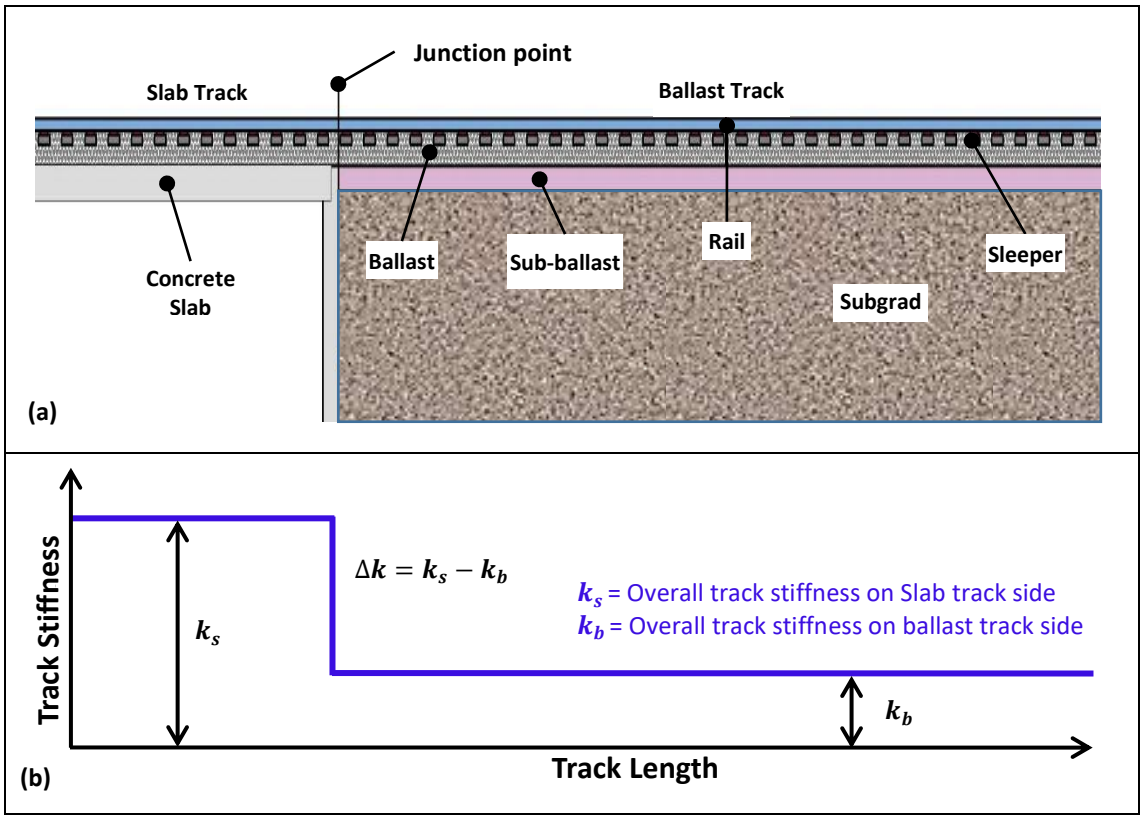

Figure 5.2: (a) A typical track transition between slab track and ballast track, (b) Abrupt stiffness variation at track transition

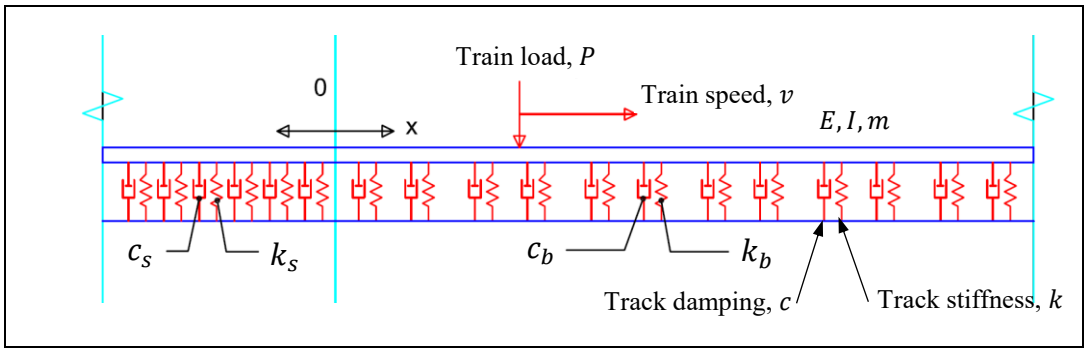

Figure 5.3: Mass, spring-dashpot model for ballast track to slab track transition

This main purpose of the above model is to find out the total differential settlement at the junction of the tracks, without the provision of any transition zone, under the train wheel load, P moving at a speed, v. The governing equations of motion for the ballast track and the slab track (Koh et al. 2003; Uzzal et al. 2008; Ding et al. 2012; Walker & Indraratna 2018) can be written as follow:

$$\frac{EI\partial^4 w_s}{\partial x^4} + \frac{m\partial^2 w_s}{\partial t^2} + c_s\frac{\partial w_s}{\partial t} + k_s w_s = -P\delta(x - vt) \qquad x \leq 0 \qquad (5.1)$$

$$\frac{EI\partial^4 w_b}{\partial x^4} + \frac{m\partial^2 w_b}{\partial t^2} + c_b\frac{\partial w_b}{\partial t} + k_b w_b = -P\delta(x - vt) \qquad x > 0 \qquad (5.2)$$

where,

E = Rail modulus of elasticity, (N/mm^2)

I = Rail moment of inertia, (mm^4)

m = mass of the rail, (kg/m)

k_b & k_s = total track stiffness for ballast track and slab track, respectively, (kN/m/m)

c_b & c_s = total track damping for ballast track and slab track, respectively, (kN/mm)

w_b & w_s = vertical deflection in ballast track and slab track, respectively, (mm)

P = Dynamic load of train wheelset, (kN)

v = moving speed of train wheelset, (m/s)

δ = Dirac-delta function

In order to find the differential settlement for both the tracks in the transition zone, the above partial differential equations can be solved separately considering the Euler-Bernoulli beam on a viscoelastic foundation with moving load, P at a speed of, v.

5.4 Effect of Stiffness Variation at Track Transition

To investigate the effect of sudden stiffness variation on the track settlement at track transition, a base case of track transition (one-step transition) is adopted where the stiffness suddenly changes from k = 80 to 5 MN/m/m at $x = 0$ (i.e. the Junction point). This case was solved analytically for four-carriage loading (P =10-tonne) using Equation (4.13) where:

$$k = k_s = 80 \text{ MN/m/m} \qquad \text{for } x \leq 0$$

and

$$k = k_b = 5 \text{ MN/m/m} \qquad \text{for } x > 0$$

In order to capture the most critical condition with respect to differential settlements, half of the train loading was considered on one side of the track junction and half on

the other side as shown in Figure 5.4. The settlements (w) under each wheel loading are calculated and plotted along the track length. It can be noted that the maximum settlements on the stiffer and softer side of the track transition are 0.69mm and 8.05mm, respectively. It shows that the settlements on ballasted track are far greater than those on the stiffer track (concrete bridge deck), resulting in a substantial differential settlement at this location. Based on the above values, the maximum differential settlement is Δw_{max} 7.36mm. This would lead to increased dynamic loading impact, causing accelerated degradation of track geometry and material. Hence, to mitigate these problems, this differential settlement needs to be reduced to a certain allowable limit through the provision of an effective transition zone.

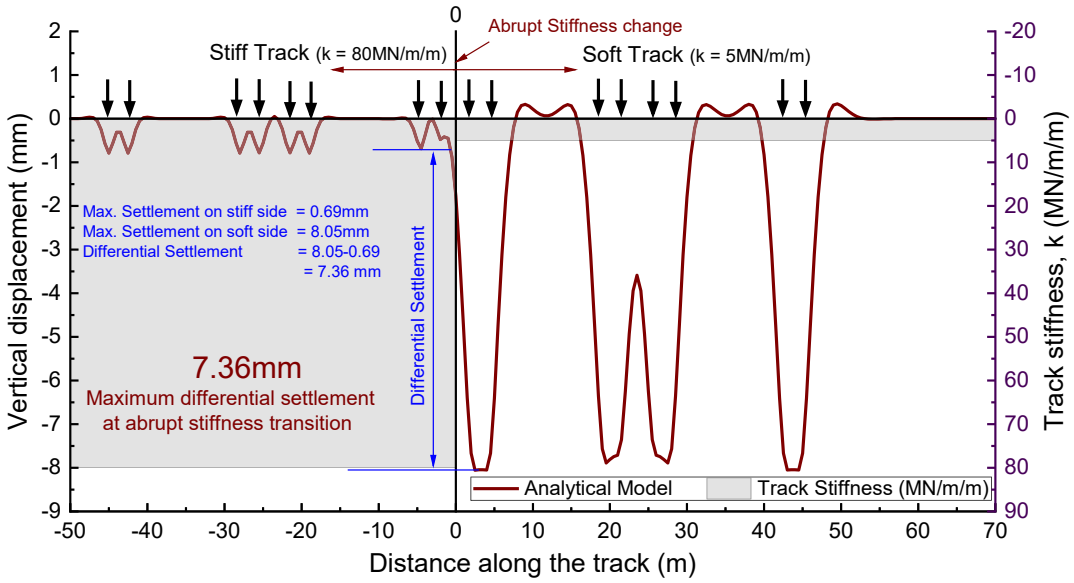

Figure 5.4: Calculated vertical displacement of rail track for one-step transition, stiffness varying from k=80 MN/m/m to k=5 MN/m/m under P=10 tonne

5.5 Wheel Load Effect on the Differential Settlement

In order to investigate the effect of wheel loading on the differential settlement for the typical transition case, Equation (4.13) is analysed for P=10, 12.5, 15 and 20-tonnes wheel loading. It is noted that the differential settlement increases significantly with the increase in wheel loading. The results obtained for track settlement on both sides of the track transition are plotted in Figure 5.5, showing an enhanced differential settlement with increased wheel loading. This Figure also designates a linear trend for

increased settlement with an increase in wheel loading. Hence, it can be concluded that the load amplification at any track transition results in higher differential settlement and this trend is expected to continue if proper mitigation measures are not implemented. A multi-step transition is now introduced as a mitigation measure to minimise the differential settlement and this is discussed in the next chapter.

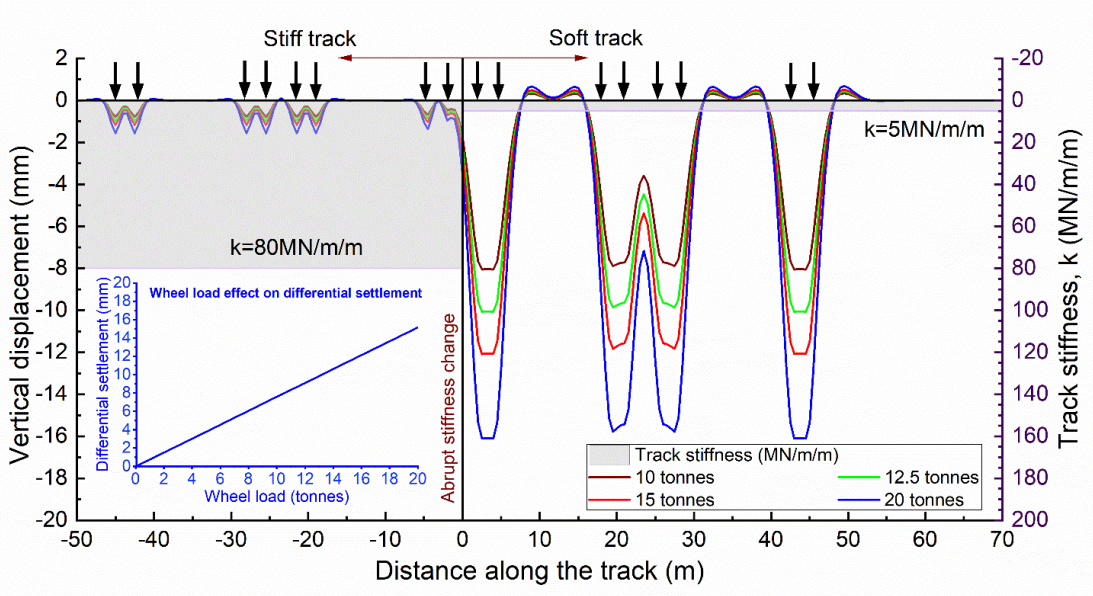

Figure 5.5: The effect of wheel load (P) on differential settlements for one-step stiffness transition varying from k=80 MN/m/m (stiff track) to k=5 MN/m/m (ballasted track)

5.6 Finite Element Modelling of One-step Transition

An abrupt change in structural characteristics at the track transition can make the design of the transition zone become complicated to be solved using an analytical approach. Additionally, the BOEF theory has several limitations for the dynamic response analysis of track substructure, especially regarding the nonlinearity of the substructure layers. Although, the simple BOEF or mass-spring-dashpot model can be utilised to understand the simple behaviour of track transition through the analytical model, extensive calculations are required to study the dynamic response at track transitions analytically. This is because of many variables involved when considering various characteristics of all the supporting layers individually, including non-linearity, inhomogeneity, and plasticity, among others (Indraratna et al. 2019). However, the

numerical modelling approach can investigate the mechanical behaviour of such complex tracks under dynamic loading conditions (Zhang et al. 2016; Heydari-Noghabi et al. 2017).

Hence, in order to develop a numerical model for the design of the transition zone, the 2D FEM layered model was further updated to incorporate the one-step transition from a stiff structure to a soft, as shown in Figure 5.6(a). This figure simulates the track transition shown in Figure 5.2(a), with an abrupt change in stiffness values from 80MN/m/m to 5MN/m/m. The transition divides the model into two portions; the left represents the stiff structure with 80MN/m/m and the right with 5MN/m/m. The rail has been modelled as a continuous beam for the whole 120m length of the model and has been kept the same for both the tracks along with the sleepers. The mechanical properties of all the materials are kept the same as given in Table 4.1, except the E values of ballast, sub-ballast and subgrade that were adjusted to match the track equivalent stiffness on both sides of the transition Table 4.2.

The deformation contour of this transition model under the effect of multiple wheel loading (P =10t) is given in Figure 5.6(b). Results obtained from the FEM show that the softer track undergoes higher deformation (8.4 mm) compared to stiffer track (0.8 mm), as expected. The vertical displacements under the effect of multiple loading and sudden stiffness variation, obtained through both analytical and numerical modelling approaches, are presented in Figure 5.6(c). This shows a good agreement between analytical and numerical results, indicating that the FEM model can be used to predict the differential settlement for a given stiffness variation at transition zones.

The author understands that a comprehensive 3D numerical model for optimizing railway transition zones would be ideal albeit much greater computational time and effort. The current 2D model is a stepping stone towards this goal by serving as a preliminary assessment tool that has been chosen for its practicality and computational efficiency. Despite its limitations, the 2D model is still adequate for determining the needs of the transition zone. Where the longitudinal direction has a very long dimension compared to the transverse direction, the true 3D condition indeed becomes close to 2D Plane Strain that still serves the purpose, as explained by many past studies (Powrie et al. 2007; Sadeghi & Askarinejad 2010).

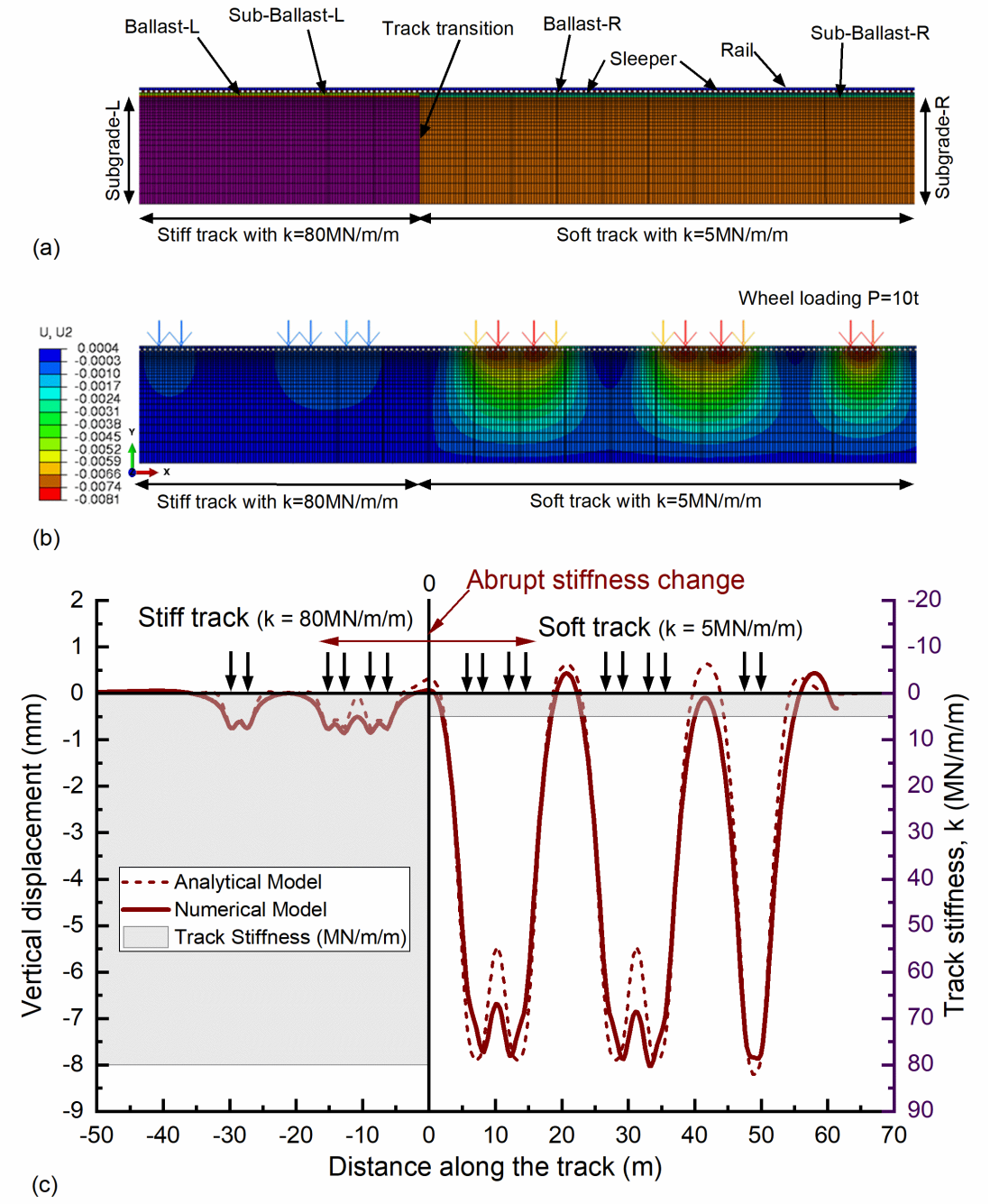

Figure 5.6: (a) 2D FEM model for ballasted track transition for k-80MN/m/m and k=5MN/m/m track; (b) Deformation contours for 2D FEM layered model with abrupt stiffness variation at track transition under *P*=10 tonne; (c) Comparison of vertical displacements of rail track for one-step transition for analytical and numerical modelling.

5.7 Chapter Summary

In this study, minimising differential settlement caused by sudden stiffness variation was analysed based on a beam on an elastic foundation subjected to various train loading conditions using analytical and numerical modelling approaches

In this chapter the dynamic response of a typical transition is investigated through analytical (considering BOEF) and numerical (2D-FEM; layered) modelling approaches. The maximum settlement on both sides of the Junction point (i.e. at $x = 0$), where the stiffness suddenly changes from k = 80 to 5 MN/m/m for the one-step transition, is determined under four-carriage loading (P =10-tonne). Due to the abrupt changes in track stiffness, a significant differential settlement occurred at the transitions, which was further exacerbated by load amplification. The FEM results of vertical displacements were found to be in good agreement with the analytical results. A maximum differential settlement (Δw_{max}) of 7.36mm could be evaluated. From a stability perspective, such differential values would be detrimental in relation to long heavy-haul trains, hence the imperative need for designing interim transition zones.

CHAPTER SIX

6. DESIGN OPTIMIZATION OF TRANSITION ZONES

6.1 Introduction

A transition zone having a smooth and gradual stiffness variation is often provided at track junctions to alleviate the problems associated with such structural discontinuities by minimising the differential settlements (Indraratna et al. 2011; Zuada Coelho 2011; Sañudo et al. 2016; Aggestam & Nielsen 2019), among others. In this regard, a novel approach to smoothen the abrupt stiffness variation along railway transitions has been proposed in this chapter to design a multistep transition zone. The influence of stiffness on track dynamic response applied to transition zones is investigated analytically, considering a beam on an elastic foundation. Vertical track displacements for varying stiffness values under different combinations of axle loads and speeds have been calculated analytically and numerically.

A mathematical process has been introduced to determine the optimum stiffness of each segment to ensure a gradual change in stiffness while minimising the corresponding differential settlement. The proposed methodology has been further validated through the Finite Element Modelling approach and worked-out examples epitomizing the effects of stiffness variation along the number of transition steps. The 2D FEM layered track model was further extended to the multistep transition zone. This model considers varied values of stiffness to simulate the moving wheel load on the layered track, where they are determined on the basis of the analytical approach. This chapter also provides the step-by-step design guidelines for the multistep transition zone, a flow chart, and two worked-out examples.

6.2 Transition Zone Design

To minimise the differential settlements at track transitions, a smooth variation of stiffness values between adjacent sections is required. This can be achieved by

providing a properly designed transition zone comprising multiple segments ensuring gradual variation in their stiffness values. A novel analytical approach for the provision of a multi-step transition zone comprised of various transition segments with varying stiffness values is introduced in this study. The concept of this proposed novel approach for transition zone design is illustrated in Figure 6.1. It presents a transition zone of length L, between a slab track with stiffness k_0 (k_{max}) and a ballasted track with stiffness k_{n+1} (k_{min}). This transition zone is comprised of a given number of transition segments (n), each with length (l). A step-by-step process of the proposed approach and the practical design guidelines for a transition zone is given in the following sections.

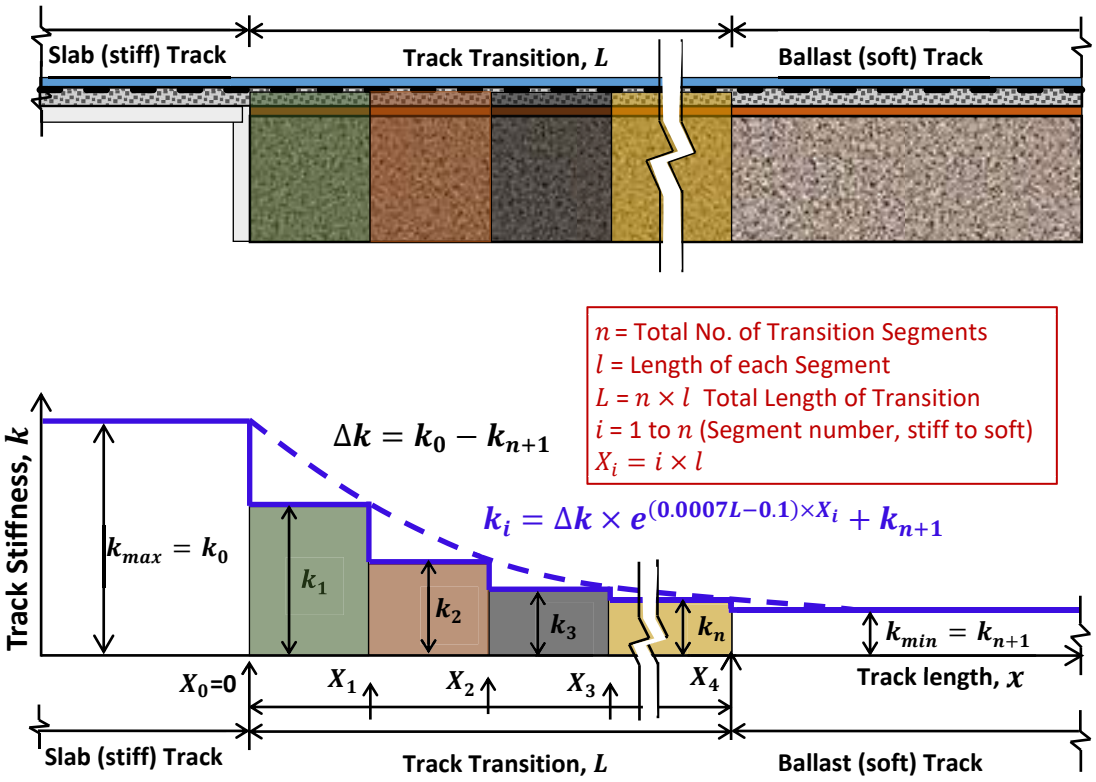

Figure 6.1: Proposed multistep transition zone design for smooth stiffness variation

In this approach, values of n and l are firstly determined, followed by the determination of stiffness of each segment (k_i). The value of k_i is then obtained through an iterative process for a gradual change of Δk and is set to minimise the differential settlement (Δw_i) between any two consecutive transition segments as an

optimisation criterion. In this study, k_i is proposed based on the total stiffness variation at any track transition Δk, and the total number of segments and their lengths (the length of each segment has been assumed constant for simplicity) in the proposed transition zone, as given:

$$k_i = \Delta k \times e^{(0.0007L-0.1)\times X_i} + k_{n+1} \tag{6.1}$$

where, k_i = Track stiffness value of segment i (MN/m/m); $\Delta k = k_s - k_b$: Total stiffness variation at track transition (MN/m/m); $L = n \times l$: Total length of the transition zone (m); n: Total number of transition segments; l: Length of each segment (m); X_i: Distance of endpoint of segment i from track junction, $i = 1$ to n. The derivation of this empirical relation is given in Appendix B.

The output parameters from the proposed method of analysis are: (i) the number of transition steps, (ii) the length of each step, and (iii) the stiffness of each step. The first two parameters will decide the total length of the transition zone, while the third parameter helps to determine the type and specifications of materials used in that specific segment. The overall track stiffness is determined from a combined stiffness of various track elements (Powrie & Le Pen 2016), as given in Equation (4.10), and the stiffness of each track element can be determined using Equation (4.11).

6.3 Design Criterion to Optimise Differential Settlement

An allowable differential settlement ($\Delta w_{allowed}$) is adopted as the main design criterion for transition zones using the proposed approach. This criterion suggests that the differential settlement between any two consecutive transition segments (e.g. difference between the settlements of track with lesser stiffness, w_{soft} and with higher stiffness, w_{stiff}) at a given transition zone must be less than ζ (zeta). In this study, the value of ζ (allowable differential settlement) has been adopted as 5 mm, as suggested by Zhou et al. (2020). However, it is noted that this value can be varied depending on the nature, scope of the project and current standard practices.

Alternatively,

$$\Delta w_{allowed} = w_{soft} - w_{stiff} \tag{6.2}$$

$$\Delta w_{allowed} \leq \zeta = 5.0 \text{ mm} \tag{6.3}$$

Hence, the number of transition segments (n) and the length of each segment (l) need to be selected to ensure that $\Delta w_{allowed}$ criterion, Equation (6.3) is fulfilled. However, if this criterion is not fulfilled for any two consecutive segments, the number of segments needs to be increased until this criterion is fully satisfied for all the segments. This criterion also serves as the initial check for the provision of a transition zone at any track transition. Hence, it can be suggested that there is no specific requirement to provide any transition zone if the differential settlement at that junction is less than ζ.

6.4 Step-by-Step Design Guidelines

Based on the solution for track transition, the following steps are introduced for the design of the track transition zone under train loadings. In addition, a complete flow chart representing the summary of the practical design steps based on the proposed approach is given in Figure 6.2.

Step 1: Find the stiffness variation for the given track transition

$$\Delta k = k_0 - k_{n+1} \tag{6.4}$$

Step 2: Calculate the maximum settlement for each track segment using Equations (4.14) to (4.16) and then maximum differential settlement, Δw_{max} at the given track junction is determined as:

$$\Delta w_{max} = w_{n+1} - w_0 \tag{6.5}$$

Step 3: Apply differential settlement check:

$$\Delta w_{max} \leq \Delta w_{allowed} = \zeta \tag{6.6}$$

However, if $\Delta w_{max} \leq \Delta w_{allowed}$ then the transition zone is not required. Otherwise, move to step 4.

Step 4: Assume the number of segments, n in the transition zone (i.e., starting with $n = 1$)

Step 5: Assume the length, l of each segment ($l = 5m - 10m$), considering the intended design purpose, as suggested by Lei (2017).

Step 6: Calculate the stiffness value for each segment as given:

$$k_i = \Delta k \times e^{(0.0007L - 0.1) \times X_i} + k_{n+1} \tag{6.7}$$

where $i = 1$ to n, $L = n \times l$, X_i = distance of endpoint of segment, i from $x = 0$

Step 7: Calculate differential settlement for every two consecutive segments under various train speeds and load, Δw_i

$$\Delta w_i = w_i - w_{i-1} \tag{6.8}$$

where, w_i: Maximum settlement under wheel load at transition segment i

Step 8: Apply differential settlement check for $\Delta w_{i,\,max}$

$$\Delta w_{i,\,max} \leq \Delta w_{allowed} = \zeta \tag{6.9}$$

if $\Delta w_{i,\,max} > \Delta w_{allowed}$, go back to Step 4 with $n = n + 1$; otherwise, if $\Delta w_{i,\,max} \leq \Delta w_{allowed}$: Total transition length, $L = n \times l$, and stiffness of each segment = k_i

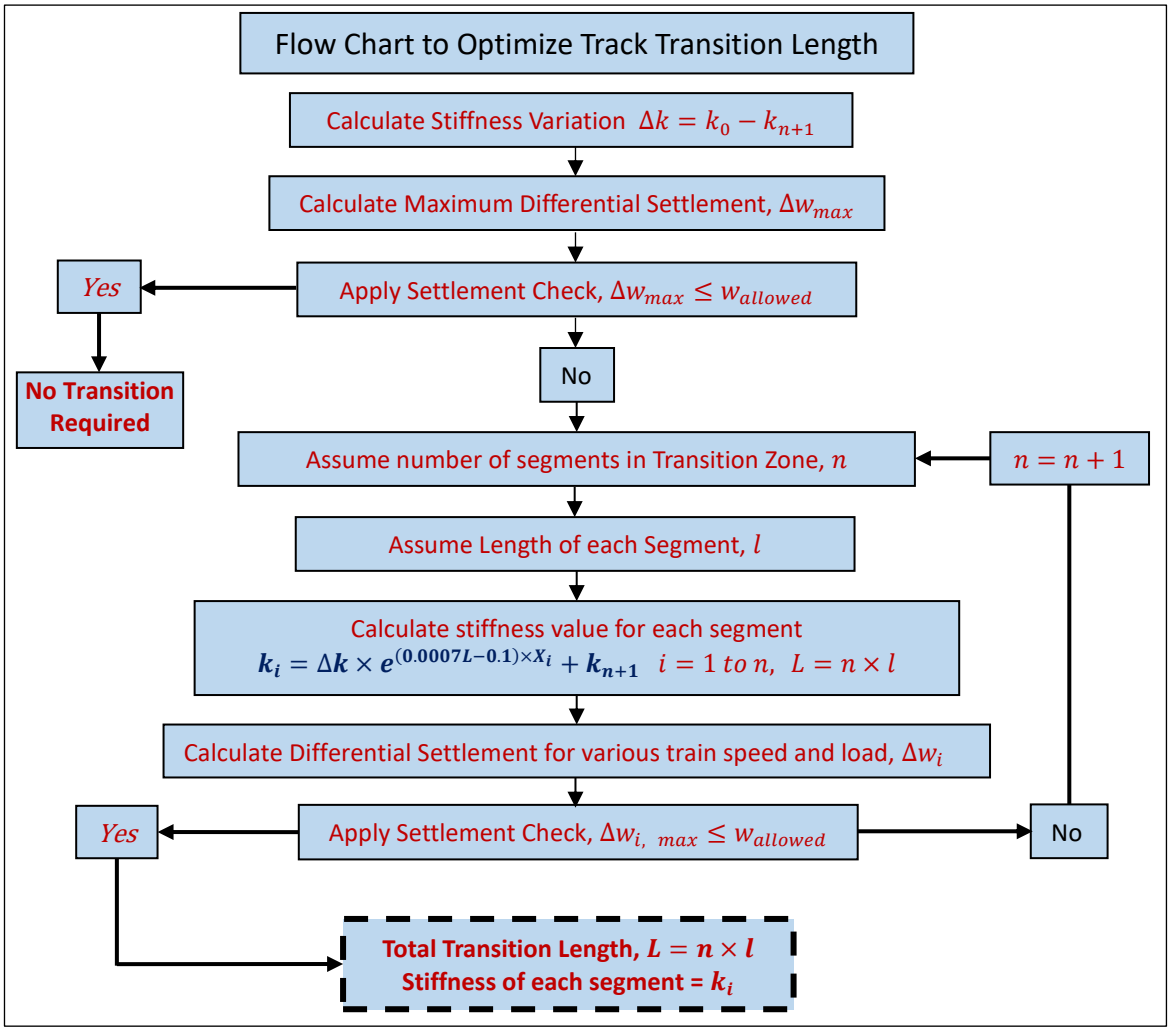

Figure 6.2: Flow chart for the proposed novel approach for the design of track transition zone

6.5 Differential Settlement for Multistep Transition

In order to minimize the differential settlement resulting from a one-step track transition case, a novel approach is introduced for the provision of multi-step transition zones. In this study, a 40m long transition zone, as suggested by Hu et al. (2019), has been adopted for a smooth variation of track stiffness. Furthermore, a five-step transition zone comprising four transition segments ($n = 4$), with length of 10m each ($l = 10m$, mainly considering lower speed, primarily for freight trains, track) is introduced and the stiffness value of each segment was calculated using Equation (6.1), which gives $k_1 = 41.5$ MN/m/m, $k_2 = 22.8$ MN/m/m, $k_3 = 13.6$ MN/m/m, and

$k_4 = 9.2$ MN/m/m, respectively. The corresponding settlements are then determined using Equation (4.13), considering the appropriate length and stiffness value for each segment.

A four-carriage static train with 10-tonne wheel loading is considered in this analysis and the predicted vertical displacements along the track are presented in Figure 6.3, showing the maximum settlement under each wheel load (w_p) and its variation with respect to the stiffness of each segment. It is also noted that with the provision of a transition zone, the track settlement changes gradually from one section to the other. It is observed that without a proper transition zone, the maximum differential settlement (Δw_{max}) was computed as 7.36mm (Figure 5.4), however this Δw_{max} becomes under the maximum allowed value of 5.0mm, for any two consecutive segments when a five-step transition zone is considered. Hence, knowing the settlement values under each wheel load, the differential settlement, Δw_i for all the transition segments can be determined by Equation (6.8). Additionally, these differential settlement values (Δw_i) can be used as a criterion for optimising the design of transition zones.

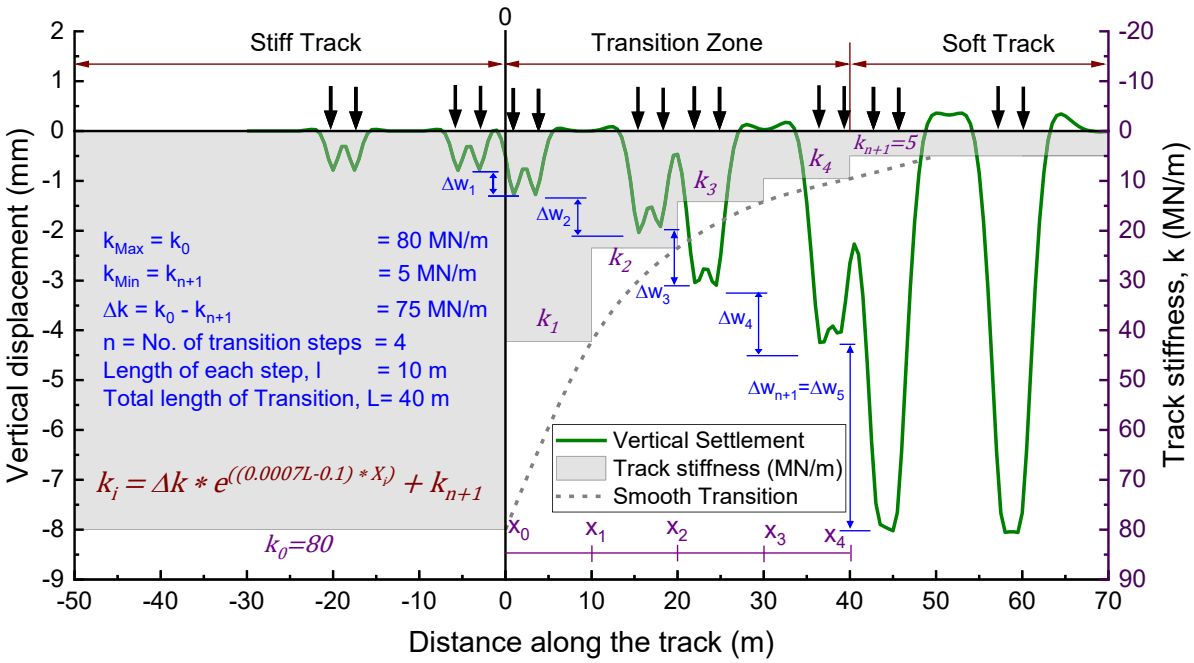

Figure 6.3: Rail deflection for a five-step transition zone under four-carriage static train loading with 10-tonne wheel loadings

6.6 Design Optimisation Through Differential Settlement Criterion

In order to design the transition zone for the given stiffness variation, the differential settlement (Δw_i) between various segments is optimised. The settlement under a given wheel load, (P_p) is compared with the settlement under the previous wheel (P_{p-1}) of a four-carriage train moving from left to right (stiff to soft). Figure 6.4 shows the differential settlement for each wheel load along the track as a result of 10-tonne and 15-tonne wheel loadings. A zero differential settlement line indicates that the settlement under any specific wheel load is the same as the settlement under the previous wheel load, which is mainly due to the same stiffness sections thus resulting in zero differential settlement, such as for $P_1, P_7,\ P_{11}, P_{14}$, among others.

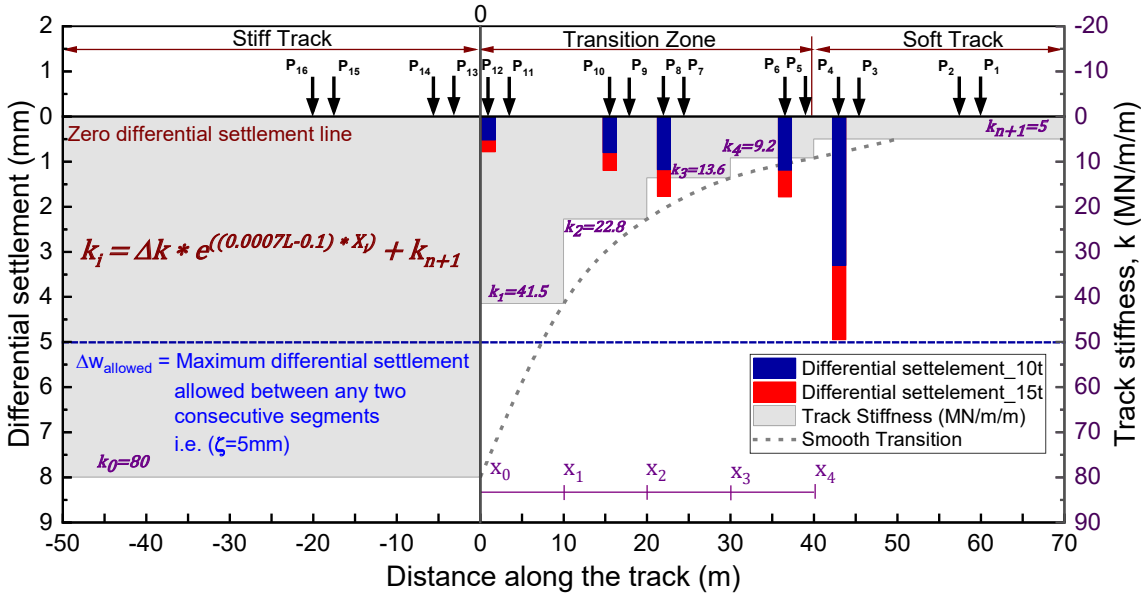

Figure 6.4: Normalised settlement for a five-step transition zone under four-carriage static train loading with 10-tonne and 15-tonne wheel loadings

Another line has also been added to demarcate the maximum allowed settlement at a level where the differential settlement is equal to 5.0mm, (ζ). This line represents the transition zone design criterion, ensuring that the settlement under any specific wheel load must not differ by more than 5mm while compared to the settlement under the previous wheel load. It is observed that differential settlement occurs only when two consecutive wheels are on different track segments with varying stiffness, such as for

P_4, P_6, P_8, P_{10}, & P_{12}. However, the values are below the allowable differential settlement ($\Delta w_{allowed}$) for both the train loadings, that indicates the effectiveness 0f the provision of the five-step transition zone through smooth stiffness variation.

6.7 Design Optimisation Through Numerical Modelling

The 2D FEM model is further developed for the transition zone design optimisation, incorporating a multi-step transition zone obtained through the analytical approach introduced in this study. In this regard, the total number of transition segments, their length and stiffness values are determined by following the first six steps of the proposed approach (Figure 6.2). These values are then incorporated into the FEM model to update it for a multistep transition zone, which can be analysed in detailed considering various characteristics of the supporting layers under dynamic loads of moving trains in different directions.

In this study, the numerical model (Figure 5.6a) was further updated for a 40m long five-step transition zone with four transition segments as shown in Figure 6.5(a). The model represents a gradual variation of abrupt stiffness change from k_0 to k_{n+1} through the provision of a transition zone consisting of four segments with stiffness values varying from k_1 to k_4.

It is worth mentioning that the stiffness values of these segments are determined through the analytical approach introduced in chapter 4; Equations (4.10) & (4.11), and they are then utilised to calculate the material properties of substructural layers as given in Table 4.2. This model was solved for the vertical displacements under the effect of multiple wheel loading (P =10t) and the results of deformation contour are shown in Figure 6.5(b). It can be observed that there is a gradual increase in the intensity of settlements and the spread of deformation contours from stiff track to soft track substructure.

The comparison for the vertical displacements of tracks subjected to 16 wheels loading obtained through analytical and numerical modelling approaches is presented in Figure 6.6. It is seen that the predicted settlements obtained from FEM simulation are in good agreement with those calculated by the analytical method, indicating the reliability of

the numerical model that can be applied in transition zone design optimisation, considering the multiple wheel loading and layered track substructure.

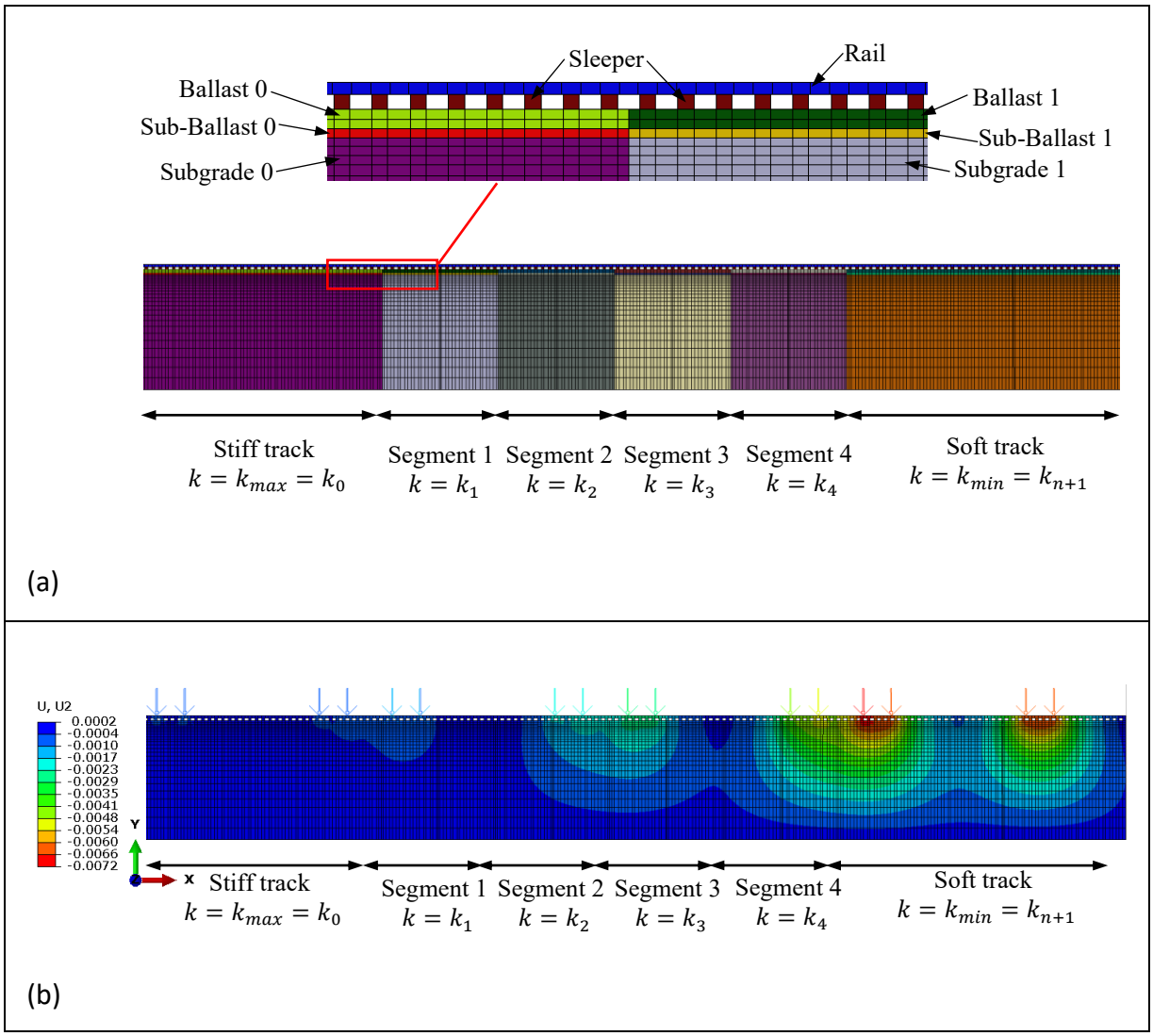

Figure 6.5: (a) 2D FEM model for 5-steps ballasted track transition for k-80MN/m/m to k=5MN/m/m; (b) Deformation contours for 2D FEM layered model for 5-steps ballasted track transition for k-80MN/m/m to k=5MN/m/m

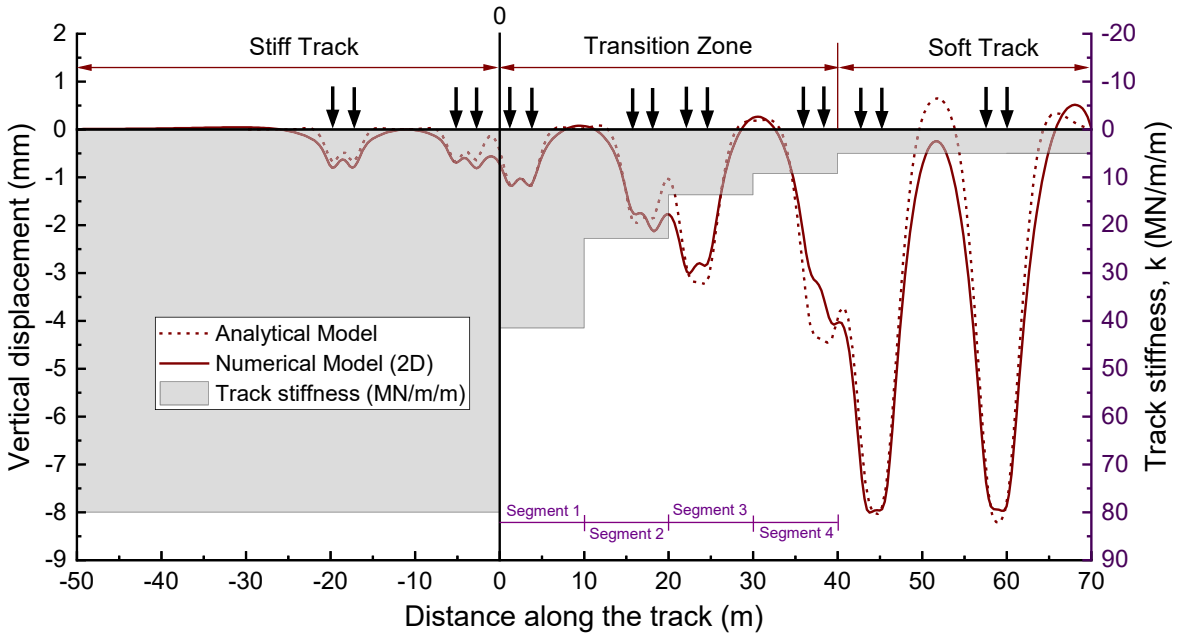

Figure 6.6: Comparison of vertical displacements of rail track for 5-step transition for analytical and numerical modelling

6.8 Practical Implications

A transition zone is essential to minimize the effect of abrupt variations in track stiffness, for instance, in the case of a gradual transition from a ballast section to a much stiffer slab track or a bridge deck. In essence, minimising the differential settlement through a gradual variation of stiffness over a number of transition zone sections is key for ensuring track stability. As explained in the flow chart (Figure 6.2), the key input parameters must correctly assess and quantify the optimum track stiffness on both sides of the transition based on fundamental mechanics and where possible supported by field data. Indeed, the proposed method will also assist in implementing the appropriate ground improvement methods to attain the required magnitudes of stiffness, as explained further via two worked-out examples below.

6.9 Worked-out Design Example-1: Design of Multistep Transition Zone between Flexible (Ballasted) Track Rigid (Slab) Track

To demonstrate the capability of the given approach, the design of a transition zone between a slab track and a ballast track is carried out. The track stiffness values for slab track and ballast track have been considered as $k_{slab} = 80$ MN/m/m, and $k_{ballast}$ =5 MN/m/m as considered by Selig & Li (1994).

Input design parameters:

- Stiffness of stiffer track section (slab track), $k_{slab} = k_0 = 80$ MN/m/m
- Stiffness of soft track section (ballast track), $k_{ballast} = k_{n+1} = 5$ MN/m/m
- 30-tonne train axle loading, $P_{Axle} = 20$ tonne
- Train speed, $v = 80$ km/h
- Allowable settlement enhancement factor, $\Delta w_{allowed} = 5$ mm

Design calculation:

Step 1: Find a stiffness variation for the given track transition using Equation (6.4):

$$\Delta k = k_0 - k_{n+1} = 75 \text{ MN/m/m}$$

Step 2: In order to check the requirement of a transition zone, we will find the differential settlement at the given track junction using Equations (4.14)-(4.16), which result in:

$$\Delta w_{max} = w_{n+1} - w_0 = 10.3 \text{ mm}$$

Step 3: Apply differential settlement check:

$$\Delta w_{max} = 10.3 > \Delta w_{allowed}$$

Check failed, so we need to design the track transition following the next steps

Step 4: $n = 1$

Step 5: $l = 10m$

Step 6: Calculate stiffness value for segment 1 using Equation (6.7):

$$k_1 = 75 \times e^{(0.0007 \times 10 - 0.1) \times 10} + 5 = 34.6 \text{ MN/m/m}$$

Step 7: Calculate the differential settlement ratio for every consecutive segment

$$\Delta w_1 = w_1 - w_0 = 1.04 \text{ mm}$$
$$\Delta w_2 = w_2 - w_1 = 8.7 \text{ mm}$$

Step 8: Apply differential settlement check:

$$\Delta w_{max} = \Delta w_2 = 8.7 > \Delta w_{allowed}$$

Check failed, so we need to go back to Step 4 with increased n as $n = n + 1$

Step 4a: $n = 1 + 1 = 2$

Step 5a: $l = 2m$

Step 6a: $k_1 = 36.7$ MN/m/m, $k_2 = 18.4$ MN/m/m

Step 7a: $\Delta w_1 = 0.9$, $\Delta w_2 = 1.4$ and $\Delta w_3 = 7.7$ (mm)

Step 8a: $\Delta w_{max} = \Delta w_3 = 7.7 > \Delta w_{allowed}$

Check failed, so we need to go back to Step 4 with increased n as $n = n + 1$

Step 4b: $n = 2 + 1 = 3$

Similarly, following steps 5b to 7b, we get

Step 8b: $\Delta w_{max} = \Delta w_4 = 5.7 > \Delta w_{allowed}$

Check failed, so we need to go back to step 4 with increased n as $n = n + 1$

Step 4c: $n = 3 + 1 = 4$

Step 5c: $l = 10m$

Step 6c: $k_1 = 41.5$ MN/m/m, $k_2 = 22.8$ MN/m/m, $k_3 = 13.6$ MN/m/m, & $k_4 = 9.2$ MN/m/m

Step 7c: $\Delta w_1 = 0.7$, $\Delta w_2 = 1.13$, $\Delta w_3 = 1.68$, $\Delta w_4 = 1.69$, & $\Delta w_5 = 4.7$ (mm)

Step 8c: Applying differential settlement check:

$$\Delta w_{max} = \Delta w_5 = 4.7 \leq \Delta w_{allowed} = 5 \text{ mm}$$

Check passed

This shows the maximum differential settlement between any two consecutive

segments in the newly designed transition zone is less than the allowable limit. Hence, the final design of the transition zone considering a gradual stiffness variation at the junction of the given slab and ballast track is as follows:

- Total number of transition segments, $n = 4$ (which gives the total number of transition steps as 5)
- Length of each transition segment, $l = 10\text{m}$
- The total length of the transition zone, $L = n \times l = 40\text{m}$

Track stiffness of each segment:

$k_0 = 80\ \text{MN/m/m},$ $k_1 = 41.5\ \text{MN/m/m},$ $k_2 = 22.8\ \text{MN/m/m},$
$k_3 = 13.6\ \text{MN/m/m},$ $k_4 = 9.2\ \text{MN/m/m},$ & $k_5 = 5\ \text{MN/m/m}$

6.10 Worked-out Design Example-2: Stiffness Variation and Transition Steps

In order to investigate the effect of total stiffness variation and the number of transition steps in any transition zone, the differential settlement for a multi-step transition zone is calculated by adopting Equations (4.14), under 15-tonne wheel load, for twelve different cases. Three types of transition zones are considered based on their number of transition steps: (i) 4-step transition, (ii) 5-step transition, and (iii) 6-step transition. Each of them is then solved for four different cases based on the total stiffness variation between stiff (concrete bridge deck) and soft (ballast) track sections; (i) $\Delta k = 75\ \text{MN/m}$ considering $k_s = 80\ \text{MN/m/m},\ \&\ k_b = 5\ \text{MN/m/m}$, (ii) $\Delta k = 60\ \text{MN/m/m}$ considering $k_s = 80\ \text{MN/m/m},\ \&\ k_b = 20\ \text{MN/m/m}$, (iii) $\Delta k = 45\ \text{MN/m/m}$ considering $k_s = 80\ \text{MN/m/m},\ \&\ k_b = 35\ \text{MN/m/m}$, and (iv) $\Delta k = 30\ \text{MN/m/m}$ considering $k_s = 80\ \text{MN/m/m},\ \&\ k_b = 50\ \text{MN/m/m}$.

The results of all these twelve cases for normalised differential settlement between various transition segments (steps) are presented in Figure 6.7. It is seen that there is a significant decrease in maximum differential settlement (from 6.4mm to 4.9mm) for a 4-step transition with $\Delta k = 75\ \text{MN/m/m}$, by increasing the number of transition steps from 4 to 5. Based on Figure 6.7, for all these cases, there is a substantial decrease in differential settlement with the increase in the number of steps in a transition zone. Similarly, it can also be noted that irrespective of the total number of steps, the higher

the stiffness variation at track transition, the larger the differential settlement occurring between various transition segments. This worked-out example demonstrates that the differential settlement within the transition zone can be controlled up to the maximum allowed value (e.g. $\zeta = 5$mm) by increasing the length of the transition zone with the addition of more transition segments for a gradual variation of track stiffness along the critical track sections.

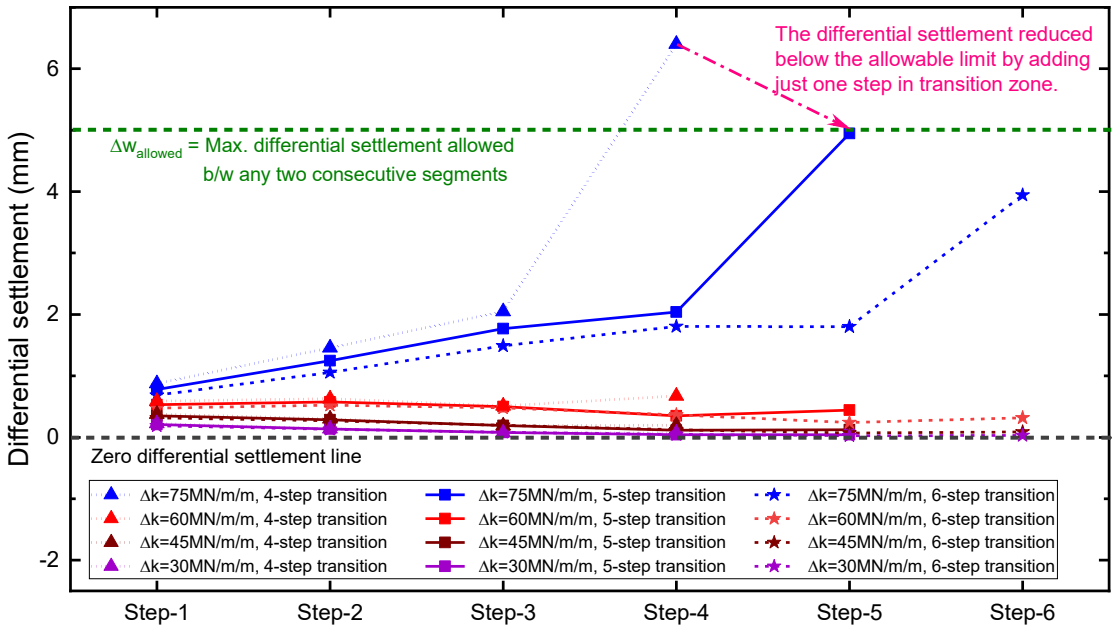

Figure 6.7: Effect of stiffness variation (Δk) and number of transition steps on the design of transition zone

6.11 Chapter Summary

This chapter presents the design optimisation of transition zones through a novel approach, providing step-by-step design guidelines and optimisation criteria. An optimization process was introduced to determine the required stiffness (k_i) for each segment to compute the minimum differential settlement. This process ensured that the number of transition steps could be selected optimally so that the differential settlement between any two consecutive segments would be less than the allowable differential settlement, ζ.

The FEM results of vertical displacements were found to be in good agreement with

the analytical results. As the actual train loading was simulated on a layered track (with measured geotechnical parameters), the soil-structure interaction and geotechnical aspects of a typical track could be properly captured in this FEM analysis. This validation proves that the BOEF approach can be reliably used for analysing the behaviour at transition zones for a given set of computational factors (number of steps, length, stiffness); thus, a minimal differential settlement could be achieved. This chapter also highlights the research significance through its practical implications along with the worked-out design examples.

CHAPTER SEVEN

7. THREE-DIMENSIONAL MODELLING OF TRACK TRANSITIONS

7.1 Introduction

In railways, a Three-dimensional (3D) numerical model becomes necessary to capture more complex track geometry and dynamic response under actual train loadings that are rather transient and dynamic (Kouroussis et al. 2011), especially, while the vibrations generated by the dynamic loads are amplified due to increased train speeds (Thach et al. 2013; Sayeed & Shahin 2016). However, it requires a high level of computational power to create and analyse an accurate and detailed model. Nevertheless, it has become an essential tool in many fields and with improved computing power and software capabilities, its use is expected to continue to grow more widely in the future. The extended utilisation of 3D modelling in railways has been discussed in Chapter 3 and is presented in Table 3.1 for comparison purposes.

In this Chapter, 3D finite element numerical modelling is utilised for the analysis of a complex system of track transitions that would have been much more difficult to study analytically or experimentally. It helped in the design optimization of multistep transition zones for various train speeds and loads to improve their performance and reliability. In order to fulfil the requirement of high level of computational power for this analysis, interactive high-performance computing (iHPC) resources, provided by the University of Technology Sydney (UTS), were utilised in an efficient manner. The main content of this Chapter is summarised and to be submitted as a journal article, titled “Enhancing multi-step transitions through comprehensive analytical solution and advanced 3D numerical modelling techniques”.

7.2 3D FEM Model

In order to perform a detailed investigation of the complex dynamic response of transition zones, under moving train loads, a comprehensive plan for 3D FEM

modelling has been devised and is presented in this chapter. Firstly, a 3D model for a conventional ballasted track is developed and calibrated with an analytical model, and then further validated with actual field measurement data. Secondly, this model is extended to incorporate a one-step transition from stiff to soft structure and analysed under various train loads moving at various speeds. Infinite boundary elements are also incorporated in this model to minimise the boundary effect on the dynamic analysis. Thirdly, this model is then further developed to incorporate the multistep transition zone as designed by the analytical approach presented in Chapter 6. A detailed analysis is then performed on these models to investigate the efficiency of the transition zone for various train loads and speeds. The details of the geometry, material properties, mesh and boundary conditions of these models are presented in the following sections.

7.2.1 Track Geometry

The first 3D model, with a total length, width, and height of 10m, 5m and 4.68m, respectively, was developed for a conventional ballasted track using FEM software ABAQUS, as shown in Figure 7.1. Due to the symmetric nature of the track in the transverse direction (i.e. parallel to sleepers), the track model has been established in half in Y-Z Plane (longitudinal Z-axis) considering the symmetric boundary at the centre of two steel rails. The steel rail is modelled as a standard I-section, for the UIC60 profile with 60kg/m as the unit mass (Shahraki et al. 2015). There are 17 reinforced concrete sleepers, each measuring 0.26 metres in width, 0.23 metres in height, and 1.25 meters in length, placed at 0.6 meter centre-to-centre spacing (Nimbalkar & Indraratna 2016). Ballast and sub-ballast layers have been simulated with thicknesses of 300 mm and 150 mm, respectively, and are situated on top of two homogenous subgrade layers with a thickness of 3m and 1m, respectively. The train load has been simulated as a rigid block sliding, from left to right, on the top surface of the steel rail. This model is utilised mainly for calibration purposes.

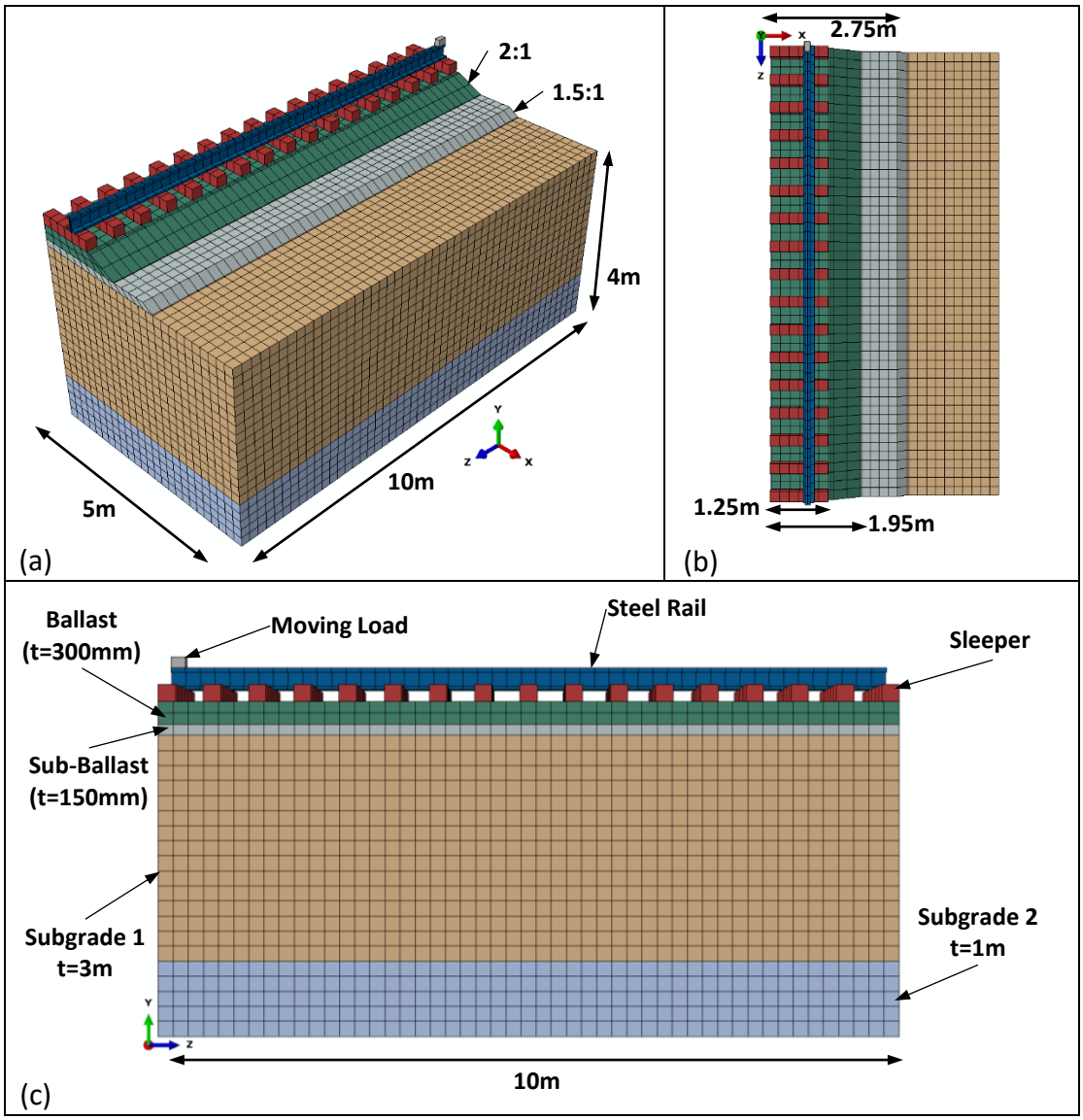

Figure 7.1: 3D FEM mesh for modelling of a conventional ballasted track: (a) Three-dimensional view, (b) Top view, (c) Front view

The length of the model (Figure 7.1) is doubled to incorporate one-step transition from a stiff structure (with stiffness, k = 80 MN/m/m) to a soft structure(stiffness, k = 5 MN/m/m). Hence, the total length of the model became as 20m and the total number of sleepers increased from 17 to 34, as shown in Figure 7.2. The model has been divided into two parts at its mid-length; where the left half (in positive Z direction) indicates the stiffer track and the right refers to the softer track. Therefore, the letters 'L' and 'R' in the figure descriptions indicate the left and right parts, respectively. All the other dimensions are kept the same as the conventional ballasted track (Figure 7.1). The train wheel load has been simulated as a rigid circular block rolling on the steel

rail. This model represents the track transition for sudden stiffness variation from a stiff track to a normal ballasted track (less stiff) to investigate the requirement of the transition zone based on the corresponding differential settlements mesured at their junction.

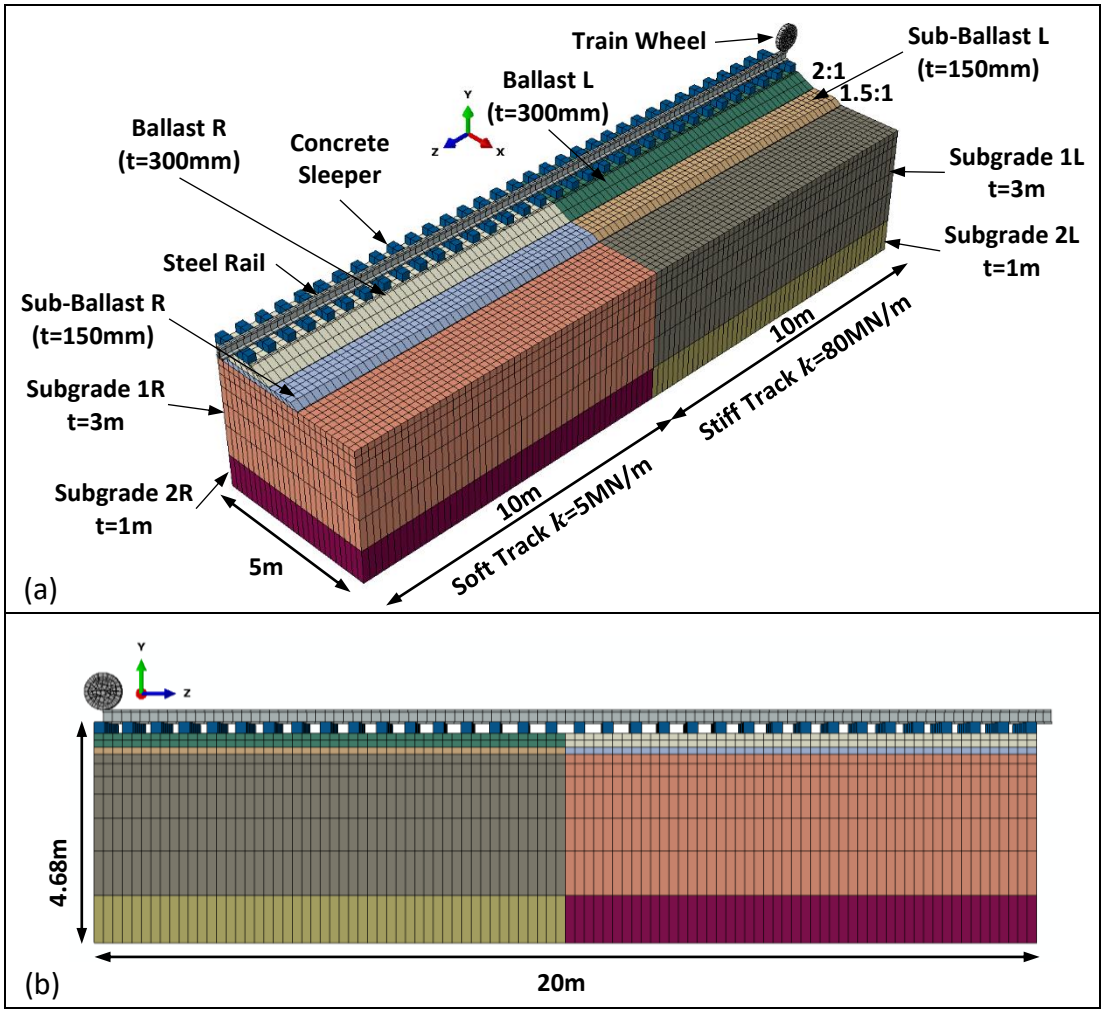

Figure 7.2: 3D FEM model for one-step track transition having stiffness of k-80MN/m/m and k=5MN/m/m tracks: (a) Three-dimensional view, (b) Front view

It should be noted that the two models described above are fairly straightforward, requiring less computational time and resources but being adequate to explore the necessity of providing a transition zone for any track. However, a more detailed model is required to optimise the design of the multistep transition zone (obtained through the proposed novel approach presented in Chapter 6) for various train speeds, loads, and directions of train movement. In order to achieve this goal, a comprehensive 3D model of a typical multistep transition zone is then developed, as presented in Figure 7.3. This figure shows the geometrical dimensions and details of the 130 meters long

full-track model incorporating various transition segments. This model is capable of accommodating up to 7-step (6 segments) transition zone with 10 meters segment length, or 13-step transition zone with 5 meters segment length. It also has the capacity to adjust the length of each segment in the multiple of 5 meters. Hence, this model can be utilised to optimise the design of any transition zone by changing the material properties of its different sections as per the design. Additionally, this model is flexible with the inclusion of infinite elements at the boundaries on its all sides to minimise the boundary effect due to energy absorption. These infinite elements introduce small viscous dampers that absorb the incident waves, hence reducing the wave reflection. Currently, this model has been developed for a 5-step transition zone with four transition segments (as proposed above in Chapter 6), each with 10 meter in length.

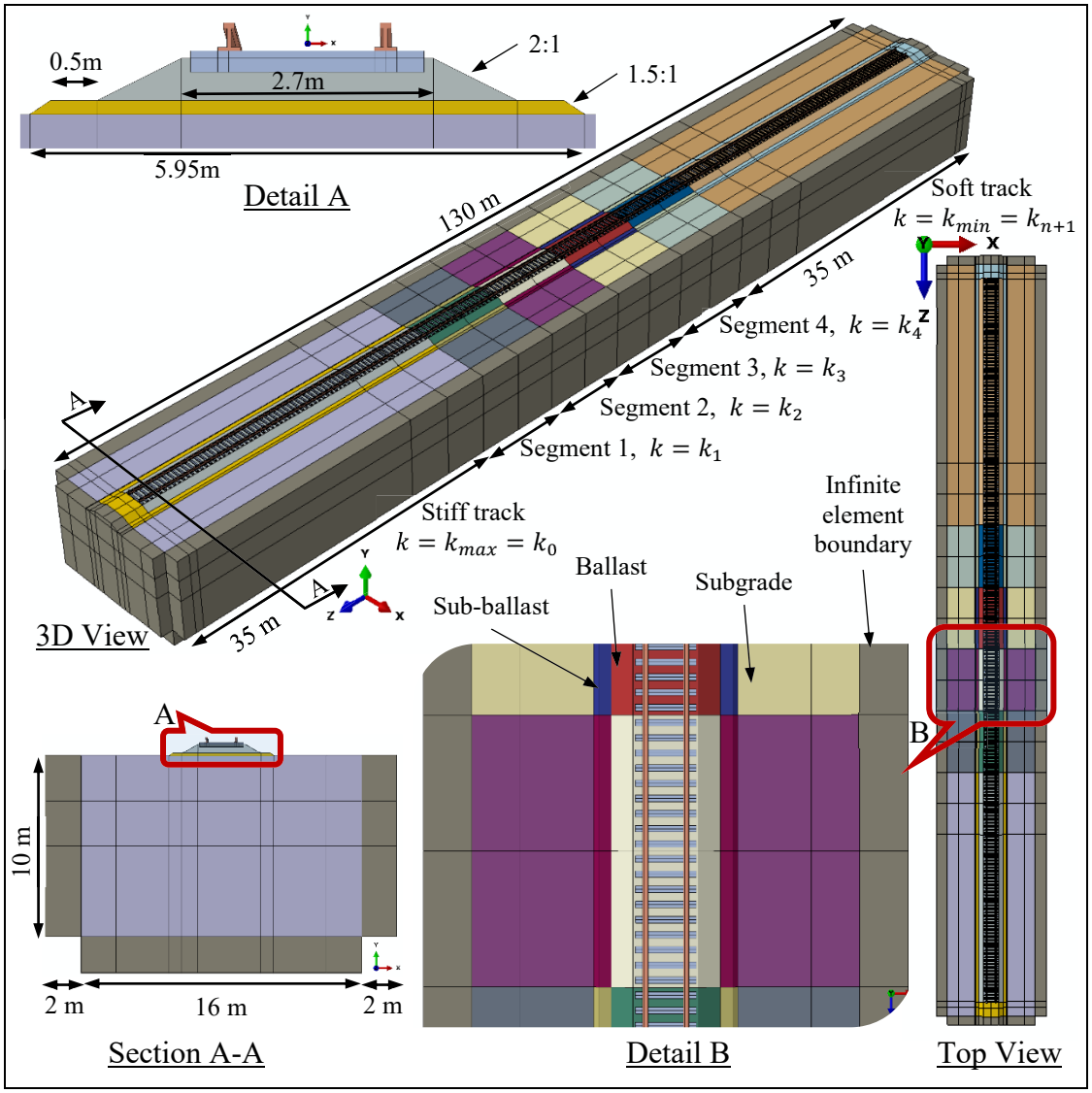

Figure 7.3: Three-dimensional model of a proposed multistep transition zone

7.2.2 Material Properties and Parameters

In this 3D FEM model, the steel rails and concrete sleepers are modelled as linear-elastic materials, as commonly adopted by other researchers (e.g., Li et al. 2018). However, in order to accurately represent the damping and nonlinear behaviour of track substructure, the ballast, sub-ballast and subgrade are modelled as elasto-plastic materials with the inclusion of damping behaviour (Nimbalkar et al. 2012; Lamprea-Pineda et al. 2021). As the ballast is a granular material and train loading is cyclic (repeated) in nature, so its dynamic response and strength depend on the train movement and the corresponding stresses and strains (Leshchinsky & Ling 2013; Shih et al. 2019). Therefore, Drucker-Prager (DP) yield criterion has been considered for ballast, whereas, sub-ballast and subgrade materials have been simulated considering Mohr-Coulomb (MC) criterion.

In order to provide the damping to the substructural materials, the Rayleigh viscous damping technique is utilised (Chumyen et al. 2022), where the global damping matrix (C) is related to the mass matrix (M), and stiffness matrix (K), through Rayleigh damping coefficients; α and β, as shown in Equation (4.9). The geometry and model input parameters for various components and the segments are obtained from Table 4.1 and adjusted for the required design parameters using Equations (4.10) & (4.11) and are given in Table 4.2.

In the interest of simplifying the analysis and maintaining a consistent approach, the damping coefficients have been kept uniform for all subgrades, regardless of their stiffness variations. While this approach may not fully capture real-world variability in damping, it provides a reasonable approximation for investigating the track's dynamic behavior and differential settlement.

To simulate the wheel load for moving trains, a point load is applied to a rigid block sliding on the top surface of the rail in the longitudinal direction. The predetermined speed of this block corresponds to the actual train speed.

7.2.3 Geometry, Mesh and Boundary Conditions for a Track at Transition Zone

In order to minimize the computational effort and owing to the symmetric nature of the track in transverse direction, the track model has been established in half in Y-Z Plane (longitudinal Z-axis) considering the symmetrical boundary at the centre of two rails. The model is further divided into finite element mesh and infinite element mesh domains, as shown in Figure 7.4. The finite element mesh domain is modelled with the hexahedral (8–nodded) elements (linear brick) with hourglass control and reduced integration (C3D8R), and the infinite element mesh domain is modelled by one-way infinite elements (CIN3D8). Furthermore, sleepers, ballast and sub-ballast are discretised for finer mesh, whereas the coarser mesh is adopted near the boundaries.

A gradual transition is introduced between finer and coarser mesh discretisation with quadratic tetrahedral elements (C3D10M). Hence, the discretised mesh grid has 119555 nodes and 73848 elements in total for the multistep transition model. In order to improve the analysis accuracy, the node continuity at the interface is well maintained between all the layers (Abaqus 2020). Additionally, surface-to-surface contact was established between various layers of the track model using a penalty method to ensure the accurate transmission of normal and shear stresses at the interface (Hibbitt et al. 2014). Similarly, a tie constraint is established between the bottom of the steel rail and the top of sleepers, whereas, the sleepers are connected to the surrounding ballast as “hard contact” with “rough” friction. The interaction between the rigid block and rail is established as “hard contact” with no friction. In total 16 rigid blocks are introduced to apply the wheel load of four moving carriages. These blocks slide on the rail at a specific rate as per the train speed and configuration.

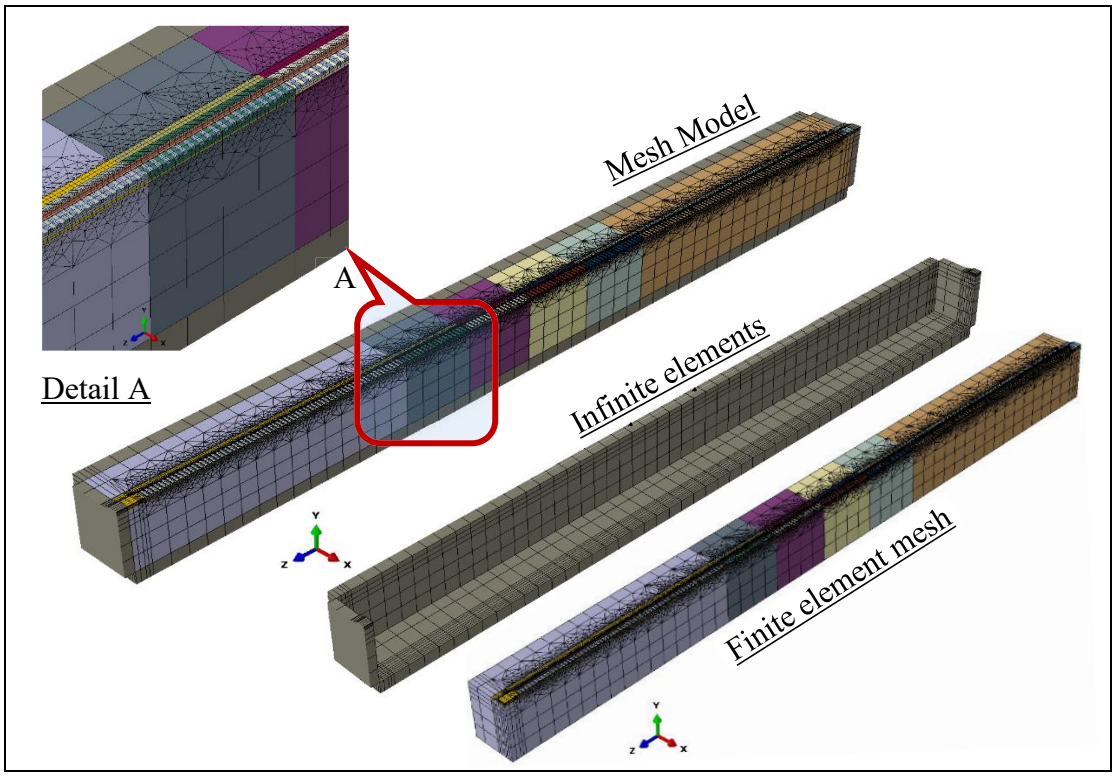

Figure 7.4: Mesh configurations of 3D FEM model for multistep transition zone

7.3 Model Validation

The first model, with relatively smaller dimensions, was developed to calibrate the 3D modelling parameters with the 2D numerical model and the analytical modelling results. To determine the maximum settlement under the applied loading, a static wheel load was applied at the centre of the 3D model, as depicted in Figure 7.1, in the form of a point load. Material parameters for each track layer were set to an equivalent track stiffness of 10 MN/m/m. The predicted deformation contour for the corresponding settlements and the deformed shape of the 3D FE layered model under 10-tonne wheel loading is shown in Figure 7.5(a).

The same model was analysed for two different wheel loadings, 10 tonnes and 20 tonnes. The maximum settlements were then plotted and compared to the maximum settlements obtained through the analytical and 2D numerical modelling, as illustrated in Figure 7.5(b). It was found that the 3D model predicted a maximum settlement of 3.89 mm under 10 tonnes wheel loading, which is almost similar to the one calculated by the analytical solution (3.90 mm). In addition, the beam on springs model and the

2D FE model predicted maximum settlements of 3.84 mm and 3.86 mm, respectively, for the same loading which shows an identical prediction. A similar trend was observed for the 20-tonne wheel loading. The similarity in settlement observed, especially between the 2D and 3D models, can be attributed to the nature of the static loading condition employed in this study.

Under static loading, the track's response to applied loads is primarily governed by the vertical stiffness of the track components and the underlying subgrade. In such cases, the lateral and longitudinal behaviour of the track may have a relatively lesser influence on the overall deformation. However, the 3D model introduces additional degrees of freedom that may influence lateral and longitudinal effects under dynamic loading conditions. Additionally, it can be noted that the settlements predicted by 3D modelling is more reliable as it is closer to the one predicted by analytical modelling and, therefore, can be used with confidence in further investigations.

The updated 3D model, now with double the length, as shown in Figure 7.2, has been validated for moving loads through a comparison with the data presented by Li et al. (2018). The model was refined by taking into account elasto-plastic material parameters and identical loading conditions to ensure a fair comparison between the two studies. The dynamic behaviour of the 3D track model, with an equivalent stiffness of 10MN/m/m, was then evaluated by analysing the vertical displacement at a specific location when subjected to a four-carriage load moving at a speed of 200km/h. The comparison of results, shown in Figure 7.6, demonstrates a reasonable agreement between the two modelling approaches under similar loading conditions. As a result, this current 3D FE model can be utilized to study the dynamic response of track transitions and optimize the design of transition zones for various train speeds and loading scenarios.

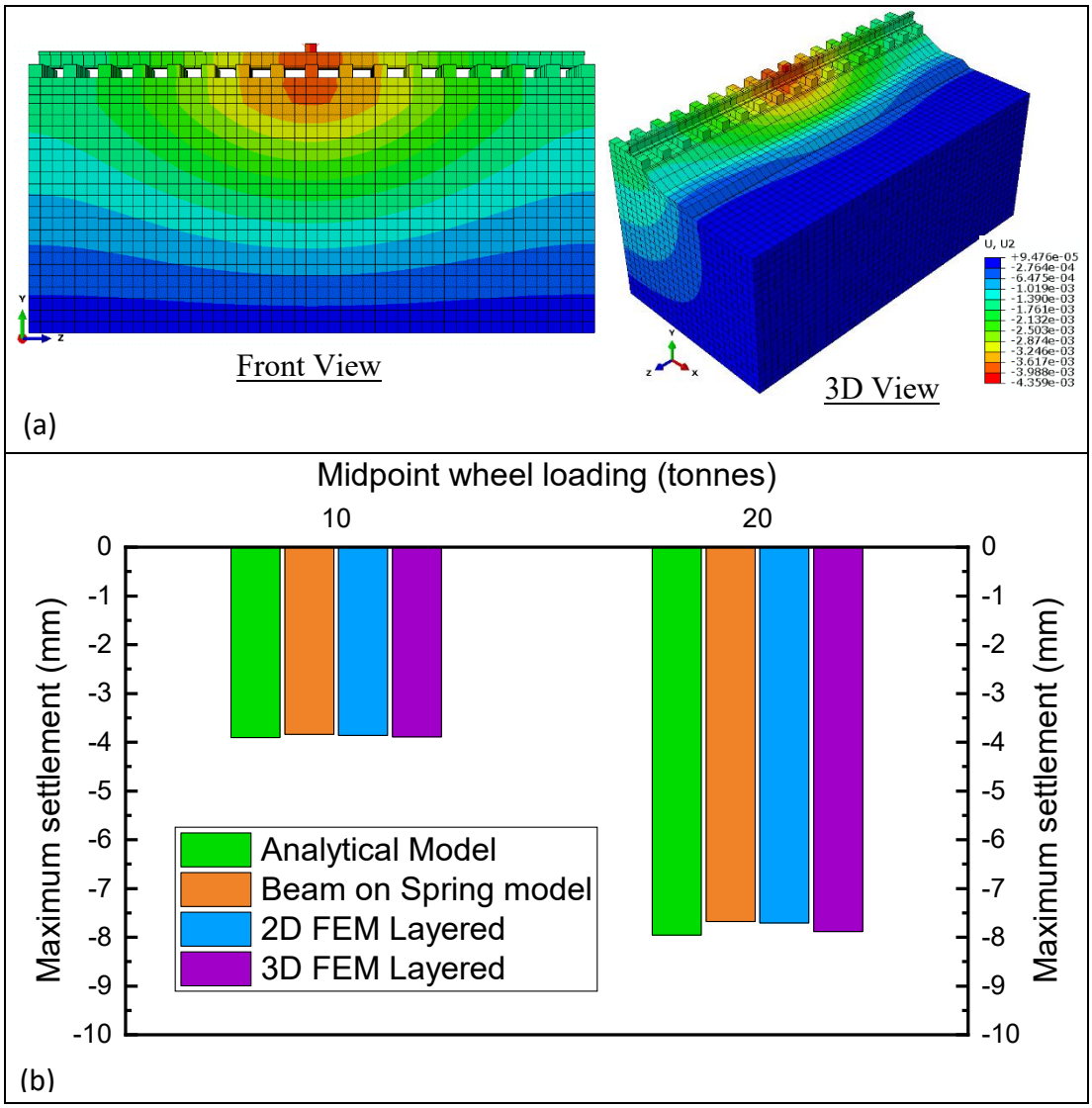

Figure 7.5: (a) Deformation contours for 3D FEM layered model with track stiffness as 10MN/m; (b) Comparison of maximum settlements obtained through analytical and numerical modellings

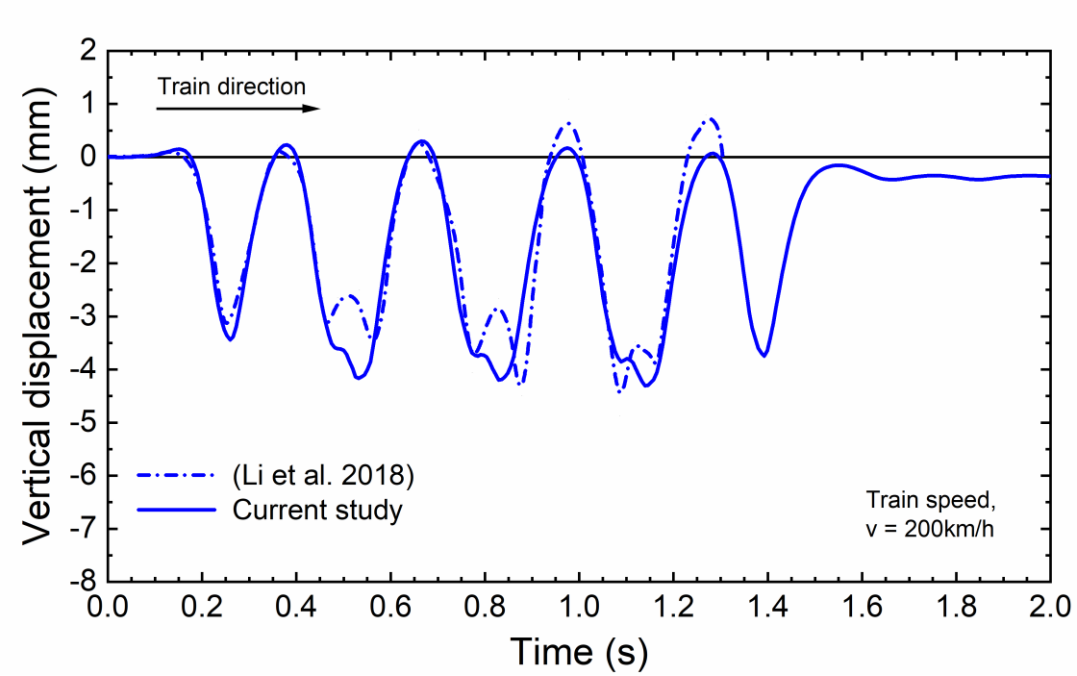

Figure 7.6: Comparison of vertical displacements of rail track with equivalent track stiffness as 10MN/m/m under four-carriage loading moving at 200km/h

7.4 Results and Discussion

The use of 3D finite element models has proven invaluable in optimizing the design of multi-step transition zones for improved performance and reliability under varying train speeds and loads. The high computational demands of these models were solved by using the interactive high-performance computing (iHPC) facilities provided by the University of Technology Sydney (UTS) to run ABAQUS models, ensuring efficient and effective analysis. The subsequent sections present the results and insights gained from this dynamic analysis.

7.4.1 Dynamic Displacements for One-Step Transition

The first step in designing a transition zone is to determine its requirements based on the maximum differential settlement that occurs at a track transition. This can be done by using a simple but effective 3D numerical model, as depicted in Figure 7.2. This model requires fewer computational resources and thus yields faster results, especially for a one-step transition. For instance, if there is a sudden change in track stiffness

values from k=80 MN/m/m to k=5 MN/m/m, the model predicts a differential settlement of around 8mm under a 10-tonne wheel load travelling at 180 km/h (Figure 7.7)

To calculate the differential settlement, the maximum vertical displacements on either side of the transition are analyzed considering the track's dynamic response subjected to moving loads, as shown in Figure 7.7. The figure displays the deformation contours for a 3D FEM layered model with a sudden change in stiffness values from k=80 MN/m/m to k=5 MN/m/m at the track transition under a moving wheel load of P=10 tonne, along with the corresponding vertical displacements for the stiff and soft tracks. It can be seen that the maximum midspan settlement on the stiffer side is approximately 0.7mm, while on the softer side, it is up to around 8.7mm, resulting in a total differential settlement of 8mm. By comparing this differential settlement with the maximum allowed value of 5mm, as per Zhou et al. (2020), the requirement of a transition zone at this junction is needed. Therefore, it can be concluded that this model can effectively determine the requirements of a transition zone for tracks under different loading conditions.

7.4.2 Dynamic Analysis of Multistep Transition Zone

The provision of a transition zone is imperative when differential settlements exceed the acceptable limits at track junctions. To design an effective transition zone, it is necessary to first determine the total differential displacement. The guidelines outlined in Chapter 6 can then be followed to create a multi-step transition zone. For the specific track transition studied in this chapter, the step-by-step design process is outlined in Worked-out Design Example 1 (Chapter 6).

To optimize the design, the comprehensive 3D numerical model depicted in Figure 7.3 should be updated to reflect the design requirements. In this study, a 5-step transition zone consisting of four segments, each 10m in length, was incorporated into the model. The model was then analyzed for a four-carriage train with 16 wheels, traveling at speeds of 60, 100, 150, 200, and 250 km/h, and subjected to two types of wheel loading (10 and 20 tonnes). The results of these analyses are presented in the subsequent

sections.

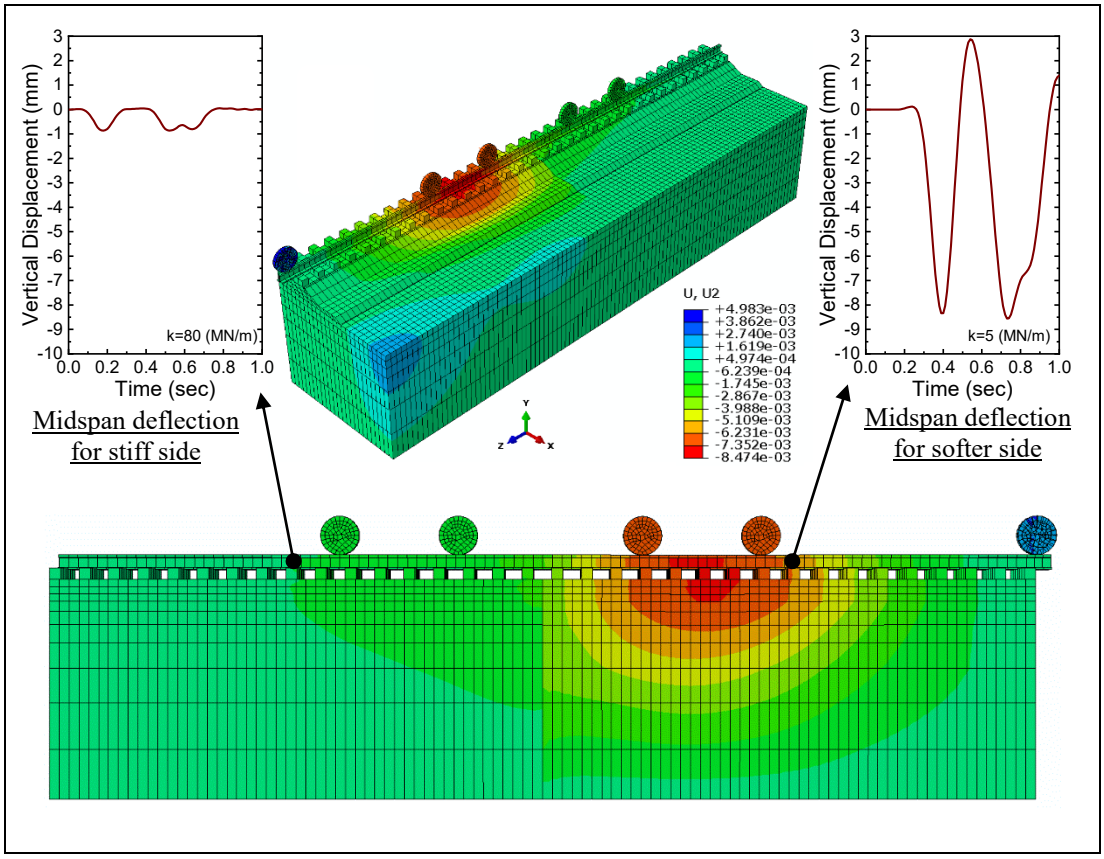

Figure 7.7: Deformation contours for 3D FEM layered model with abrupt stiffness variation at track transition under moving wheel load P=10 tonne, and corresponding vertical displacements for the stiff and soft track.

7.4.3 Effect of Train Speed on Dynamic Response of Transition Zone

The multistep transition zone is composed of multiple segments, each of which reacts differently to moving loads. During dynamic analysis of the 3D model of transition zone, the vertical displacement of each segment is analyzed in response to train loads traveling at different speeds. As illustrated in Figure 7.8, the figure shows the vertical displacements at the center of the segment with a track stiffness of k = 5 MN/m/m, when subjected to a 20-tonne axle loading moving at speeds of 60, 100, 150, 200, and 250 km/h. This segment is the weakest among the various segments in the transition zone and thus experiences the highest vertical displacements, which can be compared

to the more rigid segment with a stiffness value of k = 13.6 MN/m/m presented in Figure 7.9. The response of the other segments is included in Appendix C.

It is clear that the stiffer segments experience lower vertical displacements under similar loading conditions (as expected). For instance, subjected to 20-tonne axle load and train speed of 100km/h, the stiff track (k=13.6 MN/m/m) shows a maximum settlement of 4.7mm; in contrast, the soft track (k=5 MN/m/m) shows a settlement of up to 12mm under the same loading condition. It can also be noted that at lower speeds, the displacement peaks caused by axle loads are clearly visible, indicating the recovery of some of the elastic settlements before the next load is applied. However, at higher speeds, the displacement peaks caused by individual axle loads are no longer visible due to smaller loading intervals. This is why the displacement peaks under a single bogie are relatively smaller compared to the peaks under two consecutive bogies, such as in the case of two consecutive carriages. The impact of increased train speed on the response of each segment is discussed in detail in the following sections.

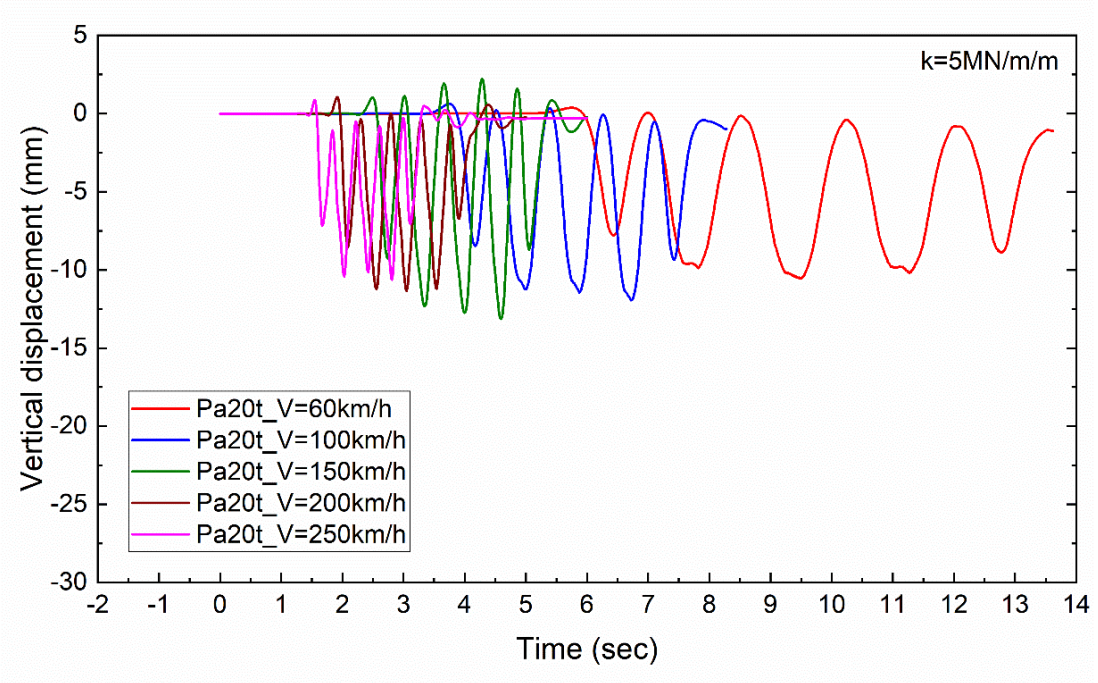

Figure 7.8: Predicted vertical displacements for 3D FEM layered model (k = 5 MN/m/m, P_{axle} = 20 t) considering four-carriage loading moving at various speeds

7.4.4 Effect of Train Load on Dynamic Response of Transition Zone

In order to assess the impact of train loads on the dynamic response of the track, a 3D model of the transition zone was analysed for two different axle loadings (20 tonnes and 40 tonnes). The results from the preceding section were based on a 20-tonne axle load, however, the dynamic response of the transition zones under a 40-tonne axle load is shown in Figure 7.10. This figure illustrates the vertical displacements at the center of a segment with a track stiffness of k=5 MN/m/m when subjected to a 40-tonne axle load traveling at speeds of 60, 100, 150, 200, and 250 km/h. The response of the other segments under the 40-tonne axle load is included in Appendix C.

It can be seen that an increase in axle load results in a corresponding increase in vertical displacements of the track. For example, by comparing Figure 7.10 and Figure 7.8, it can be observed that doubling the axle load leads to a doubling of the corresponding displacements. A similar trend can also be seen by comparing Figure 7.10 with Figure 4.6, although the magnitude of the displacements will differ as the displacements shown in Figure 7.10 take into account both the train speed and loads, whereas Figure 4.6 only demonstrates the effect of the train load under static loading conditions.

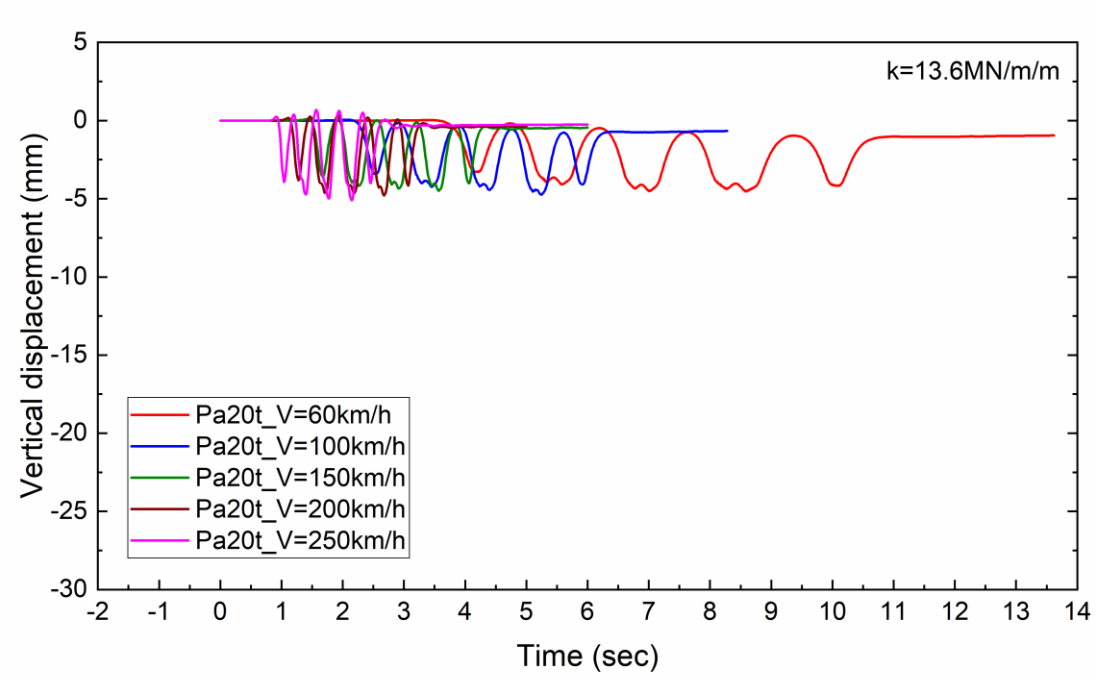

Figure 7.9: Predicted vertical displacements for 3D FEM layered model (k = 13.6 MN/m/m, P_{axle} = 20 t) considering four-carriage loading moving at various speeds

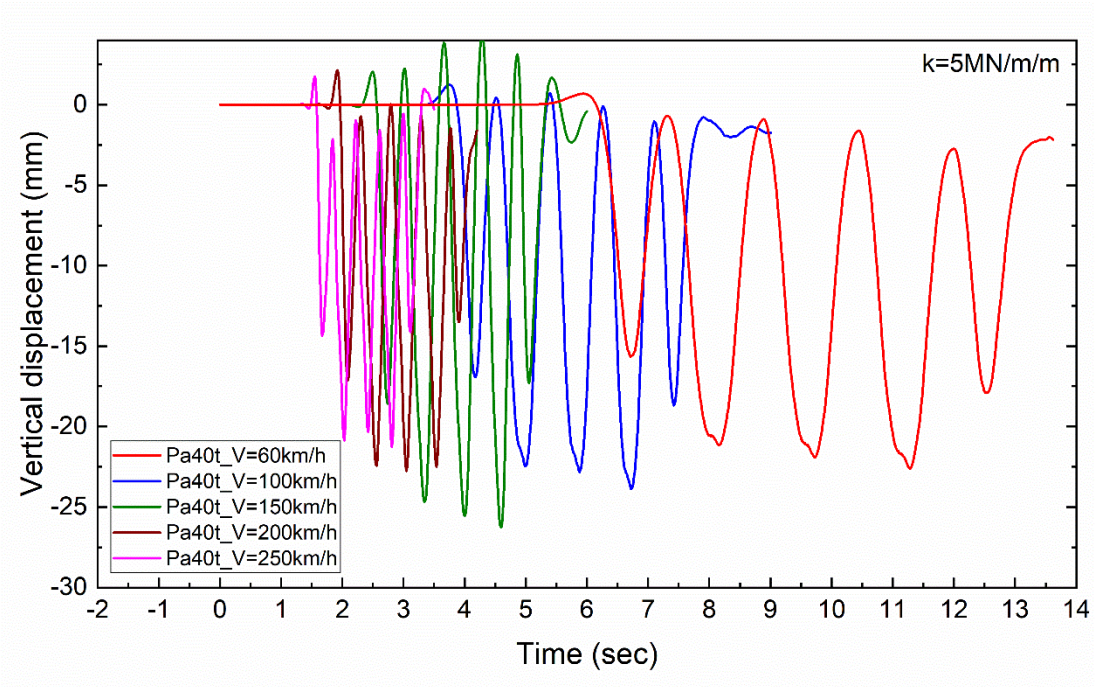

Figure 7.10: Predicted vertical displacements for 3D FEM layered model (k = 5 MN/m/m, P_{axle} = 40 t) considering four-carriage loading moving at various speeds

7.4.5 Effect of Train Speed and Load on the Dynamic Response of Transition Zone

The impact of train speed and load on the dynamic behaviour of the proposed transition zone is demonstrated in Figure 7.11, which shows the variation in the maximum vertical displacements for different transition segments under varying train speeds and loading conditions. It is seen that there is a nearly 100% increase in the maximum displacement of each segment as the train axle load increases from 20 to 40 tonnes. For instance, under 20 tonne axle load and train speed of 100km/h, the maximum settlement is predicted as 11.8 mm for the track with k=5 MN/m/m, however, under 40 tonne axle loads, this settlement increases up to 23.8 mm. On the other hand, the trend in the change of displacements for different segments with increasing train speed remains almost the same, indicating the effect of train speed on the settlement is not pronounced as compared to the increased loads.

However, the trend is not consistent within the segments, meaning that each segment responds differently to the changes in train speed. For instance, there is a decreasing

trend in track displacements as the train speed increases for segments with higher track stiffness (k = 80 & 41.5 MN/m/m). In contrast, for segments with lower track stiffness (i.e. k = 9.2 & 5 MN/m/m), the vertical displacement initially increases with increasing train speed up to 150km/h and then decreases.

To further clarify the above observation, the predicted settlements is normalised and the results are shown in Figure 7.12. The normalized settlement was calculated by normalizing the settlement (vertical displacement) of a segment for a given train speed by its highest settlement among all simulated speeds. To illustrate, consider a track segment with a stiffness value of 5 MN/m/m, the highest settlement for this segment occurs at a train speed of 150 km/h, as seen in Figure 7.11. Hence, the normalized settlement for this segment was obtained by dividing its settlement at any other speed by its settlement at a speed of 150 km/h. As a result, for this given speed, the normalized settlement of this particular segment becomes equal to one.

Similarly, the normalized settlement was calculated for all other segments and is presented in Figure 7.12. The result indicates that the track with a higher stiffness value (i.e. k = 80 MN/m/m) experiences higher settlement at lower speeds (i.e. v = 60 km/h) as compared to the higher speed. In contrast, the track with a lower stiffness value (i.e. k = 5 MN/m/m) experiences higher settlement at higher speeds (i.e. v = 150 km/h). Similarly, for other tracks having stiffness values ranging from 80 to 5 MN/m/m, the maximum settlement occurs at speeds ranging from 60 to 150 km/h.
Therefore, it can be inferred that the different segments in a transition zone may exhibit diverse behaviour for varying train speeds and may result in an excessive settlement if the train speed reaches to its critical speed. As a result, it is advisable to optimize the design of the transition zone for various train speeds in order to prevent excessive settlements during train operations.

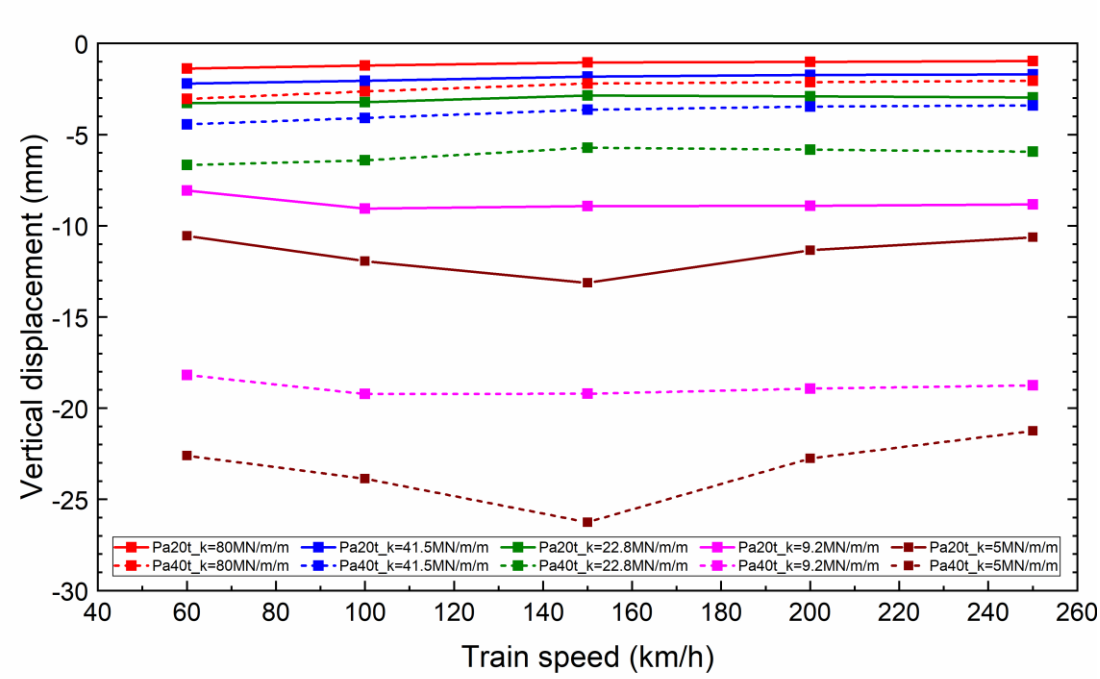

Figure 7.11: Predicted maximum vertical displacements for 3D FEM layered model of the proposed transition zone considering various train loading and speed

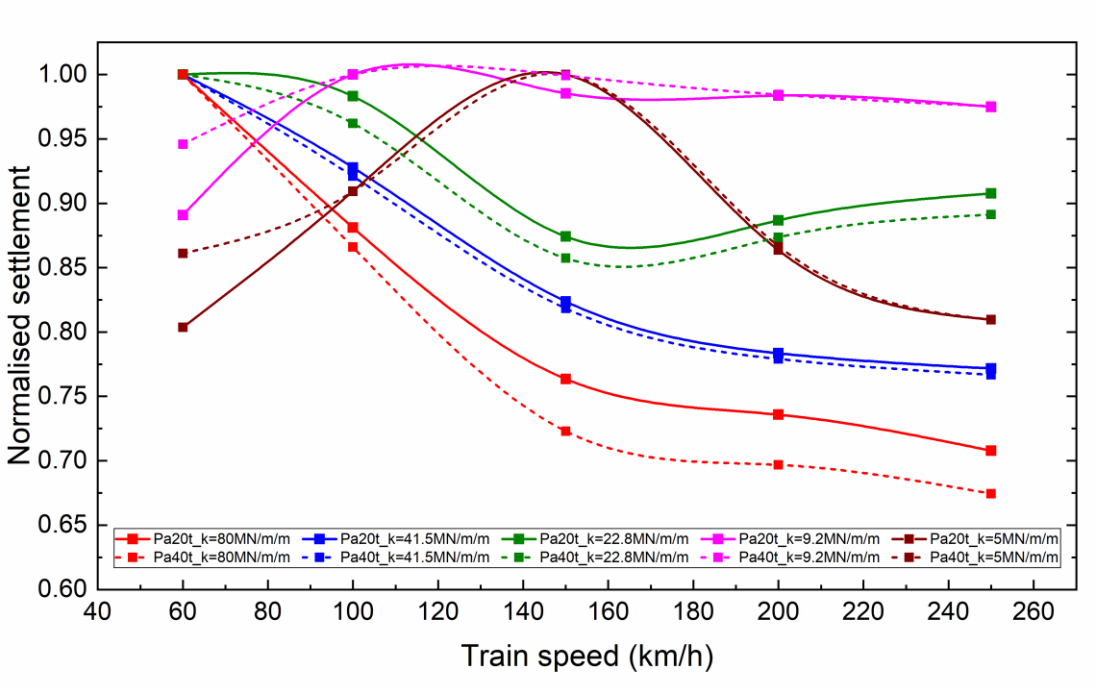

Figure 7.12: Predicted normalised settlement for 3D FEM layered model of the proposed transition zone considering various train loading and speed.

7.4.6 Effect of track stiffness on the Dynamic Response of Transition Zone

The impact of the stiffness values of the proposed transition segments can be analysed through the dynamic analysis conducted on a 3D model of the transition zone. The results are presented in Figure 7.13, which displays the relationship between the vertical displacements and the respective track stiffness for different speed and loading conditions. The results indicate that tracks with stiffness, *k* more than 20 MN/m/m exhibit reduced settlements, resulting in a smaller differential settlement even with significant variations in stiffness. Conversely, the transition segments with stiffness, *k* less than 20 MN/m/m demonstrate greater vertical displacements and correspondingly higher differential settlements, even with minor stiffness variations.

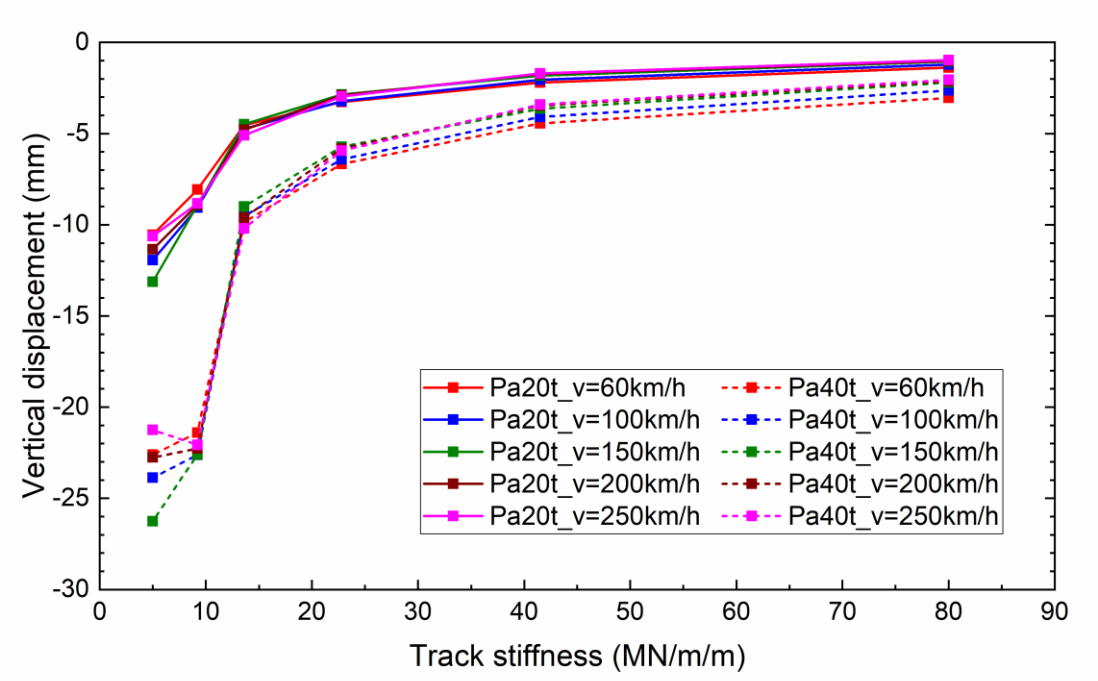

Figure 7.13: Predicted maximum vertical displacements for 3D FEM layered model of the proposed transition zone considering stiffness values of its various segments

The results presented in Figure 7.13 validate the efficacy of the analytical approach described in Chapter-6 for designing multistep transition zones. The approach incorporates an empirical relation, presented in Chapter 6, to determine the stiffness values of the various segments in the transition zone. This relation ensures a smooth

and gradual variation in stiffness values, rather than relying on simple arithmetic means. As a result, the proposed analytical approach considers the track dynamic response in designing the multistep transition zone, and leads to larger variations in stiffness on its stiffer side, as compared to the softer side.

7.5 Design Optimization of the Multistep Transition Zone

The design of the transition zone is based on the criterion of differential settlement between consecutive segments, Δw_{max}. The proposed approach states that the maximum differential settlement must be less than a permitted value of 5mm, i.e. $\Delta w_{max} \leq \Delta w_{allowed} = 5$mm. To optimize the design, it is necessary to determine the differential settlement caused by the variation in stiffness between consecutive segments and this can be done by analysing the 3D model of the multistep transition zone.

The initial calculation focuses on the differential settlement resulting from the shift from a stiff segment (track with k = 80 MN/m/m) to any specific segment in the proposed multistep transition zone. The results of this analysis are presented in Figure 7.14, and provide the differential settlement of various transition segments with respect to the stiffest segment under different speed and loading conditions.

The results show that the differential settlement between segments with k = 80 and k = 5 MN/m/m can reach up to 12mm under the influence of a 20-tonne axle load moving at 150 km/h. This highlights the need for a transition zone to accommodate this stiffness variation. Additionally, predicted results indicate that the differential settlement increases almost doubles as the axle load increases from 20 to 40-tonne axle load, establishing a direct relationship between train load and differential settlement, as previously presented in Figure 5.5.

To evaluate the effectiveness of the proposed multistep transition zone, its efficiency must be analysed for various train speeds and loading conditions. To accomplish this, the differential settlement between consecutive segments is calculated for different speeds subjected to a given 20-tonne axle load and compared with the acceptable limit, as shown in Figure 7.15. Results demonstrate that the differential settlement between

two consecutive segments remains within the allowable limit for all train speeds, indicating the effectiveness of the proposed design.

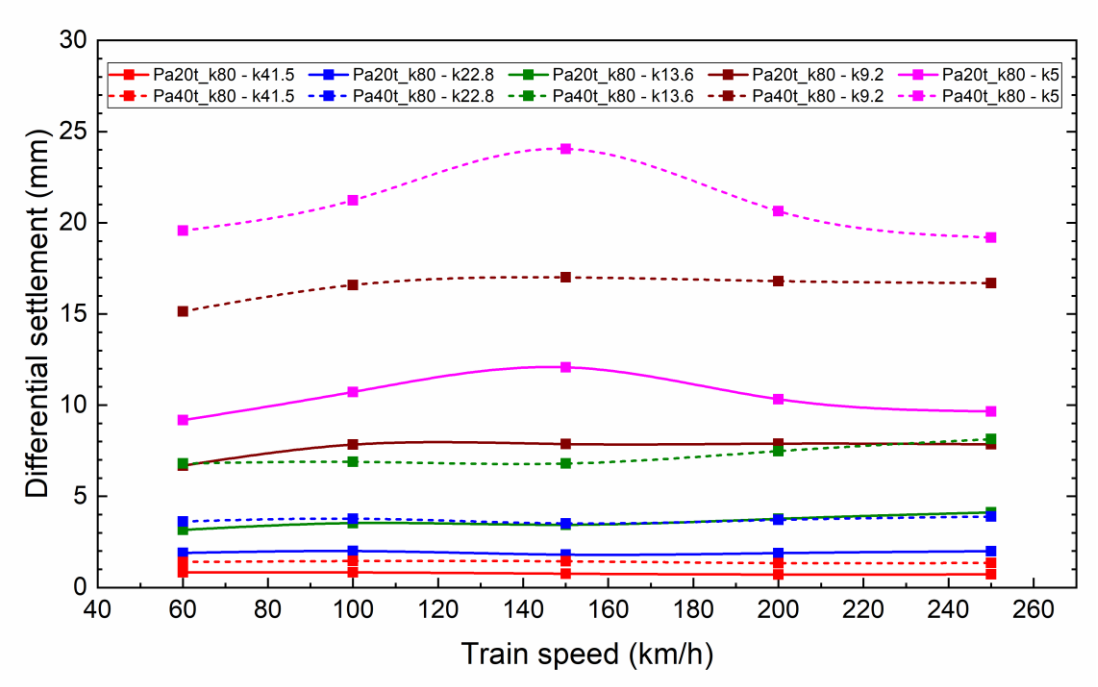

Figure 7.14: Predicted maximum differential settlement for 3D layered model of the proposed transition zone between its various segments

On the other hand, when the proposed multistep transition zone FEM model is simulated for 40-tonne axle load, it fails to meet the established criterion of the allowable differential settlement. The results of this analysis are presented in Figure 7.16, which shows that the differential settlement between segments with k = 13.6 MN/m/m and k = 9.2 MN/m/m exceeds 5 mm. Furthermore, for segments with k = 9.2 and k = 5 MN/m/m, the differential settlement exceeds the acceptable limit of 5 mm for some speeds. This highlights the ineffectiveness of the proposed design under 40-tonne axle loading.

In conclusion, the proposed design of the multistep transition zone is effective under 20-tonne axle loading, but requires optimization for higher axle loads. The design optimization can be achieved by increasing the number of transition steps in accordance with the novel approach outlined in Chapter 6, and analysing the new design using the above 3D FEM model subjecte to various train speeds and loading conditions.

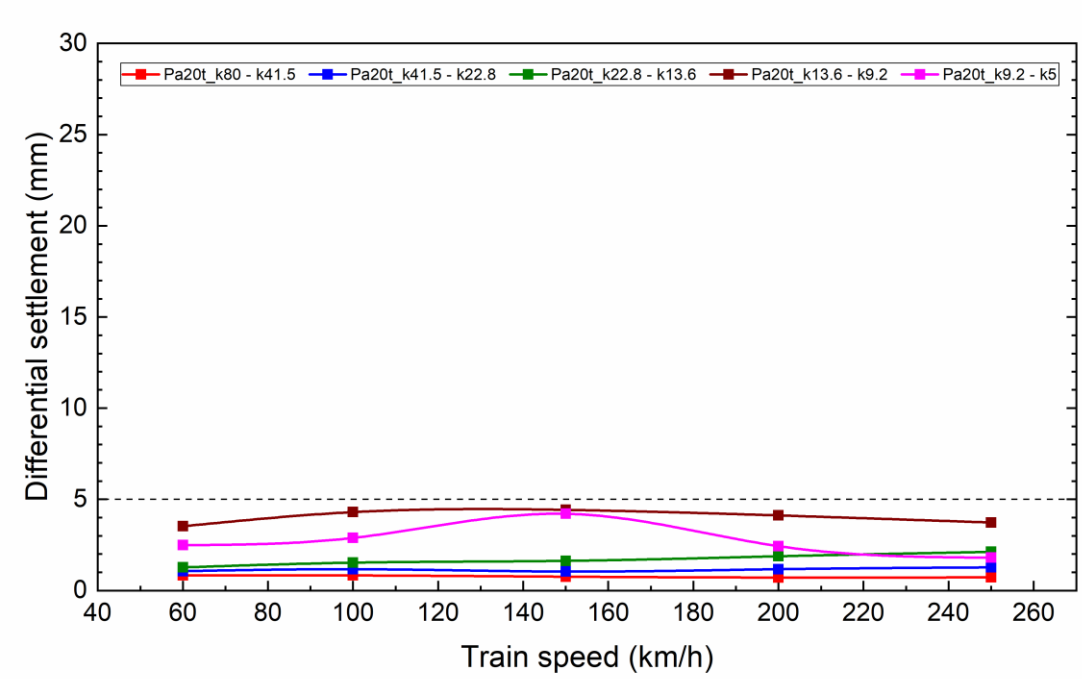

Figure 7.15: Predicted maximum differential settlement for 3D FEM model of the proposed transition zone between its consecutive segments under 20t axle loading

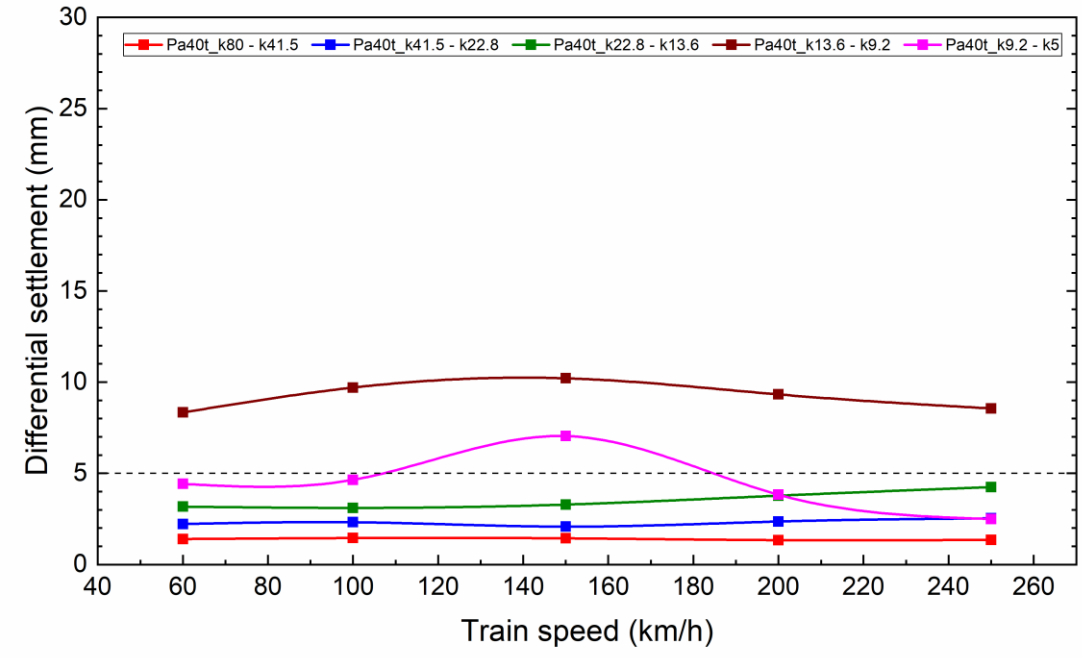

Figure 7.16: Predicted maximum differential settlement for 3D FEM model of the proposed transition zone between its consecutive segments under 40t axle loading

7.6 Design Recommendations

Based on the results of the FEM analysis, design recommendations can be made for any track transition. These recommendations involve the provision of transition zone, imposing restrictions on train speed and axle load, or proposing soil improvement techniques to achieve the required track stiffness as per the proposed design. For instance, in the case of a track transition changing from k = 80 MN/m/m to k = 5 MN/m/m, the recommendation can be presented after a thorough analysis of the outcomes. This includes an evaluation of the necessity for a transition zone and its efficacy under specific loading conditions at the site.

The results of the study on the requirement for a transition zone or the safe range of stiffness variation in the absence of a transition zone are presented graphically in Figure 7.17 and Figure 7.18. These Figures illustrate the relationship between stiffness variation, train speed, and differential settlement under the influence of 20-tonnes and 40-tonnes axle loads, respectively. The green region in the Figures signifies that the differential settlements are below the acceptable limit of 5 mm, indicating that there is no need for a transition zone under the relevant loading conditions. On the other hand, the red region in the Figures indicates that the differential settlements exceed the acceptable limit of 5 mm, suggesting that a transition zone is required if the stiffness variation falls within that region under the corresponding loading conditions.

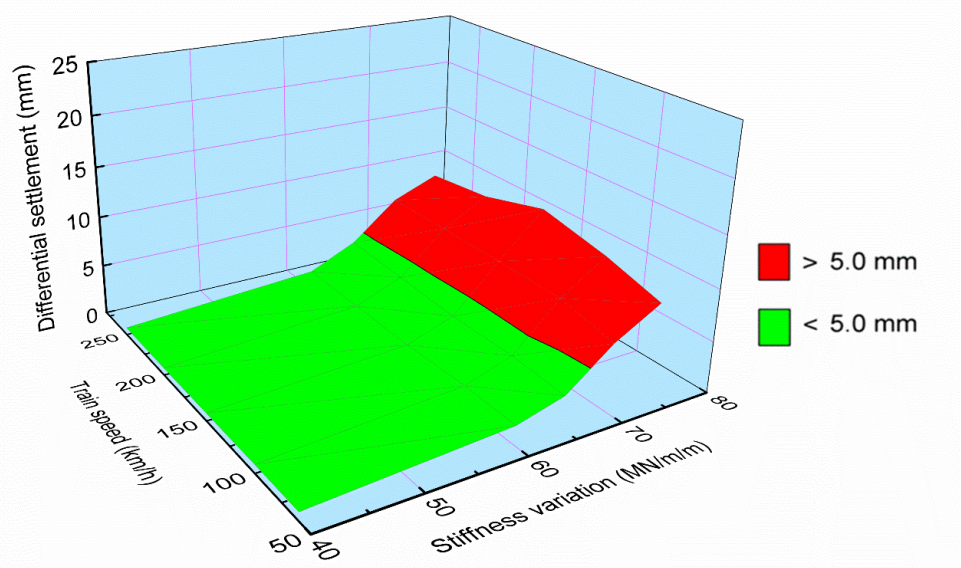

Figure 7.17: Relationship between stiffness variation, train speed and the differential settlement under 20-tonnes axle load, for track transition from k = 80 to 5 MN/m/m

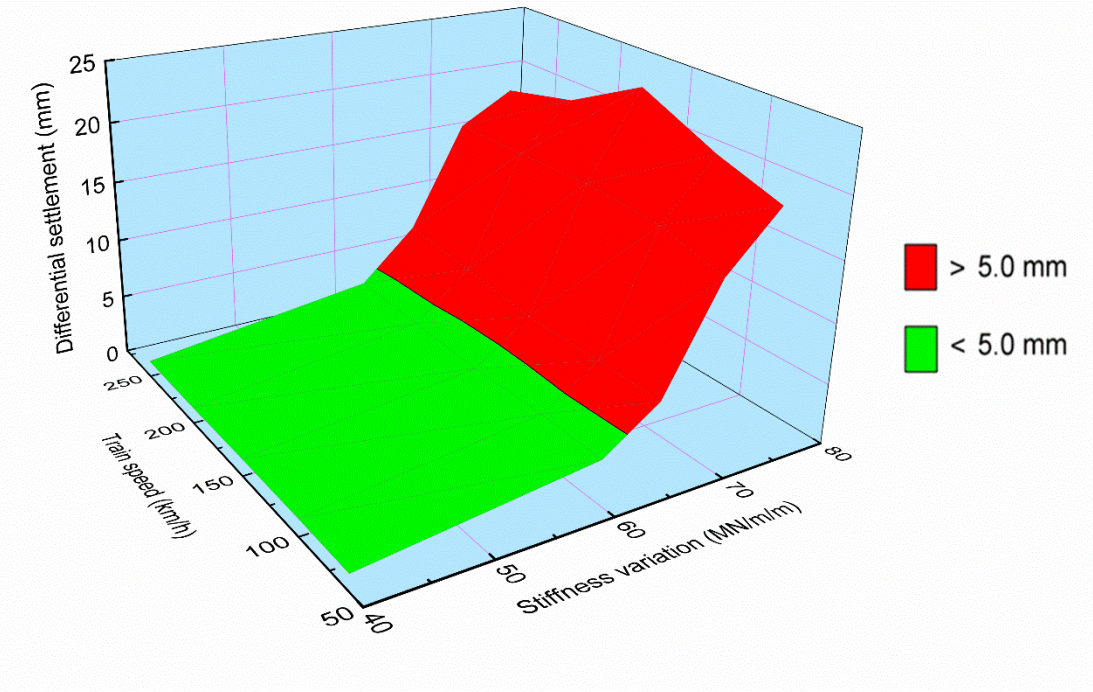

Figure 7.18: Relationship between stiffness variation, train speed and the differential settlement under 40-tonnes axle load, for track transition from k = 80 to 5 MN/m/m

Similarly, the results of the study on the effectiveness of the proposed five-step transition zone under the effect of 20-tonnes and 40-tonnes axle loads are presented graphically in Figure 7.19 and Figure 7.20, respectively. These figures demonstrate the maximum differential settlements between each consecutive step of the transition zone for various train speeds under the corresponding loading conditions.

It is evident from Figure 7.19 (20-tonne axle load) that the differential settlement between all consecutive steps remains within the acceptable limit for the 20-ton axle load. However, for the 40-tonne axle load, Figure 7.20 illustrates that the differential settlement exceeds the limit for some transition steps (as shown with red regions), indicating the inadequacy of the proposed transition zone under such loading conditions. This necessitates the optimization of the design, either by increasing the number of transition steps or by imposing restrictions on train speed and load while using the same design.

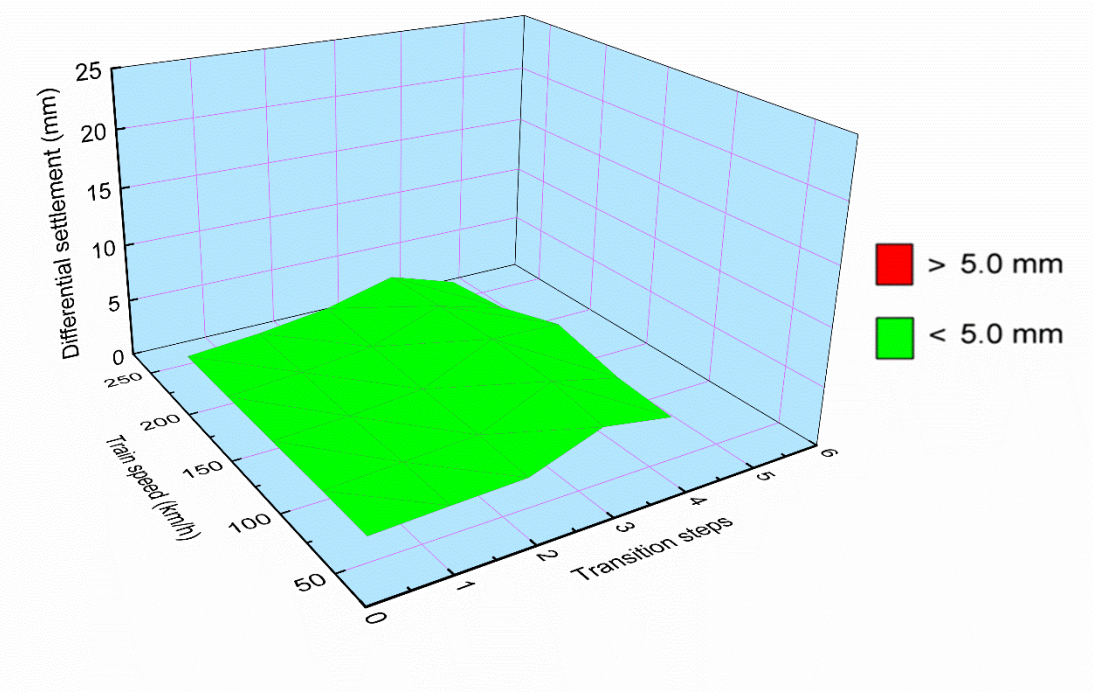

Figure 7.19: Maximum differential settlements for the proposed five-step transition zone between its various consecutive segments under 20t axle loading

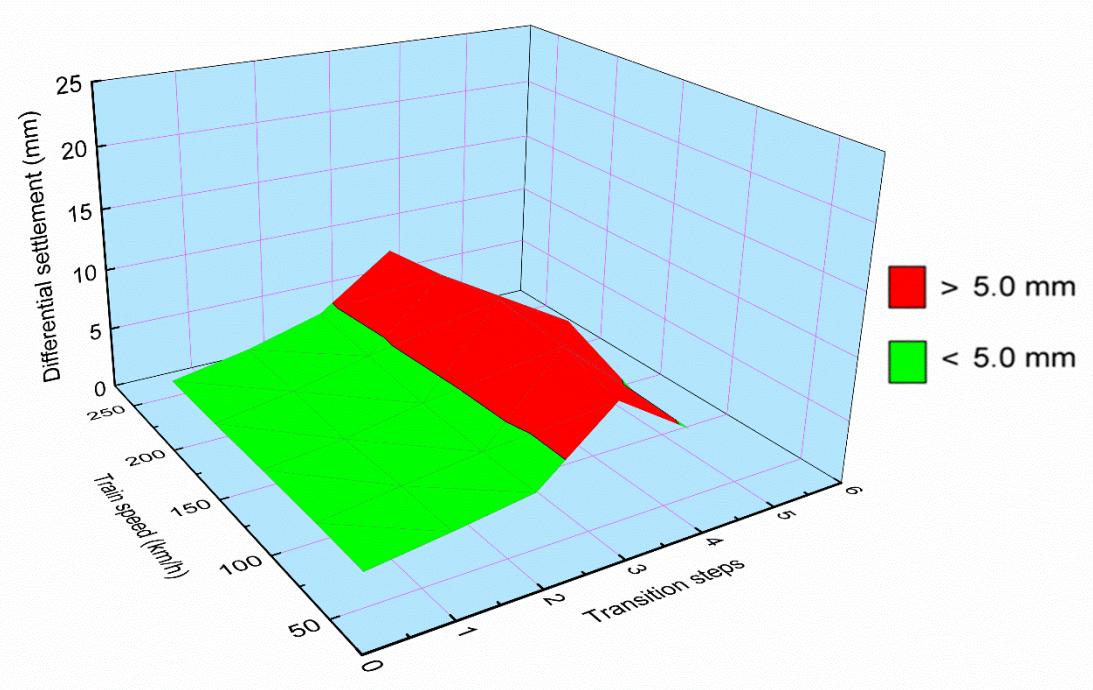

Figure 7.20: Maximum differential settlements for the proposed five-step transition zone between its various consecutive segments under 40t axle loading

Hence, the train speed limit for any track transition will depend on adhering to the allowable differential settlement criteria. There is no predetermined specific speed limit based solely on the differential settlement; rather, the maximum speed limit for any track transition will be determined by ensuring that the allowable differential settlement of 5 mm is not exceeded. Therefore, the speed limit will vary depending on the stiffness and design characteristics of each specific transition zone to maintain the differential settlement within the acceptable range.

Finally, recommendations for soil improvement techniques can be presented to achieve the desired track stiffness for each segment in accordance with the final proposed design of the multi-step transition zone. A variety of techniques are available to adjust the track stiffness to the required values, which have been thoroughly discussed in Chapter 3. However, determining the most appropriate technique for a specific stiffness value requires a comprehensive analysis and is beyond the scope of this study.

7.7 Guidelines for the Optimal Design of Transition Zone

The purpose of this study is to establish guidelines for the optimal design of transition zones at track transitions. This involves determining the requirement for the provision of the transition zone, conducting a preliminary design, and optimizing the design for various train speeds and loading conditions. The design and analysis process is performed through a combination of analytical and numerical modelling techniques presented throughout the thesis. The following steps summarize the guidelines for optimal transition zone design:

Step 1: The initial step is to determine the stiffness variation (Δk) at the track transition. The track stiffness on either side of the transition is normally known or can be determined otherwise from field measurements either by measuring rail/sleeper deflection under actual train passing or by falling weight techniques (Powrie & Le Pen 2016).

Step 2: The next step is to calculate the requirement for the transition zone based on

the stiffness variation at the track transition. This is done by determining the differential settlement and comparing it to the acceptable value (e.g. 5mm). The differential settlement can be calculated using an analytical model or 2D FEM layered model.

Step 3: The multistep transition zone is then designed following the given flowchart for the proposed novel approach presented in Chapter 6.

Step 4: The 3D FEM layered model of the multistep transition zone is updated by incorporating the design parameters from Step 3. The fundamental parameters of the substructural layers can be calculated using Equations (4.10) & (4.11) based on the required equivalent stiffness.

Step 5: The 3D FEM layered model is analysed for site-specific train speed and loading conditions to ensure compliance with design criteria for all loading conditions.

Step 6: The final step is to provide design recommendations.

These design guidelines are also presented in the form of a flow chart, as given in Figure 7.21.

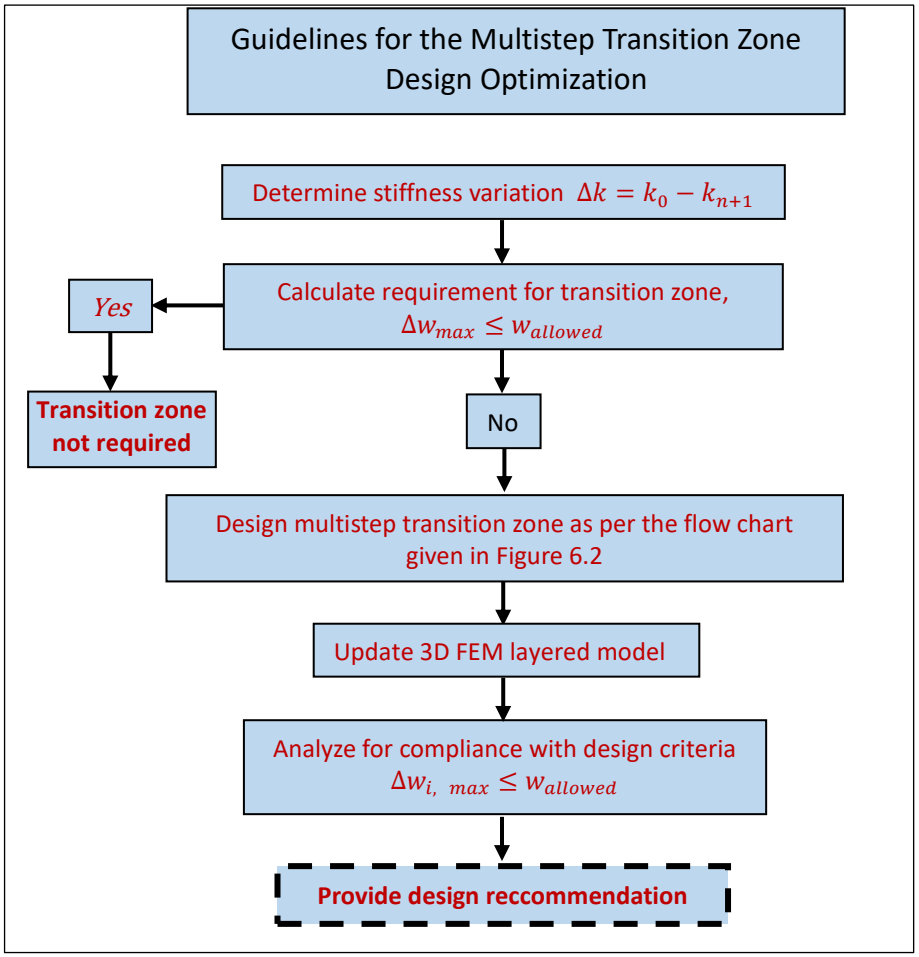

Figure 7.21: Flow Chart for Guidelines for the Multistep Transition Zone Design Optimization

7.8 Chapter Summary

This chapter presents the design optimization of multistep transition zones using 3D finite element numerical modelling. The process involves gradually developing a comprehensive 3D finite element model through model calibration and validation. Dynamic response analysis is conducted for various speed and loading conditions, and differential settlements are calculated and discussed. Finally, design optimization and design recommendations are provided. In addition, this chapter offers design optimization guidelines based on the analytical and numerical modelling presented in the thesis.

The analysis of the five-step transition zone subjected to a four-carriage train with 16 wheels travelling at various speeds and incorporating two types of axle loadings shows that different segments in a multistep transition zone may exhibit diverse behaviour for varying train speeds and may result in excessive settlement. Therefore, it is recommended to optimize the design of the transition zone for various train speeds. The results also indicate that tracks with stiffness, k more than 20 MN/m/m exhibit reduced settlements, while the transition segments with stiffness, k less than 20 MN/m/m demonstrate greater vertical displacements and correspondingly higher differential settlements.

The proposed empirical relation to determining the stiffness values of the various segments in the transition zone is validated, which ensures a smooth and gradual variation in stiffness values. The proposed analytical approach considers the track dynamic response in designing the multistep transition zone and leads to larger variations in stiffness on its stiffer side compared to the softer side.

The proposed design of the five-step transition zone is effective under 20-tonne axle loading but requires optimization for higher axle loads. The design optimization can be achieved by increasing the number of transition steps and analyzing the new design using the 3D model for various speed and loading conditions.

Based on the analysis results, several recommendations for any track transition can be made. These recommendations may include deciding on the provision of a transition zone, imposing restrictions on train speed and load, or suggesting soil improvement techniques to achieve the required track stiffness in line with the proposed design.

CHAPTER EIGHT

8. CONCLUSIONS AND RECOMMENDATIONS

8.1 Conclusions

In this study, an extensive investigation into rail track transitions has been conducted to explore the associated issues and potential solutions. The research encompasses a critical analysis of current approaches to designing transition zones with the objective of mitigating the effects of sudden changes in track structural properties. In this doctoral study, by designing a multistep transition zone, the author has proposed a novel approach to mitigate sudden changes in structural properties of track (e.g. change from a concrete bridge deck to a soft alluvial terrain). The study includes design optimization guidelines and analyses the effect of abrupt stiffness variation at transition zones under different loading conditions, using a mathematical process to determine the optimum stiffness of each segment. The proposed methodology is subsequently validated through Finite Element Modelling, supplemented with worked-out examples. The study provides novel insights into improving the performance of ballasted tracks at transition zones.

The present study provides a comprehensive review of ongoing research in the area of rail track transition, highlighting differential settlements and enhanced dynamic loads as significant issues that lead to track degradation and increased maintenance costs. The study also emphasizes the need for more precise and effective design approaches to address these issues, as current design practices rely heavily on empirical approaches that assume an elastic medium.

To mitigate these issues, transition zones must be designed with consideration for variations in stiffness and possible initial settlement, which can differ from case to case. The design of transition zones is challenging due to the interaction of multiple track structural components in a composite structure, further complicated by sudden variations in the structural properties of the track at transition zones.

The study also delves into the issue of minimizing differential settlement caused by sudden stiffness variations in transition zones, demonstrating through analytical and numerical modelling approaches that abrupt changes in track stiffness cause significant differential settlement at the track transitions, which can be further amplified by load.

The outcomes of this study have the potential to inspire better design solutions and revised specifications and practical guidelines for track transition zones by identifying an appropriate length for transition zones to gradually transform track stiffness, reducing differential settlement at these critical locations and minimizing track degradation. Overall, the study underscores the need for continued research to develop more precise and cost-effective design approaches to address these issues in rail track transitions.

Based on the findings of this study, the following specific conclusions can be drawn:

- Results obtained from the analytical and numerical modelling approaches showed that an increase in track stiffness from k=5MN/m/m (ballasted track) to k=80MN/m/m (slab track) would result in a significant reduction in track settlements, w_{max} (i.e., reduced from w_{max} =4.9 mm to w_{max} =0.6 mm, respectively). At any track transition, the maximum differential settlement (Δw_{max}) significantly higher than the allowable limit (i.e. 5mm) could be evaluated. From a stability perspective, such differential values would be detrimental in relation to long heavy-haul trains, hence the imperative need for designing interim transition zones.
- For a given track stiffness (k), the settlements of track increased with an increase in train speed. For instance, under a given wheel load of P=10 tonnes and track stiffness k=5 MN/m per linear meter, the analytical model showed an increase in maximum track settlement from w_{max}=8 mm to w_{max}=15.8 mm, when the train speed increased from 60 km/h to 200km/h. This demonstrated the enhanced dynamic loading effect attributed to moving loads.

- The absolute differential settlement (Δw) between any two tracks having different values of stiffness increased with the train speed. For a given stiffness variation of Δk = 75MN/m/m, the values of Δw were calculated as 10.5mm and 17.8mm for speeds of v=100km/h and v=300km/h, respectively. These analyses confirmed that trains moving at higher speeds would lead to higher differential settlements.
- An optimization process was introduced to determine the required stiffness (k_i) for each segment to ensure the minimum differential settlement. This process allowed the number of transition steps could be selected optimally so that the differential settlement between any two consecutive segments would be less than the allowable differential settlement, α. In a practical sense, knowing the value of α as set by the design criteria, the required number of transition steps and their corresponding stiffness could be determined iteratively.
- An empirical relation was introduced through an iterative process to find out the preliminary stiffness (k_i) of each segment in the proposed multistep transition zone design. This incorporated the total stiffness variation at any track transition Δk, and the total number of segments and their lengths in the proposed design. The value of (k_i) was obtained for a gradual change of Δk and was set to minimize the differential settlement (Δw_i) between any two consecutive transition segments as an optimization criterion.
- The FEM results of vertical displacements were found to be in good agreement with the analytical results. As the actual moving wheel loading was simulated on a layered track (with measured geotechnical parameters), the soil-structure interaction and geotechnical aspects of a typical track could be properly captured in this FEM analysis. This validation proved that the BOEF approach could be reliably used for analyzing the behavior at transition zones for a given set of computational factors (number of steps, length, stiffness), thus, a minimal differential settlement could be achieved.
- The results of 3D modelling of the proposed multistep transition zone indicated that tracks with a value of stiffness (*k)* more than 20 MN/m/m exhibited reduced settlements, while the transition segments with *k* less than 20 MN/m/m demonstrated greater vertical displacements and correspondingly higher

differential settlements. This validated the effectiveness of the proposed empirical relation, in determining the stiffness values offering larger variations in stiffness on its stiffer side compared to the softer side.

- The results also showed that an increase in axle load would result in a corresponding increase in vertical displacements of the track. It was seen that there was nearly a 100% increase in the maximum displacement of each segment as the train axle load increased from 20 to 40 tonnes. For instance, under 20-tonne axle load and train speed of 100km/h, a maximum track settlement of 11.8 mm was predicted with k=5 MN/m/m; however, under 40-tonne axle load, this settlement increased to 23.8 mm.
- The study found that the stiffness value of a track had a significant effect on settlement, where the track experienced a higher settlement at lower speeds if the stiffness value was higher (k = 80 MN/m/m), and greater settlement at higher speeds would occur if the stiffness was lesser (k = 5 MN/m/m). The study highlighted the diverse behavior of different segments in a transition zone for varying train speeds and the potential risk of excessive settlement if train speed reached the critical speed. Therefore, it can be recommended that the design of the transition zone be optimized for various train speeds to prevent excessive settlements during train operations, and designers and practicing engineers should consider the potential impact of train speed and track stiffness on the settlement to ensure safe and efficient train operations.
- The analysis showed that the proposed design of the multistep transition zone was effective in limiting the differential settlement between consecutive segments to within the acceptable limit of 5mm for all train speeds when the axle loading was 20-tonne. However, when the axle loading was increased to 40-tonne, the differential settlement exceeded the allowable limit for given speeds. This implies that the design of the multistep transition zone needs to be optimized for higher axle loads to ensure that the differential settlement remains within the acceptable limit for operational train speeds.
- Based on the results of the analysis, design recommendations can be made for any track transition. These recommendations involve the provision of a transition zone, imposing restrictions on train speed and load, or proposing soil

improvement techniques to achieve the desired track stiffness for each segment in accordance with the final proposed design of the multi-step transition zone. Various techniques can be utilized to adjust the track stiffness, as discussed in the literature review, but determining the most suitable technique for a specific stiffness value requires a comprehensive analysis that falls beyond the scope of this study.

The current study provided a significant extension for design rejuvenation of transition zones by minimising the differential settlement at any two consecutive transition segments. The outcomes of this study will assist the practitioners to design transition zone, taking into account the total length with the number of transition steps and appropriate stiffness values and their variation along the track.

8.2 Limitations

While the analytical approach and methodology for tracks at transition zones presented in the current study are useful, it is important to note that they have certain obvious limitations. These include:

(i) The analytical approach assumes substructure soil conditions (layered track) using a representative spring with an equivalent stiffness, k, which may not fully capture the complexity of real-world soil conditions,

(ii) The numerical modelling does not account for groundwater contribution, which may have a significant impact on the behavior of the track;

(iii) The study focuses on the dynamic response of the track transitions in terms of vertical displacements (i.e. strain-based analysis), but the stress analysis has not been considered for design optimization, and;

(iv) The study does not provide a specific method to determine the most appropriate soil improvement technique for a given stiffness value of a proposed transition zone, which may be a crucial factor in the success of the design.

8.3 Future Recommendations

On the basis of this study, the following are some recommendations for future research in this field:

- The analytical approach described in this thesis assumed substructure soil conditions (layered track) using a representative spring with an equivalent stiffness, k, considering the BOEF model. Although, the use of finite element analysis (FEA) of comprehensive 3D models have provided more accurate and detailed representations of the soil behavior, it is recommended that future research investigates alternative analytical approaches to model the substructure soil conditions at track transition zones.
- Effects of different types of subgrade conditions, groundwater tables have not been considered in the current analysis. In this study, the track substructure was assumed to be fully drained; hence the effect of any pore pressure build-up was not considered. In real life, excess pore pressure can develop when a soft subgrade is subjected to prolonged cyclic loading from long and heavy trains, resulting in fluidization and mud pumping. This process can contaminate ballasted tracks, resulting in differential settlement and instability.
- To enhance the design of track transition zones, it is recommended that future studies incorporate stress-based analysis as one of a design criterion in addition to differential settlement. By doing so, potential areas of stress concentration and stress rotation can be identified under the impact of axle loads moving at varying speeds. This may then enable the development of more robust and durable design recommendations that can better withstand the stresses and strains of regular train operation.
- It is recommended that future research develops a method for determining the most appropriate soil improvement technique for a given stiffness value of a proposed transition zone. This can be achieved by evaluating the performance of different soil improvement methods or mitigation measures (e.g., geosynthetics, soil stabilization, USP, additional rails, etc.) under various soil conditions, and developing guidelines or decision-making tools for selecting the most appropriate technique for a given scenario.

- It is recommended that a practical method on using the marginal and waste materials (e.g., mixture of fly ash, coal wash and rubber granulates for capping layer) at transition zone should be implemented to reduce the abrupt change in track stiffness while adopting an environmentally-friendly solution.
- Adverse effect of ballast breakage on the differential settlement at the track at transition zone has not been covered in this study. This can be investigated by adopting an advanced coupled discrete-continuum modeling approach where the ballast layer is simulated in discrete element method (DEM) and beyond which the continuum media (capping, subgrade) can be modelled by FEM.
- The design of multistep transition zone should be further update to incorporate varying lengths of individual transition segments.
- The analytical and beam on spring models provide valuable insights and are effective for analyzing static loading scenarios, assisting in the identification of initial design configurations, and enhancing the understanding of fundamental track behavior. However, to achieve a fully automated design process for multistep transition zones that consider varying stiffness, train loads, speeds, and ground conditions, it is advisable to explore more advanced analytical models or 3D models. These sophisticated models can encompass dynamic loading effects, lateral track behavior, and other intricate factors, contributing to a comprehensive and accurate optimization process.

REFERENCES

Abadi, T., Pen, L.L., Zervos, A. & Powrie, W. 2019, 'Effect of Sleeper Interventions on Railway Track Performance', *Journal of Geotechnical and Geoenvironmental Engineering*, vol. 145, no. 4, p. 04019009.

Abaqus 2020, 'ABAQUS User's Manual Ver. 2020', Series ABAQUS User's Manual Ver. 2020 Dassault Systemes Vélizy-Villacoublay, France.

Admetlla Pérez, N. 2010, 'Transición vía en placa-vía con balasto mediante traviesas cuadro', Minor thesis thesis, Universitat Politècnica de Catalunya · BarcelonaTech (UPC).

Aggestam, E. & Nielsen, J.C. 2019, 'Multi-objective optimisation of transition zones between slab track and ballasted track using a genetic algorithm', *Journal of Sound and Vibration*, vol. 446, pp. 91-112.

Alves Ribeiro, C., Paixão, A., Fortunato, E. & Calçada, R. 2015, 'Under sleeper pads in transition zones at railway underpasses: numerical modelling and experimental validation', *Structure and Infrastructure Engineering*, vol. 11, no. 11, pp. 1432-49.

Banimahd, M. 2008, 'Advanced finite element modelling of coupled train-track systems: a geotechnical perspective', PhD thesis thesis, Heriot-Watt University.

Banimahd, M. & Woodward, P. 2007, '3-Dimensional finite element modelling of railway transitions'.

Banimahd, M., Woodward, P.K., Kennedy, J. & Medero, G.M. 2012, 'Behaviour of train–track interaction in stiffness transitions', vol. 165, Thomas Telford Ltd, pp. 205-14.

Berggren, E. 2009, 'Railway track stiffness: dynamic measurements and evaluation for efficient maintenance', PhD thesis thesis, Stockholm; Royal Institute of Technology (KTH).

Beskou, N.D. & Theodorakopoulos, D.D. 2011, 'Dynamic effects of moving loads on road pavements: a review', *Soil Dynamics and Earthquake Engineering*, vol. 31, no. 4, pp. 547-67.

Bian, X., Li, W., Qian, Y. & Tutumluer, E. 2019, 'Micromechanical Particle Interactions in Railway Ballast through DEM Simulations of Direct Shear Tests', *International Journal of Geomechanics*, vol. 19, no. 5, p. 04019031.

Boler, H., Mishra, D., Tutumluer, E., Chrismer, S. & Hyslip, J.P. 2019, 'Stone blowing as a remedial measure to mitigate differential movement problems at railroad bridge approaches', *Proceedings of the Institution of Mechanical Engineers, Part F: Journal of Rail and Rapid Transit*, vol. 233, no. 1, pp. 63-72.

Briaud, J.-L. 1997, *Settlement of Bridge Approaches:(the Bump at the End of the Bridge)*, vol. 234, Transportation Research Board.

Cai, C., Shi, X., Voyiadjis, G. & J Zhang, Z. 2005, *Structural Performance of Bridge Approach Slabs under Given Embankment Settlement*, vol. 10.

Carrascal, I., Casado, J., Polanco, J. & Gutiérrez-Solana, F. 2005, 'Comportamiento dinámico de placas de asiento de sujeción de vía de ferrocarril', vol. 22, pp. 372-7.

Chen, C. 2013, 'Discrete element modelling of geogrid-reinforced railway ballast and track transition zones', PhD thesis thesis, University of Nottingham.

Chen, C. & Mcdowell, G.R. 2016, 'An investigation of the dynamic behaviour of track

transition zones using discrete element modelling', *Proceedings of the Institution of Mechanical Engineers, Part F: Journal of Rail and Rapid Transit*, vol. 230, no. 1, pp. 117-28.
Choi, J. 2013, 'Influence of track support stiffness of ballasted track on dynamic wheel-rail forces', *Journal of transportation engineering*, vol. 139, no. 7, pp. 709-18.
Choudhury, D., Bharti, R.K., Chauhan, S. & Indraratna, B. 2008, 'Response of Multilayer Foundation System beneath Railway Track under Cyclic Loading', *Journal of Geotechnical and Geoenvironmental Engineering*, vol. 134, no. 10, pp. 1558-63.
Chumyen, P., Connolly, D., Woodward, P. & Markine, V. 2022, 'The effect of soil improvement and auxiliary rails at railway track transition zones', *Soil Dynamics and Earthquake Engineering*, vol. 155, p. 107200.
Coelho, B., Hölscher, P., Priest, J., Powrie, W. & Barends, F. 2011, 'An assessment of transition zone performance', *Proceedings of the Institution of Mechanical Engineers, Part F: Journal of Rail and Rapid Transit*, vol. 225, no. 2, pp. 129-39.
Coelho, B., Priest, J. & Hölscher, P. 2018, 'Dynamic behaviour of transition zones in soft soils during regular train traffic', *Journal of Rail and Rapid Transit*, vol. 232, no. 3, pp. 645-62.
Cui, J. & Nelson, J.D. 2019, 'Underground transport: An overview', *Tunnelling and Underground Space Technology*, vol. 87, pp. 122-6.
Czyczula, W., Koziol, P. & Blaszkiewicz, D. 2017, 'On the Equivalence between Static and Dynamic Railway Track Response and on the Euler-Bernoulli and Timoshenko Beams Analogy', *Shock and Vibration*, vol. 2017, p. 13.
Dahlberg, T. 2001, 'Some railroad settlement models—a critical review', *Proceedings of the Institution of Mechanical Engineers, Part F: Journal of Rail and Rapid Transit*, vol. 215, no. 4, pp. 289-300.
Dahlberg, T. 2003, *Railway track settlements-a literature review*.
Dahlberg, T. 2010, 'Railway track stiffness variations - consequences and countermeasures', *International Journal of Civil Engineering*, vol. 8, no. 1, pp. 1-12.
De Oliveira Barbosa, J.M. & Van Dalen, K.N. 2019, 'Dynamic response of an infinite beam periodically supported by sleepers resting on a regular and infinite lattice: Semi-analytical solution', *Journal of Sound and Vibration*, vol. 458, pp. 276-302.
Dimitrovová, Z. & Varandas, J. 2009, 'Critical velocity of a load moving on a beam with a sudden change of foundation stiffness: Applications to high-speed trains', *Computers & Structures*, vol. 87, no. 19-20, pp. 1224-32.
Ding, H., Chen, L.-Q. & Yang, S.-P. 2012, 'Convergence of Galerkin truncation for dynamic response of finite beams on nonlinear foundations under a moving load', *Journal of Sound and Vibration*, vol. 331, no. 10, pp. 2426-42.
Duan, R. & Yang, J. 2013, 'Modelling and simulation of a bridge interacting with a moving vehicle system', Series Modelling and simulation of a bridge interacting with a moving vehicle system.
Esmaeili, M., Heydari-Noghabi, H. & Kamali, M. 2018, 'Numerical investigation of railway transition zones stiffened with auxiliary rails', Thomas Telford Ltd, pp. 1-10.
Esmaeili, M., Zakeri, J.A. & Babaei, M. 2017, 'Laboratory and field investigation of

the effect of geogrid-reinforced ballast on railway track lateral resistance', *Geotextiles and Geomembranes*, vol. 45, no. 2, pp. 23-33.
Estaire, J., Cuéllar, V. & Santana, M. 2017, 'Testing railway tracks at 1: 1 scale at CEDEX Track Box', *Proceedings of the Intern. Cong. on High-Speed Rail. Technologies and Long Term Impacts*.
Esveld, C. 2001, *Modern Railway Track. 2nd Edition*, 2nd edn, MRT-Productions, The Netherlands.
Esveld, C. 2009, 'The significance of track resilience', *Eur. Railway Rev. News*, vol. 10, no. 1420, p. 28.
Esveld, C. 2010, 'Recent developments in high-speed track', University of Zagreb Zagreb (Croatia).
Esveld, C., Markine, V. & Duškov, M. 2001, 'Feasibility of EPS as a lightweight sub-base material in railway track structures', pp. 1-10.
Fara, A. 2014, 'Transition Zones for Railway Bridges: A Study of the Sikån Bridge', Master`s thesis thesis, Sweden; Luleå University of Technology.
Fortunato, E., Paixão, A. & Calçada, R. 2013, 'Railway track transition zones: design, construction, monitoring and numerical modelling', *International Journal of Railway Technology*, vol. 2, no. 4, pp. 33-58.
Frohling, R., Scheffel, H. & Ebersöhn, W. 1996, 'The vertical dynamic response of a rail vehicle caused by track stiffness variations along the track', *Vehicle System Dynamics: International Journal of Vehicle Mechanics and Mobility*, vol. 25, no. S1, pp. 175-87.
Frohling, R.D. 1997, 'Deterioration of railway track due to dynamic vehicle loading and spatially varying track stiffness', PhD thesis thesis, University of Pretoria, South Africa.
Froio, D., Rizzi, E., Simões, F.M. & Da Costa, A.P. 2018, 'Universal analytical solution of the steady-state response of an infinite beam on a Pasternak elastic foundation under moving load', *International Journal of Solids and Structures*, vol. 132, pp. 245-63.
Gallage, C., Dareeju, B. & Dhanasekar, M. 2013, 'State-of-the-art: track degradation at bridge transitions', pp. 40-52.
Gallego Giner, I. & López Pita, A. 2009, 'Numerical simulation of embankment—structure transition design', *Proceedings of the Institution of Mechanical Engineers, Part F: Journal of Rail and Rapid Transit*, vol. 223, no. 4, pp. 331-43.
Gallego Giner, I., López Pita, A., Vieira Chaves, E.W. & Rivas Álvarez, A.M. 2012, 'Design of embankment–structure transitions for railway infrastructure', vol. 165, Thomas Telford Ltd, pp. 27-37.
Gallego, I., Muñoz, J., Rivas, A. & Sanchez-Cambronero, S. 2011, 'Vertical track stiffness as a new parameter involved in designing high-speed railway infrastructure', *Journal of transportation engineering*, vol. 137, no. 12, pp. 971-9.
Galvín, P., Romero, A. & Dominguez, J. 2010, 'Vibrations induced by HST passage on ballast and non-ballast tracks', *Soil Dynamics and Earthquake Engineering*, vol. 30, no. 9, pp. 862-73.
Galvín, P., Romero, A. & Domínguez, J. 2010, 'Fully three-dimensional analysis of high-speed train–track–soil-structure dynamic interaction', *Journal of Sound and Vibration*, vol. 329, no. 24, pp. 5147-63.

Germonpré, M., Degrande, G. & Lombaert, G. 2017, 'A track model for the prediction of ground-borne vibrations due to parametric excitation', vol. 199, pp. 2663-8.
Gonzalez, D. 2019, 'Traffic Congestion in California: Implementation of Congestion Pricing in Los Angeles County as an Effective Traffic-Reducing Strategy', California State University, Northridge.
Gubler, D. 2012, *Local train crossing the Brusio spiral viaduct, Switzerland*, <https://bahnbilder.ch/picture/11543>.
Gundavaram, D. & Hussaini, S.K.K. 2019, 'Polyurethane-based stabilization of railroad ballast–a critical review', *International Journal of Rail Transportation*, pp. 1-22.
Hay, W.W. 1982, *Railroad engineering*, vol. 1, John Wiley & Sons.
Hendry, M.T. 2007, 'Train-induced dynamic response of railway track and embankments on soft peaty foundations'.
Heydari-Noghabi, H., Varandas, J.N., Esmaeili, M. & Zakeri, J. 2017, 'Investigating the Influence of Auxiliary Rails on Dynamic Behavior of Railway Transition Zone by a 3D Train-Track Interaction Model', *Latin American Journal of Solids and Structures*, vol. 14, pp. 2000-18.
Heydari-Noghabi, H., Zakeri, J., Esmaeili, M. & Varandas, J. 2018, 'Field study using additional rails and an approach slab as a transition zone from slab track to the ballasted track', *Journal of Rail and Rapid Transit*, vol. 232, no. 4, pp. 970-8.
Hibbitt, D., Karlsson, B. & Sorensen, P. 2014, 'ABAQUS standard user's and reference manuals', *Dassault Systèmes*.
Hölscher, P. & Meijers, P. 2007, 'Literature study of knowledge and experience of transition zones', *Delft: report*, no. 415990-0011.
Hu, P., Zhang, C., Wen, S. & Wang, Y. 2019, 'Dynamic responses of high-speed railway transition zone with various subgrade fillings', *Computers and Geotechnics*, vol. 108, pp. 17-26.
Huang, H. & Brennecke, B. 2013, 'Track stiffness transition zone studied with three-dimensional sandwich track model', *Transportation Research Record: Journal of the Transportation Research Board*, no. 2374, pp. 136-42.
Huang, H., Tutumluer, E., Hashash, Y.M. & Ghaboussi, J. 2009, 'Discrete element modeling of aggregate behavior in fouled railroad ballast', pp. 33-41.
Hunt, H. & Winkler 1997, 'Settlement of railway track near bridge abutments.(third paper in young railway engineer of the year (1996) award)', vol. 123, Thomas Telford-ICE Virtual Library, pp. 68-73.
Hussaini, S.K.K., Indraratna, B. & Vinod, J.S. 2016, 'A laboratory investigation to assess the functioning of railway ballast with and without geogrids', *Transportation Geotechnics*, vol. 6, pp. 45-54.
Hyslip, J.P., Li, D. & Mcdaniel, C. 2009, 'Railway bridge transition case study'.
Indraratna, B. & Ionescu, D. 2000, 'State of the art large scale testing of ballast', vol. 24, pp. 24.1-.13.
Indraratna, B., Ionescu, D. & Christie, H. 1998, 'Shear behavior of railway ballast based on large-scale triaxial tests', *Journal of geotechnical and geoenvironmental Engineering*, vol. 124, no. 5, pp. 439-49.
Indraratna, B., Khabbaz, H., Salim, W. & Christie, D. 2006, 'Geotechnical properties of ballast and the role of geosynthetics', *Proceedings of the ICE: Ground Improvement*, vol. 10, no. 3, pp. 91-101.
Indraratna, B. & Ngo, T. 2018, *Ballast Railroad Design: SMART-UOW Approach*,

Book, vol. First edition, CRC Press, United States.
Indraratna, B., Nimbalkar, S., Christie, D., Rujikiatkamjorn, C. & Vinod, J. 2010, 'Field assessment of the performance of a ballasted rail track with and without geosynthetics', *Journal of Geotechnical and Geoenvironmental Engineering*, vol. 136, no. 7, pp. 907-17.
Indraratna, B., Nimbalkar, S. & Neville, T. 2014, 'Performance assessment of reinforced ballasted rail track', *Proceedings of the ICE: Ground Improvement*, vol. 167, no. 1, pp. 24-34.
Indraratna, B., Qi, Y., Ngo, T.N., Rujikiatkamjorn, C., Neville, T., Ferreira, F.B. & Shahkolahi, A. 2019, 'Use of Geogrids and Recycled Rubber in Railroad Infrastructure for Enhanced Performance', *Geosciences*, vol. 9, no. 1, p. 30.
Indraratna, B., Sajjad, M.B., Ngo, T., Correia, A.G. & Kelly, R. 2019, 'Improved Performance of Ballasted Tracks at Transition Zones: A Review of Experimental and Modelling Approaches', *Transportation Geotechnics*, vol. 21, p. 100260.
Indraratna, B., Salim, W. & Rujikiatkamjorn, C. 2011, *Advanced rail geotechnology–ballasted track*, CRC press, Netherlands.
Indraratna, B., Sun, Y. & Nimbalkar, S. 2016, 'Laboratory assessment of the role of particle size distribution on the deformation and degradation of ballast under cyclic loading', *Journal of geotechnical and geoenvironmental engineering*, vol. 142, no. 7, p. 04016016.
Insa, R., Salvador, P., Inarejos, J. & Roda, A. 2012, 'Analysis of the influence of under sleeper pads on the railway vehicle/track dynamic interaction in transition zones', *Proceedings of the Institution of Mechanical Engineers, Part F: Journal of Rail and Rapid Transit*, vol. 226, no. 4, pp. 409-20.
Iwnicki, S., Grassie, S. & Kik, W. 2000, 'Track settlement prediction using computer simulation tools', Project report thesis, Manchester Metropolitan University.
J. Pires, H.T.M. Phuong, A.G. Dumont, M. Vajdić, S. Lenart & Oslaković, I.S. 2014, 'SMARTRAIL – DEL 3.2 Rehabilitation of Open Tracks and Transition Zones', Project report thesis, 7th Framework Programme.
Jayasuriya, C., Indraratna, B. & Ngo, T.N. 2019, 'Experimental Study to Examine the Role of Under Sleeper Pads for Improved Performance of Ballast under Cyclic Loading', *Transportation Geotechnics*, vol. 19, pp. 61-73.
Kang, Y., Yang, S., Lee, H., Kim, Y., Jang, S. & Kim, E. 2008, 'A study of track and train dynamic behavior of transition zone between concrete slab track and ballasted track', Report thesis, Korea Railroad Research Institute, Uiwang, South Korea.
Karlsson, N. & Hjelm, M. 2016, 'Dynamic response of railway bridges subjected to high speed trains-Parametrical case studies', Thesis thesis, CHALMERS University of Technology, Sweden.
Kennedy, J., Woodward, P., Medero, G. & Banimahd, M. 2013, 'Reducing railway track settlement using three-dimensional polyurethane polymer reinforcement of the ballast', *Construction and Building Materials*, vol. 44, pp. 615-25.
Kenney, J. 1954, 'Steady-state vibrations of beam on elastic foundation for moving load', *J. appl. Mech.*, vol. 21, pp. 359-64.
Kerr, A.D. & Bathurst, L.A. 2001, 'A Method for Upgrading the Performance at Track Transitions for High-Speed Service', Report thesis, U.S. Department of Transportation.

Kerr, A.D. & Moroney, B.E. 1993, 'Track transition problems and remedies', *Bulletin American Railway Engineering Association*, no. 742, pp. 267-98.
Koch, E., Hudacsek, P., Szepesházi, R. & Kegyes-Brassai, O. 2018, '3D modelling of train-track interaction at bridge transition', paper presented to the *XVI Danube - European Conference on Geotechnical Engineering*.
Koh, C., Ong, J., Chua, D. & Feng, J. 2003, 'Moving element method for train-track dynamics', *International Journal for Numerical Methods in Engineering*, vol. 56, no. 11, pp. 1549-67.
Kouroussis, G., Connolly, D.P. & Verlinden, O. 2014, 'Railway-induced ground vibrations–a review of vehicle effects', *International Journal of Rail Transportation*, vol. 2, no. 2, pp. 69-110.
Kouroussis, G., Verlinden, O. & Conti, C. 2011, 'Free field vibrations caused by high-speed lines: measurement and time domain simulation', *Soil Dynamics and Earthquake Engineering*, vol. 31, no. 4, pp. 692-707.
Labrado Palomo, M., Roca Barceló, F., Ribes Llario, F. & Real Herráiz, J. 2018, 'Effect of vehicle speed on the dynamics of track transitions', *Journal of Vibration and Control*, vol. 24, no. 21, pp. 5118-28.
Lackenby, J., Indraratna, B., Mcdowell, G. & Christie, D. 2007, 'Effect of confining pressure on ballast degradation and deformation under cyclic triaxial loading', *Institution of Civil Engineers: Geotechnique*, vol. 57, no. 6, pp. 527-36.
Lamas-Lopez, F., Cui, Y.-J., Calon, N., D'aguiar, S.C. & Zhang, T. 2017, 'Impact of train speed on the mechanical behaviours of track-bed materials', *Journal of Rock Mechanics and Geotechnical Engineering*, vol. 9, no. 5, pp. 818-29.
Lamprea-Pineda, A.C., Connolly, D.P. & Hussein, M.F. 2021, 'Beams on elastic foundations–a review of railway applications and solutions', *Transportation Geotechnics*, p. 100696.
Lazorenko, G., Kasprzhitskii, A., Khakiev, Z. & Yavna, V. 2019, 'Dynamic behavior and stability of soil foundation in heavy haul railway tracks: A review', *Construction and Building Materials*, vol. 205, pp. 111-36.
Le Pen, L. & Powrie, W. 2011, 'Contribution of base, crib, and shoulder ballast to the lateral sliding resistance of railway track: a geotechnical perspective', *Proceedings of the Institution of Mechanical Engineers, Part F: Journal of Rail and Rapid Transit*, vol. 225, no. 2, pp. 113-28.
Lei, X. 2017, *High Speed Railway Track Dynamics*, Springer, Singapore.
Lei, X. & Mao, L. 2004, 'Dynamic response analyses of vehicle and track coupled system on track transition of conventional high speed railway', *Journal of Sound Vibration*, vol. 271, pp. 1133-46.
Lei, X. & Zhang, B. 2010, 'Influence of track stiffness distribution on vehicle and track interactions in track transition', *Journal of Rail and Rapid Transit*, vol. 224, no. 6, pp. 592-604.
Lei, X. & Zhang, B. 2011, 'Analyses of dynamic behavior of track transition with finite elements', *Journal of Vibration and Control*, vol. 17, no. 11, pp. 1733-47.
Leshchinsky, B. & Ling, H.I. 2013, 'Numerical modeling of behavior of railway ballasted structure with geocell confinement', *Geotextiles and Geomembranes*, vol. 36, pp. 33-43.
Li, D. 2000, 'Deformations and remedies for soft railroad subgrades subjected to heavy axle loads', *Advances in transportation and geoenvironmental systems using geosynthetics*, pp. 307-21.

Li, D. & Davis, D. 2005, 'Transition of Railroad Bridge Approaches', *Journal of Geotechnical and Geoenvironmental Engineering*, vol. 131, no. 11, pp. 1392-8.
Li, D., Hyslip, J., Sussmann, T. & Chrismer, S. 2016, *Railway geotechnics*, CRC Press, London.
Li, D., Otter, D. & Carr, G. 2010, 'Railway bridge approaches under heavy axle load traffic: problems, causes, and remedies', *Proceedings of the Institution of Mechanical Engineers, Part F: Journal of Rail and Rapid Transit*, vol. 224, no. 5, pp. 383-90.
Li, D. & Selig, E.T. 1998, 'Method for railroad track foundation design. I: Development', *Journal of geotechnical and geoenvironmental engineering*, vol. 124, no. 4, pp. 316-22.
Li, D. & Selig, E.T. 1998, 'Method for railroad track foundation design. II: Applications', *Journal of geotechnical and geoenvironmental engineering*, vol. 124, no. 4, pp. 323-9.
Li, L., Nimbalkar, S. & Zhong, R. 2018, 'Finite element model of ballasted railway with infinite boundaries considering effects of moving train loads and Rayleigh waves', *Soil Dynamics and Earthquake Engineering*, vol. 114, pp. 147-53.
Li, Z. & Wu, T. 2008, 'Vehicle/track impact due to passing the transition between a floating slab and ballasted track', *Noise and Vibration Mitigation for Rail Transportation Systems*, Springer, pp. 94-100.
Lima, A.D.O., Dersch, M., Qian, Y., Tutumluer, E. & Edwards, J. 2017, 'Laboratory evaluation of under-ballast mat effectiveness to mitigate differential movement problem in railway transition zones'.
Long, J.H., Olson, S.M., Stark, T.D. & Samara, E.A. 1998, 'Differential movement at embankment-bridge structure interface in Illinois', *Transportation Research Record*, vol. 1633, no. 1, pp. 53-60.
Luna, R. 2004, *Evaluation of bridge approach slabs, performance and design*.
Lundqvist, A. & Dahlberg, T. 2005, 'Load impact on railway track due to unsupported sleepers', *Journal of Rail and Rapid Transit*, vol. 219, no. 2, pp. 67-77.
Lundqvist, A., Larsson, R. & Dahlberg, T. 2006, 'Influence of railway track stiffness variations on wheel/rail contact force', *Track for High-Speed Railways, Porto, Portugal*.
Mallik, A.K., Chandra, S. & Singh, A.B. 2006, 'Steady-state response of an elastically supported infinite beam to a moving load', *Journal of sound and vibration*, vol. 291, no. 3-5, pp. 1148-69.
Mcdowell, G.R. & Li, H. 2016, 'Discrete element modelling of scaled railway ballast under triaxial conditions', *Granular matter*, vol. 18, no. 3, p. 66.
Mills, J.A. 2006, 'THE MYTH OF THE STANDARD GAUGE: RAIL GAUGE CHOICE IN AUSTRALIA', GRIFFITH UNIVERSITY.
Mishra, D., Boler, H., Tutumluer, E., Hou, W. & Hyslip, J.P. 2017, 'Deformation and dynamic load amplification trends at railroad bridge approaches: effects caused by high-speed passenger trains', *Transportation research record*, vol. 2607, no. 1, pp. 43-53.
Mishra, D., Qian, Y., Huang, H. & Tutumluer, E. 2014, 'An integrated approach to dynamic analysis of railroad track transitions behavior', *Transportation Geotechnics*, vol. 1, no. 4, pp. 188-200.
Mishra, D., Tutumluer, E., Boler, H., Hyslip, J. & Sussmann, T. 2014, 'Railroad track

transitions with multidepth deflectometers and strain gauges', *Transportation Research Record: Journal of the Transportation Research Board*, no. 2448, pp. 105-14.
Mishra, D., Tutumluer, E., Stark, T.D., Hyslip, J.P., Chrismer, S.M. & Tomas, M. 2012, 'Investigation of differential movement at railroad bridge approaches through geotechnical instrumentation', *Journal of Zhejiang University SCIENCE A*, vol. 13, no. 11, pp. 814-24.
Momoya, Y., Sekine, E. & Tatsuoka, F. 2005, 'Deformation characteristics of railway roadbed and subgrade under moving-wheel load', *Soils and Foundations*, vol. 45, no. 4, pp. 99-118.
Momoya, Y., Takahashi, T. & Nakamura, T. 2016, 'A study on the deformation characteristics of ballasted track at structural transition zone by multi-actuator moving loading test apparatus', *Transportation Geotechnics*, vol. 6, pp. 123-34.
Namura, A., Kohata, Y. & Miura, S. 2004, 'Effect of sleeper size on ballasted track settlement', *Quarterly Report of RTRI*, vol. 45, no. 3, pp. 156-61.
Namura, A. & Suzuki, T. 2007, *Evaluation of Countermeasures against Differential Settlement at Track Transitions*, vol. 48, 3.
Nassif, H., Vittilo, N. & Abu Amra, T. 2003, 'Analysis and Design of Bridge Approach and Transition Slabs in New Jersey'.
Navaratnarajah, S.K., Indraratna, B. & Ngo, N.T. 2018, 'Influence of under sleeper pads on ballast behavior under cyclic loading: experimental and numerical studies', *Journal of Geotechnical and Geoenvironmental Engineering*, vol. 144, no. 9, p. 04018068.
Ngo, N.T., Indraratna, B. & Rujikiatkamjorn, C. 2016, 'Micromechanics-based investigation of fouled ballast using large-scale triaxial tests and discrete element modeling', *Journal of Geotechnical and Geoenvironmental Engineering*, vol. 143, no. 2, p. 04016089.
Ngo, N.T., Indraratna, B. & Rujikiatkamjorn, C. 2016, 'Simulation ballasted track behavior: numerical treatment and field application', *International Journal of Geomechanics*, vol. 17, no. 6, p. 04016130.
Ngo, N.T., Indraratna, B. & Rujikiatkamjorn, C. 2018, 'Load-Deformation Responses of Ballasted Rail Tracks: Laboratory and Discrete-Continuum Modelling', Springer, pp. 189-98.
Nguyen, V.-H. & Duhamel, D. 2008, 'Finite element procedures for nonlinear structures in moving coordinates. Part II: Infinite beam under moving harmonic loads', *Computers & Structures*, vol. 86, no. 21-22, pp. 2056-63.
Nicks, J.E. 2009, 'The bump at the end of the railway bridge', thesis thesis, Texas A&M University.
Nimbalkar, S. & Indraratna, B. 2016, 'Improved performance of ballasted rail track using geosynthetics and rubber shockmat'.
Nimbalkar, S., Indraratna, B., Dash, S.K. & Christie, D. 2012, 'Improved performance of railway ballast under impact loads using shock mats', *Journal of geotechnical and geoenvironmental engineering*, vol. 138, no. 3, pp. 281-94.
Onesteel, L. 2017, 'Rail Track Material: Steel Rails and Trak-Lok Steel Sleeper Systems, 2017', Series Rail Track Material: Steel Rails and Trak-Lok Steel Sleeper Systems, 2017, 2017.
Paixão, A. 2014, 'Transition zones in railway tracks: an experimental and numerical

study on the structural behaviour', PhD Thesis thesis, Porto: University of Porto, Faculty of Engineering, Porto.
Paixao, A., Fortunato, E. & Calçada, R. 2015, 'Design and construction of backfills for railway track transition zones', *Proceedings of the Institution of Mechanical Engineers, Part F: Journal of Rail and Rapid Transit*, vol. 229, no. 1, pp. 58-70.
Paixão, A., Fortunato, E. & Calçada, R. 2014, 'Transition zones to railway bridges: track measurements and numerical modelling', *Engineering structures*, vol. 80, pp. 435-43.
Paixão, A., Fortunato, E. & Calçada, R. 2016, 'A numerical study on the influence of backfill settlements in the train/track interaction at transition zones to railway bridges', *Proceedings of the Institution of Mechanical Engineers, Part F: Journal of Rail and Rapid Transit*, vol. 230, no. 3, pp. 866-78.
Paixão, A., Varandas, J.N., Fortunato, E. & Calçada, R. 2018, 'Numerical simulations to improve the use of under sleeper pads at transition zones to railway bridges', *Engineering Structures*, vol. 164, pp. 169-82.
Pita, A.L., Teixeira, P.F. & Robuste, F. 2004, 'High speed and track deterioration: The role of vertical stiffness of the track', *Journal of Rail and Rapid Transit*, vol. 218, no. 1, pp. 31-40.
Plotkin, D. & Davis, D. 2008, *Bridge approaches and track stiffness*, Project report, U.S. Department of Transportation.
Powrie, W. & Le Pen, L. 2016, *A Guide to Track Stiffness*, University of Southampton.
Powrie, W., Yang, L. & Clayton, C.R. 2007, 'Stress changes in the ground below ballasted railway track during train passage', *Proceedings of the Institution of Mechanical Engineers, Part F: Journal of Rail and Rapid Transit*, vol. 221, no. 2, pp. 247-62.
Priest, J. & Powrie, W. 2009, 'Determination of dynamic track modulus from measurement of track velocity during train passage', *Journal of geotechnical and geoenvironmental engineering*, vol. 135, no. 11, pp. 1732-40.
Punetha, P., Nimbalkar, S. & Khabbaz, H. 2020, 'Analytical Evaluation of Ballasted Track Substructure Response under Repeated Train Loads', *International Journal of Geomechanics*, vol. 20, no. 7, p. 04020093.
Punetha, P., Nimbalkar, S. & Khabbaz, H. 2021, 'Simplified geotechnical rheological model for simulating viscoelasto-plastic response of ballasted railway substructure', *International Journal for Numerical and Analytical Methods in Geomechanics*, vol. 45, no. 14, pp. 2019-47.
Puppala, A.J., Archeewa, E., Saride, S., Nazarian, S. & Hoyos, L. 2012, 'Recommendations for design, construction, and maintenance of bridge approach slabs', Technical report thesis, The University of Texas at Arlington.
Puppala, A.J., Saride, S., Archeewa, E., Hoyos, L.R. & Nazarian, S. 2009, *Recommendations for design, construction, and maintenance of bridge approach slabs: Synthesis report*.
Puppala, A.J., Saride, S., Archeewa, E., Hoyos, L.R. & Nazarian, S. 2009, 'Recommendations for design, construction, and maintenance of bridge approach slabs: Synthesis report', Technical report thesis, The University of Texas at Arlington.
Puzavac, L., Popović, Z. & Lazarević, L. 2012, 'Influence of track stiffness on track behaviour under vertical load', *PROMET-Traffic & Transportation*, vol. 24, no.

5, pp. 405-12.
Qian, Y., Tutumluer, E., Mishra, D. & Kazmee, H. 2018, 'Triaxial testing and discrete-element modelling of geogrid-stabilised rail ballast', *Proceedings of the Institution of Civil Engineers-Ground Improvement*, vol. 171, no. 4, pp. 223-31.
Read, D. & Li, D. 2006, 'Design of track transitions', *TCRP Research Results Digest*, no. 79.
Real, T., Zamorano, C., Hernández, C., García, J. & Real, J. 2016, 'Static and dynamic behavior of transitions between different railway track typologies', *KSCE Journal of Civil Engineering*, vol. 20, no. 4, pp. 1356-64.
Rose, J., Walker, L. & Li, D. 2002, 'Heavy-Haul Asphalt (HMA) underlayment trackbeds: Pressures/deflections/materials properties measurements'.
Sadeghi, J. & Askarinejad, H. 2010, 'Development of nonlinear railway track model applying modified plane strain technique', *Journal of transportation engineering*, vol. 136, no. 12, pp. 1068-74.
Sañudo, R., Cerrada, M., Alonso, B. & Dell'olio, L. 2017, 'Analysis of the influence of support positions in transition zones. A numerical analysis', *Construction and Building Materials*, vol. 145, pp. 207-17.
Sañudo, R., Dell'olio, L., Casado, J., Carrascal, I. & Diego, S. 2016, 'Track transitions in railways: A review', *Construction and Building Materials*, vol. 112, pp. 140-57.
Sañudo, R., Miranda, M. & Markine, V. 2016, 'The influence of train running direction and track supports position on the behaviour of transition zones', vol. 18, pp. 281-8.
Sasaoka, C.D. & Davis, D. 2005, 'Implementing track transition solutions for heavy axle load service', Citeseer.
Sato, Y. 1995, 'Japanese studies on deterioration of ballasted track', *Vehicle system dynamics*, vol. 24, no. sup1, pp. 197-208.
Sayeed, M.A. & Shahin, M.A. 2016, 'Three-dimensional numerical modelling of ballasted railway track foundations for high-speed trains with special reference to critical speed', *Transportation Geotechnics*, vol. 6, pp. 55-65.
Sayeed, M.A. & Shahin, M.A. 2017, 'Design of ballasted railway track foundations using numerical modelling Part I: Development', *Canadian Geotechnical Journal*, no. ja.
Seara, I. & Correia, A.G. 2008, *Zonas de transição de vias-férreas. A importância de uma solução geoestrutural*, 9899574023.
Selig, E.T. & Li, D. 1994, 'Track modulus: Its meaning and factors influencing it', *Transportation Research Record*, no. 1470.
Selig, E.T. & Waters, J.M. 1994, *Track geotechnology and substructure management*, Thomas Telford.
Senalp, A.D., Arikoglu, A., Ozkol, I. & Dogan, V.Z. 2010, 'Dynamic response of a finite length euler-bernoulli beam on linear and nonlinear viscoelastic foundations to a concentrated moving force', *Journal of Mechanical Science and Technology*, vol. 24, no. 10, pp. 1957-61.
Sew, I.D.G.S. & Chin, I.T.Y. 2001, 'Geotechnical Solutions for High Speed Track Embankment–A Brief Overview'.
Shahraki, M., Warnakulasooriya, C. & Witt, K.J. 2015, 'Numerical study of transition zone between ballasted and ballastless railway track', *Transportation*

Geotechnics, vol. 3, pp. 58-67.
Shan, Y., Albers, B. & Savidis, S.A. 2013, 'Influence of different transition zones on the dynamic response of track–subgrade systems', *Computers and Geotechnics*, vol. 48, pp. 21-8.
Shan, Y., Shu, Y. & Zhou, S. 2017, 'Finite-infinite element coupled analysis on the influence of material parameters on the dynamic properties of transition zones', *Construction and Building Materials*, vol. 148, pp. 548-58.
Shan, Y., Zhou, S. & Shu, Y. 2018, 'Differential Settlement and Soil Dynamic Stress of a Culvert-embankment Transition Zone Due to an Adjacent Shield Tunnel Construction', *KSCE Journal of Civil Engineering*, vol. 22, no. 7, pp. 2325-33.
Shih, J.-Y., Grossoni, I. & Bezin, Y. 2019, 'Settlement analysis using a generic ballasted track simulation package', *Transportation Geotechnics*, vol. 20, p. 100249.
Sol-Sánchez, M., Moreno-Navarro, F. & Rubio-Gámez, M.C. 2015, 'The use of elastic elements in railway tracks: A state of the art review', *Construction and building materials*, vol. 75, pp. 293-305.
Stanislav, L., Karmen, F.B., Karin, N.-C., Amir, M.K., Miha, K., Marko, V., Kangle, C. & Julie, C. 2018, *Guidelines on the Use of Novel Construction and Maintenance Techniques within the Operational Railway Environment*, 636285, vol. D4.1, DESTination RAIL – Decision Support Tool for Rail Infrastructure Managers, H2020-MG 2014-2015.
Stark, T.D. & Wilk, S.T. 2016, 'Root cause of differential movement at bridge transition zones', *Proceedings of the Institution of Mechanical Engineers, Part F: Journal of Rail and Rapid Transit*, vol. 230, no. 4, pp. 1257-69.
Stark, T.D. & Wynn, L. 2018, 'Reinforced Railway Transitions to Mitigate Differential Displacements', *American Association of Railroads, Technology Digest, TD-18-0XX, Transportation Tech. Center, Inc., Pueblo, CO*.
Steffens, D.M. 2005, 'Identification and development of a model of railway track dynamic behaviour', Master`s thesis thesis, Queensland University of Technology.
Sterling, R. & Nelson, P. 2013, 'City resiliency and underground space use', *Zhou, Cai, Sterling (Eds.), Advances in Underground Space Development, Copyright*, pp. 56-14.
Suiker, A.S. & De Borst, R. 2003, 'A numerical model for the cyclic deterioration of railway tracks', *International journal for numerical methods in engineering*, vol. 57, no. 4, pp. 441-70.
Sun, Q.D., Indraratna, B. & Nimbalkar, S. 2015, 'Deformation and degradation mechanisms of railway ballast under high frequency cyclic loading', *Journal of Geotechnical and Geoenvironmental Engineering*, vol. 142, no. 1, p. 04015056.
Sung, D., Chang, S. & Kim, S. 2020, 'Effect of additional anti-vibration sleeper track considering sleeper spacing and track support stiffness on reducing low-frequency vibrations', *Construction and Building Materials*, vol. 263, p. 120140.
Sussman, T., Ebersöhn, W. & Selig, E. 2001, 'Fundamental nonlinear track load-deflection behavior for condition evaluation', *Transportation research record: journal of the transportation research board*, no. 1742, pp. 61-7.
Teixeira, P.F., Casas-Esplugas, C., López-Pita, A. & Ubalde, L. 2006, *Deterioration*

in geometric track quality on high speed lines: the experience of the Madrid-Seville high speed line (1992-2002).

Thach, P.-N., Liu, H.-L. & Kong, G.-Q. 2013, 'Vibration analysis of pile-supported embankments under high-speed train passage', *Soil Dynamics and Earthquake Engineering*, vol. 55, pp. 92-9.

Tutumluer, E., Huang, H., Hashash, Y. & Ghaboussi, J. 2007, 'Discrete element modeling of railroad ballast settlement'.

Tutumluer, E., Qian, Y., Hashash, Y.M., Ghaboussi, J. & Davis, D.D. 2013, 'Discrete element modelling of ballasted track deformation behaviour', *International Journal of Rail Transportation*, vol. 1, no. 1-2, pp. 57-73.

Tutumluer, E., Stark, T.D., Mishra, D. & Hyslip, J.P. 2012, 'Investigation and mitigation of differential movement at railway transitions for US high speed passenger rail and joint passenger/freight corridors', American Society of Mechanical Engineers, pp. 75-84.

Ugural, A.C. & Fenster, S.K. 2003, *Advanced strength and applied elasticity*, Pearson education.

Uzzal, R.U.A., Ahmed, W. & Rakheja, S. 2008, 'Dynamic analysis of railway vehicle-track interactions due to wheel flat with a pitch-plane vehicle model', *Journal of Mechanical Engineering*, vol. 39, no. 2, pp. 86-94.

Van Dalen, K. 2006, 'Ground vibration induced by a high-speed train running over inhomogeneous subsoil, transition radiation in two-dimensional inhomogeneous elastic systems', Master`s thesis thesis, Department of Structural Engineering, TUDelft.

Varandas, J., Hölscher, P. & Silva, M. 2010, 'A settlement model for ballast at transition zones'.

Varandas, J., Hölscher, P. & Silva, M. 2016, 'Three-dimensional track-ballast interaction model for the study of a culvert transition', *Soil Dynamics and Earthquake Engineering*, vol. 89, pp. 116-27.

Varandas, J.N. 2013, 'Long-term behaviour of railway transitions under dynamic loading application to soft soil sites', PhD Thesis thesis, Lisboa: Faculdade de Ciências e Tecnologia da Universidade Nova de Lisboa.

Varandas, J.N., Hölscher, P. & Silva, M.A. 2011, 'Dynamic behaviour of railway tracks on transitions zones', *Computers & structures*, vol. 89, no. 13-14, pp. 1468-79.

Wahls, H.E. 1990, *Design and construction of bridge approaches*, vol. 159, Transportation Research Board.

Walker, R.T. & Indraratna, B. 2018, 'Moving Loads on a Viscoelastic Foundation with Special Reference to Railway Transition Zones', *International Journal of Geomechanics*, vol. 18, no. 11, p. 04018145.

Wang, H., Chang, L. & Markine, V. 2018, 'Structural health monitoring of railway transition zones using satellite radar data', *Sensors*, vol. 18, no. 2, p. 413.

Wang, H. & Markine, V. 2018, 'Modelling of the long-term behaviour of transition zones: Prediction of track settlement', *Engineering Structures*, vol. 156, pp. 294-304.

Wang, H., Markine, V. & Liu, X. 2018, 'Experimental analysis of railway track settlement in transition zones', *Proceedings of the Institution of Mechanical Engineers, Part F: Journal of rail and rapid transit*, vol. 232, no. 6, pp. 1774-89.

Wang, H., Markine, V., Shevtsov, I. & Dollevoet, R. 2015, 'Analysis of the dynamic behaviour of a railway track in transition zones with differential settlement', American Society of Mechanical Engineers, pp. V001T01A24-VT01A24.
Wang, H. & Markine, V.L. 2018, 'Methodology for the comprehensive analysis of railway transition zones', *Computers and Geotechnics*, vol. 99, pp. 64-79.
Wang, H., Silvast, M., Markine, V. & Wiljanen, B. 2017, 'Analysis of the dynamic wheel loads in railway transition zones considering the moisture condition of the ballast and subballast', *Applied Sciences*, vol. 7, no. 12, p. 1208.
Wei, K., Liu, Z.-X., Liang, Y.-C. & Wang, P. 2017, 'An investigation into the effect of temperature-dependent stiffness of rail pads on vehicle-track coupled vibrations', *Proceedings of the Institution of Mechanical Engineers, Part F: Journal of Rail and Rapid Transit*, vol. 231, no. 4, pp. 444-54.
Wilk, S.T., Stark, T.D. & Rose, J.G. 2016, 'Evaluating tie support at railway bridge transitions', *Proceedings of the Institution of Mechanical Engineers, Part F: Journal of Rail and Rapid Transit*, vol. 230, no. 4, pp. 1336-50.
Witt, S. 2008, 'The influence of under sleeper pads on railway track dynamics', Master`s Thesis thesis, Dept. of Management and Engineering, Linkoping Univ. Institute of Technology.
Woldringh, R. & New, B. 1999, 'Embankment design for high speed trains on soft soils'.
Woodward, P., Kennedy, J. & Medero, G. 2009, 'Three-dimensional track reinforcement using polymer geocomposites', *Proceedings of the American Railway Engineering and Maintenance of Way Association (AREMA), Chicago, USA*.
Woodward, P., Kennedy, J. & Medero, G. 2010, 'Improving the safety of the railway track infrastructure using insitu polyurethane geocomposites'.
Woodward, P., Kennedy, J., Medero, G. & Banimahd, M. 2012, 'Application of in situ polyurethane geocomposite beams to improve the passive shoulder resistance of railway track', *Proceedings of the Institution of Mechanical Engineers, Part F: Journal of Rail and Rapid Transit*, vol. 226, no. 3, pp. 294-304.
Woodward, P., Kennedy, J., Medero, G. & Banimahd, M. 2012, 'Maintaining absolute clearances in ballasted railway tracks using in situ three-dimensional polyurethane geocomposites', *Proceedings of the Institution of Mechanical Engineers, Part F: Journal of Rail and Rapid Transit*, vol. 226, no. 3, pp. 257-71.
Wu, Q., Spiryagin, M., Cole, C. & Mcsweeney, T. 2018, 'Parallel computing in railway research', *International Journal of Rail Transportation*, pp. 1-24.
Yu, H. & Yuan, Y. 2013, 'Analytical solution for an infinite Euler-Bernoulli beam on a viscoelastic foundation subjected to arbitrary dynamic loads', *Journal of Engineering Mechanics*, vol. 140, no. 3, pp. 542-51.
Yu, H., Zhang, Z., Chen, J., Bobet, A., Zhao, M. & Yuan, Y. 2018, 'Analytical solution for longitudinal seismic response of tunnel liners with sharp stiffness transition', *Tunnelling and Underground Space Technology*, vol. 77, pp. 103-14.
Zakeri, J.-A. & Ghorbani, V. 2011, 'Investigation on dynamic behavior of railway track in transition zone', *Journal of Mechanical Science and Technology*, vol. 25, no. 2, pp. 287-92.
Zaman, M., Gopalasingam, A. & Laguros, J.G. 1991, 'Consolidation settlement of

bridge approach foundation', *Journal of Geotechnical Engineering*, vol. 117, no. 2, pp. 219-40.
Zarembski, A. & Palese, J. 2003, 'Transitions eliminate impact at crossings', *Railway track and structures*, vol. 99, no. 8.
Zhai, W. & True, H. 2000, 'Vehicle-track dynamics on a ramp and on the bridge: simulation and measurements', *Vehicle System Dynamics*, vol. 33, pp. 604-15.
Zhai, W., Wang, K. & Cai, C. 2009, 'Fundamentals of vehicle–track coupled dynamics', *Vehicle System Dynamics*, vol. 47, no. 11, pp. 1349-76.
Zhai, W., Wang, S., Zhang, N., Gao, M., Xia, H., Cai, C. & Zhao, C. 2013, 'High-speed train–track–bridge dynamic interactions–Part II: experimental validation and engineering application', *International Journal of Rail Transportation*, vol. 1, no. 1-2, pp. 25-41.
Zhai, W., Xia, H., Cai, C., Gao, M., Li, X., Guo, X., Zhang, N. & Wang, K. 2013, 'High-speed train–track–bridge dynamic interactions–Part I: theoretical model and numerical simulation', *International Journal of Rail Transportation*, vol. 1, no. 1-2, pp. 3-24.
Zhang, S., Xiao, X., Wen, Z. & Jin, X. 2008, 'Effect of unsupported sleepers on wheel/rail normal load', *Soil Dynamics and Earthquake Engineering*, vol. 28, no. 8, pp. 662-73.
Zhang, T.-W., Lamas-Lopez, F., Cui, Y.-J., Calon, N. & D'aguiar, S.C. 2017, 'Development of a simple 2D model for railway track-bed mechanical behaviour based on field data', *Soil Dynamics and Earthquake Engineering*, vol. 99, pp. 203-12.
Zhang, X., Zhao, C. & Zhai, W. 2016, 'Dynamic behavior analysis of high-speed railway ballast under moving vehicle loads using discrete element method', *International Journal of Geomechanics*, vol. 17, no. 7, p. 04016157.
Zhang, Y.-J., Murray, M. & Ferreira, L. 1998, 'A mechanistic approach for estimation of track modulus', Central Queensland University Rockhampton, Qld, pp. 9-14.
Zhao, L., Wang, X., Stoeter, J., Sun, Y., Li, H., Hu, Q. & Li, M. 2019, 'Path Optimization Model for Intra-City Express Delivery in Combination with Subway System and Ground Transportation', *Sustainability*, vol. 11, no. 3, p. 758.
Zhou, S., Wang, B. & Shan, Y. 2020, 'Review of research on high-speed railway subgrade settlement in soft soil area', *Railway Engineering Science*, vol. 28, no. 2, pp. 129-45.
Zhu, J., Thompson, D. & Jones, C. 2011, 'On the effect of unsupported sleepers on the dynamic behaviour of a railway track', *Vehicle system dynamics*, vol. 49, no. 9, pp. 1389-408.
Zuada Coelho, B. 2011, 'Dynamics of railway transition zones in soft soils', PhD Thesis thesis, Delft University of Technology.

APPENDIX A: MATLAB CODE FOR BOEF ANALYSIS

```
clear all
close all
clc
syms Y(x) w E I k f
assume([E I k] > 0)

u = symunit;
Eu = E*u.Pa;     % Pascal
Iu = I*u.m^4;    % meter^4
ku = k*u.N/u.m^2;  % Newton/meter^2
X = x*u.m;
F = f*u.N/u.m;

eqn = diff(Y,X,4) + ku/(Eu*Iu)*Y ==
F/(Eu*Iu)*dirac(x)
eqnFT = fourier(eqn)
eqnFT = isolate(eqnFT, fourier(Y(x),x,w))
YSol = ifourier(rhs(eqnFT));
YSol = simplify(YSol)
checkUnits(subs(eqn,Y,YSol));
YSol = separateUnits(YSol);


values = [205e9 3.0422e-5 80e6 0.0981e6];
YSol2 = subs(YSol,[E I k f],values);
YSol2 = vpa(YSol2,16);
figure('Renderer', 'painters', 'Position',
[75 140 1050 500])
fplot(-YSol2, 'linewidth',2); hold on

values1 = [205e9 3.0422e-5 40e6 0.0981e6];
YSol3 = subs(YSol,[E I k f],values1);
YSol3 = vpa(YSol3,16)
fplot(-YSol3, 'linewidth',2)
hold on

values = [205e9 3.0422e-5 20e6 0.0981e6];
YSol1 = subs(YSol,[E I k f],values);
YSol1 = vpa(YSol1,16)
fplot(-YSol1, 'linewidth',2)
```

```
hold on

values = [205e9 3.0422e-5 10e6 0.0981e6];
YSol4 = subs(YSol,[E I k f],values);
YSol4 = vpa(YSol4,16)
fplot(-YSol4, 'linewidth',2)
hold on

values1 = [205e9 3.0422e-5 5e6 0.0981e6];
YSol5 = subs(YSol,[E I k f],values1);
YSol5 = vpa(YSol5,16)
fplot(-YSol5, 'linewidth',2)
hold on


 grid on
ax = gca;
ax.GridColor = [0 0 0];
ax.GridLineStyle = '--';
ax.GridAlpha = 0.5;
ax.Layer = 'bottom';
xlabel('Distance from the load, along the
track (m)', 'FontSize', 22);
ylabel('Vertical displacement (m)',
'FontSize', 22);
set(gca,'FontSize',18);
```

APPENDIX B: DERIVATION OF EMPIRICAL RELATION FOR k_i.

B.1 Calculation of wheel deflection

The calculation of stiffness for various segments of the multistep transition is based on the differential settlement between two consecutive segments. Therefore, the first step was to calculate the track deflection under each wheel load, considering the effect of multiple loadings of a four-carriage train. In order to achieve that, a comprehensive spreadsheet (as given in Figure B-1) was prepared that has the ability to calculate track deflection under each wheel load for any given stiffness values. This spreadsheet is also capable of selecting the stiffness value based on the wheel location. The Equation used in this spreadsheet for calculating the wheel deflection is as follows:

$$w(0,t) = \sum_{n=1}^{N} \frac{F_n}{2k_{system}L} e^{-\frac{vt-d_n}{L}} \left(cos\left(\frac{vt-d_n}{L}\right) + sin\left(\frac{vt-d_n}{L}\right)\right)$$

where

$$L = \sqrt[4]{\frac{4EI}{k}}$$

B.2 Calculation of stiffness change at track transition

In order to design a transition zone, the total stiffness variation is calculated for the given transition. This can be done using below equation:

$$\Delta k = k_{max} - k_{min}$$

Wheel 1			Wheel 2			Wheel 3			Wheel 4		
x	*k*	*w*	*x*	*k*	*w*	*x*	*k*	*w*	*x*	*k*	*w*
-90	5	6.24E-29	-87.5	5	-1.2E-28	-75.5	5	-9.1E-25	-73	5	3.28E-24
-89.5	5	7.54E-29	-87	5	-3E-28	-75	5	-9.7E-25	-72.5	5	6.42E-24
-89	5	7.7E-29	-86.5	5	-5.7E-28	-74.5	5	-7.7E-25	-72	5	1.05E-23
-88.5	5	5.62E-29	-86	5	-9.1E-28	-74	5	-1.3E-25	-71.5	5	1.53E-23
-88	5	-2.1E-30	-85.5	5	-1.3E-27	-73.5	5	1.14E-24	-71	5	1.98E-23
-87.5	5	-1.2E-28	-85	5	-1.6E-27	-73	5	3.28E-24	-70.5	5	2.24E-23
-87	5	-3E-28	-84.5	5	-1.8E-27	-72.5	5	6.42E-24	-70	5	2.04E-23
-86.5	5	-5.7E-28	-84	5	-1.6E-27	-72	5	1.05E-23	-69.5	5	1.02E-23
-86	5	-9.1E-28	-83.5	5	-6E-28	-71.5	5	1.53E-23	-69	5	-1.3E-23
-85.5	5	-1.3E-27	-83	5	1.47E-27	-71	5	1.98E-23	-68.5	5	-5.4E-23
-85	5	-1.6E-27	-82.5	5	5.07E-27	-70.5	5	2.24E-23	-68	5	-1.2E-22
-84.5	5	-1.8E-27	-82	5	1.05E-26	-70	5	2.04E-23	-67.5	5	-2E-22
-84	5	-1.6E-27	-81.5	5	1.78E-26	-69.5	5	1.02E-23	-67	5	-3.1E-22
-83.5	5	-6E-28	-81	5	2.65E-26	-69	5	-1.3E-23	-66.5	5	-4.2E-22
-83	5	1.47E-27	-80.5	5	3.53E-26	-68.5	5	-5.4E-23	-66	5	-5E-22
-82.5	5	5.07E-27	-80	5	4.13E-26	-68	5	-1.2E-22	-65.5	5	-5.1E-22
-82	5	1.05E-26	-79.5	5	4.01E-26	-67.5	5	-2E-22	-65	5	-3.6E-22
-81.5	5	1.78E-26	-79	5	2.52E-26	-67	5	-3.1E-22	-64.5	5	4.74E-23
-81	5	2.65E-26	-78.5	5	-1.2E-26	-66.5	5	-4.2E-22	-64	5	8.24E-22
-80.5	5	3.53E-26	-78	5	-8E-26	-66	5	-5E-22	-63.5	5	2.08E-21
-80	5	4.13E-26	-77.5	5	-1.9E-25	-65.5	5	-5.1E-22	-63	5	3.89E-21
-79.5	5	4.01E-26	-77	5	-3.4E-25	-65	5	-3.6E-22	-62.5	5	6.2E-21
-79	5	2.52E-26	-76.5	5	-5.3E-25	-64.5	5	4.74E-23	-62	5	8.77E-21
-78.5	5	-1.2E-26	-76	5	-7.4E-25	-64	5	8.24E-22	-61.5	5	1.1E-20
-78	5	-8E-26	-75.5	5	-9.1E-25	-63.5	5	2.08E-21	-61	5	1.2E-20
-77.5	5	-1.9E-25	-75	5	-9.7E-25	-63	5	3.89E-21	-60.5	5	1.02E-20
-77	5	-3.4E-25	-74.5	5	-7.7E-25	-62.5	5	6.2E-21	-60	5	3.41E-21
-76.5	5	-5.3E-25	-74	5	-1.3E-25	-62	5	8.77E-21	-59.5	5	-1.1E-20
-76	5	-7.4E-25	-73.5	5	1.14E-24	-61.5	5	1.1E-20	-59	5	-3.5E-20
-75.5	5	-9.1E-25	-73	5	3.28E-24	-61	5	1.2E-20	-58.5	5	-7.2E-20
-75	5	-9.7E-25	-72.5	5	6.42E-24	-60.5	5	1.02E-20	-58	5	-1.2E-19
-74.5	5	-7.7E-25	-72	5	1.05E-23	-60	5	3.41E-21	-57.5	5	-1.8E-19
-74	5	-1.3E-25	-71.5	5	1.53E-23	-59.5	5	-1.1E-20	-57	5	-2.4E-19
-73.5	5	1.14E-24	-71	5	1.98E-23	-59	5	-3.5E-20	-56.5	5	-2.8E-19
-73	5	3.28E-24	-70.5	5	2.24E-23	-58.5	5	-7.2E-20	-56	5	-2.6E-19
-72.5	5	6.42E-24	-70	5	2.04E-23	-58	5	-1.2E-19	-55.5	5	-1.6E-19
-72	5	1.05E-23	-69.5	5	1.02E-23	-57.5	5	-1.8E-19	-55	5	9.9E-20
-71.5	5	1.53E-23	-69	5	-1.3E-23	-57	5	-2.4E-19	-54.5	5	5.68E-19
-71	5	1.98E-23	-68.5	5	-5.4E-23	-56.5	5	-2.8E-19	-54	5	1.31E-18
-70.5	5	2.24E-23	-68	5	-1.2E-22	-56	5	-2.6E-19	-53.5	5	2.34E-18
-70	5	2.04E-23	-67.5	5	-2E-22	-55.5	5	-1.6E-19	-53	5	3.62E-18
-69.5	5	1.02E-23	-67	5	-3.1E-22	-55	5	9.9E-20	-52.5	5	5E-18
-69	5	-1.3E-23	-66.5	5	-4.2E-22	-54.5	5	5.68E-19	-52	5	6.12E-18
-68.5	5	-5.4E-23	-66	5	-5E-22	-54	5	1.31E-18	-51.5	5	6.39E-18
-68	5	-1.2E-22	-65.5	5	-5.1E-22	-53.5	5	2.34E-18	-51	5	4.92E-18
-67.5	5	-2E-22	-65	5	-3.6E-22	-53	5	3.62E-18	-50.5	5	5.13E-19
-67	5	-3.1E-22	-64.5	5	4.74E-23	-52.5	5	5E-18	-50	5	-8.3E-18
-66.5	5	-4.2E-22	-64	5	8.24E-22	-52	5	6.12E-18	-49.5	5	-2.3E-17
-66	5	-5E-22	-63.5	5	2.08E-21	-51.5	5	6.39E-18	-49	5	-4.4E-17
-65.5	5	-5.1E-22	-63	5	3.89E-21	-51	5	4.92E-18	-48.5	5	-7.2E-17
-65	5	-3.6E-22	-62.5	5	6.2E-21	-50.5	5	5.13E-19	-48	5	-1E-16
-64.5	5	4.74E-23	-62	5	8.77E-21	-50	5	-8.3E-18	-47.5	5	-1.3E-16
-64	5	8.24E-22	-61.5	5	1.1E-20	-49.5	5	-2.3E-17	-47	5	-1.5E-16
-63.5	5	2.08E-21	-61	5	1.2E-20	-49	5	-4.4E-17	-46.5	5	-1.3E-16
-63	5	3.89E-21	-60.5	5	1.02E-20	-48.5	5	-7.2E-17	-46	5	-6.2E-17
-62.5	5	6.2E-21	-60	5	3.41E-21	-48	5	-1E-16	-45.5	5	9.81E-17
-62	5	8.77E-21	-59.5	5	-1.1E-20	-47.5	5	-1.3E-16	-45	5	3.79E-16
-61.5	5	1.1E-20	-59	5	-3.5E-20	-47	5	-1.5E-16	-44.5	5	8.1E-16
-61	5	1.2E-20	-58.5	5	-7.2E-20	-46.5	5	-1.3E-16	-44	5	1.4E-15
-60.5	5	1.02E-20	-58	5	-1.2E-19	-46	5	-6.2E-17	-43.5	5	2.11E-15
-60	5	3.41E-21	-57.5	5	-1.8E-19	-45.5	5	9.81E-17	-43	5	2.83E-15

Wheel 5			Wheel 6			Wheel 7			Wheel 8		
x	*k*	*w*	*x*	*k*	*w*	*x*	*k*	*w*	*x*	*k*	*w*
-69	9.2	2.34E-26	-66.5	9.2	-1.2E-25	-54.5	13.65	9.88E-24	-52	13.65	-1.6E-22
-68.5	9.2	2.65E-26	-66	9.2	-2.4E-25	-54	13.65	3.4E-24	-51.5	13.65	-2.2E-22
-68	9.2	2.14E-26	-65.5	9.2	-3.9E-25	-53.5	13.65	-1.4E-23	-51	13.65	-2.4E-22
-67.5	9.2	6.75E-28	-65	9.2	-5.3E-25	-53	13.65	-4.7E-23	-50.5	13.65	-1.5E-22
-67	9.2	-4.5E-26	-64.5	9.2	-6.1E-25	-52.5	13.65	-9.8E-23	-50	13.65	1.66E-22
-66.5	9.2	-1.2E-25	-64	9.2	-5.1E-25	-52	13.65	-1.6E-22	-49.5	13.65	8.06E-22
	9.2	-0.00415	-63.5	9.2	-5.7E-26	-51.5	13.65	-2.2E-22	-49	13.65	1.86E-21
-65.5	9.2	-3.9E-25	-63	9.2	9.58E-25	-51	13.65	-2.4E-22	-48.5	13.65	3.3E-21
-65	9.2	-5.3E-25	-62.5	9.2	2.74E-24	-50.5	13.65	-1.5E-22	-48	13.65	4.82E-21
-64.5	9.2	-6.1E-25	-62	9.2	5.4E-24	-50	13.65	1.66E-22	-47.5	13.65	5.66E-21
-64	9.2	-5.1E-25	-61.5	9.2	8.78E-24	-49.5	13.65	8.06E-22	-47	13.65	4.44E-21
-63.5	9.2	-5.7E-26	-61	9.2	1.22E-23	-49	13.65	1.86E-21	-46.5	13.65	-9.7E-22
-63	9.2	9.58E-25	-60.5	9.2	1.42E-23	-48.5	13.65	3.3E-21	-46	13.65	-1.3E-20
-62.5	9.2	2.74E-24	-60	9.2	1.21E-23	-48	13.65	4.82E-21	-45.5	13.65	-3.5E-20
-62	9.2	5.4E-24	-59.5	9.2	2.25E-24	-47.5	13.65	5.66E-21	-45	13.65	-6.6E-20
-61.5	9.2	8.78E-24	-59	9.2	-2E-23	-47	13.65	4.44E-21	-44.5	13.65	-1E-19
-61	9.2	1.22E-23	-58.5	9.2	-6E-23	-46.5	13.65	-9.7E-22	-44	13.65	-1.3E-19
-60.5	9.2	1.42E-23	-58	9.2	-1.2E-22	-46	13.65	-1.3E-20	-43.5	13.65	-1.2E-19
-60	9.2	1.21E-23	-57.5	9.2	-2E-22	-45.5	13.65	-3.5E-20	-43	13.65	-2.9E-20
-59.5	9.2	2.25E-24	-57	9.2	-2.8E-22	-45	13.65	-6.6E-20	-42.5	13.65	1.99E-19
-59	9.2	-2E-23	-56.5	9.2	-3.3E-22	-44.5	13.65	-1E-19	-42	13.65	6.26E-19
-58.5	9.2	-6E-23	-56	9.2	-2.9E-22	-44	13.65	-1.3E-19	-41.5	13.65	1.28E-18
-58	9.2	-1.2E-22	-55.5	9.2	-7.2E-23	-43.5	13.65	-1.2E-19	-41	13.65	2.1E-18
-57.5	9.2	-2E-22	-55	9.2	4.3E-22	-43	13.65	-2.9E-20	-40.5	13.65	2.83E-18
-57	9.2	-2.8E-22	-54.5	9.2	1.33E-21	-42.5	13.65	1.99E-19	-40	13.65	2.96E-18
-56.5	9.2	-3.3E-22	-54	9.2	2.7E-21	-42	13.65	6.26E-19	-39.5	13.65	1.58E-18
-56	9.2	-2.9E-22	-53.5	9.2	4.48E-21	-41.5	13.65	1.28E-18	-39	13.65	-2.6E-18
-55.5	9.2	-7.2E-23	-53	9.2	6.34E-21	-41	13.65	2.1E-18	-38.5	13.65	-1.1E-17
-55	9.2	4.3E-22	-52.5	9.2	7.55E-21	-40.5	13.65	2.83E-18	-38	13.65	-2.4E-17
-54.5	9.2	1.33E-21	-52	9.2	6.8E-21	-40	13.65	2.96E-18	-37.5	13.65	-4.3E-17
-54	9.2	2.7E-21	-51.5	9.2	2.12E-21	-39.5	13.65	1.58E-18	-37	13.65	-6.1E-17
-53.5	9.2	4.48E-21	-51	9.2	-9E-21	-39	13.65	-2.6E-18	-36.5	13.65	-7E-17
-53	9.2	6.34E-21	-50.5	9.2	-2.9E-20	-38.5	13.65	-1.1E-17	-36	13.65	-5.2E-17
-52.5	9.2	7.55E-21	-50	9.2	-6E-20	-38	13.65	-2.4E-17	-35.5	13.65	2.15E-17
-52	9.2	6.8E-21	-49.5	9.2	-1E-19	-37.5	13.65	-4.3E-17	-35	13.65	1.82E-16
-51.5	9.2	2.12E-21	-49	9.2	-1.4E-19	-37	13.65	-6.1E-17	-34.5	13.65	4.59E-16
-51	9.2	-9E-21	-48.5	9.2	-1.7E-19	-36.5	13.65	-7E-17	-34	13.65	8.51E-16
-50.5	9.2	-2.9E-20	-48	9.2	-1.6E-19	-36	13.65	-5.2E-17	-33.5	13.65	1.29E-15
-50	9.2	-6E-20	-47.5	9.2	-5.9E-20	-35.5	13.65	2.15E-17	-33	13.65	1.6E-15
-49.5	9.2	-1E-19	-47	9.2	1.89E-19	-35	13.65	1.82E-16	-32.5	13.65	1.43E-15
-49	9.2	-1.4E-19	-46.5	9.2	6.44E-19	-34.5	13.65	4.59E-16	-32	13.65	1.94E-16
-48.5	9.2	-1.7E-19	-46	9.2	1.35E-18	-34	13.65	8.51E-16	-31.5	13.65	-2.8E-15
-48	9.2	-1.6E-19	-45.5	9.2	2.28E-18	-33.5	13.65	1.29E-15	-31	13.65	-8.4E-15
-47.5	9.2	-5.9E-20	-45	9.2	3.28E-18	-33	13.65	1.6E-15	-30.5	13.65	-1.7E-14
-47	9.2	1.89E-19	-44.5	9.2	4E-18	-32.5	13.65	1.43E-15	-30	13.65	-2.7E-14
-46.5	9.2	6.44E-19	-44	9.2	3.77E-18	-32	13.65	1.94E-16	-29.5	13.65	-3.6E-14
-46	9.2	1.35E-18	-43.5	9.2	1.58E-18	-31.5	13.65	-2.8E-15	-29	13.65	-3.6E-14
-45.5	9.2	2.28E-18	-43	9.2	-3.9E-18	-31	13.65	-8.4E-15	-28.5	13.65	-1.7E-14
-45	9.2	3.28E-18	-42.5	9.2	-1.4E-17	-30.5	13.65	-1.7E-14	-28	13.65	3.88E-14
-44.5	9.2	4E-18	-42	9.2	-3E-17	-30	13.65	-2.7E-14	-27.5	13.65	1.48E-13
-44	9.2	3.77E-18	-41.5	9.2	-5.1E-17	-29.5	13.65	-3.6E-14	-27	13.65	3.22E-13
-43.5	9.2	1.58E-18	-41	9.2	-7.5E-17	-29	13.65	-3.6E-14	-26.5	13.65	5.49E-13
-43	9.2	-3.9E-18	-40.5	9.2	-9.2E-17	-28.5	13.65	-1.7E-14	-26	13.65	7.75E-13
-42.5	9.2	-1.4E-17	-40	9.2	-8.9E-17	-28	13.65	3.88E-14	-25.5	13.65	8.67E-13
-42	9.2	-3E-17	-39.5	9.2	-4.1E-17	-27.5	13.65	1.48E-13	-25	13.65	5.93E-13
-41.5	9.2	-5.1E-17	-39	9.2	8.05E-17	-27	13.65	3.22E-13	-24.5	13.65	-3.9E-13
-41	9.2	-7.5E-17	-38.5	9.2	3.1E-16	-26.5	13.65	5.49E-13	-24	13.65	-2.5E-12
-40.5	9.2	-9.2E-17	-38	9.2	6.71E-16	-26	13.65	7.75E-13	-23.5	13.65	-6.1E-12
-40	9.2	-8.9E-17	-37.5	9.2	1.16E-15	-25.5	13.65	8.67E-13	-23	13.65	-1.1E-11
-39.5	9.2	-4.1E-17	-37	9.2	1.7E-15	-25	13.65	5.93E-13	-22.5	13.65	-1.6E-11
-39	9.2	8.05E-17	-36.5	9.2	2.12E-15	-24.5	13.65	-3.9E-13	-22	13.65	-2E-11

Wheel 9			Wheel 10			Wheel 11			Wheel 12		
x	*k*	*w*	*x*	*k*	*w*	*x*	*k*	*w*	*x*	*k*	*w*
-48	22.8	6.9E-24	-45.5	22.8	-1.4E-22	-33.5	41.5	-5.1E-20	-31	41.50642	9.56E-19
-47.5	22.8	2.05E-24	-45	22.8	-1.7E-22	-33	41.5	-5.4E-20	-30.5	41.50642	1.31E-18
-47	22.8	-1.2E-23	-44.5	22.8	-1.2E-22	-32.5	41.5	-1.3E-21	-30	41.50642	9.12E-19
-46.5	22.8	-4.1E-23	-44	22.8	1.1E-22	-32	41.5	1.64E-19	-29.5	41.50642	-1.4E-18
-46	22.8	-8.6E-23	-43.5	22.8	6.24E-22	-31.5	41.5	4.93E-19	-29	41.50642	-6.9E-18
-45.5	22.8	-1.4E-22	-43	22.8	1.5E-21	-31	41.5	9.56E-19	-28.5	41.50642	-1.6E-17
-45	22.8	-1.7E-22	-42.5	22.8	2.67E-21	-30.5	41.5	1.31E-18	-28	41.50642	-2.7E-17
-44.5	22.8	-1.2E-22	-42	22.8	3.7E-21	-30	41.5	9.12E-19	-27.5	41.50642	-2.9E-17
-44	22.8	1.1E-22	-41.5	22.8	3.53E-21	-29.5	41.5	-1.4E-18	-27	41.50642	-3.8E-18
-43.5	22.8	6.24E-22	-41	22.8	3.49E-22	-29	41.5	-6.9E-18	-26.5	41.50642	8.03E-17
-43	22.8	1.5E-21	-40.5	22.8	-8.4E-21	-28.5	41.5	-1.6E-17	-26	41.50642	2.51E-16
-42.5	22.8	2.67E-21	-40	22.8	-2.5E-20	-28	41.5	-2.7E-17	-25.5	41.50642	4.96E-16
-42	22.8	3.7E-21	-39.5	22.8	-5E-20	-27.5	41.5	-2.9E-17	-25	41.50642	6.95E-16
-41.5	22.8	3.53E-21	-39	22.8	-7.7E-20	-27	41.5	-3.8E-18	-24.5	41.50642	5.23E-16
-41	22.8	3.49E-22	-38.5	22.8	-8.9E-20	-26.5	41.5	8.03E-17	-24	41.50642	-6.1E-16
-40.5	22.8	-8.4E-21	-38	22.8	-5.2E-20	-26	41.5	2.51E-16	-23.5	41.50642	-3.4E-15
-40	22.8	-2.5E-20	-37.5	22.8	8.81E-20	-25.5	41.5	4.96E-16	-23	41.50642	-8.3E-15
-39.5	22.8	-5E-20	-37	22.8	3.91E-19	-25	41.5	6.95E-16	-22.5	41.50642	-1.4E-14
-39	22.8	-7.7E-20	-36.5	22.8	8.91E-19	-24.5	41.5	5.23E-16	-22	41.50642	-1.6E-14
-38.5	22.8	-8.9E-20	-36	22.8	1.53E-18	-24	41.5	-6.1E-16	-21.5	41.50642	-3.6E-15
-38	22.8	-5.2E-20	-35.5	22.8	2.02E-18	-23.5	41.5	-3.4E-15	-21	41.50642	3.9E-14
-37.5	22.8	8.81E-20	-35	22.8	1.77E-18	-23	41.5	-8.3E-15	-20.5	41.50642	1.27E-13
-37	22.8	3.91E-19	-34.5	22.8	-2.8E-19	-22.5	41.5	-1.4E-14	-20	41.50642	2.57E-13
-36.5	22.8	8.91E-19	-34	22.8	-5.5E-18	-22	41.5	-1.6E-14	-19.5	41.50642	3.69E-13
-36	22.8	1.53E-18	-33.5	22.8	-1.5E-17	-21.5	41.5	-3.6E-15	-19	41.50642	2.97E-13
-35.5	22.8	2.02E-18	-33	22.8	-2.9E-17	-21	41.5	3.9E-14	-18.5	41.50642	-2.7E-13
-35	22.8	1.77E-18	-32.5	22.8	-4.3E-17	-20.5	41.5	1.27E-13	-18	41.50642	-1.7E-12
-34.5	22.8	-2.8E-19	-32	22.8	-4.7E-17	-20	41.5	2.57E-13	-17.5	41.50642	-4.3E-12
-34	22.8	-5.5E-18	-31.5	22.8	-2.1E-17	-19.5	41.5	3.69E-13	-17	41.50642	-7.4E-12
-33.5	22.8	-1.5E-17	-31	22.8	6.48E-17	-19	41.5	2.97E-13	-16.5	41.50642	-8.6E-12
-33	22.8	-2.9E-17	-30.5	22.8	2.42E-16	-18.5	41.5	-2.7E-13	-16	41.50642	-2.7E-12
-32.5	22.8	-4.3E-17	-30	22.8	5.24E-16	-18	41.5	-1.7E-12	-15.5	41.50642	1.88E-11
-32	22.8	-4.7E-17	-29.5	22.8	8.66E-16	-17.5	41.5	-4.3E-12	-15	41.50642	6.45E-11
-31.5	22.8	-2.1E-17	-29	22.8	1.1E-15	-17	41.5	-7.4E-12	-14.5	41.50642	1.33E-10
-31	22.8	6.48E-17	-28.5	22.8	8.65E-16	-16.5	41.5	-8.6E-12	-14	41.50642	1.95E-10
-30.5	22.8	2.42E-16	-28	22.8	-4.4E-16	-16	41.5	-2.7E-12	-13.5	41.50642	1.67E-10
-30	22.8	5.24E-16	-27.5	22.8	-3.6E-15	-15.5	41.5	1.88E-11	-13	41.50642	-1.1E-10
-29.5	22.8	8.66E-16	-27	22.8	-9.1E-15	-15	41.5	6.45E-11	-12.5	41.50642	-8.5E-10
-29	22.8	1.1E-15	-26.5	22.8	-1.7E-14	-14.5	41.5	1.33E-10	-12	41.50642	-2.2E-09
-28.5	22.8	8.65E-16	-26	22.8	-2.4E-14	-14	41.5	1.95E-10	-11.5	41.50642	-3.9E-09
-28	22.8	-4.4E-16	-25.5	22.8	-2.4E-14	-13.5	41.5	1.67E-10	-11	41.50642	-4.7E-09
-27.5	22.8	-3.6E-15	-25	22.8	-6.8E-15	-13	41.5	-1.1E-10	-10.5	41.50642	-1.8E-09
-27	22.8	-9.1E-15	-24.5	22.8	4.52E-14	-12.5	41.5	-8.5E-10	-10	41.50642	9.03E-09
-26.5	22.8	-1.7E-14	-24	22.8	1.48E-13	-12	41.5	-2.2E-09	-9.5	41.50642	3.26E-08
-26	22.8	-2.4E-14	-23.5	22.8	3.07E-13	-11.5	41.5	-3.9E-09	-9	41.50642	6.89E-08
-25.5	22.8	-2.4E-14	-23	22.8	4.89E-13	-11	41.5	-4.7E-09	-8.5	41.50642	1.03E-07
-25	22.8	-6.8E-15	-22.5	22.8	5.93E-13	-10.5	41.5	-1.8E-09	-8	41.50642	9.31E-08
-24.5	22.8	4.52E-14	-22	22.8	4.06E-13	-10	41.5	9.03E-09	-7.5	41.50642	-4.5E-08
-24	22.8	1.48E-13	-21.5	22.8	-4.1E-13	-9.5	41.5	3.26E-08	-7	41.50642	-4.2E-07
-23.5	22.8	3.07E-13	-21	22.8	-2.3E-12	-9	41.5	6.89E-08	-6.5	41.50642	-1.1E-06
-23	22.8	4.89E-13	-20.5	22.8	-5.4E-12	-8.5	41.5	1.03E-07	-6	41.50642	-2E-06
-22.5	22.8	5.93E-13	-20	22.8	-9.6E-12	-8	41.5	9.31E-08	-5.5	41.50642	-2.5E-06
-22	22.8	4.06E-13	-19.5	22.8	-1.3E-11	-7.5	41.5	-4.5E-08	-5	41.50642	-1.2E-06
-21.5	22.8	-4.1E-13	-19	22.8	-1.2E-11	-7	41.5	-4.2E-07	-4.5	41.50642	4.3E-06
-21	22.8	-2.3E-12	-18.5	22.8	-9.6E-13	-6.5	41.5	-1.1E-06	-4	41.50642	1.65E-05
-20.5	22.8	-5.4E-12	-18	22.8	3.04E-11	-6	41.5	-2E-06	-3.5	41.50642	3.56E-05
-20	22.8	-9.6E-12	-17.5	22.8	9.02E-11	-5.5	41.5	-2.5E-06	-3	41.50642	5.46E-05
-19.5	22.8	-1.3E-11	-17	22.8	1.79E-10	-5	41.5	-1.2E-06	-2.5	41.50642	5.16E-05
-19	22.8	-1.2E-11	-16.5	22.8	2.75E-10	-4.5	41.5	4.3E-06	-2	41.50642	-1.6E-05
-18.5	22.8	-9.6E-13	-16	22.8	3.16E-10	-4	41.5	1.65E-05	-1.5	41.50642	-0.00021
-18	22.8	3.04E-11	-15.5	22.8	1.79E-10	-3.5	41.5	3.56E-05	-1	41.50642	-0.00057

Wheel 13			Wheel 14			Wheel 15			Wheel 16		
x	*k*	*w*	*x*	*k*	*w*	*x*	*k*	*w*	*x*	*k*	*w*
-27	80	1.63E-19	-24.5	80	-5.5E-18	-12.5	80	6.1E-11	-10	80	-1.8E-09
-26.5	80	4.53E-19	-24	80	-1.3E-17	-12	80	1.11E-10	-9.5	80	-2.8E-09
-26	80	7.65E-19	-23.5	80	-1.9E-17	-11.5	80	1.09E-10	-9	80	-1.8E-09
-25.5	80	6.15E-19	-23	80	-7.7E-18	-11	80	-9.2E-11	-8.5	80	5.21E-09
-25	80	-1E-18	-22.5	80	4.74E-17	-10.5	80	-7E-10	-8	80	2.28E-08
-24.5	80	-5.5E-18	-22	80	1.75E-16	-10	80	-1.8E-09	-7.5	80	4.99E-08
-24	80	-1.3E-17	-21.5	80	3.54E-16	-9.5	80	-2.8E-09	-7	80	6.6E-08
-23.5	80	-1.9E-17	-21	80	4.18E-16	-9	80	-1.8E-09	-6.5	80	1.18E-08
-23	80	-7.7E-18	-20.5	80	-6.8E-17	-8.5	80	5.21E-09	-6	80	-2.2E-07
-22.5	80	4.74E-17	-20	80	-1.8E-15	-8	80	2.28E-08	-5.5	80	-7.1E-07
-22	80	1.75E-16	-19.5	80	-5.3E-15	-7.5	80	4.99E-08	-5	80	-1.3E-06
-21.5	80	3.54E-16	-19	80	-9.3E-15	-7	80	6.6E-08	-4.5	80	-1.4E-06
-21	80	4.18E-16	-18.5	80	-8.3E-15	-6.5	80	1.18E-08	-4	80	7.85E-07
-20.5	80	-6.8E-17	-18	80	1E-14	-6	80	-2.2E-07	-3.5	80	7.78E-06
-20	80	-1.8E-15	-17.5	80	6.21E-14	-5.5	80	-7.1E-07	-3	80	2.08E-05
-19.5	80	-5.3E-15	-17	80	1.52E-13	-5	80	-1.3E-06	-2.5	80	3.42E-05
-19	80	-9.3E-15	-16.5	80	2.29E-13	-4.5	80	-1.4E-06	-2	80	2.52E-05
-18.5	80	-8.3E-15	-16	80	1.22E-13	-4	80	7.85E-07	-1.5	80	-5.3E-05
-18	80	1E-14	-15.5	80	-5E-13	-3.5	80	7.78E-06	-1	80	-0.00026
-17.5	80	6.21E-14	-15	80	-2E-12	-3	80	2.08E-05	-0.5	80	-0.00059
-17	80	1.52E-13	-14.5	80	-4.2E-12	-2.5	80	3.42E-05	0	80	-0.00082
-16.5	80	2.29E-13	-14	80	-5.3E-12	-2	80	2.52E-05	0.5	80	-0.00059
-16	80	1.22E-13	-13.5	80	-1E-13	-1.5	80	-5.3E-05	1	80	-0.00026
-15.5	80	-5E-13	-13	80	1.98E-11	-1	80	-0.00026	1.5	80	-5.3E-05
-15	80	-2E-12	-12.5	80	6.1E-11	-0.5	80	-0.00059	2	80	2.52E-05
-14.5	80	-4.2E-12	-12	80	1.11E-10	0	80	-0.00082	2.5	80	3.42E-05
-14	80	-5.3E-12	-11.5	80	1.09E-10	0.5	80	-0.00059	3	80	2.08E-05
-13.5	80	-1E-13	-11	80	-9.2E-11	1	80	-0.00026	3.5	80	7.78E-06
-13	80	1.98E-11	-10.5	80	-7E-10	1.5	80	-5.3E-05	4	80	7.85E-07
-12.5	80	6.1E-11	-10	80	-1.8E-09	2	80	2.52E-05	4.5	80	-1.4E-06
-12	80	1.11E-10	-9.5	80	-2.8E-09	2.5	80	3.42E-05	5	80	-1.3E-06
-11.5	80	1.09E-10	-9	80	-1.8E-09	3	80	2.08E-05	5.5	80	-7.1E-07
-11	80	-9.2E-11	-8.5	80	5.21E-09	3.5	80	7.78E-06	6	80	-2.2E-07
-10.5	80	-7E-10	-8	80	2.28E-08	4	80	7.85E-07	6.5	80	1.18E-08
-10	80	-1.8E-09	-7.5	80	4.99E-08	4.5	80	-1.4E-06	7	80	6.6E-08
-9.5	80	-2.8E-09	-7	80	6.6E-08	5	80	-1.3E-06	7.5	80	4.99E-08
-9	80	-1.8E-09	-6.5	80	1.18E-08	5.5	80	-7.1E-07	8	80	2.28E-08
-8.5	80	5.21E-09	-6	80	-2.2E-07	6	80	-2.2E-07	8.5	80	5.21E-09
-8	80	2.28E-08	-5.5	80	-7.1E-07	6.5	80	1.18E-08	9	80	-1.8E-09
-7.5	80	4.99E-08	-5	80	-1.3E-06	7	80	6.6E-08	9.5	80	-2.8E-09
-7	80	6.6E-08	-4.5	80	-1.4E-06	7.5	80	4.99E-08	10	80	-1.8E-09
-6.5	80	1.18E-08	-4	80	7.85E-07	8	80	2.28E-08	10.5	80	-7E-10
-6	80	-2.2E-07	-3.5	80	7.78E-06	8.5	80	5.21E-09	11	80	-9.2E-11
-5.5	80	-7.1E-07	-3	80	2.08E-05	9	80	-1.8E-09	11.5	80	1.09E-10
-5	80	-1.3E-06	-2.5	80	3.42E-05	9.5	80	-2.8E-09	12	80	1.11E-10
-4.5	80	-1.4E-06	-2	80	2.52E-05	10	80	-1.8E-09	12.5	80	6.1E-11
-4	80	7.85E-07	-1.5	80	-5.3E-05	10.5	80	-7E-10	13	80	1.98E-11
-3.5	80	7.78E-06	-1	80	-0.00026	11	80	-9.2E-11	13.5	80	-1E-13
-3	80	2.08E-05	-0.5	80	-0.00059	11.5	80	1.09E-10	14	80	-5.3E-12
-2.5	80	3.42E-05	0	80	-0.00082	12	80	1.11E-10	14.5	80	-4.2E-12
-2	80	2.52E-05	0.5	80	-0.00059	12.5	80	6.1E-11	15	80	-2E-12
-1.5	80	-5.3E-05	1	80	-0.00026	13	80	1.98E-11	15.5	80	-5E-13
-1	80	-0.00026	1.5	80	-5.3E-05	13.5	80	-1E-13	16	80	1.22E-13
-0.5	80	-0.00059	2	80	2.52E-05	14	80	-5.3E-12	16.5	80	2.29E-13
0	80	-0.00082	2.5	80	3.42E-05	14.5	80	-4.2E-12	17	80	1.52E-13
0.5	80	-0.00059	3	80	2.08E-05	15	80	-2E-12	17.5	80	6.21E-14
1	80	-0.00026	3.5	80	7.78E-06	15.5	80	-5E-13	18	80	1E-14
1.5	80	-5.3E-05	4	80	7.85E-07	16	80	1.22E-13	18.5	80	-8.3E-15
2	80	2.52E-05	4.5	80	-1.4E-06	16.5	80	2.29E-13	19	80	-9.3E-15
2.5	80	3.42E-05	5	80	-1.3E-06	17	80	1.52E-13	19.5	80	-5.3E-15
3	80	2.08E-05	5.5	80	-7.1E-07	17.5	80	6.21E-14	20	80	-1.8E-15

Figure B-1: Spreadsheet to calculate the track deflection under each wheel

B.3 Calculation of differential settlement

The next step was to calculate the differential settlement between any two consecutive wheels. Following equation was used to calculate the differential settlement:

$$\Delta w_n = \frac{w_n}{w_{n-1}}$$

B.4 Differential settlement criterion

In order to provide a smooth and gradual variation in the stiffness values along the track, the preliminary value of maximum differential settlement was set to be 1.5. i.e.

$$\Delta w_n \leq 1.5$$

B.5 Stiffness variation with random values

Initially the stiffness variation was made by selecting some random values between the maximum and minimum stiffness. For instance, for a typical transition (that has been considered in this study) the maximum stiffness is 80 Mn/m/m, whereas, minimum is 5 MN/m/m, which results in abrupt stiffness variation of 75 MN/m/m at their junction. A gradual variation was provided at this junction by selecting some random values such as; 5, 10, 20, 40, 60, and 80 Mn/m/m. This variation has been

presented in Figure B-2. In order to fulfill the differential settlement criteria, the random stiffness variation is adjusted as shown in Figure B-2.

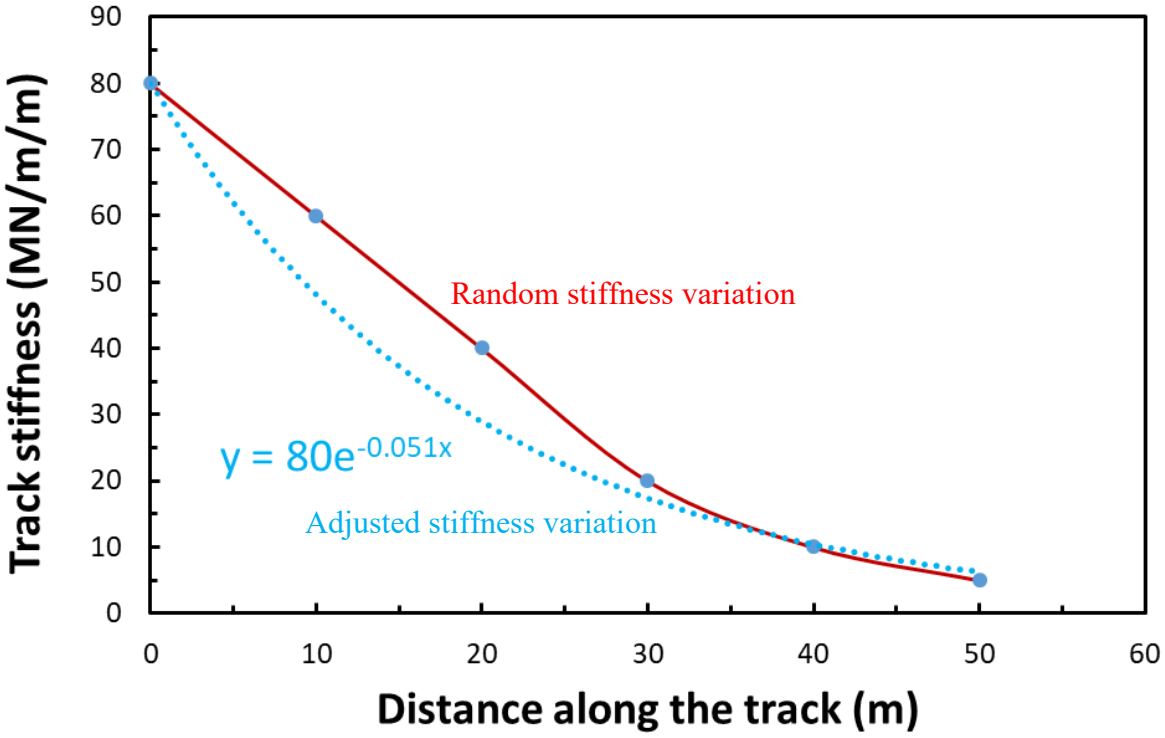

Figure B-2: 5-steps stiffness variation with random values

B.6 Trial and error method for the selection of final equation

Considering the above adjusted variation equation, various trials were made to determine their suitability for different stiffness values and transition steps. Various trials considered in this study are as below:

Trial 1

$$k_i = k_{max} \times e^{(-0.05)\times X_i}$$

Trial 2

$$k_i = \Delta k \times e^{(-0.05)\times X_i}$$

Trial 3

$$k_i = \Delta k \times e^{(-0.05)\times X_i} + k_{n+1}$$

Trial 4

$$k_i = \Delta k \times e^{(-0.07)\times X_i} + k_{n+1}$$

Trial 5

Linear Variation

Trial 6

Final Proposed Equation

$$k_i = \Delta k \times e^{(0.0007L-0.1)\times X_i} + k_{n+1}$$

The comparison of stiffness variations based on the above trials, considering multistep transition zone for various steps, is given below.

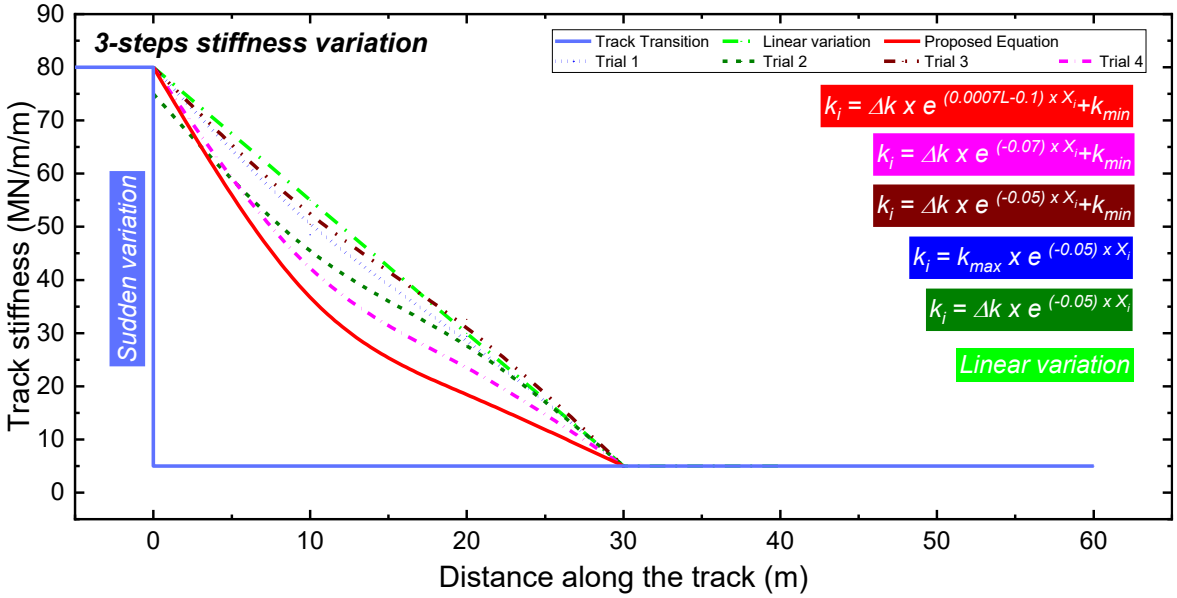

Figure B-3: Comparison of stiffness variation calculated by various trials for a 3-step transition zone design

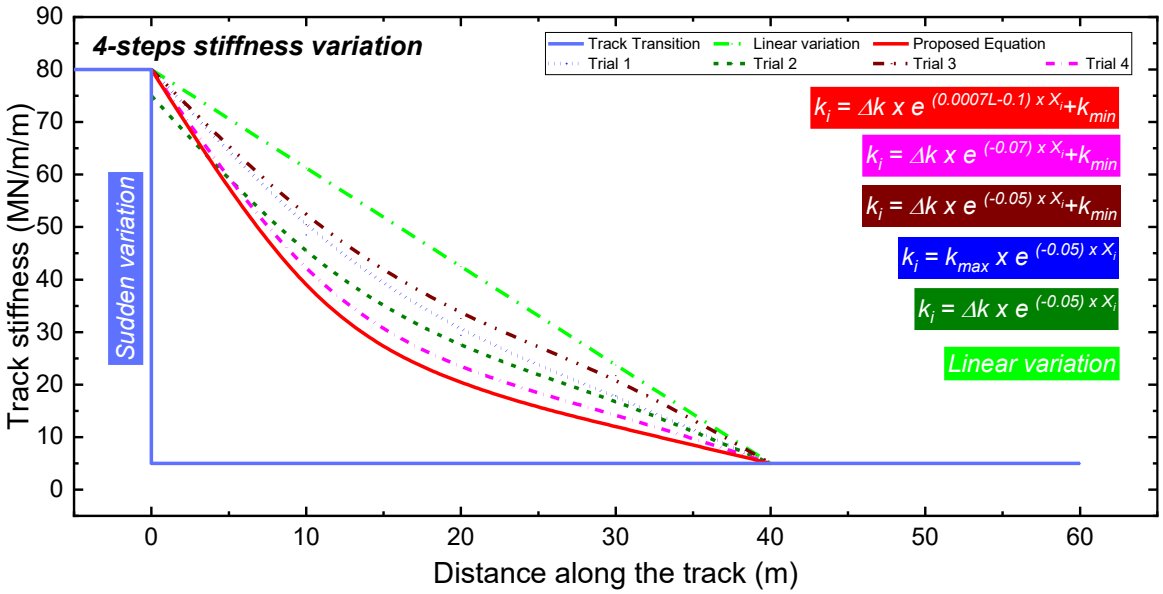

Figure B-4: Comparison of stiffness variation calculated by various trials for a 4-step transition zone design

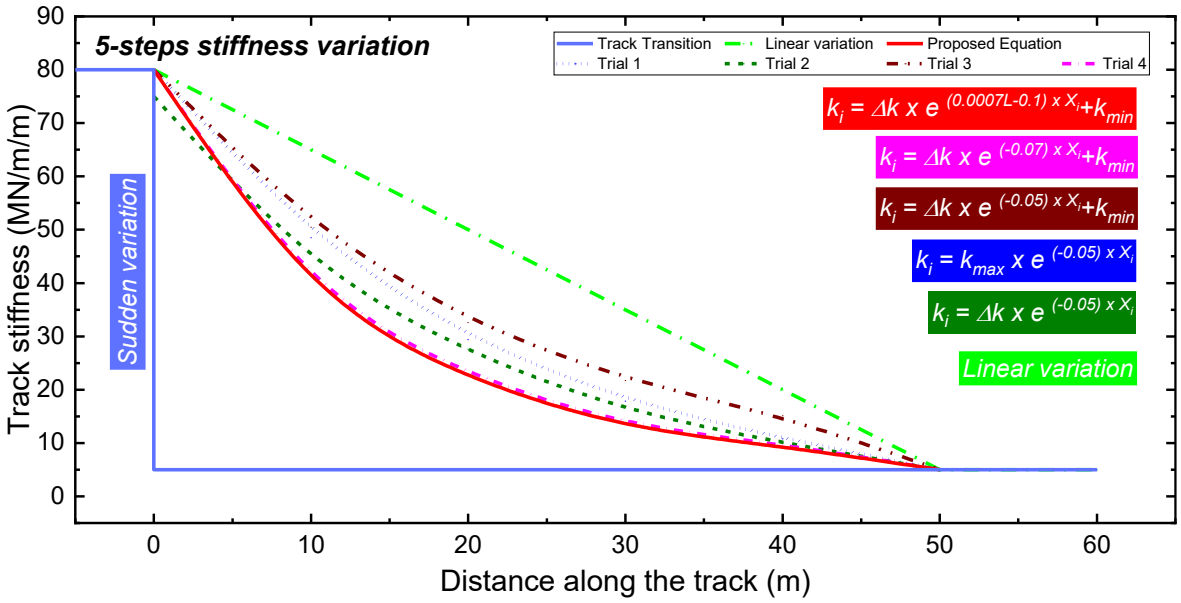

Figure B-5: Comparison of stiffness variation calculated by various trials for a 5-step transition zone design

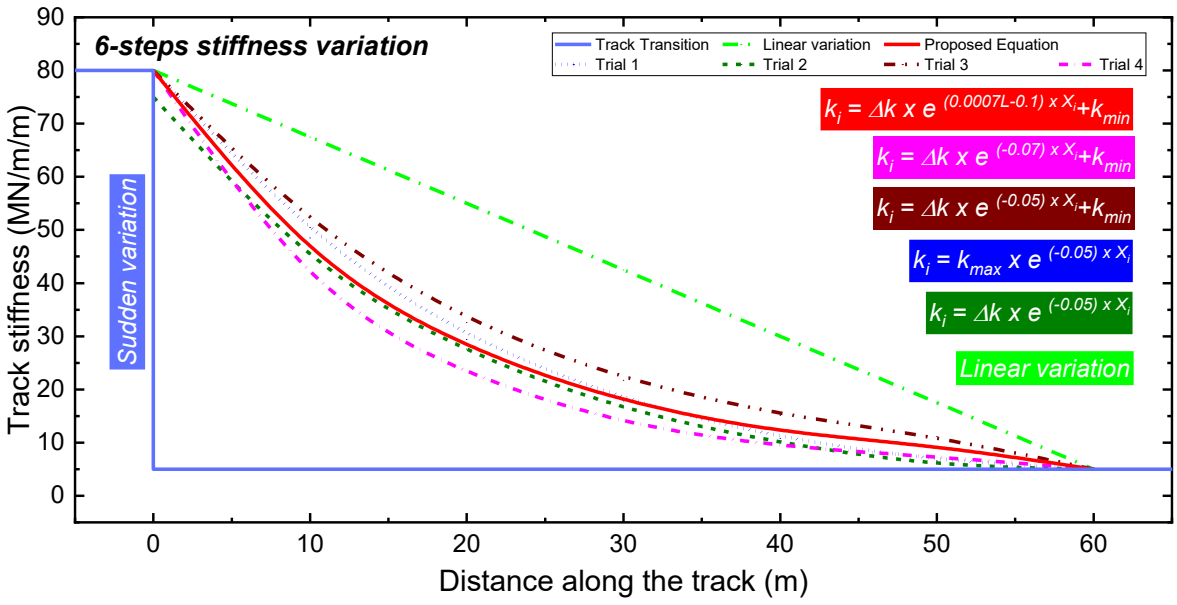

Figure B-6: Comparison of stiffness variation calculated by various trials for a 6-step transition zone design

B.6 Proposed empirical equation for stiffens variation

Based on the trial and error method, it was noted that the proposed equation showed better results for different combinations of stiffness variation and the number of transition steps. This equation incorporates not only the actual stiffness difference at any transition, but also the number of total steps and their lengths, as given below:

$$k_i = \Delta k \times e^{(0.0007L-0.1)\times X_i} + k_{n+1}$$

This relation ensures a smooth and gradual variation in stiffness values, rather than relying on simple arithmetic means. As a result, the proposed analytical approach considers the track dynamic response in designing the multistep transition zone, and leads to larger variations in stiffness on its stiffer side, as compared to the softer side. The stiffness variation for a 6-steps transition zone, based on the proposed empirical equation is presented in Figure B-7. This figure also demonstrates the calculated stiffness values of various transition segments in the proposed transition zone.

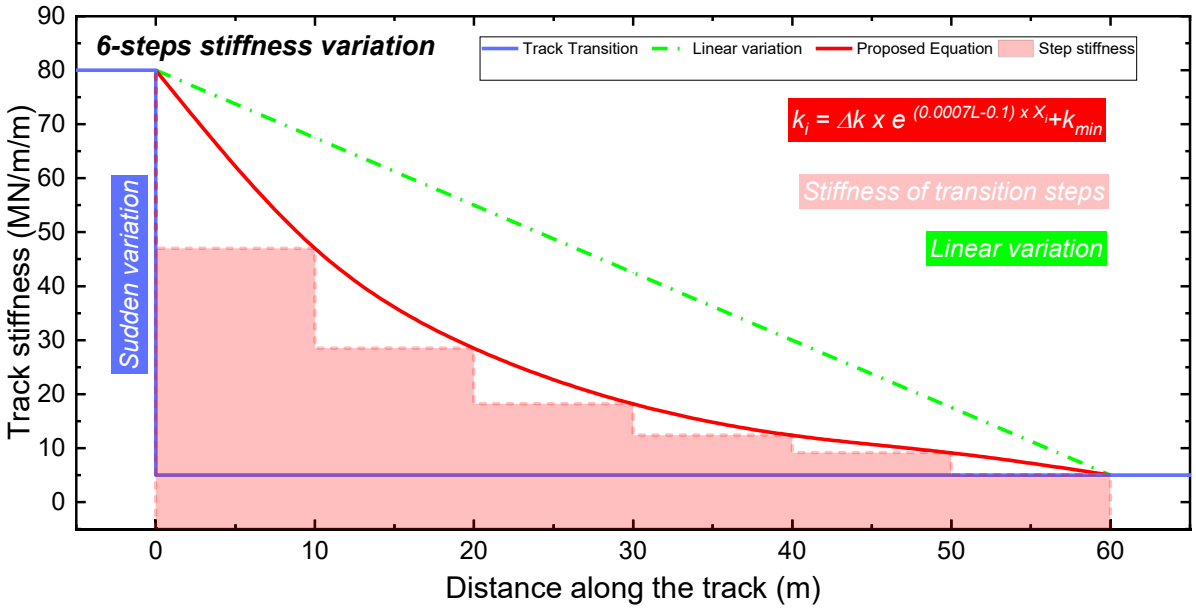

Figure B-7: Stiffness variation for a 6-steps transition zone, based on the proposed empirical equation

APPENDIX C: 3D ANALYSIS

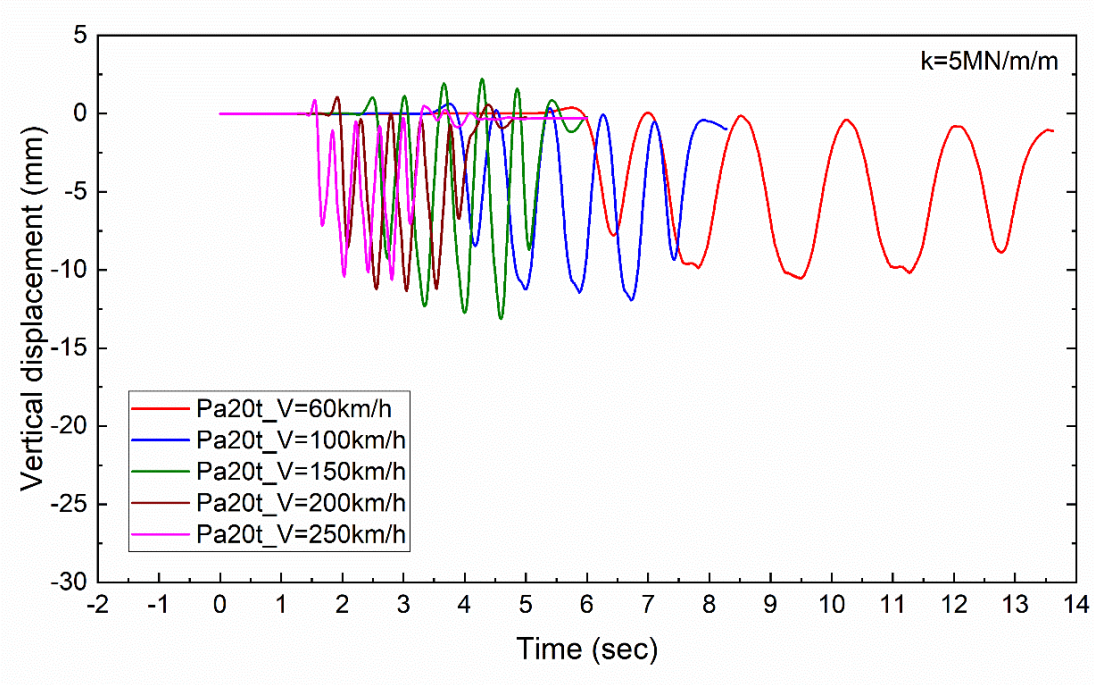

Figure C-1: Predicted vertical displacements for 3D FEM layered model (k = 5 MN/m/m, P_{axle} = 20 t) considering four-carriage loading moving at various speeds

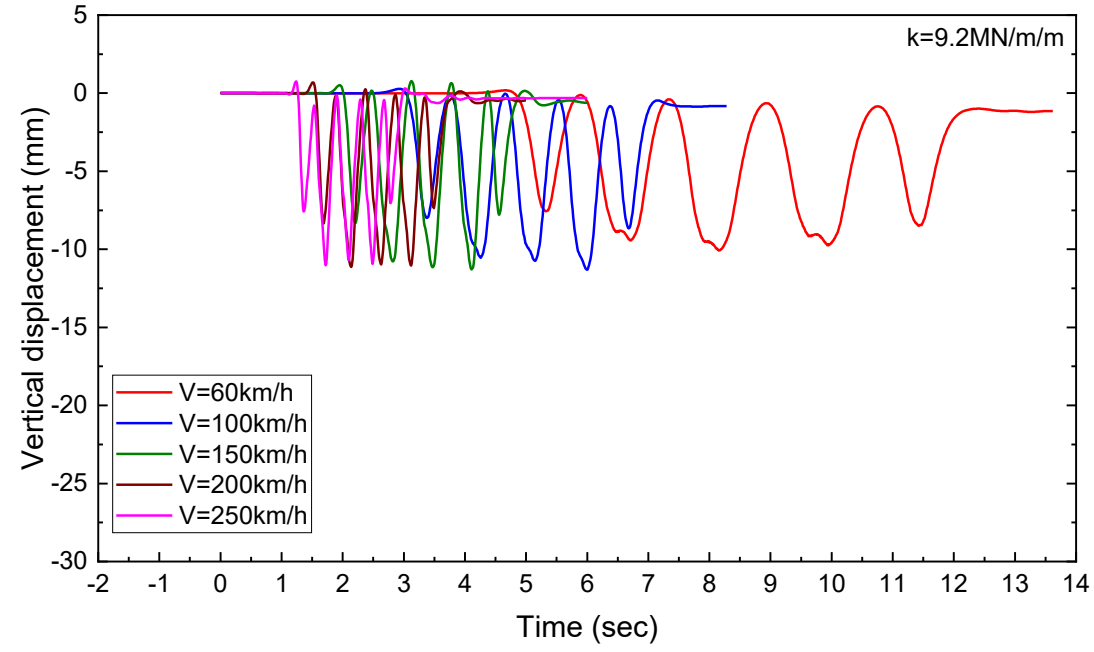

Figure C-2: Predicted vertical displacements for 3D FEM layered model (k = 9.2 MN/m/m, P_{axle} = 20 t) considering four-carriage loading moving at various speeds

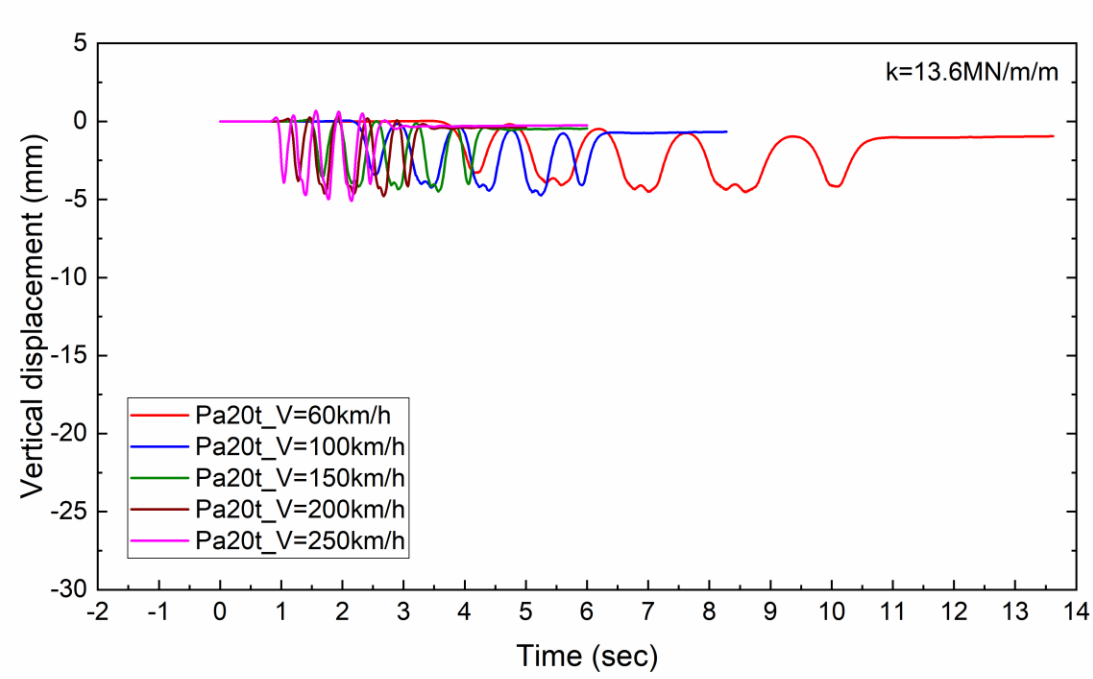

Figure C-3: Predicted vertical displacements for 3D FEM layered model (k = 13.6 MN/m/m, P_{axle} = 20 t) considering four-carriage loading moving at various speeds

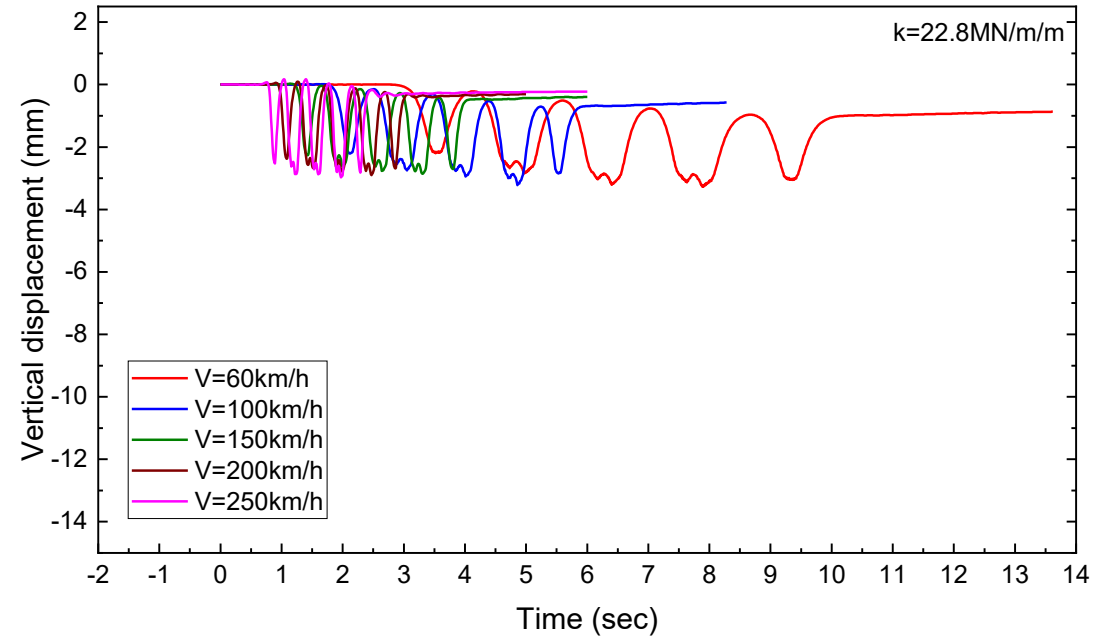

Figure C-4: Predicted vertical displacements for 3D FEM layered model (k = 22.8 MN/m/m, P_{axle} = 20 t) considering four-carriage loading moving at various speeds

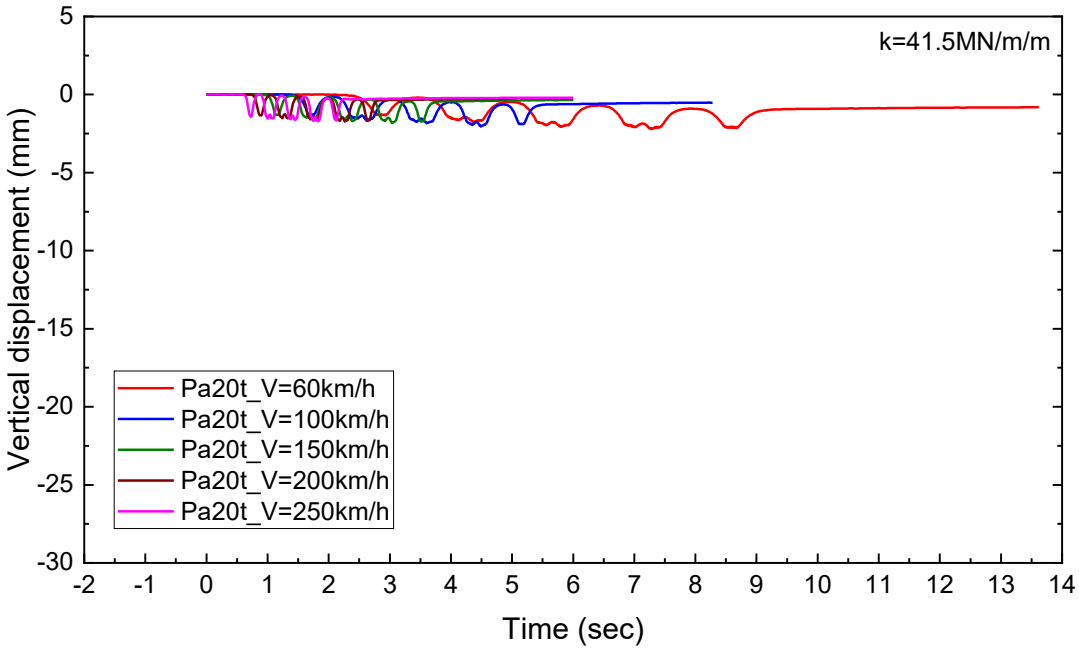

Figure C-5: Predicted vertical displacements for 3D FEM layered model (k = 41.5 MN/m/m, P_{axle} = 20 t) considering four-carriage loading moving at various speeds

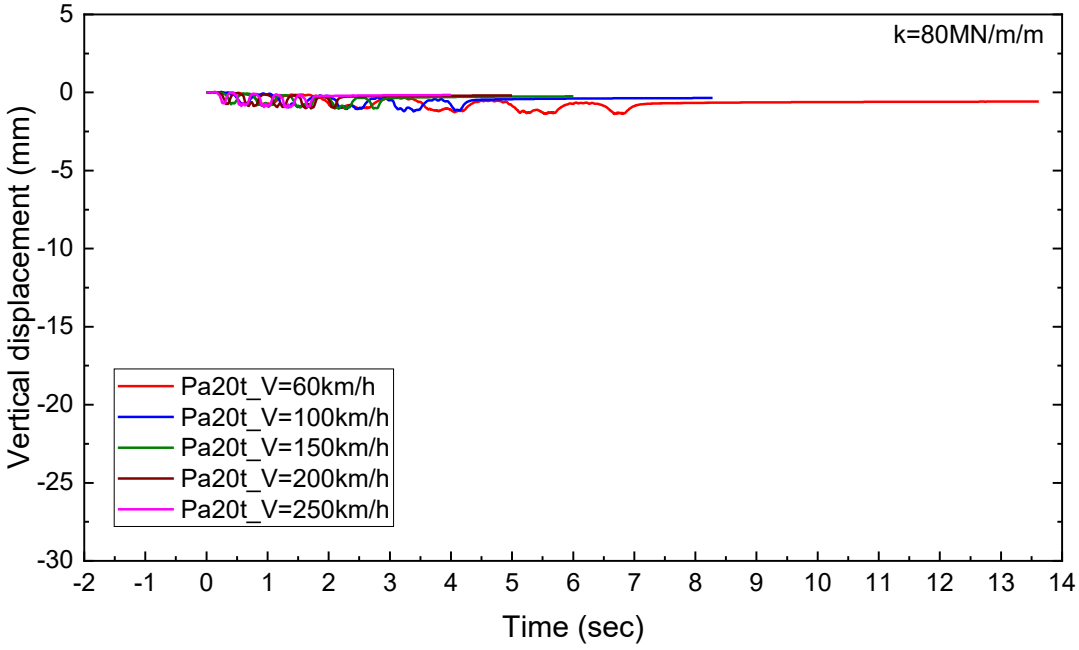

Figure C-6: Predicted vertical displacements for 3D FEM layered model (k = 80 MN/m/m, P_{axle} = 20 t) considering four-carriage loading moving at various speeds

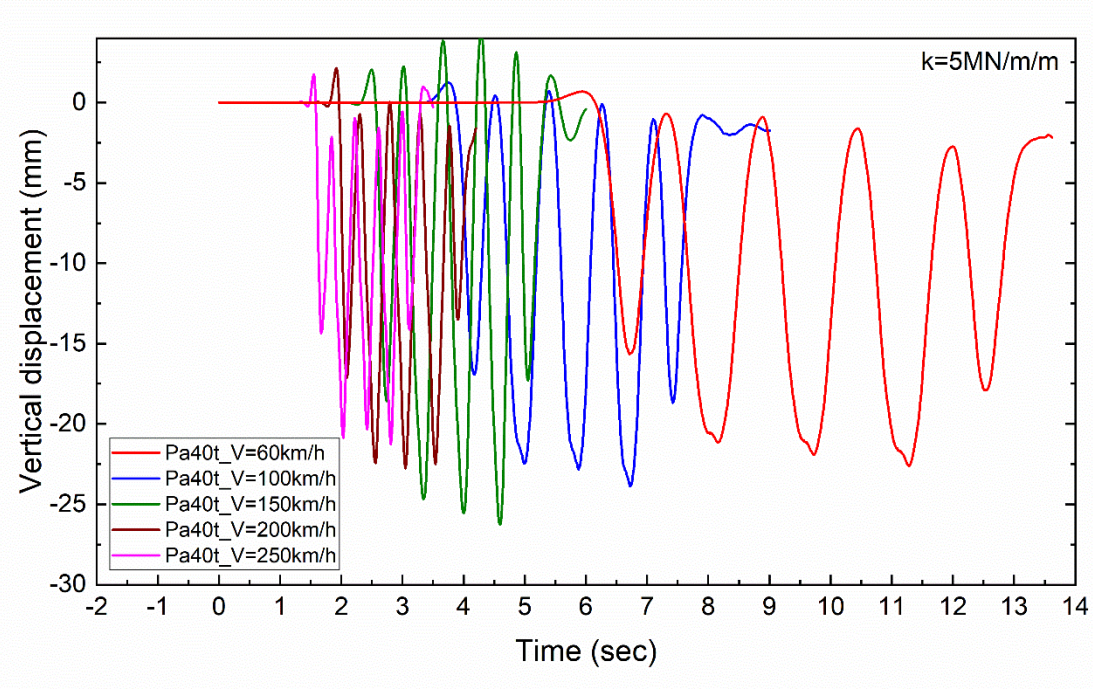

Figure C-7: Predicted vertical displacements for 3D FEM layered model (k = 5 MN/m/m, P_{axle} = 40 t) considering four-carriage loading moving at various speeds

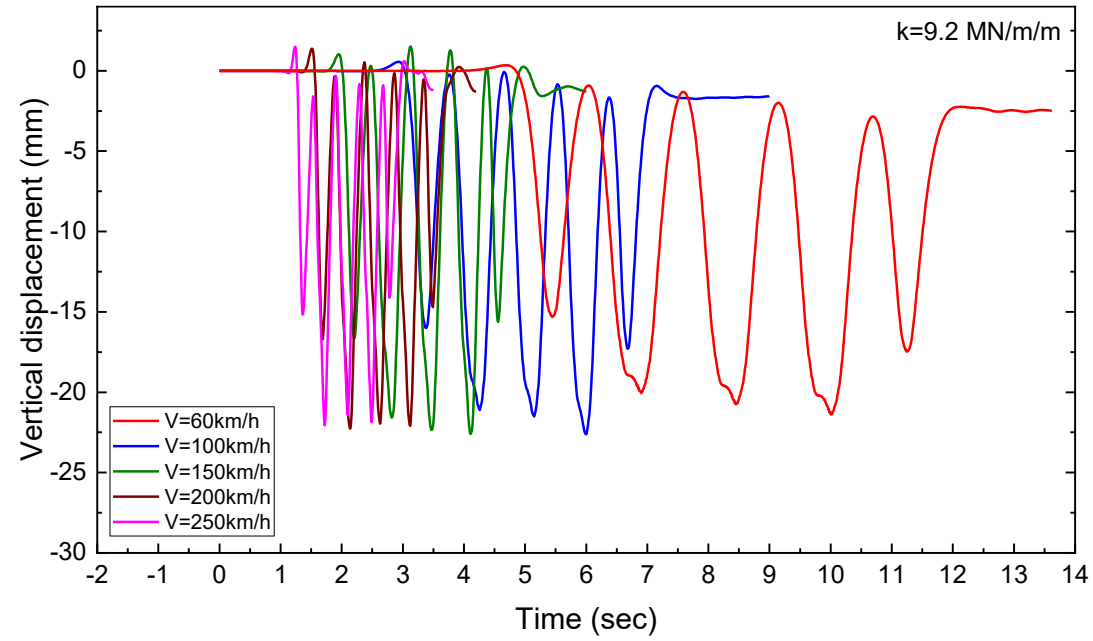

Figure C-8: Predicted vertical displacements for 3D FEM layered model (k = 9.2 MN/m/m, P_{axle} = 40 t) considering four-carriage loading moving at various speeds

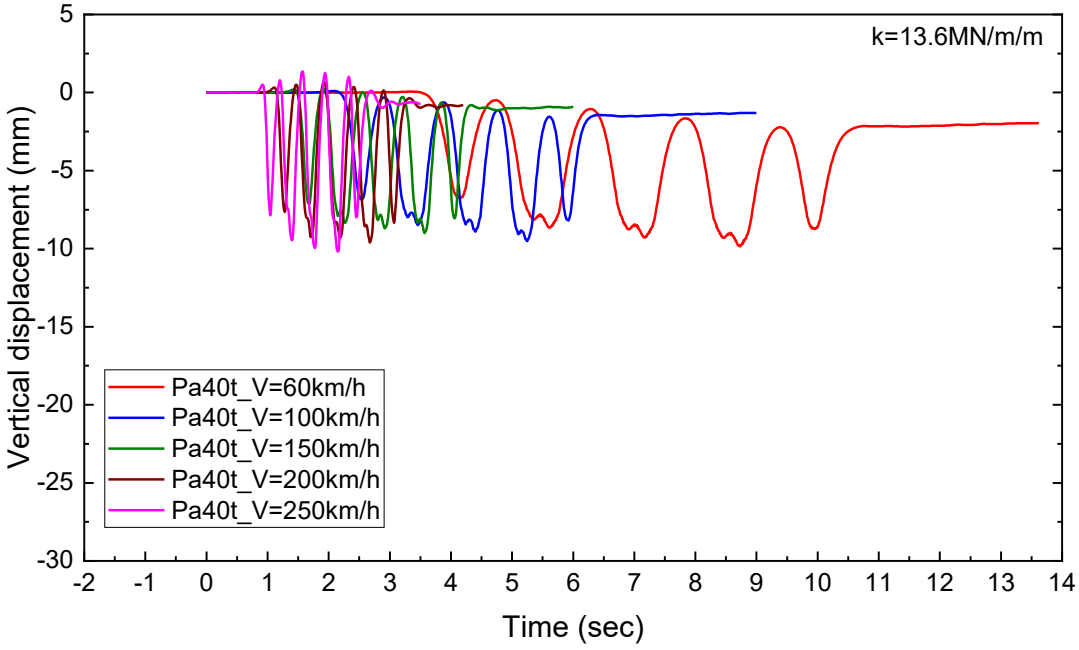

Figure C-9: Predicted vertical displacements for 3D FEM layered model (k = 13.6 MN/m/m, P_{axle} = 40 t) considering four-carriage loading moving at various speeds

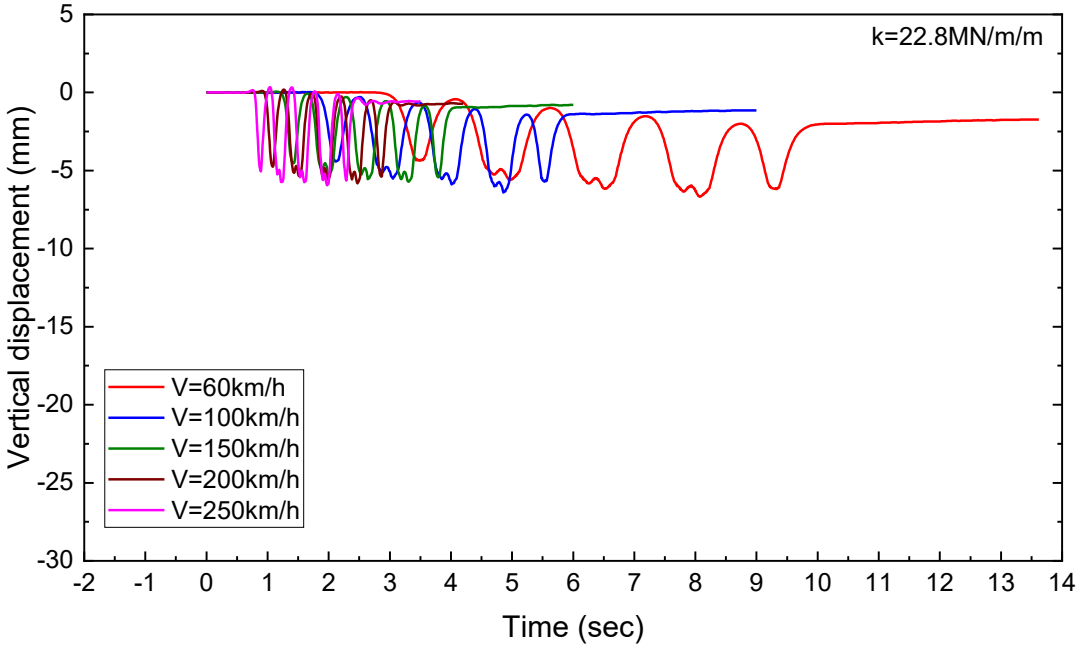

Figure C-10: Predicted vertical displacements for 3D FEM layered model (k = 22.8 MN/m/m, P_{axle} = 40 t) considering four-carriage loading moving at various speeds

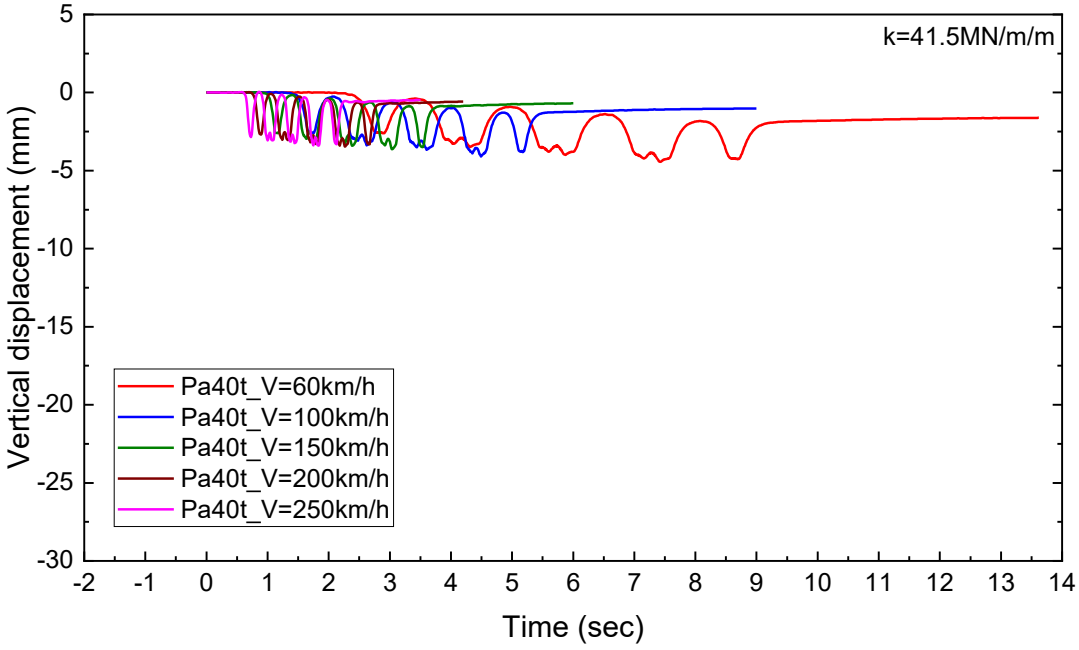

Figure C-11: Predicted vertical displacements for 3D FEM layered model (k = 41.5 MN/m/m, P_{axle} = 40 t) considering four-carriage loading moving at various speeds

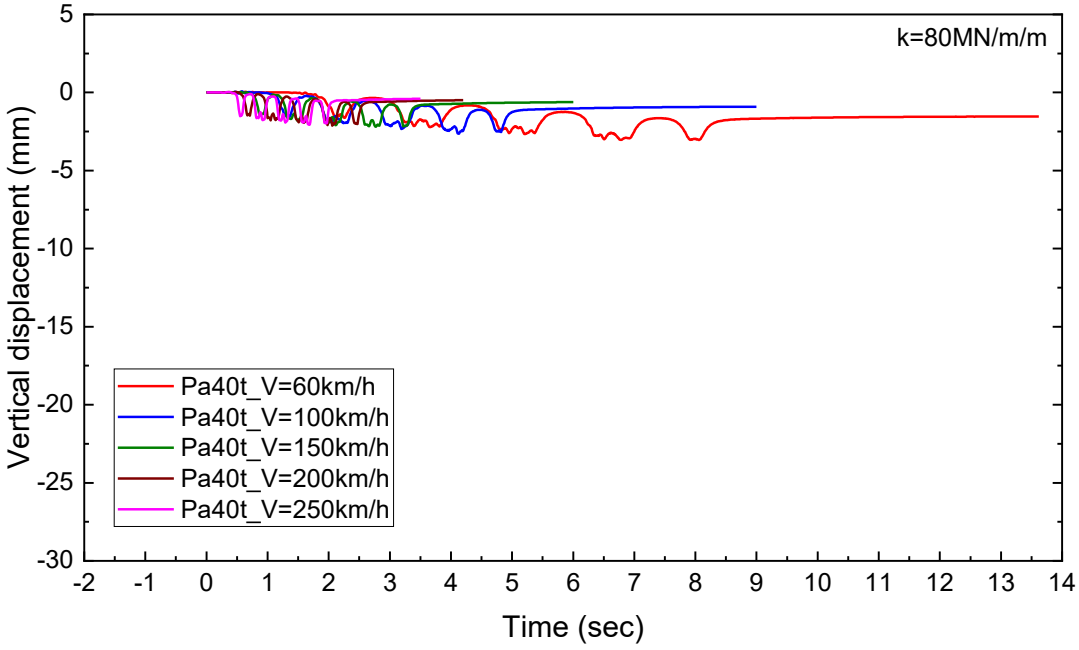

Figure C-12: Predicted vertical displacements for 3D FEM layered model (k = 80 MN/m/m, P_{axle} = 40 t) considering four-carriage loading moving at various speeds